

EXPERIMENTAL STUDIES OF DYNAMIC  
RESPONSE OF FOUNDATIONS

Thesis by  
Behnam Hushmand

In Partial Fulfillment of the Requirements  
for the Degree of  
Doctor of Philosophy

California Institute of Technology  
Pasadena, California  
1983

(Submitted November 15, 1983)



**ABSTRACT**

An investigation was made into the behavior of rigid foundations and structures resting on the surface or embedded in a cohesionless soil and subjected to transient active or passive excitations and forced vibrations using the centrifuge modeling technique. The investigation was aimed at studying both low and high amplitude vibrations of foundations under machine type loadings, earthquake or wave induced vibrations, and other sources of dynamic loads. Rigid "prototype" foundations of mass and size comparable to foundations of a low rise building were simulated in the centrifuge at a centrifugal acceleration of 50g. Rigid model structures (aluminum towers) attached to foundations of different shapes, sizes, masses, and moments of inertia were tested. The effect of soil depth, boundary conditions, and depth of foundation embedment were investigated. Mainly rocking and horizontal modes of vibration were studied. The impulse rocking-horizontal excitation of the models was provided by actively perturbing the model structures using explosive energy or by passively exciting them by shaking the whole soil bucket using a hydraulic shaking system. The forced vibration was produced by a miniature air-driven counterrotating eccentric mass shaker mounted on the model structures. During the tests detailed measurements of the static and dynamic contact pressure distributions, displacement components of the model, and acceleration amplitudes at different elevations of the model structure were obtained. The acceleration ratios were used to determine the modes of vibration of the foundation systems. Natural frequencies and damping coefficients of the modes were calculated by fitting the amplitude-frequency response of a single degree of freedom mass-spring-dashpot oscillator to the experimental response curves derived from the test data. Experimental results provided information regarding the influence of different geometrical, inertial, and loading conditions on the vibrational characteristics of the soil-structure system. In particular the effect of foundation

embedment was to increase the model resonant frequencies and to cause an appreciable change in contact pressure distribution underneath the footing. However, the resonant frequencies predicted by the lumped parameter analysis for a simple two-degree-of-freedom (rocking and translation) model were about 20 to 55 per cent higher than those measured experimentally. These results were consistent with the comparisons made in similar theoretical and experimental studies such as those performed by Morris in the Cambridge centrifuge and those performed on full-scale footings by Stokoe and Richart. Damping ratios of the rocking-sliding vibration did not change considerably when footing size or depth of embedment changed. The existence of rigid boundaries around the soil mass in the bucket, and an inefficient contact between soil and the foundation side walls and lower surface could account for these observations. Uplift and nonlinear large amplitude vibrations were consistently observed during the steady-state vibration tests. Uplift led to a softer vibrating system which behaved non-linearly. As a result the frequency of vibration decreased with the amount of lift-off. In transient vibration uplift reduced the intensity of higher frequency vibration. Soil around the foundation edge yielded and plastic deformations and subsequent softening of the contact soil increased the material damping while it decreased the resonant frequency of the system. It was concluded that elastic half-space theory does not satisfy the needs for analysis of foundation behavior under high amplitude vibrations and more sophisticated methods of analysis are required.

## ACKNOWLEDGEMENTS

I wish to express my sincere gratitude to my advisor, Professor R. F. Scott, for his guidance, encouragement and helpful suggestions provided during the course of this investigation. The assistance of the other members of the faculty of Civil Engineering, and specially of Professors G. W. Housner, P. C. Jennings, J. L. Beck, and J. F. Hall is also acknowledged. Special thanks are due to Professor Nick Warren of the University of California in Los Angeles and Dr. Carol Tosaya formerly with Stanford University, California, for their valuable suggestions and assistance in ultrasonic wave velocity measurement tests.

The financial support of the National Science Foundation and the California Institute of Technology is gratefully acknowledged.

I would like to thank Mr. J. R. Lee for his great assistance with centrifuge testing. Thanks are also expressed to my friends A. Allard, S. J. Lee, S. Jain, K. Chelvakumar, and R. Relles for their help in numerous ways. Special thanks are owed to Miss Martha Nyiri, Mrs. Gloria Jackson, Mrs. Sharon Beckenbach, and my sister Elahe for all they have done in preparing this manuscript.

Finally, I wish to express heartfelt gratitude to the members of my family, especially my wife, Simin, for her steadfast love and support through years of hard work.

## TABLE OF CONTENTS

	<u>Page</u>
ABSTRACT . . . . .	.iii
ACKNOWLEDGEMENTS . . . . .	v
Chapter I INTRODUCTION	
1.1 GENERAL . . . . .	1
1.2 DYNAMIC RESPONSE OF FOOTINGS. . . . .	4
1.3 HISTORICAL BACKGROUND . . . . .	9
1.3.1 Theoretical Studies. . . . .	10
1.3.1.1 Early Empirical Models. . . . .	10
1.3.1.2 Rigid Footings on Linear Elastic Half-Space. . . . .	11
1.3.1.3 Viscoelastic Half-Space . . . . .	13
1.3.1.4 Rigid Footings on Homogeneous Soil or Layered Medium . . . . .	14
1.3.1.5 Foundations with Arbitrary Shapes and Rigidity. . . . .	15
1.3.1.6 Nonlinearity, Inhomogeneity, Anisotropy. . . . .	16
1.3.1.7 Embedded Footings . . . . .	17
1.3.2 Experimental Studies . . . . .	17
1.4 SUMMARY OF PAST THEORETICAL AND EXPERIMENTAL RESULTS. . . . .	20
1.4.1 Effect of Size, Shape, and Inertia . . . . .	20
1.4.2 Effect of Finite Depth of Stratum over Bedrock . . . . .	20
1.4.3 Effect of Nonlinearity and Hysteretic Damping in Soil. . . . .	21
1.4.4 Effect of Embedment. . . . .	21
1.5 OBJECTIVES. . . . .	22
1.6 ORGANIZATION OF THE REPORT. . . . .	24
CHAPTER REFERENCES. . . . .	26
Chapter 2 CENTRIFUGE MODEL TESTING. . . . .	
2.1 INTRODUCTION. . . . .	32
2.2 CENTRIFUGE MODELING . . . . .	33
CHAPTER REFERENCES. . . . .	41

## TABLE OF CONTENTS (Continued)

	<u>Page</u>
Chapter 3 PRELIMINARY EXPERIMENTS ON FOAM RUBBER. . . . .	42
3.1 INTRODUCTION . . . . .	42
3.2 ELASTIC MEDIUM AND FOOTINGS. . . . .	42
3.3 EQUIPMENT AND INSTRUMENTATION. . . . .	44
3.3.1 Loading Equipment . . . . .	44
3.3.2 Measuring Equipment . . . . .	47
3.4 CALIBRATION OF TRANSDUCERS . . . . .	50
3.5 EXPERIMENTAL PROCEDURE AND RESULTS . . . . .	50
3.5.1 Wave Propagation Tests. . . . .	51
3.5.2 Vertical Vibration of Footings. . . . .	53
3.6 COMPARISON OF THEORETICAL AND EXPERIMENTAL RESULTS . . . . .	56
CHAPTER REFERENCES . . . . .	65
Chapter 4 SOIL. . . . .	66
4.1 INTRODUCTION . . . . .	66
4.2 GENERAL PROPERTIES OF SOIL . . . . .	69
4.3 DYNAMIC SOIL PROPERTIES. . . . .	69
4.3.1 Resonant Column Tests . . . . .	71
4.3.2 Ultrasonic Pulse Tests. . . . .	87
4.4 SUMMARY. . . . .	94
CHAPTER REFERENCES . . . . .	96
Chapter 5 EQUIPMENT AND INSTRUMENTATION . . . . .	98
5.1 GENERAL PRESENTATION OF CENTRIFUGE . . . . .	98
5.2 EQUIPMENT . . . . .	100
5.2.1 The Centrifuge. . . . .	100
5.2.2 Loading Equipment . . . . .	100
5.2.2.1 Explosion Generating Loading System. . . . .	103
5.2.2.2 Counterrotating Eccentric Mass Shaker. . . . .	103
5.2.2.3 The Continuous Earthquake Generating Mechanism. . . . .	108
5.2.2.3a The Bucket Frame and Shaking System . . . . .	108
5.2.2.3b The Controller MTS 406 . . . . .	110
5.2.3 Model Structures. . . . .	113

## TABLE OF CONTENTS (Continued)

	<u>Page</u>
5.2.4 Soil Containers . . . . .	116
5.3 INSTRUMENTATION . . . . .	118
5.3.1 Description of Different Devices . . . . .	118
5.3.2 The Circuitry. . . . .	122
5.4 CALIBRATION OF TRANSDUCERS. . . . .	125
5.5 DATA ACQUISITION AND REDUCTION SYSTEMS. . . . .	128
5.5.1 Data Acquisition. . . . .	128
5.5.2 Data Reduction. . . . .	129
CHAPTER REFERENCES . . . . .	131
Chapter 6 TEST PROCEDURE AND DATA REDUCTION. . . . .	132
6.1 GENERAL STEPS OF EXPERIMENT SETUP . . . . .	132
6.2 SPECIAL TESTING METHODS . . . . .	137
6.2.1 Explosion Generated Free Oscillation Tests. . . . .	137
6.2.2 Steady-State Forced Vibration Tests Using Air-Driven Shaker . . . . .	142
6.2.3 Transient Shaking of the Soil Container . . . . .	149
6.3 DATA REDUCTION. . . . .	150
CHAPTER REFERENCES . . . . .	154
Chapter 7 EXPERIMENTAL RESULTS . . . . .	155
7.1 EXPLOSION-GENERATED FREE OSCILLATION. . . . .	155
7.2 STEADY-STATE FORCED VIBRATION TESTS . . . . .	167
7.2.1 Presentation and Analysis Methods of the Results . . . . .	167
7.2.2 Effect of Soil Depth and Side Boundaries. . . . .	176
7.2.3 Influence of Foundation Size and Shape. . . . .	180
7.2.4 Variation of Rocking Resonant Frequency with Centrifugal Acceleration . . . . .	184
7.2.5 Variation of Resonant Frequency with Eccentric Mass of Shaker. . . . .	186
7.2.6 Effect of Mass Moment of Inertia ( $I_b$ ) . . . . .	189
7.2.7 Effect of the $\frac{\sqrt{M}}{I_b}$ Ratio. . . . .	189
7.2.8 Influence of Footing Embedment. . . . .	191
7.2.9 Static and Dynamic Pressure Distribution Over the Footing-Soil Contact Area . . . . .	197
7.2.9.1 Static Pressure Distribution . . . . .	197



## TABLE OF CONTENTS (Continued)

	<u>Page</u>
7.2.9.2 Mechanism of Yielding, Liftoff and Separation During Rocking of the Tower . . . . .	198
7.2.9.3 Dynamic Pressure Distribution. . . . .	202
7.2.10 Nonlinear Inelastic Behavior of the Soil-Tower System . . . . .	209
7.2.11 Imperfection of the Axisymmetry and Soil Homogeneity . . . . .	212
7.2.12 Determination of Response Modes . . . . .	214
7.3 MODEL TESTS IN TRANSIENT HYDRAULIC SHAKER. . . . .	221
7.4 MODELLING AT DIFFERENT SCALES. . . . .	224
7.5 CONCLUSION . . . . .	227
CHAPTER REFERENCES . . . . .	230
Chapter 8 THEORETICAL RESULTS, SUMMARY AND CONCLUSIONS . . . . .	231
8.1 INTRODUCTION TO METHODS OF ANALYSIS . . . . .	231
8.2 LUMPED PARAMETER ANALYSIS . . . . .	233
8.2.1 One-Degree-of-Freedom Lumped Parameter Analog . . . . .	234
8.2.2 Two-Degree-of-Freedom Lumped Parameter Analog . . . . .	242
8.2.3 Foundation-Soil Impedances . . . . .	246
8.2.4 Impedance Functions for Viscoelastic Foundations . . . . .	248
8.2.5 Impedance Functions for Analysis of Embedded Foundations . . . . .	252
8.2.6 Presentation of Theoretical Results for the 2-D Model . . . . .	253
8.2.6.1 Theoretical Values of Resonant Frequencies . . . . .	256
8.2.6.2 Comparison of Experimental and Theoretical Response Amplitudes . . . . .	259
8.2.6.3 Theoretical Modal Analysis . . . . .	259
8.2.6.4 Theoretical Results for Embedded Footings . . . . .	265
8.2.6.5 Theoretical Results for Foundations of Different Sizes . . . . .	266
8.2.6.6 Reasons for Discrepancy Between Predicted and Measured Results . . . . .	269
8.3 SUMMARY AND CONCLUSIONS . . . . .	270
CHAPTER REFERENCES . . . . .	274

Appendix A . . . . .	275
Appendix B . . . . .	285
Appendix C . . . . .	298

## CHAPTER 1

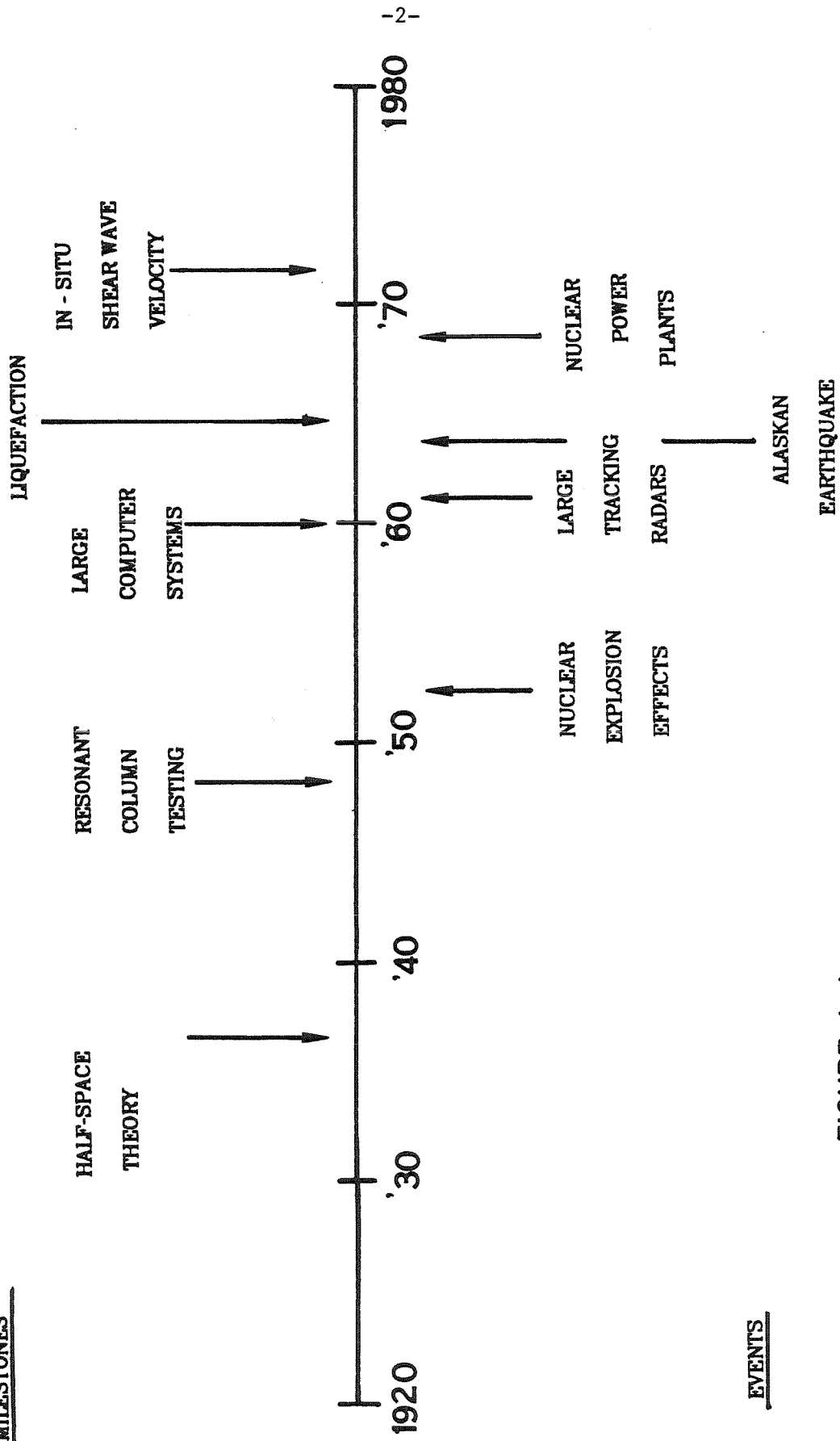
### INTRODUCTION

This introductory chapter is divided into four sections. The first section indicates the scope of soil dynamics and significance of soil-structure interaction analysis. Section 1.2 delves briefly into the past work and presents the state of the art in dynamic design of foundations subjected to machine-type loadings, and foundations of buildings to resist seismic and other-large amplitude dynamic loads. Section 1.3 describes the objectives and scope of this study. The last section of this chapter outlines the proposed test program and the organization of this investigation.

#### 1.1. GENERAL

Soil dynamics is a branch of soil mechanics which studies the behavior of soil masses and foundations on or in soil under dynamic stresses. Interest in development and growth of this subject arose originally from the need to design foundations subjected to machine-type loads and the need for compaction of soils under vibratory loads. There are many engineering problems which involve soil dynamics, such as: design of machine foundations and foundations of tracking radars; analysis and design of earthquake-resistant foundations for buildings and energy-producing structures such as nuclear power plants, offshore platforms and earth dams; determination of soil profiles using in-situ wave propagation velocity measurements; pile driving; and compaction of loose soils using vibratory loads. While many developments have influenced the evolution of soil dynamics, a few contributions have had especially important impacts. These special events and investigations are milestones in the evolution of soil dynamics (see Fig. 1).

MILESTONES



EVENTS

FIGURE 1.1

Machine foundations are the most frequently encountered problems in soil dynamics and many of the early books and references on soil dynamics deal with this problem (Barkan 1962, Richart *et al.* 1970). Careful and sound engineering design of machine foundations is required to provide satisfactory operation of machinery and nearby equipment and to minimize the disturbance to people working in the immediate vicinity. Therefore the key ingredient in design of foundations under dynamic loads anticipated from operation of machinery is a careful engineering analysis to limit the motion to amplitudes which are in the safe range both for human beings and machines.

Continuous growth and increased population in seismically active regions has contributed to the growing concern regarding the safe behavior of structures during earthquakes. A successful design of a structure to resist seismic loads is only possible through inclusion of the effect of the underlying soil on the dynamic behavior of the structure. Experience with structures subjected to earthquake shaking, and analysis of collected earthquake data (Ohsaki 1969, Seed 1968), and forced vibration tests of real buildings, eg. Foutch (1976), have shown that behavior of structures strongly depends on the fabric of the underlying soil layer and on the character of the soil-structure interface. Only when a structure is founded on the surface of a stiff soil or rock, for example, is the motion of its foundation similar to the earthquake free field motion, and then the dynamic response of the structure can be analysed using the "fixed base" model.

Although the existence of the soil-structure interaction effect has been recognized and investigated in Japan since the 1930's, this problem did not receive considerable attention in the United States up to the 1960 Chilean earthquake, the Alaskan earthquake of 1964 and the earthquake in Niigata, Japan in 1964. The other great factor in growth of concern for this problem was because of the surge in nuclear power plant construction during the 1970's, caused by fear of

shortage of other sources of energy. Because of catastrophic consequences in case of the failure of a nuclear power plant during strong ground shaking the requirement for safety analysis of each plant must consider the possible effect of earthquakes.

Therefore motivated to a large extent by the need to understand the soil-structure interaction phenomenon and to design machine foundations to operate in a satisfactory fashion, analysis of the dynamic response of foundations has been selected for this study.

In the following sections of this introductory chapter after a brief description of the physical and mathematical aspects of the foundation vibration theory a review of previous studies is made and requirements for a good soil-structure interaction analysis for design of machine foundations and other types of foundations are discussed.

## 1.2. DYNAMIC RESPONSE OF FOOTINGS

Footings of machines, buildings, dams, and other structures have arbitrary shapes and rigidities and are usually embedded partially in the soil. The supporting soil is of a discrete nature and is a three-phase material: solid grains, water and air. Thus soil is not a continuum, nor isotropic or homogeneous and behaves in a complex nonlinear inelastic manner under applied loads. Therefore an analytical approach to the dynamic behavior of footings similar to all other problems in soil mechanics is not possible unless a great deal of simplifying assumptions are introduced into the problem. The basic assumption is to treat soil as a continuum, provided that all the phenomena to be considered include a large number of particles. In case of dynamic and wave propagation problems, it means that only vibrations with wavelengths much larger than grainsize are considered. This, fortunately, is the case for most of the phenomena of practical interest in soil mechanics.

The basic original mathematical model for the foundation vibration problem was that of a rigid circular disc resting on the surface of a linear elastic, isotropic, and homogeneous half-space, called also a semi-infinite idealized soil. Further improvements in this model include the following aspects of the real problem:

- (1) Internal (material) damping of soils
- (2) Layering, inhomogeneity and anisotropy of soils
- (3) Approximate nonlinear and inelastic behavior of soils
- (4) Arbitrary shapes of footings
- (5) Embedment of footings
- (6) Flexibility of footings

The problem is usually solved for the response of a massless rigid plate attached to the surface of an elastic half-space where the resulting relations can be placed in a form comparable to that developed for the conventional one-degree-of-freedom system with viscous damping. This analogy will result in evaluation of foundation-soil impedance functions, which in effect model the soil as a system of elastic springs and viscous dashpots which provide restorative and dissipative forces. In general the values of these impedance functions are dependent upon soil properties, foundation geometry and the frequency of vibration.

The problem is quite complex because of the mixed boundary conditions on the surface of the half-space. Displacements at the contact area between the rigid plate and half-space are uniform or linearly varying depending on the mode of vibration (translational or rotational), while stresses are zero on the rest of half-space. The contact stress distributions are unknown and can be derived only by an exact treatment of the mixed boundary value problem. In order to reduce these rather complicated mixed boundary conditions to a simpler but approximate one, stress distributions over the contact area of footing and half-space were assumed to be known. In this way stresses over the

entire surface of the half-space are defined which leads to a simple boundary value problem. The resulting solution was approximate, however, since it gave rise to surface displacements incompatible with the rigid plate.

In a more rigorous approach mixed boundary value problem was solved assuming some of the contact stress components to be zero. This so called "relaxed mixed boundary value problem" was followed by the exact solution of the problem, deriving the true stress distribution on the contact area between disk and the half-space. All these methods will result in relations between displacement and force which define the compliance functions, as the ratio of displacement to force, or the impedance functions as the inverse of compliance. The following equations are a condensation of the solution to the problem.

Assuming that the elastic half-space has a shear modulus,  $G$ , a Poisson's ratio,  $\nu$ , and a mass density of  $\rho = \gamma/g$ , the harmonic response  $q$  to an input force  $P = P_0 e^{i\omega t}$  can be written as

$$q = \frac{P_0}{Gr_0} [ f_1 + if_2 ] e^{i\omega t} \quad (1.1)$$

in which the frequency dependent compliance functions  $f_1$  and  $f_2$  are the in-phase and out-of-phase responses of the disk to unit harmonic inputs, and  $r_0$  is the disk radius. Following the Hsieh's approach (1962) in deriving the stiffness and dashpot coefficients of the foundation-soil system we take the derivative of equation 1.1 with respect to time to obtain

$$\frac{dq}{dt} = \frac{P_0 \omega}{Gr_0} [ if_1 - f_2 ] e^{i\omega t} \quad (1.2)$$

combining equations 1.1 and 1.2 will result to equation

$$f_1 \omega q - f_2 \frac{dq}{dt} = \frac{P_0 \omega}{Gr_0} [ f_1^2 + f_2^2 ] e^{i\omega t} = \frac{P \omega}{Gr_0} [ f_1^2 + f_2^2 ] \quad (1.3a)$$



or

$$P = -\frac{Gr_o}{\omega} \left[ \frac{f_2}{f_1^2 + f_2^2} \right] \frac{dq}{dt} + Gr_o \left[ \frac{f_1}{f_1^2 + f_2^2} \right] q \quad (1.3b)$$

Equation 1.3b indicates that force transmitted to the elastic half-space is a function not only of the displacement of the disk, but also is a function of its velocity. If a massive plate of radius  $r_o$  and mass  $m_o$  is placed on the weightless rigid disk and subjected to a vertical exciting force  $Q_z$ , the equation of motion is

$$m_o \frac{d^2q}{dt^2} = Q_z + P \quad (1.4)$$

by substituting equation 1.3b into equation 1.4

$$m_o \frac{d^2q}{dt^2} + C_v \frac{dq}{dt} + K_v q = Q_z \quad (1.5)$$

where  $K_{sub v}$  and  $C_{sub v}$  are

$$K_v = -Gr_o \left[ \frac{f_1}{f_1^2 + f_2^2} \right] \quad (1.6a)$$

$$C_v = \frac{Gr_o}{\omega} \left[ \frac{f_2}{f_1^2 + f_2^2} \right] \quad (1.6b)$$

Equation 1.5 is similar to the equation for the one-degree-of-freedom system with viscous damping,

$$m \frac{d^2x}{dt^2} + c \frac{dx}{dt} + Kx = Q_x \quad (1.7)$$

with the exception that both  $K_v$  and  $C_v$  depend on frequency. Therefore,  $K_v$  and  $C_v$  are the stiffness and damping coefficients for the vibrating foundation on the elastic half-space. A similar approach results in the following functions for the rocking impedance,

$$K_\varphi = -Gr_o^3 \left[ \frac{f_1}{f_1^2 + f_2^2} \right] \quad (1.8)$$

$$C_\varphi = \frac{Gr_o^3}{\omega} \left[ \frac{f_2}{f_1^2 + f_2^2} \right] \quad (1.9)$$

In addition to Poisson's ratio, dimensionless frequency factor and mass ratio are the only parameters affecting the response of the vibrating footing. The frequency factor  $a_o$  and the mass ratio  $b$  are defined as

$$a_o = \omega r_o \sqrt{\frac{\rho}{G}} = \frac{\omega r_o}{v_s} = \frac{2\pi r_o}{L_s} \quad (1.10)$$

$$b = \frac{m}{\rho r_o^3} \quad (1.11)$$

in which  $V_s$  and  $L_s$  are the shear wave velocity and wave length. Functions  $f_1$  and  $f_2$  depend on frequency factor  $a_o$  and poisson's ratio  $\nu$ . Defining functions  $F_1$  and  $F_2$  as

$$F_1 = \frac{4}{(1-\nu)} f_1 \quad (1.12a)$$

$$F_2 = \frac{4}{(1-\nu)} f_2 \quad (1.12b)$$

and a mass ratio as

$$B_z = \frac{1-\nu}{4} b = \frac{1-\nu}{4} \frac{m}{\rho r_o^3} \quad (1.13)$$

Lysmer (1965) derived results which were essentially independent of Poisson's ratio. Amplitude of the disk motion can be expressed in terms a magnification factor  $M$ . For example in case of the vertically vibrating footing

$$A_z = \frac{(1-\nu)Q_o}{4Gr_o} M \quad (1.14)$$

where  $M$  is

$$M = \frac{4Gr_o A_z}{(1-\nu)Q_o} = \sqrt{\frac{F_1^2 + F_2^2}{(1 - B_z a_o^2 F_1)^2 + (B_z a_o^2 F_2)^2}} \quad (1.15)$$

Theoretical curves defining the relation between the magnification factor and the frequency parameter for different mass ratios  $B_z$  are derived in literature

and are used extensively for analysis and design.

### 1.3. HISTORICAL BACKGROUND

Many investigation of both an analytical and experimental nature on the dynamic response of footings have been conducted. A great wealth of references regarding the past work in this area since the early years of the present century can be found in the literature. Particularly in the last fifteen years considerable progress in this area of soil dynamics has been made and many researchers have studied different aspects of the problem. A comprehensive account of the past work up to the year 1969 can be found in McNeill (1969), or Richart, Hall, and Woods (1970), and a review of the present state of the art in dynamic analysis of foundations is presented in the recent study by Gazetas (1983). Here the main purpose is not to cover in detail all the pertinent work conducted in the past, but is to outline all the empirical, analytical and numerical models studied since early in the 20th century up to now.

For analysis different approximate methods have been used in the early years which were mainly based on engineering intuition and empirical rules. The cornerstone of the evolution of analytical techniques with a more scientific basis was the year 1904 when Lamb formulated and solved the problem of a harmonically varying point force acting on the surface of an elastic half-space. In the 1930's the first engineering application of Lamb's problem (dynamic Boussinesq' problem) was employed by Reissner (1936), to study the response of a vertically loaded cylindrical disk on the surface of an elastic half-space. This work even though an approximate solution to the dynamic response of foundations on the surface of an elastic half-space was a pioneering effort in this area and prompted many more investigations in the years after it. Because of its idealized nature, certain mathematical simplifications which are not quite realistic had to be introduced. Over many years, a great deal of progress has been made

in narrowing the gap between the results of theory and real behavior of foundation-soil system. In the following parts of this section a summary of the different mathematical improvements in the half-space theory will be presented.

### 1.3.1. Theoretical Studies

In early years of this century, as was pointed out previously, some approximate methods of analysis were employed in design of foundations for dynamic loadings, thereby avoiding the extreme difficulties inherent to a fully theoretical solution of this mixed boundary value problem. After 1950 the main stream of research in the area of foundation vibration was directed toward improving the half-space model; very recently some of the more realistic aspects of soil behavior and foundation-soil interface have been studied.

#### 1.3.1.1. *Early Empirical Models*

Major empirical methods were originated after the pioneering experimental investigations carried out by the Deutschen Forschungsgesellschaft für Bodenmechanik (DEGEBO) in Germany during the period 1928-1936. "In-Phase Mass" method, "Reduced Natural Frequency", and "Dynamic Subgrade or Dynamic Winkler" model were the main three techniques used in design of foundations for machine-type dynamic loadings. These methods primarily focused on determination of resonant frequency of the system and did not study the complete dynamic characteristics of the foundation-soil system. For example, they did not include the dissipation of energy carried by the waves propagating away from the foundation (radiation damping).

The "In-Phase Mass" method (Crockett and Hammond 1949, Rao 1961), assumes that a finite mass of soil underlying the foundation vibrates rigidly in phase with the foundation. In fact this idea was completely contradictory to the wave propagation nature of energy emanating from foundation-soil interface for

a foundation subjected to machine-type loadings. Moreover the in-phase mass may be appreciably varied with the dimensions, shape, and mass of foundation, mass density of soil and frequency of oscillation.

"Reduced Natural Frequency" method (Tschebotarioff and Ward 1948), was based on the assumption that the main factors affecting the natural frequency of the foundation are the soil bearing pressure, type of the soil, and the contact area. Therefore it did not include the effect of all the other factors influencing dynamic response of foundation.

Among these methods the "Dynamic Winkler" model (Hayashi 1921, Terzaghi 1943, 1955, Hetenyi 1946, Barkan 1962) was the most accepted one among engineers and it is still used in some countries around the world. The main approximation in this method was to regard the soil underlying the foundation as a bed of weightless independent springs resting on a rigid base.

In the above methods soil properties were considered in the calculation of resonant frequency by bearing coefficients of subgrade reaction derived from static or dynamic bearing resistance tests, required in any particular case of soil conditions and foundation properties.

#### 1.3.1.2. *Rigid Footings on Linear Elastic Half-Space*

The half-space studies are mainly concerned with the dynamic response of rigid circular foundations, and the soil medium is simulated by a homogeneous isotropic elastic half-space. The following studies are all directed at surface footings. Investigations on embedment effect of foundations are collected in section 1.3.1.7.

As it was explained before this mixed boundary value problem was originally solved by assuming different stress distributions over the contact area between footing and half-space. Based on the classic work by Lamb (1904), E. Reissner

(1936) integrated the solution for a vertical dynamic point load on the surface of the idealized solid over a circular area and presented an analytical solution for the oscillation of a rigid circular footing, resting on the surface of elastic half-space, and subjected to a vertical harmonic load. He (1937,1944) extended his work to the case of a torsional load about an axis through the center of the circular footing. Sung (1953), and Quinlan (1953), considered different distributions of contact pressures (uniform, parabolic, and rigid) and presented results for vertical oscillations. Arnold et al. (1955), and Bycroft (1956), studied other modes of vibration (horizontal and rocking) for different contact pressure distributions. Thomson and Kobori (1963), presented solutions for different vibration modes of rectangular foundations.

These solutions are only approximate because in reality the pressure distribution required to maintain a uniform or linear displacement for a rigid footing in different modes of vibration is not constant but will vary with frequency of excitation. Consequently the next development was mixed boundary-value treatment of the problem. Gladwell (1968), solved for forced tangential and rotatory vibration of a rigid circular disk. Awojobi (1969), investigated the harmonic torsional oscillations of a rigid circular body. Grootenhuis (1970), studied dynamic response of a rigid circular or rectangular foundation block resting on an half space. Luco and Westmann (1971), studied all the vibration modes of a rigid footing on the surface ,i.e. vertical, torsional, sliding (tangential mode of vibration without any slipping), rocking, and coupled rocking and sliding. A wide range of dimensionless frequencies was employed. Veletsos and Wei (1971), used analytical methods and presented numerical data for the steady state rocking and sliding response of a rigid, circular, massless disk. Numerical results were presented in the form of graphs for flexibility, stiffness, and damping coefficients to be used in an equivalent spring-dashpot representation of the soil-footing system. Dynamic impedance functions for a rigid circular

foundation were also tabulated by Veletsos and Verbic (1974). Different modes of vibration of a rigid strip footing and rigid rectangular foundations were studied by Karasudhi et al (1968), Oien (1971), Gazetas (1975), Gazetas and Roesset (1976), Wong and Luco (1976), Savidis (1977), and Kitamura and Sakurai (1979).

All of these methods give rise to frequency-dependent impedance functions relating applied force and foundation response. In applying these solutions to real soil-structure interaction problems by means of the "lumped-parameter method" the frequency-dependent coefficients of the subgrade impedance functions should be employed as restraints imposed on the base of a structure. In fact, the frequency dependence of the impedance coefficients often is ignored in practice and the coefficients are viewed as representing dashpots (including only effect of radiation damping) and springs, on which the structure bears (Hsieh 1962, Lysmer 1965, Hall 1967).

#### 1.3.1.3. *Viscoelastic Half-Space*

Material damping for the soil supporting foundation should be considered in order to achieve a realistic estimate of foundation-soil response. Experimental observations have proven that energy loss in soils in unit element tests is mainly because of internal friction (see Chap. 4). Therefore, material damping in soils is of an hysteretic nature and overall is not frequency dependent but varies with the amplitude of strains during shear deformations. Because of low values of radiation damping in rotational modes of vibration (torsion, rocking) incorporation of material damping in these modes of vibration will have a great effect on the response of vibrating footings. Veletsos and Verbic (1973), Luco (1976), and Lysmer (1980), formulated and solved the problem of the response of rigid foundations on the surface of a viscoelastic half-space or layered medium. They showed that in the case of the half-space the so-called "correspondence principle" enables the use of elastic-case impedance functions for the viscoelastic

material by just multiplying them by the factor  $(1+2i\xi)$ , where  $\xi$  is the hysteretic damping ratio and is defined by

$$\xi = \frac{\Delta W_h}{4\pi W} \quad (1.16)$$

in which  $W_h$  is the dissipated energy in each cycle of motion and  $W$  is the maximum energy of the system in the cycle.

#### 1.3.1.4. *Rigid Footings on Homogeneous Soil Stratum or Layered Medium*

Soil deposits in nature are usually inhomogeneous and soil profiles are composed of layers with distinct material properties. In most cases a layer of soft soil is underlain by a much stiffer medium or even by bedrock. Response of foundations on the surface of a soil stratum over a rigid base has been studied by many investigators for circular and strip footings (Kausel 1974, Kausel et al 1975,1979, Roesset 1980, and Gazetas and Roesset 1976,1979). Numerical solutions for the response of circular foundations on a finite stratum over a half-space have been reported by Hadjian and Luco (1977), and for strip footings by Gazetas and Roesset (1976). In these solutions the finite layer and the half-space have different material properties but they are regarded as homogeneous, isotropic, and linearly elastic. The ratio of the elastic moduli and depth of the layer to a characteristic length of footing are two more parameters affecting the response of the vibrating footing.

Dynamic response of rigid footings on the surface of homogeneous, isotropic, and elastic or viscoelastic layered media has been studied by Kausel (1974), Lysmer et al (1974), using the finite element technique. A distinct character of these finite element methods is the need for special boundary conditions to represent the infinite distance to the boundaries. By the use of appropriate conditions it is possible to prevent energy waves from reflecting at the boundaries back to the foundation-soil interface, and thereby to correctly model the



loss of energy in soil through radiation damping. 'Viscous', 'consistent', 'silent', and other special energy absorbing boundaries were studied by Lysmer et al (1974), Waas(1972), Kausel (1974), and Cohen (1980).

#### 1.3.1.5. *Foundations with Arbitrary Shapes and Rigidity*

Only a few studies in recent years have been carried out analysing response of foundations with arbitrary shape. Wong and Luco (1976), used the fundamental solution of Thomson and Kobori (1963), to define subregions within a basic arbitrarily-shaped region, i.e., the foundation. Gaul (1977), considers the same problem for a viscoelastic half-space. In another attempt by Luco and Wong (1979), they use the concept of a point-load solution of suitably adjusted strength to represent each rectangular subdivision of the footing, thereby avoiding the need for considerable computer time in calculating double integrals for the subregions. Adeli et al (1981), calculated compliances of arbitrarily- shaped footings on an elastic half-space by also breaking up the foundation into rectangular subregions. However, they used the results for an equivalent circular load for each subregion. This way the double integration procedure for rectangular subregions reduced to the numerical evaluation of only a single integral for each subregion.

The effect of the flexibility of circular and rectangular foundations on the surface of an elastic or viscoelastic half-space have been addressed in some recent studies (Lin 1978, Iguchi and Luco 1981, and Whittaker and Christiano 1982). Semi-analytical methods were used in most of these studies, where the supporting soil medium was treated using analytical methods, and the foundation was discretized to subregions in a finite elements representation. The expressions relating displacements and unit forces at nodal points on the foundation-soil interface were used to derive final solutions.

1.3.1.6. *Nonlinearity, Inhomogeneity, Anisotropy*

Real soils behave nonlinearly and permanent deformations will usually develop under medium to high amplitude loadings. In order to include the influence of nonlinearity on response of vibrating foundations some relatively simple nonlinear constitutive models have been used. The Ramberg-Osgood model was used by Funston and Hall (1967), and Jakub and Roesset (1977). Nonlinear behavior of soils has been included in many finite element solutions of soil-structure interaction problem (Lysmer et al 1974, Kausel et al 1976, etc). However, in these methods the nonlinear behavior is approximated through a series of iterative linear analyses, where the material soil properties at each step are derived from the last step of iteration using the calculated strains in the elements and experimental curves relating shear moduli and damping coefficients of soil with strain amplitude of deformation. Plastic properties of soil, i.e. permanent deformations in the soil mass under footing are not included in the above methods.

Inhomogeneity of soils has been accounted for in some of the analytical and numerical studies (Gazetas 1981e, Awojobi 1980, etc). Using the finite element method, material properties of the soil medium can be varied from element to element. In some analytical approaches models of an elastic half-space or a stratum over bedrock with linearly varying increasing moduli or wave velocities with depth have been studied for static and dynamic response of footings (Brown and Gibson 1972, Gazetas 1980, etc).

Observations have shown that soil deposits will usually behave mechanically differently in various directions, a characteristic of general behavior of materials called anisotropy. Because of sedimentation and subsequent one-dimensional consolidation in clays, and gravity effects in deposition of sands, soils usually show cross-anisotropy with a vertical axis of symmetry. Kirkner (1982), studied the vibration of a rigid disc on a transversely isotropic elastic

half-space and presented his results in the form of compliance and impedance coefficients as functions of dimensionless frequency for all modes of vibration. Gazetas (1981a, 1981f), presented solutions for response of dynamically loaded rigid strip footing on the surface of a cross-anisotropic soil layer and a visco-elastic cross -anisotropic half space.

#### 1.3.1.7. *Embedded Footings*

Foundations of most structures such as buildings, nuclear power plants, electricity towers, etc. and of machines are usually placed partially below the soil surface. Piles are extreme case of embedded foundations. Embedment has a great effect on the vibration characteristics of the foundations and has been much investigated in recent years. Several analytical and numerical methods, including the finite element method, have been used. Baranov (1967), Tajimi (1969), Novak and Beredugo (1971,1972), Novak (1973), Bielak (1975), Harada et al (1981), and many others have employed various analytical techniques to predict dynamic response of embedded footings by continuum formulation of the problem. Kuhlemeyer (1969), Waas (1972), Kausel (1974), Kausel and Roesset (1975), and several others have made use of the finite element method in dealing with this problem.

In most of these studies it is assumed that a complete bond between soil and the embedded part of footing including sidewalls exists. This is not, however, true in real cases where separation and sliding at the soil-foundation interface will happen during vibration (Tassoulas 1981, Novak and Sheta 1980, and Johnson and Epstein 1977).

#### 1.3.2. **Experimental Studies**

Theoretical methods for analyzing the dynamic response of foundation-soil systems are based on a number of simplifying assumptions regarding soil

properties and system geometry. In particular, real non-linear hysteretic soil properties are generally not included, or are approximated only. As a result, the application of theoretical results is questionable in many cases, such as, in particular, high amplitude vibration of the foundation-soil system during strong earthquake ground motion. Therefore there has existed a great need for experimental studies to evaluate theoretical techniques and to clarify the ambiguities produced by using simplified mathematical models.

Experimental studies on the dynamic behavior of surface and embedded foundations have been reported by many investigators. Pauw (1953), Novak (1960,1970), Barkan (1962), Fry (1963), Chae (1964,1969), Chae, Hall, and Richart (1965), Drnevich and Hall (1966), Stokoe (1972), Erden (1974), Varadhi and Saxena (1980) and many others studied the vertical mode of vibration of surface footings while Novak (1960, 1963,1970), Barkan (1962), Fry (1963), Chae (1971), Beredugo (1971), Gupta (1972), Stokoe (1972), Tiedemann (1972), Erden (1974) and others studied the vertical mode of vibration of embedded footings. Some experimental studies have also been conducted on torsional and sliding modes of vibration (e.g. Novak 1960,1963,1970, Barkan 1962, Fry 1963, Moore 1971, Beredugo 1971, Novak and Beredugo 1971, Stokoe 1972, Erden 1974, Stokoe and Richart 1974, Sankaran et al 1980, Sreekantiah 1982, Lin 1982, Henke et al 1983).

All the experimental work cited above has been performed on model or small prototype footings in the field or in the laboratory in soil bins with dimensions in the range of a few feet. The largest size foundations tested in the field were generally foundations for one-story buildings, electric towers, or machine foundations. The largest model foundations used in laboratory tests were comparable with some machine foundations, but in general were about 1/10 to 1/5 of prototype foundations for larger structures such as buildings with several stories.

Some experimental tests of small, and rigid model structures of order of few inches in height, of various shapes and soil densities, have been run on a shaking table to study the effect of geometry, soil, and embedment on response (e.g. Hadjian, Howard, and Smith 1975).

Since the stress conditions on a soil element have a considerable effect on its behavior under both static and dynamic loadings it is expected that a soil mass behaves differently between full-scale and model conditions. Running full-scale tests on foundations of real structures is very expensive and in some cases even impossible. The centrifuge modelling technique, which has been used increasingly in soil mechanics in recent years, overcomes these difficulties. This comes about because under the appropriate centrifugal acceleration it is possible to scale a model correctly to duplicate the behavior of a full-size prototype by preserving correct stress and strain distributions in the soil and linearly scaling all dimensions. However, because of difficulties in instrumentation and control of the experimental process, very few dynamic tests have been performed using centrifuge modeling.

In a recent study of a foundation vibration problem in a centrifuge, Morris (1979,1981) conducted a series of transient tests on the behavior of rigid circular and square footings. A parametric study on the effect of footing size, centrifugal acceleration, and moment of inertia of the footing was performed for the fundamental mode of rocking-sliding vibration. Quantitative measurement of resonant frequency and damping was done, but the effect of embedment and soil saturation was considered only qualitatively. In more recent work by Prevost and Scanlan (1983) a study of soil-structure interaction by centrifuge modeling was performed in Princeton University. In this study steady-state rocking-sliding vibration of a rigid model structure was tested in a centrifuge and a response curve for displacement amplitude was compared with some well known theoretical results. A more detailed summary of centrifuge testing

technique and the historical background of its development as a tool for experimental research in geotechnical engineering will be presented in Chapter 2, "Centrifuge Testing".

#### **1.4. SUMMARY OF PAST THEORETICAL AND EXPERIMENTAL RESULTS**

In this section a general review of the results of parametric studies on dynamic response of foundations will be presented.

##### **1.4.1. Effect of Size, Shape, and Inertia**

Increasing footing mass or moment of inertia will on the average decrease resonant frequency and effective damping, but increase amplitude of motion at resonance.

It has been found that foundation shape does not have a great influence on response of footings with equal areas and moderate aspect ratios (e.g., length-to-width ratio for rectangular geometries). In the case of very long and narrow footings it is a common practice to idealize the shape to that of an infinitely long strip. There are only three modes of vibration for a strip footing, namely vertical, rocking, and horizontal. A general similarity between the impedance functions of strip and circular foundations exists except at low frequencies where the vertical and horizontal impedance functions of a strip footing on an elastic half-space ( i.e. the static stiffnesses ) because of indeterminacy of 2-d problem are zero.

##### **1.4.2. Effect of Finite Depth of Stratum over Bedrock**

Soil deposits very rarely have uniform structure extending deep into the ground and usually are intercepted by bedrock or a very stiff soil at some shallow depth. The following effects of the presence of the bedrock are worthy of note:

In case of vertical and horizontal modes of vibration a greater influence of the bedrock has been observed, where a decrease in the depth of soil stratum over bedrock decreases the radiation damping and increases the resonant frequency of the foundation-soil system. Furthermore, modes with higher frequency of vibration might also be excited because of the finite depth of the layer. Rocking and torsional modes of vibration are only influenced by the soil close to the surface. For a layer-depth over footing-radius ratio greater than about 3 to 5 the half-space model can be used satisfactorily.

#### 1.4.3. **Effect of Nonlinearity and Hysteretic Damping in Soil**

With an increase in the amplitude of strains developed, the nonlinear behavior of soils will be more profoundly reflected in the dynamic response of foundations. Resonant frequency usually decreases and material damping increases, as a result of the softening characteristic of soils.

Material damping which is of a hysteretic nature should be incorporated in the torsional and rocking modes of vibration. This is because the radiational loss of energy in these two modes is much smaller than with vertical and horizontal modes of vibration, and therefore unrealistic values of motion amplitude will exist at resonance if material damping is omitted. However, with little loss in accuracy material damping may be neglected in the translational modes of vibration (vertical and horizontal modes) in the presence of much higher radiation damping.

#### 1.4.4. **Effect of Embedment**

Embedment overall increases the stiffness of the soil-foundation system; therefore, resonant frequency increases and amplitude at resonance decreases. Embedment also causes an increase in radiation damping. Effect of embedment

is more pronounced in the two rotational modes of footing vibration, in contrast to translational modes that are much less affected.

Embedment also amplifies the effect of coupling between horizontal and rocking modes of vibration and therefore, in the impedance matrix for a two degree of freedom rocking-sliding system, cross-coupling stiffness terms are no longer negligible in comparison with the case of surface foundations.

The above review is by no means a complete one and is only a brief and general reminder emphasizing the effect of some critical parameters on dynamic response of footings. For more detailed discussion of parametric studies of this problem see Richart, Woods, and Hall (1970), Prakash (1981), and Gazetas (1983).

#### 1.5. OBJECTIVES

As stated previously, a rational design of foundations to resist dynamic loads involves a number of separate, yet interrelated, steps: 1) establishment of criteria for performance of footing-structure system after construction, 2) determination of the loads on the foundation or input motions at foundation-soil interface, 3) evaluation of soil properties and profile at the site, 4) reduction of real conditions to idealized model, 5) selection of an appropriate analytical or numerical method of analysis for calculation of stresses and deformations in the system. Out of these steps the most crucial one is to choose an analytical method whose approximate nature fits the particular situation of the problem as close as possible. An engineer can only be confident in using a theoretical method when its validation has been verified experimentally. Once the basic ideas of a theoretical technique have been evaluated and confirmed by a limited number of experiments, it is acceptable to expand this theory and study the effect of all parameters of interest on the results of analysis.



The results of an experiment are valid when in a model, the true conditions, which exist in the real prototype problem, are modeled correctly or when the experiment is performed on the prototype itself under approximately the same conditions as will exist in a real event.

None of the above requirements is easy to fulfil, particularly when dynamic behavior of massive foundations supporting giant structures or machinery is of interest. As was mentioned before, running full-scale experiments on foundations comparable in size and weight with foundations of real structures is very expensive and in some cases even impossible. The performance of scale model tests at the earth's gravitational field cannot offer a correct answer to the solution of soil mechanic problems because of the dependence of soil behavior on ambient stress conditions. Centrifuge modelling is a powerful technique to overcome these limitations to study both static and dynamic behavior of soils and structures supported on or buried in soil. A centrifuge simulates gravity-induced stresses at a reduced geometrical scale through centrifugal loading. More reliable and complete evaluation of present analytical techniques in predicting the dynamic response of foundations and in formulating soil-structure interaction problems requires such comprehensive quantitative experiments as only the centrifuge can provide economically.

This study consists of centrifuge experiments on the dynamics of foundations, with the goal of obtaining an extensive amount of experimental data on dynamic behavior of rigid structures on sand. The proposed objectives of this investigation are:

1. To study the effect of different parameters such as shape, size, mass, and moment of inertia on the dynamic response of rigid foundations placed on a mass of dry uniform fine sand.
2. To investigate the effect of embedment on the dynamic response of such

foundations.

3. To measure dynamic pressure distributions on the contact area of footing and soil.
4. To study the effect of rigid boundaries around the soil.
5. To provide a basis for a finite element model of the test problem for comparison of the experimental results with some of the finite element calculations used for prediction of foundation behavior under dynamic loads.
6. To compare test results with existing theories.

Model foundations and structures will be excited by a range of different types of loading, i.e., impact, steady state harmonic, and random, the latter simulating an earthquake motion. The first two are active loadings acting directly upon the footing, and the third will be passive, imparted to the structure through the soil by waves emanating from the motion of the soil bucket.

#### **1.6. ORGANIZATION OF THE REPORT**

The remainder of this report is divided into seven additional chapters. Chapter 2 describes the modeling laws applied to geotechnical problems particularly in centrifuge model testing. A review of the history of the centrifuge modeling technique in geotechnical engineering is also presented. Chapter 3 contains the preliminary footing vibration tests performed in the laboratory at 1-g gravitational acceleration. The chapter includes a discussion of the boundary effects on dynamic response of a footing vibrating on a bounded medium. Physical properties of the soil employed in centrifuge tests are provided in Chapter 4. Results of laboratory tests such as grain distribution analysis, minimum and maximum density evaluation, and other conventional tests measuring soil properties are reported in this chapter. Dynamic properties of

the soil are also measured through resonant column tests and ultrasonic wave propagation velocity measurements. The equipment, instrumentation, electronic circuitry, and data acquisition system are discussed in Chapter 5. Test procedures, and data acquisition and reduction techniques are reviewed in Chapter 6. Model footings and structures and other information related to each particular experiment are also discussed in this chapter.

The results of the experiments, as well as some limited analysis of the results are contained in Chapter 7. The results include the time-amplitude plots, Fourier amplitude spectra, and response curves obtained from forced vibration and transient tests. Pressure distributions on the soil-foundation contact area, and mode shapes of vibrating rigid structures are derived experimentally. A summary discussion of the results related to each parametric study is presented in this chapter. Chapter 8 presents the lumped parameter analysis of the model specimen structures. Existing methods of calculating foundation-soil impedances and embedment factors are presented and compared. These methods are used to obtain analytical response curves that are compared with the experimental results. A summary, conclusions, and recommendations concerning the entire contents of the report is presented at the end of this chapter.

CHAPTER REFERENCES.

- [1] Adeli, Hojjat, Hejazi, Mehdi S., Keer, Leon M., and Nemat-Nasser, Siavouche, "Dynamic Response of Foundations with Arbitrary Geometries," *Journal of the Engrg. Mechanics Division, Proc., ASCE*, Vol. 107, No. EM5, October 1981, pp. 953-967.
- [2] Arnold, R. N., Bycroft, G. N., and Warburton, G. B., "Forced Vibrations of a Body on an Infinite Elastic Solid," *ASME Journal of Applied Mechanics*, Sept. 1955, pp. 391-401.
- [3] Awojobi, A. O., "Torsional Vibration of a Rigid Circular Body on an Infinite Elastic Stratum," *Int. Journal Solid Struc.*, Vol. 5, 1969, pp. 369-378.
- [4] Awojobi, A. O., "Vertical Vibrations of a Rigid Circular Body on a Non-Homogeneous Half-Space Interrupted by a Frictionless Plane," *Int. Journal for Numerical and Analytical Methods in Geomechanics*, Vol. 4, 1980, pp. 159-174.
- [5] Baranov, V. A., "On the Calculation of Excited Vibrations of an Embedded Foundation," (In Russian), *Voprosy Dinamiki, Prochnosti, Polytechnical Institute of Riga*, No. 14, 1967, pp. 195-206.
- [6] Barkan, D. D., "Dynamics of Bases and Foundations," McGraw-Hill Book Co., Inc., New York, N.Y., 1962, 434 pp.
- [7] Beredugo, Y. O., "Vibration of Embedded Symmetric Footings," Ph.D. Thesis, Faculty of Engineering Science, The University of Western Ontario, London, Canada, 1971.
- [8] Bielak, J., "Dynamic Behavior of Structures with Embedded Foundations," *Int. Journal of Earthq. Engrg. and Struct. Dyn.*, Vol. 3, No. 3, Jan.-March 1975, pp. 259-274.
- [9] Brown, P. T., and Gibson, R. E., "Surface Settlement of a Deep Elastic Stratum whose Modulus Increases Linearly with Depth," *Canadian Geotech. Journal*, 1972, 9, 467.
- [10] Bycroft, G. N., "Forced Vibrations of a Rigid Circular Plate on a Semi-Infinite Elastic Space and on an Elastic Stratum," *Philosophical Trans., Royal Society, London*, Ser.A, Vol. 248, 1956, pp. 327-368.
- [11] Chae, Y. S., "Dynamic Pressure Distribution at the Base of a Rigid Footing Subjected to Vibratory Loads," Ph.D. Dissertation, Univ. of Michigan, 1964, 214 pp.
- [12] Chae, Y. S., "Vibration of Non-Circular Foundations," *Journal of the Soil Mech. and Found. Div., ASCE*, Vol. 95, No. SM6, Nov., 1969, pp. 1411-1430.
- [13] Chae, Y. S., "Dynamic Behavior of Embedded Foundation-Soil Systems," *Highway Research Record*, No. 323, 1971, pp.49-59.
- [14] Chae, Y. S., Hall, J. R., Jr., and Richart, F. E., Jr., "Dynamic Pressure Distribution Beneath a Vibrating Footing," *Proc. 8th Int. Conf. Soil Mech. Found. Engng.*, Vol. 2, 1965, pp. 22-26.
- [15] Cohen, M. F., "Silent Boundary Method for Transient Wave Analysis," *Earthquake Engineering Research Laboratory (EERL) 80-09, California Institute of Technology (Caltech), Pasadena, California*, 1980.

- [16] Crockett, J. N. A., and Hammond, R. E. R., "The Dynamic Principles of Machine Foundations and Ground," Proc. Institution of Mechanical Engineers, London, Vol. 160, No. 4, 1949, pp. 512-523.
- [17] Drnevich, V. P., and Hall, J. R., Jr., "Transient Loading Tests on a Circular Footing," Journal of Soil Mech. and Found. Div., Proc. ASCE, Vol. 92, No. SM 6, Nov. 1966, pp. 153-167.
- [18] Erden, S. M., "Influence of Shape and Embedment on Dynamic Foundation Response," Ph.D. Thesis, University of Massachusetts, Massachusetts, March, 1974.
- [19] Foutch, D. A., "A Study of the Vibrational Characteristics of Two Multistory Buildings," EERL 76-03, Caltech, Pasadena, California, Sept. 1976.
- [20] Fry, Z. B., "Development and Evaluation of Soil Bearing Capacity, Foundations of Structures," WES, Tech. Rep. No. 3-632, Report No. 1, Jul. 1963.
- [21] Funston, N. E., and Hall, W. J., "Footing Vibration with Nonlinear Subgrade Support," Journal of Soil Mech. and Found. Div., Proc. ASCE, Vol. 93, No. SM 5, Sept. 1967, pp. 191-211.
- [22] Gaul, L., "Dynamische Wechselwirkung eines Fundamentes mit dem Viscoelastischen Halbraum," Ingenieur-Archiv, Vol. 46, 1977, pp. 401-422.
- [23] Gazetas, G., "Dynamic Stiffness Functions of Strip and Rectangular Footings on Layered Soil," S.M. Thesis, MIT, 1975.
- [24] Gazetas, G., "Static and Dynamic Displacements of Foundations on Heterogeneous Multilayered Soils," Geotechnique, 1980, Vol. 30, No. 2, 159.
- [25] Gazetas, G., "Strip Foundations on Cross-Anisotropic Soil Layer Subjected to Static and Dynamic Loading," Geotechnique, 1981a, Vol. 30, No. 2, 161.
- [26] Gazetas, G., "Torsional Displacements and Stresses in Nonhomogeneous Soil," Geotechnique, 1981e, Vol. 31, No. 4, 487.
- [27] Gazetas, G., "Dynamic Compliance Matrix of Rigid Strip Footing Bonded to a Viscoelastic Cross-Anisotropic Halfspace," Int. Journal of Mech. Sci., 1981f, Vol. 23, No. 9, 547.
- [28] Gazetas, G., "Analysis of Machine Foundation Vibrations: State of Art," Soil Dynamics and Earthquake Engrg., Vol. 2, No. 1, 1983, pp. 2-42.
- [29] Gazetas, G., and Roesset, J. M., "Forced Vibrations of Strip Footings on Layered Soils," Meth. Struct. Anal., ASCE, 1976, 1, 115.
- [30] Gazetas, G. and Roesset, J. M. "Vertical Vibration of Machine Foundations," Journal of Geotech. Engrg. Div., ASCE, 1979, Vol. 105, No. GT12, 1435.
- [31] Gladwell, G. M. L., "Forced Tangential and Rotatory Vibration of a Rigid Circular Disc on a Semi-infinite Solid," Int. Journal of Engng. Sci., 1968, Vol. 6, 591.
- [32] Grootenhuis, P., "The Dynamics of Foundation Blocks," Proc. Conf. Sec. Earthg. Civil Engng. Dyn., "Dynamic Waves in Civil Eng.," Swansea, July 1970, pp. 95-105.
- [33] Gupta, B. N., "Effect of Foundation Embedment on the Dynamic Behavior of the Foundation-Soil System," Geotechnique, Vol. 22, No. 1, March 1972, pp. 129-137.
- [34] Hadjian, A. H., Howard, G. E., and Smith, C. B., "A Comparison of Experimental and Theoretical Investigations of Embedment Effects on Seismic Response," Proceedings of the Third International Conference on SMIRT,

Sept. 1975, Paper K2/5.

- [35] Hadjian, A. H., and Luco, J. E., "On the Importance of Layering on Impedance Functions," Proc. 6th WCEE, New Delhi, 1977.
- [36] Hall, J. R., Jr., "Coupled Rocking and Sliding Oscillations of Rigid Circular Footings," Proc. International Symposium on Wave Propagation and Dynamic Properties of Earth Materials, Albuquerque, N.M., Aug. 1967.
- [37] Harada, T., Kubo, K., and Katayama, T., "Dynamic Soil Structure Interaction by Continuum Formulation Method," Inst. Indus. Sc., University of Tokyo, Vol. 29, No. 5, 1981.
- [38] Hayashi, K., "Theorie des Tragers auf elastischer Unterlage," Julius Springer (Berlin), 1921, 301 pp.
- [39] Henke, R., Richart, F. E., Jr., and Woods, R. D., "Nonlinear Torsional Dynamic Response of Footing," Journal of Geotech. Engrg. Div., ASCE, Vol. 109, No. 1, 1983, pp. 72-88.
- [40] Hetenyi, M., "Beams on Elastic Foundation," The University of Michigan Press (Ann Arbor), 1946, 255 pp.
- [41] Hsieh, T. K., "Foundation Vibrations," Proc. Institution of Civil Engineers, Vol. 22, 1962, pp. 211-226.
- [42] Iguchi, M. and Luco, J. E., "Dynamic Response of Flexible Rectangular Foundations on an Elastic Halfspace," Earthq. Engrg. Struct. Dyn., 1981, 9, 239.
- [43] Johnson, G. R. and Epstein, H. I., "Backfill Effects on Circular Foundation Stiffnesses," Journal of Geotech. Engrg. Div., ASCE, 1977, Vol. 103, No. GT8, 899.
- [44] Karasudhi, P., Keer, L. M., and Lee, S. L., "Vibratory Motion of a Body on an Elastic Half Plane," Journal of Appl. Mech., ASME, 1968, Vol. 35, E, 697.
- [45] Kausel, E., "Forced Vibrations of Circular Foundations on Layered Media," Thesis Submitted to the Massachusetts Institute of Technology, in Partial Fulfillment of the Requirements for the Degree of Doctor of Science, 1974.
- [46] Kausel, E., and Roesset, J. M., "Dynamic Stiffness of Circular Foundations," Journal of Engrg. Mech. Div., ASCE, 1975, Vol. 101, No. EM12, 771.
- [47] Kausel, E., Ushijima, R., "Vertical and Torsional Stiffness of Cylindrical Footings," Research Rep. Rr76-6, MIT, 1979.
- [48] Kausel, E., Roesset, J. M. and Christian, J. T., "Nonlinear Behavior in Soil-Structure Interaction," Journal of Geotech. Engrg. Div., ASCE, 1976, Vol. 102, No. GT12, 1159.
- [49] Kirkner, D. J., "Vibration of a Rigid Disk on a Transversely Isotropic Elastic Half Space," Int. Journal for Numerical and Analytical Meth. in Geomech., Vol. 6, 1982, pp. 293-306.
- [50] Kitamura, Y., and Sakurai, S., "Dynamic Stiffness for Rectangular Rigid Foundations on a Semi-Infinite Elastic Medium," Int. Journal for Numerical and Analytical Meth. in Geomech., 1979.
- [51] Kuhlemeyer, R., "Vertical Vibrations of Footings Embedded in Layered Media," Ph.D. Thesis, University of California, Berkeley, 1969.
- [52] Lamb, H., "On the Propagation of Tremors over the Surface of an Elastic Solid," Philosophical Transactions of the Royal Society, London, Ser. A, Vol. 203, 1904, pp. 1-42.

- [53] Lin, Y. J., "Dynamic Response of Circular Plates on Viscoelastic Halfspace," *Journal of Appl. Mech.*, ASME, 1978, Vol. 45, E, 379.
- [54] Lin, A. N., "Experimental Observations of the Effect of Foundation Embedment on Structural Response," *Earthquake Engineering Research Laboratory (EERL) 82-01*, California Institute of Technology, Pasadena, California, 1982.
- [55] Luco, J. E., "Vibrations of a Rigid Disc on a Layered Viscoelastic Medium," *Nucl. Engrg. Des.*, 1976, Vol. 36, 325.
- [56] Luco, J. E. and Westmann, R. A., "Dynamic Response of Circular Footings," *Journal of Engrg. Mech. Div.*, ASCE, 1971, Vol. 97, No. EM5, 1381.
- [57] Luco, J. E., and Wong, H. L., "Response of Structures to Nonvertically Incident Seismic Waves," UCSD Technical Report, 1979.
- [58] Lysmer, J., "Vertical Motion of Rigid Footings," Dept. of Civil Eng., Univ. of Michigan Report to WES Contract Report No. 3-115 under Contract No. DA-22-079-eng-340; also a Ph.D. dissertation, Univ. of Michigan, Aug. 1965.
- [59] Lysmer, J., "Foundation Vibrations with Soil-Structure Damping," *Civ. Engrg. & Nucl. Power*, ASCE, 1980, II, 10/4/1-18.
- [60] Lysmer, J., Udaka, T., Seed, H. B. and Hwang, R., "LUSH A Computer Program for Complex Response Analysis of Soil-Structure Systems," Report No. EERC 74-4, University of California, Berkeley, 1974.
- [61] McNeill, R. L., "Machine Foundations: The State of Art.," *Proc. Soil Dyn. Spec. Sess. 7th ICSMFE*, 1969, pp.67-100.
- [62] Moore, P. J., "Calculated and Observed Vibration Amplitudes," *Journal of Soil Mech. Found. Div.*, Proc. ASCE, Vol. 97, No. SM1, Jan. 1971, pp. 141-158.
- [63] Morris, D. V., "The Centrifugal Modelling of Dynamic Soil-Structure Interaction and Earthquake Behavior," Ph.D. Thesis, University of Cambridge, Cambridge, England, 1979.
- [64] Morris, D. V., "Dynamic Soil-Structure Interaction Modelled Experimentally on a Geotechnical Centrifuge," *Canadian Geotechnical Journal*, Vol. 18, No. 1, Feb. 1981, pp. 40-51.
- [65] Novak, M., "The Vibrations of Massive Foundations on Soil," *Int. Assoc. Bridge Struct. Eng.*, Publ. No. 20, 1960, pp. 263-281.
- [66] Novak, M., "On Some Dynamical Problems of Turbomachinery Frame Foundations," *Proc. Int. Symp. Meas. Eval. Dyn. Effects Vibr. Constr.*, RILEM, Budapest, Vol. 1, 1963, pp. 215-234.
- [67] Novak, M., "Prediction of Footing Vibrations," *Journal of Soil Mech. Found. Div.*, Proc. ASCE, Vol. 96, No. SM3, May 1970, pp. 337-361.
- [68] Novak, M., "Vibrations of Embedded Footings and Structures," Preprint 2029, ASCE, Nat. Struct. Eng. Mtg., San Francisco, Calif., April 1973, 25 pp.
- [69] Novak, M., and Beredugo, Y. O., "The Effect of Embedment on Footing Vibrations," *Proc. 1st Can. Conf. Earthq. Engrg. Research*, Vancouver, B.C., May 1971, pp. 1-14.
- [70] Novak, M., and Beredugo, Y. O., "Vertical Vibration of Embedded Footings," *Journal of Soil Mech. Found. Div.*, Proc. ASCE, Vol. 98, No. SM12, Dec. 1972, pp. 1291-1310.
- [71] Novak, M., and Sheta, M., "Approximate Approach to Contact Effects of Piles," *Dyn. Resp. Pile Fdns.*, ASCE, 1980 (O'Neil and Dobry, eds.).

- [72] Oien, M. A., "Steady Motion of a Rigid Strip Bonded to an Elastic Half-space," *Journal of Appl. Mech.*, Trans. ASME, 1971, Vol. 38, 328.
- [73] Ohsaki, Y., "The Effect of Local Soil Conditions on Earthquake Damage," *Proc. of Soil Dynamics Specialty Session during 7th Int. Conf. Soil Mechanics and Foundation Engrg.*, Published by Woodward-Clyde Consultants, San Francisco, 1969, pp. 3-32.
- [74] Pauw, A., "A Dynamic Analogy for Foundation-Soil Systems," *Symp. Dyn. Test. Soils ASTM*, STP No. 156, July 1953, pp. 90-112.
- [75] Prakash, S., "Soil Dynamics," McGraw-Hill, 1981, pp. 361-7.
- [76] Prevost, J. H., and Scanlan, R. H., "Dynamic Soil-Structure Interaction: Centrifugal Modeling," Department of Civil Engineering, Report 83-SM-1, Princeton University, Princeton, New Jersey, 1983.
- [77] Quinlan, P. M., "The Elastic Theory of Soil Dynamics," *Symposium on Dynamic Testing of Soils*, ASTM STP No. 156, 1953, pp.3-34.
- [78] Rao, H. A. Balakrishna, "The Design of Machine Foundations Related to the Bulb of Pressure," *Proc. 5th ICSMFE*, Vol. 1, 1961, pp. 563-568.
- [79] Reissner, E., "Stationare, axialsymmetrische durch eine Schuttelnde Masse erregte Schwingungen eines homogenen elastischen Halbraumes," *Ingenieur-Archiv*, Vol. 7, Part 6, Dec. 1936, pp. 381-396.
- [80] Reissner, E., "Freie und erzwungene Torsionschwingungen des elastischen Halbraumes," *Ingenieur-Archiv*, Vol. 8, No. 4, 1937, pp. 229-245.
- [81] Reissner, E., and Sagoci, H. F., "Forced Torsional Oscillations of an Elastic Half-Space," *Journal of Appl. Phys.*, Vol. 15, 1944, pp. 652-662.
- [82] Richart, F. E., Jr., Hall, J. R., Jr., and Woods, R. D., "Vibrations of Soils and Foundations," Prentice-Hall, Inc., Englewood Cliffs, N.J., 1970, 414pp.
- [83] Roesset, J. M., "The Use of Simple Models In Soil-Structure Interaction," *Civ. Engrg. & Nucl. Power*, ASCE, 1980b, II, 10/3/1-25.
- [84] Sankaran, K. S., Krishnaswamy, N. R., and Bhaskaran Nair, P. G., "Torsional Vibration Tests on Embedded Footings," *Journal of the Geotech. Engrg. Div.*, ASCE, Vol. 106, No. GT3, March 1980, pp. 325-331.
- [85] Savidis, S. A., "Analytical Methods for the Computation of Wavefields," *Dyn. Meth. Soil Rock Mech.*, 1977, 1, 225.
- [86] Seed, H. B., "The Fourth Terzaghi Lecture: Landslides During Earthquakes due to Liquefaction," *Journal of Soil Mech. and Found. Div.*, Proc. ASCE, Vol. 94, No. SM5, Sept. 1968, pp. 1053-1122.
- [87] Seed, H. B., "The Influence of the Local Soil Conditions on Earthquake Damage," *Proc. of Soil Dynamics Specialty Session during 7th Int. Conf. Soil Mechanics and Foundation Engrg.*, Published by Woodward-Clyde Consultants, San Francisco, 1969, pp. 33-66.
- [88] Sreekantiah, H. R., "Rocking Vibrations of Footings," *Journal of Geotech. Engrg. Div.*, ASCE, Vol. 108, No. GT7, July 1982, pp. 905-917.
- [89] Stokoe, K. H., II, "Dynamic Response of Embedded Foundations," Ph.D. Dissertation, Univ. of Michigan, Jan. 1972, 251pp.
- [90] Stokoe, K. H., II, and Richart, F. E., Jr., "Dynamic Response of Embedded Machine Foundations," *Journal of the Geotech. Engrg. Div.*, ASCE, Vol. 100, No. GT4, Proc. Paper 10499, Apr. 1974, pp. 427-447.



- [91] Sung, T. Y., "Vibrations in Semi-Infinite Solids due to Periodic Surface Loadings," Symposium on Dynamic Testing of Soils, ASTM-STP No. 156, 1953, pp. 35-64.
- [92] Tajimi, H., "Dynamic Analysis of a Structure Embedded in an Elastic Stratum," Proc. of the 4th WCEE, Santiago, Chile, 1969, pp. 53-69.
- [93] Tassoulas, J. L., "Elements for the Numerical Analysis of Wave Motion in Layered Media," Research Rep. R 81-2, MIT, 1981.
- [94] Terzaghi, K., "Theoretical Soil Mechanics," John Wiley and Sons, Inc. (New York), 1943.
- [95] Terzaghi, K., "Evaluation of Coefficients of Subgrade Reaction," Geotechnique, Vol. 5, 1955, pp. 297-326.
- [96] Thomson, W. T., and Kobori, T., "Dynamical Compliance of Rectangular Foundations on an Elastic Half-Space," J. Appl. Mech., Trans. ASME, Vol. 30, Dec. 1963, pp. 579-584.
- [97] Tiedemann, D. A., "Vertical Dynamic Response of Embedded Footings," Bureau of Recl. Report, REC-ERC-72-34, Eng. Research Center, Sept. 1972, 22 pp.
- [98] Tschebotarioff, G. P., and Ward, E. R., "The Resonance of Machine Foundations and the Soil Coefficients Which Affect It," Proc. 2nd ICSMFE, Vol. 1, 1948, pp. 309-313.
- [99] Varadhi, S. N., and Saxena, S. K., "Foundation Response to Soil Transmitted Loads," Journal of Geotech. Engrg. Div., ASCE, Vol. 106, No. GT10, Oct. 1980, pp. 1121-1139.
- [100] Veletsos, A. S. and Verbic, B., "Vibration of Viscoelastic Foundations," Int. Journal of Earthq. Engrg. and Struct. Dyn., 1973, 2, 87.
- [101] Veletsos, A. S., and Verbic, B., "Basic Response Functions for Elastic Foundations," Journal of Engrg. Mech. Div., ASCE, 1974, Vol. 100, No. EM2, 189.
- [102] Veletsos, A. S., and Wei, Y. T., "Lateral and Rocking Vibrations of Footings," Journal of Soil Mech. Found. Div., ASCE, 1971, 97, SM9, 1227.
- [103] Waas, G., "Linear Two-Dimensional Analysis of Soil Dynamic Problems in Semi-Infinite Layered Media," Ph.D. Thesis, University of California, Berkeley, California, 1972.
- [104] Whittaker, W. L., and Christiano, P., "Dynamic Response of Plate on Elastic Half-Space" J. Engrg. Mech. Div., ASCE, 1982, 108, EM1, 133.
- [105] Wong, H. L. and Luco, J. E., "Dynamic Response of Rigid Foundations of Arbitrary Shape," Earthq. Engrg. Struct. Dyn., 1976, Vol. 4, 579.

## CHAPTER 2

### CENTRIFUGE MODEL TESTING

#### 2.1 INTRODUCTION

Many problems in physical sciences are not amenable to complete mathematical modeling in order to discover the reasons and philosophy behind their existence. The horizons of theoretical techniques in searching for solutions of the puzzles set forth by nature are limited. Nevertheless, a great number of problems in physics can be solved successfully by application of these methods. But, in many cases the analytical methods fail to yield a thorough and clear picture of complex problems. Many simplified and even sometimes unrealistic assumptions have to be introduced which lead to very conservative or misleading results. In search for solutions of unresolved questions which arise in the course of theoretical efforts, many scientists and researchers in different fields of science have turned to experimental techniques to elucidate the complex physical processes. Stress and strain distributions in bodies with nonlinear behavior, deformation and flow of multi-phase materials, and interaction of fluids and solids constitute examples of these complicated phenomena.

Experiments on full-scale existing systems, such as giant civil engineering structures, are often very expensive, difficult and even sometimes impossible. Moreover, before undertaking expensive engineering projects an engineer tries to find out how the structure would behave after it is constructed. In both cases exact analysis and direct experimentation is precluded and therefore the best alternative is to construct a model, i.e. a small scale replica of the structure and to perform tests on it to obtain empirically the desired information.

In recent years civil engineers have shown an increasing desire to study behavior of structures and particularly soil masses through the application of models. Soil mechanics was not appreciated as a branch of science up to the

late nineteenth century, and consequently application of model studies in this field is still very new in comparison with other areas of science. Rocha (1957) published one of the original papers on general modeling laws in soil mechanics. Roscoe (1968) presented a paper in which he covered general model theory in soil mechanics, and the advantages of centrifuge model testing. A collection of selected papers on modeling techniques in soil mechanics and geology with special emphasis on centrifuge testing methods was compiled by Scott (1975).

## 2.2 CENTRIFUGE MODELING

In recent years application of the centrifuge as a powerful tool in solving geotechnical engineering problems by modelling, has been widely accepted by researchers and engineers. Perhaps the first use of a centrifuge for geotechnical purposes was made by Bucky (1931). On the use of the machine to study models under the effect of stresses arising from the weight of the material itself he noted :

"To produce at corresponding points in a small-scale model the same unit stresses that exist in the full-scale structure, the weight of the material of the model must be increased in the same ratio that the scale of the model is decreased with respect to the full-scale structure. The effect of an increase in weight may be obtained by the use of centrifugal force, the model being placed in a suitable revolving apparatus."

Most soil properties strongly depend upon the confining pressure which is largely gravity-induced. Thus, in soils, for the model and prototype to behave similarly, the confining stress must be identical in both systems at homologous points. If model tests on soil are to be performed in the earth's gravity field, then the mass density of the model material must be increased in the same ratio that its size has been reduced. In case of soil, because of its complex stress-strain behavior, it is difficult or impossible to construct the model with a material other than prototype soil. The other alternative is to use the same soil in the model as in the prototype, but perform the tests in a centrifuge as Bucky

indicated. A centrifuge uses centrifugal acceleration to simulate gravitational loading on soil. The ratio of the accelerations in model and prototype structures must be inversely proportional to the ratio of their linear dimensions. Thus, for a model 100 times reduced in size, it should be subjected to an acceleration 100 times the earth gravitational acceleration. Appendix (A) provides an analytical example deriving scaling relations of the model and prototype.

If the ratio of linear prototype dimensions to those of a centrifuge model is  $N$ , then the ratio of areas and volumes are  $N^2$  and  $N^3$  respectively. According to the scaling relations, forces in the prototype will be  $N^2$  times those in model and moments  $N^3$  times, so that stresses (force per unit area) remain unchanged. Because the same material is used in both model and prototype, strains are also equivalent in both systems, and thus, displacements (strains times length) in the prototype are  $N$  times larger than in the model. Therefore, using the same material in model and prototype and placing the model in a centrifuge acceleration field  $N$  times normal terrestrial gravity results in the same strains and stresses at homologous points.

The principles of centrifuge modelling can be extended to the modelling of time-dependent events, such as dynamic soil-structure interaction systems. It can be shown that time in the prototype is  $N$  times the time in the model, so dynamic events take place  $N$  times faster in the model. As a result, frequencies and accelerations are higher by a factor of  $N$  in the model, while velocities remain the same. Energy in the prototype is  $N^3$  times the energy in the model and power is  $N^2$  times larger in the prototype. Table 2.1 lists the scaling relationships between prototype and model (centrifuge) parameters at a modelling scale of  $N$ .

In this investigation the soil-structure interaction of model towers and simple

TABLE 2.1  
SCALE RATIOS

Quantity	Full Scale (Prototype)	Centrifugal Model at N g's
Linear Dimension	1	1/ n
Area	1	1/ n <sup>2</sup>
Volume	1	1/ n <sup>3</sup>
Time		
In Dynamic Terms	1	1/ n
In Diffusion Cases	1	1/ n <sup>2</sup>
In Viscous Flow Cases	1	1
Velocity (Distance/ Time)	1	1
Acceleration (Distance/ Time <sup>2</sup> )	1	n
Mass	1	1/ n <sup>3</sup>
Force	1	1/ n <sup>2</sup>
Energy	1	1/ n <sup>3</sup>
Stress (Force/ Area)	1	1
Strain (Displacement/ Unit Length)	1	1
Density	1	1
Energy Density	1	1
Frequency		
In Dynamic Problems	1	n

footings on a foundation of dry sand were studied. Rigid prototype footings of different shapes and sizes were simulated using model footings with high rigidity in comparison with soil stiffness. Thus, only geometrical and inertial characteristics of models were scaled to the required ratios.

The centrifuge method was used for these experiments because of its attractiveness that the stresses in the model are identical to those in the prototype so that it avoids problems associated with testing, at earth gravity, small soil models involving materials with strongly nonlinear behavior, Scott(1977). The disadvantages lie in performing tests with models in flight at speeds of 100 to 500 rpm while trying to control the test process, and to transfer power and electrical signals in and out of the centrifuge through electric and hydraulic sliprings. In dynamic modelling tests any shaking system used to simulate passive (earthquake-like motions), or active loadings (e.g., steady state shaking by a shaker mounted on model structure) must have frequency and acceleration output capability  $N$  times the prototype values. Thus, for prototype structures with natural frequencies in a range of 1 to 20 HZ the shaker frequency output at a model scale of 100, for example, must be from 100 to 2000 HZ.

Several questions in evaluating the results of a centrifuge test program must be answered. How well does a model test predict a prototype behavior? Do the scaling relationships apply to all features of the problem? Considering the first question, it is desirable to check the centrifuge modelling method, whenever possible, by direct comparison with field tests (e.g., Lyndon and Schofield, 1978; Scott et al., 1982). However this is not always possible. In many cases indirect evidence can be provided to prove validity of centrifuge modelling tests (Schofield, 1981). In order to demonstrate the internal consistency of a test series, similar models at different scales, all simulating the same prototype structure, are tested. It is obvious that all these models should deliver the same results for the desired prototype. This indirect check of modelling technique is

called "modelling of models". In relation to the second question, referring to Scott (1977) when the same soil is used in the model as in the prototype, there is a problem in deciding at what soil grain scale the application of continuum and constitutive laws to both model and prototype soils will break down. In the case of very fine-grained soils such as clays there will be many grains in a representative soil element in both prototype and model. In this case the bulk material properties of both model and prototype material are identical. On the other hand, in a coarse sand with grains around a millimeter in diameter, there will be fewer grains in a model soil element than in the prototype. In this case, stress-strain relations of model and prototype may not be the relevant factors, but the individual grains in the model represent the behavior of gravel or even boulders in the prototype. Thus, the soil material in the model may not represent a continuum any more.

It is noted that there is a contradiction between the scale factor for time in dynamic events (scale factor  $\frac{1}{N}$ ) and for time in diffusion effects such as pore pressure dissipation (scale factor  $\frac{1}{N^2}$ ). In seismic events where the inertial effects must be considered and when there is pore water pressure dissipation in soil, such as in liquefaction of a saturated sand layer, the above problem may cause difficulties in centrifuge modelling. One way to cure this problem is to decrease the permeability of the soil for flow through the pores (Schofield, 1981). However, in the present study the sand used was fully dry, thus, there was no flow of water in the pores to cause any problem in the scaling laws.

In dynamic tests in the centrifuge the vibrating model has a relative motion with respect to the rotating reference frame of the centrifuge arm. This will cause a Coriolis acceleration,  $\vec{a}_c$ , on the model. This acceleration is equal to the vector product of angular velocity of centrifuge arm ( $\vec{\omega}$ ) and the relative velocity of the model motion,  $\vec{V}$ , with respect to the rotating frame of the centrifuge

arm. The angular velocity  $\vec{\omega}$  is parallel to the centrifuge rotational axis and the velocity  $\vec{V}$  may be in any direction depending on the experiment set up. Figure 2.1 shows a model tower oscillating in the test bucket and the direction of the vectors  $\vec{\omega}$  and  $\vec{V}$ . To minimize the adverse effect of Coriolis acceleration on the test results, the model should vibrate parallel to the axis of rotation. Pokrovsky and Fyodorov (1968) realized this problem during their tests on cratering and suggested that for a model container velocity in flight at around 30 m/s (98.4 ft/s) there is a region of prototype velocities for which modeling errors occur between 1.5 m/s (4.92 ft/s) and 60 m/s (196.8 ft/s). Since velocity of the model towers fall in the above-mentioned undesirable range of velocities it was tried to excite the towers in a direction parallel to the centrifuge axis whenever possible.

As was mentioned previously, the first use of a centrifuge in the geotechnical area dates back to the early 1930's when Bucky used one to study some simple mining problems. A little later in the Soviet Union, a centrifuge was used in soil mechanics testing by Pokrovsky and a number of co-workers. The use of the centrifuge was not widespread in the western hemisphere, particularly in the United States up to about 15 or 20 years ago, when it started undergoing a rebirth. Scott and Morgan (1977) through a literature survey, presented a proof of desirability for different uses of centrifuge testing procedure. In a recent paper Schofield (1981) reviewed applications of centrifuge modelling technique in dynamic and earthquake geotechnical problems.

At present, a number of centrifuges have been built and used for soil testing around the world. There are four in the United Kingdom, one at Liverpool, two at Manchester and one at Cambridge, with radii up to 5 meters and acceleration capabilities up to 200g. In Russia, Polshin *et al* (1973) reported that "several dozen" centrifuges have been employed for soil testing purposes. In addition, centrifuges are currently used for geotechnical research in Sweden, Denmark, France, and Japan. In the United States other than the National Centrifuge



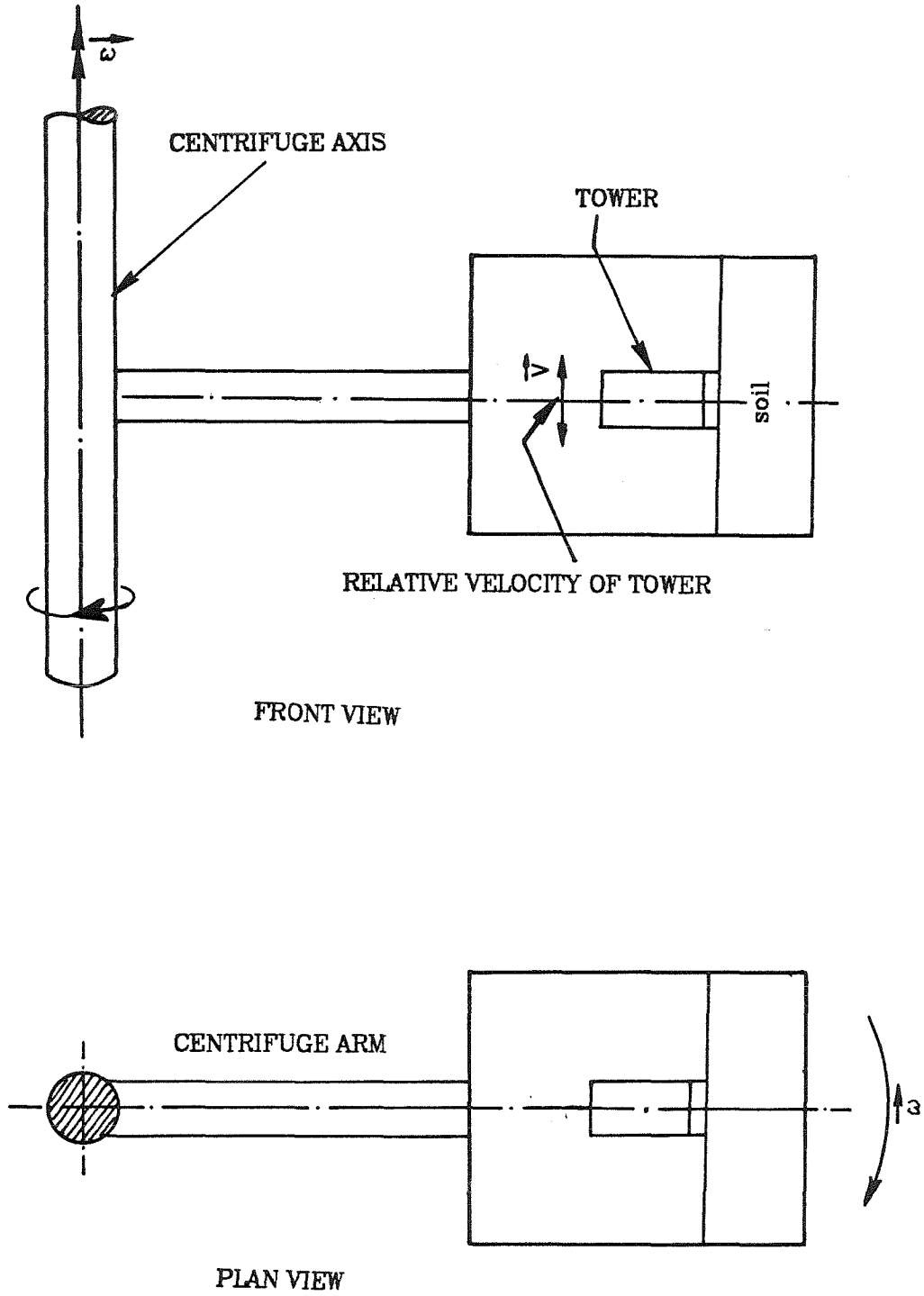


FIG. 2.1 TOWER MOTION RELATIVE TO CENTRIFUGE ARM

facility in the Ames Research Center which is currently still under construction for soil mechanics studies, only a few small centrifuges have been used, although the technique was originated here by Bucky.

Even with so many centrifuges built and operational around the world, and the number of tests performed, there is not sufficient evidence of quantitative centrifugal test results nor have many comparisons been made between models and prototypes. In many cases only a qualitative agreement between model and prototype behavior has been reported. In view of these inadequacies there is a great need for more quantitative test results, as well as comparisons of model and prototype behavior, or verifications through the method of "modeling of models". This is one of the major goals of the particular research program, the dynamic centrifuge testing of soil-structure interaction phenomenon, cited in this report.

CHAPTER REFERENCES.

- [1] Bucky, P. B., "Use of Models for the Study of Mining Problems," Am. Inst. Mining and Metallurgical Engineers. Tech. Pub. No. 425, 1931, pp. 3-28.
- [2] Lyndon, A., and Schofield, A. N., "Centrifugal Model Tests of the Lodalen Landslide," Canadian Geotechnical Journal, Vol. 15, No. 1, 1978, pp. 1-13.
- [3] Pokrovsky, G. I., and Fyodorov, I.S., "Centrifugal Model Testing in the Construction Industry (in Russian). Publishing House of Literature for the Construction Industry, Moscow, 1968.
- [4] Polshin, D. E., et al., "Centrifugal Model Testing of Foundation Soils of Building Structures," Proceedings of the Eighth International Conference on Soil Mechanics and Foundation Engineering, Vol. 1.3, 1973, pp. 203-208.
- [5] Rocha, M., "The Possibility of Solving Soil Mechanics Problems by the Use of Models," Proceedings of the Fourth International Conference on Soil Mechanics and Foundation Engineering, Vol. 1, 1957, pp. 183-188.
- [6] Roscoe, K. H., "Soils and Model Tests," Journal of Strain Analysis, Vol. 3, 1968, pp. 57-64.
- [7] Schofield, A. N., "Dynamic and Earthquake Geotechnical Centrifuge Modeling," Proceedings, Int. Conf. Recent Advances in Geotech. Eng. and Soil Dynamics, St. Louis, Missouri, 1981, pp.1-18.
- [8] Scott, R. F., "The Centrifugal Technique in Geotechnology, Selected Papers," Soil Mechanics Laboratory, California Institute of Technology, Pasadena, California, November 1975.
- [9] Scott, R. F., "Centrifuge Studies of Cyclic Lateral Load-Displacement Behavior of Single Piles," Soil Mechanics Laboratory, California Institute of Technology, Pasadena, California, 1977.
- [10] Scott, R. F., and Morgan, N. R., "Feasibility and Desirability of Constructing a Very Large Centrifuge for Geotechnical Studies," Report 760-170, California Institute of Technology and Jet Propulsion Laboratory, March 1977.
- [11] Scott, R. F., Ting, J. M., and Lee, J., "Comparison of Centrifuge and Full Scale Dynamic Pile Tests," International Conf. on Soil Dynamics and Earthq. Engrg., Southampton, UK, July 1982.

## CHAPTER 3

### PRELIMINARY EXPERIMENTS ON FOAM RUBBER

#### 3.1. INTRODUCTION

A series of experiments on dynamic response of rigid circular footings resting on the surface of a large piece of foam rubber was performed at earth gravitational acceleration field in the laboratory. The main purpose of these tests was to study the difficulties which might arise during dynamic testing in a centrifuge and to discover the relevant factors in design and construction of model structures, shaking equipment, and electronic circuitry for signal conditioning and controlling centrifuge tests. Results of these experiments were compared with common theoretical techniques in dynamic design of footings as a guide for later analysis of centrifuge experiments.

An experimental investigation of the same nature was performed by Arnold, et al (1955) where they studied all rigid body modes of vibration (i.e. rocking, sliding, vertical, and torsion) of rigid circular footings. Their main goal, however, was to present an experimental proof to elastic half-space theory.

In the present experiments, the vertical mode of vibration of two circular footings with different masses was studied.

#### 3.2. ELASTIC MEDIUM and FOOTINGS

In modelling dynamic response of rigid footings on elastic half-space with geometrical similarity between model and prototype, the mass ratio  $B_z$  (Eqn. 1.13) remains constant if the same density ratios of footing mass to elastic medium in addition to equal Poisson's ratios exist. Referring to the expression for magnification factor  $M$  ( Eqn. 1.15) functions  $F_1$  and  $F_2$  must also be the same for both systems to have identical dimensionless amplitude ratios. These are mainly functions of  $a_0$ , the dimensionless frequency. Therefore if model

footings are subjected to dynamic loads in the same range of dimensionless frequencies as the prototype, the magnification factor  $M$  should be the same for both systems.

Theoretically the elastic medium should have infinite extent, but in an experiment a finite model can be used provided wave reflections from the model boundaries can be eliminated. A piece of foam rubber (Urethane foam, density 1.5 pcf) 4 ft square in area and 2 ft high was provided to simulate the semi-infinite medium. Since complete elastic properties and damping characteristics of the material were not available, a series of extension and compression tests on samples with rod and cube configurations was performed. They produced values of elastic modulus  $E$ , Poisson's ratio  $\nu$ , and shear modulus  $G$  equal to 16.8 psi, 0.325, and 6.3 psi respectively. However, it was realized that the behavior of the material is dependent on the time rate of loading which is a characteristic of 'visco-elastic' materials. Thus, elastic properties had to be calculated from dynamic testing of the material, such as wave propagation methods. Propagation velocities of energy waves emanating from a vibrating footing at the center of the rubber surface were measured. The test procedure and method of calculation of the elastic coefficients from the measured velocities are described later. It was expected that damping in the rubber was sufficient to prevent random reflections without producing any adverse effect on experimental results in comparison with the behavior of a theoretical undamped medium. However, the material damping in the foam did not fully serve the desired purposes. It reduced amplitude of vibration in comparison with theoretical results, especially around the resonance peak. In one case at low frequencies where the wave lengths are large compared with lateral dimensions of the medium it could not completely prevent reflection of the waves from the boundaries.

Two wooden disks with the same base radii but different masses were used as the rigid footings (footings A and B). Their rigidity was checked during

experiments by recording amplitudes of vibration at a few points on the footings. They were attached to the surface of the rubber at the center of the surface area. The values of their masses and dimensions are given in Table 3.1.

Table 3.1 Footings Masses and Dimensions

Footing	Radius $r_o$ (in)	Thickness $t$ (in)	Weight (lbf) (including the coil and load cell)	Mass Ratio $B_z$
A	2.51	0.125	0.384	4.7
B	2.51	0.325	0.573	7.0
Weight of the Coil and the Load Cell = 0.285 lbf				
Weight of the Load Cell = 0.074 lbs				

Note that the footing mass includes mass of a load cell and an electrical coil mounted on the footing (see Section 3.3.1). The value of Poisson's ratio of the foam required in evaluation of mass ratio  $B_z$  is derived from Table 3.2 presented in a later section.

### 3.3. EQUIPMENT and INSTRUMENTATION

The equipment used is divided in two groups, one to generate the exciting force and the other to measure applied force and output signals (see Fig. 3.1). These and the test procedure are explained next.

#### 3.3.1. Loading Equipment

An electromagnetic shaker was used to vibrate the footings vertically. The force was produced by the interaction of a permanent magnet and a coil through which an alternating current was passed. The coil was mounted on a load cell which was fixed on the footing at the center of its surface area. The permanent magnet of the shaker was fixed at the mid-span of a steel I beam

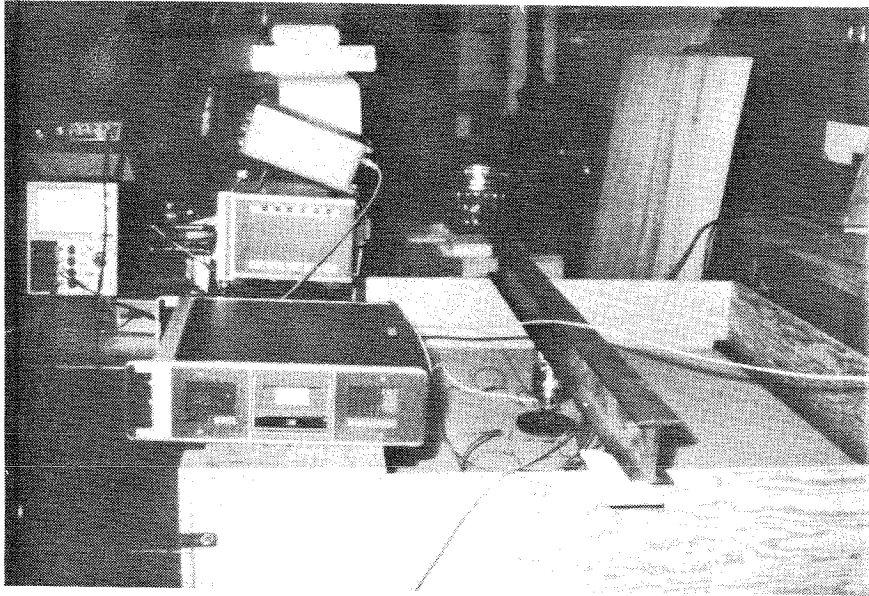


**FIGURE 3.1: EXPERIMENTAL EQUIPMENT**

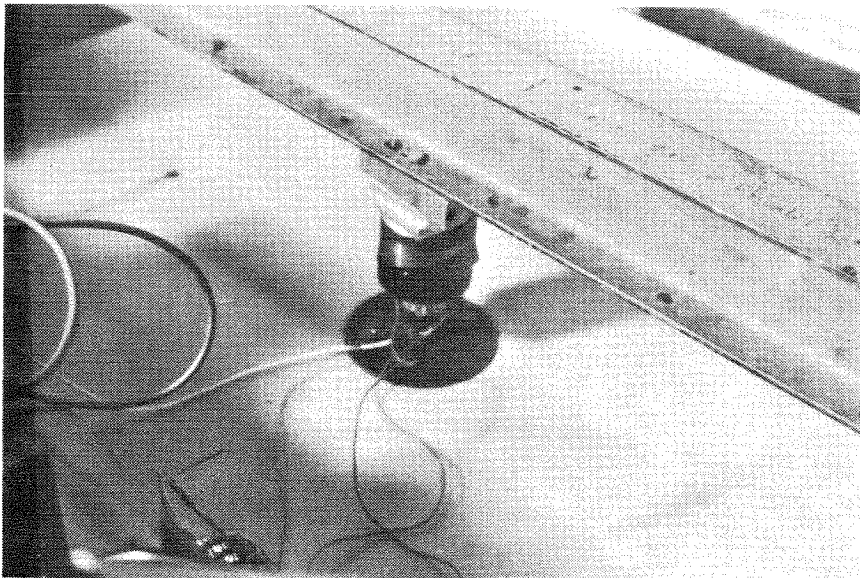


**FIGURE 3.2: FOOTING, LOAD CELL, ELECTROMAGNET SHAKER AND SUPPORTING BEAM**

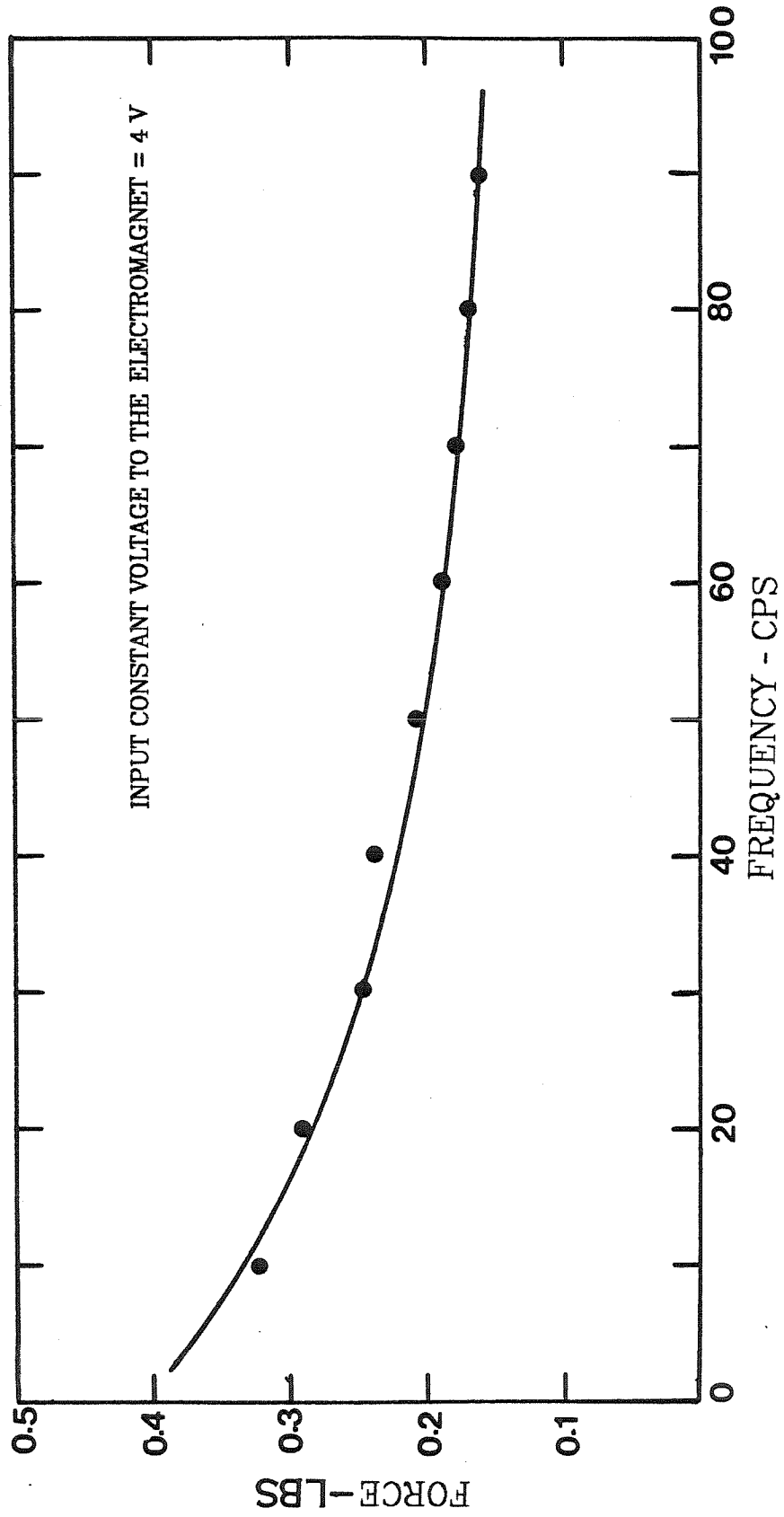


FIG. 3.3 OUTPUT FORCE OF THE ELECTROMAGNETIC SHAKER VS FREQUENCY



exactly above the coil (Fig. 3.2). Together, the coil and the load cell, formed part of the footing weight. Input voltage to the coil was generated by a Dynascan Model B&K Precision 3020 sweep/function generator, and amplified by the Hafler DH-200 power amplifier, both available commercially. In steady state vibration tests a sinusoidal voltage signal was generated by the function generator and applied to the coil after being amplified. Frequency of oscillation could be varied continuously and the load amplitude could be controlled by reading the output from the load cell and adjusting the input voltage. Variation of the shaker force with frequency of oscillation, at a constant input voltage to the coil, is shown in Figure 3.3. As is seen from the figure force amplitude reduces as the frequency increases which requires higher input voltage to the coil to keep the force amplitude constant. In transient tests, an electrical voltage pulse was fed into the coil by the function generator and power amplifier. In order to synchronize application time of the pulse and start time of recording equipment, the output pulse from the function generator was passed through a relay and then it was used simultaneously to activate the coil and to trigger the measuring equipment.

### 3.3.2. Measuring Equipment

Transducers, signal conditioning and recording equipment comprise the measuring system which includes the following equipment:

- a) Accelerometers: Three Entran Devices Inc. Model EGAL-125F-10D miniature accelerometers were used. They were labeled in these experiments as accelerometer (A1), Serial No. 10UOU-V2-2; (A2), Serial No. 10UOU-V3-3; and (A3), Serial No. 10UOU-V1-1. They only weigh about 1 gram and were rigidly glued to the footing or rubber surface by double sided adhesive tape. The accelerometers have a range of 10 g with a nominal sensitivity of about 12 mv/g (varies slightly from this with each

particular unit), an input impedance of about 900 ohms, an output impedance of about 400 ohms, and a useful frequency range of DC to about 600 Hz. They were powered by a +15 volt DC power supply. Similar accelerometers with some different specifications have been used in later centrifuge experiments and are described in more detail in Chapter 5, "Equipment and Instrumentation" for centrifuge tests.

b) Load Cell: A metallic ring on which 4 strain gages are fixed and connected in such a way that they constitute a Wheatstone bridge, was constructed to measure applied magnetic forces on the footing. Upon loading, the ring deforms and the strain gages deliver a voltage proportional to tangential strain, and consequently, for small deformations, to the developed load in the ring. The resonant frequency of the load cell fixed on a rigid floor was determined from its free vibration after being excited by an initial impulse force. This frequency was about 850 Hz which is approximately 15 times the resonant frequency of the footing-foam rubber system as will be seen later. The load cell was powered by a +5 volts excitation.

c) Heathkit Model IP-2718 TRI-Power Supply: It was used to power accelerometers and the load cell.

d) Signal Amplifier: A four channel voltage follower instrumentation amplifier, LF352 (Fig. 3.4), was designed particularly for these experiments. Output signals from the accelerometers, and the load cell were amplified before being recorded. Required power input to the amplifier ( $\pm 15$  volts) was provided by a standard adjustable dual tracking power supply, (CA4194).

e) Oscilloscope Tektronix 5103N: This provided a visual display of the wave forms being measured, from which it was possible to obtain accurate measures of voltage and time.

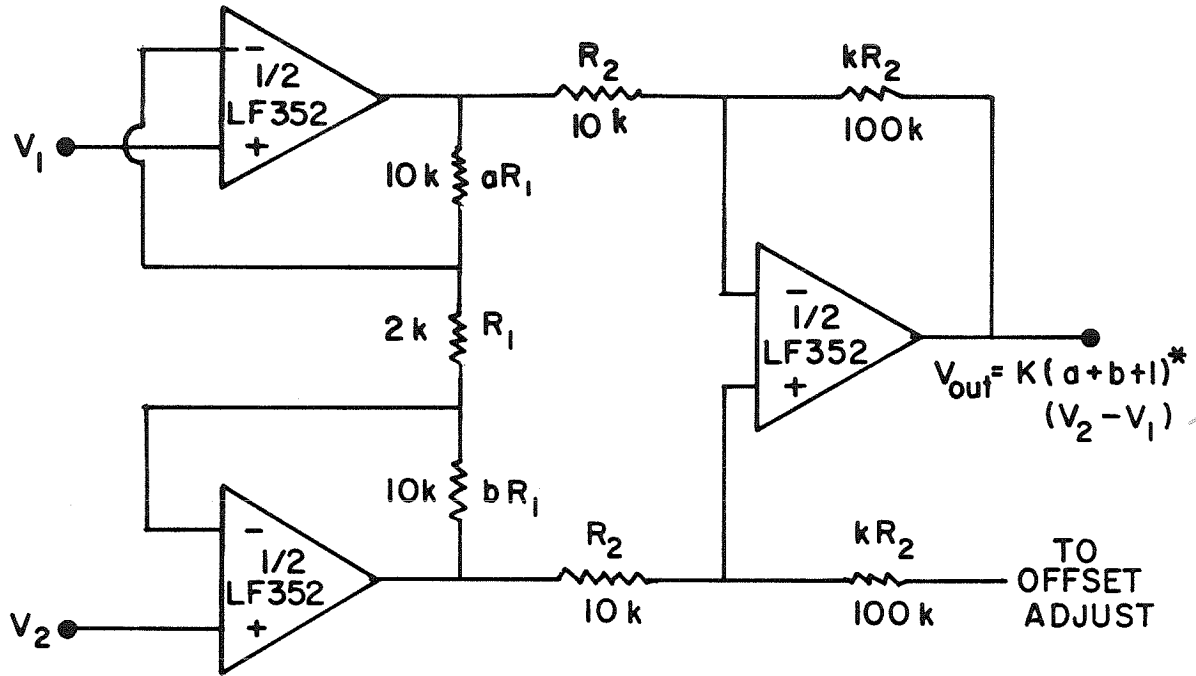


FIGURE 3.4 AMPLIFIER FOR ACCELEROMETERS AND LOAD CELL

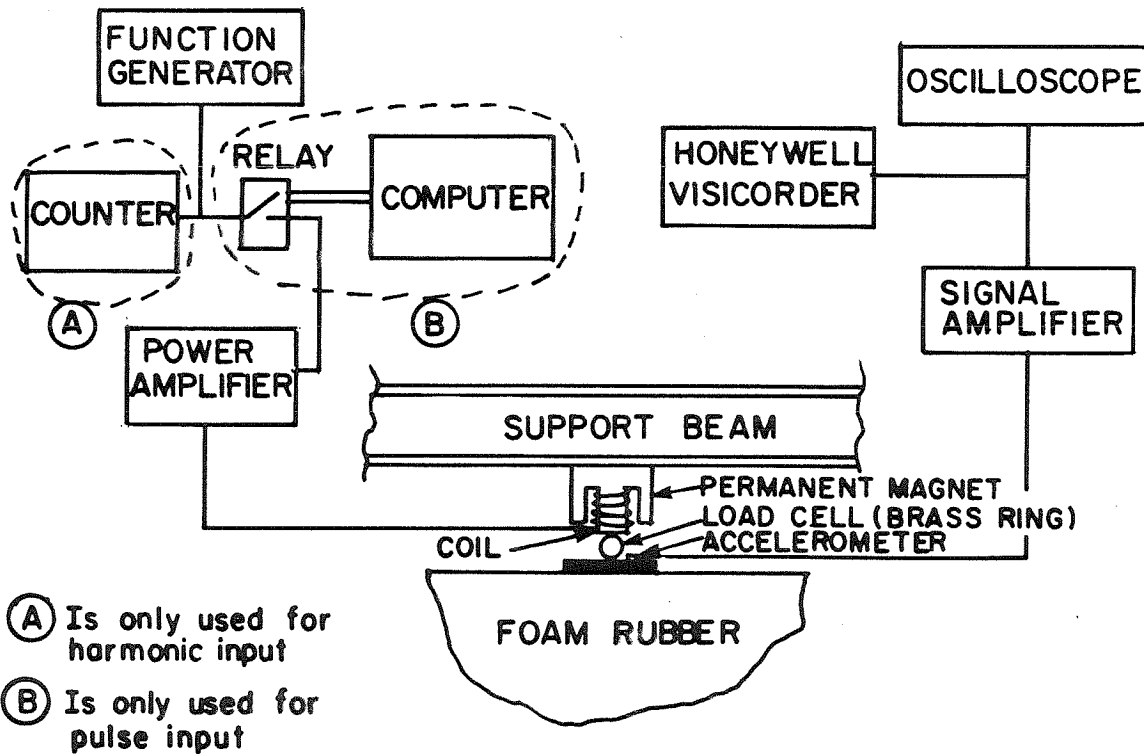


FIGURE 3.5 EXPERIMENTAL SET UP FOR HARMONIC AND PULSE INPUTS

f) Monsanto Model 100A Counter - Timer: Precise frequency measurements

from DC to high frequencies were made possible by this digital counter.

g) Recorder: Originally a Honeywell Model 1858 CRT Visicorder was used, but

later a micro-computer with an ADC unit (Analog to Digital Converter) was employed in recording the data. Only the Visicorder is described here and the computer will be referred to in Chapter 5. The Visicorder allows inertialess analog recording of the data from DC to 5 KHz. The analog signals are recorded on Kodak Type UV 1920-80330Y Visicorder Recording Paper. The sensitivity of recording in the tests was 200 mv/division (1 division= 2.5 cm). Recording of dynamic tests usually took place at a paper speed of 20 to 50 inches per second depending on the particular test.

A complete diagram of the test set-up for steady state and transient shaking of the footings in their vertical mode of vibration is depicted in Figure 3.5.

### 3.4. CALIBRATION OF TRANSDUCERS

The load cell was calibrated by placing known weights on a plate attached to its top and reading the output voltage of the strain gages at each load. A straight line was fitted through the data points by minimizing sum of the squares of deviations. Y-intercept and slope coefficients of this line were calculated as -0.005 lbf and 3.113 lbf/mv respectively. Accelerometers were calibrated on a tilt table which permits varying the acceleration from -1 g to +1 g continuously. Slope coefficients of calibration lines for accelerometers (A1), (A2), and (A3) were equal to 11.175 mv/g, 11.375 mv/g, and 11.300 mv/g respectively.

### 3.5. EXPERIMENTAL PROCEDURE AND RESULTS

The following two groups of experiments were performed:

a) Wave propagation tests to measure dynamic properties of the foam rubber.

b) Steady state and transient (pulse) shaking of footings A and B in their vertical mode of vibration.

### 3.5.1. Wave Propagation Tests

Compression and Rayleigh wave velocities were both measured. In the first case two accelerometers were attached to the rubber surface on a line passing through the center of the surface area at a fixed distance from each other. These two accelerometers served as receiving stations for an incoming pulse wave generated at the footing by the magnetic shaker. An electrical pulse produced by the function generator passed through a relay before it was amplified by the power amplifier to energize the coil (see Fig. 3.5). Thus the width of the pulse depended on the wave form generated by the function generator and the time interval between closure and opening of the relay. This was controlled by the computer, which sent signals to another relay inside the ADC to energize and close the main relay. Just before closure of the relay, the computer started the ADC to take data at a rate of 25 KHz per channel. This was made possible by an appropriate software and hardware package built into the system; the package will be explained in chapter 5. If the Visicorder is used for recording, the relay was closed manually, and the input pulse to the coil used to trigger the recorder as well. For wave speeds of 150 ft/sec to 400 ft/sec, and distances of 12 to 20 inches between transducers, a maximum of 1.5% error may occur in measuring the velocities. The travel time of pressure waves between the two recording stations was measured from the recorded acceleration signals. Wave velocity was calculated from the expression

$$V_p = \frac{d}{\Delta t} \quad (3.1)$$

where  $V_p$  is the pressure wave velocity,  $d$  the distance between recording

stations, and  $\Delta t$  the travel time.

Rayleigh-wave velocities were measured by applying a source of harmonic vibration at the rubber surface and measuring the wave length of the resulting surface waves (see Richart et al, 1970). The distance between points oscillating in phase with the source of vibration and the location point of the source is equal to a multiple of wavelength,  $L_R$ . Wave velocity  $V_R$ , was then calculated from the measured wave length and the frequency of vibration  $f_R$ , according to the following relation

$$V_R = L_R \cdot f_R \quad (3.2)$$

Steady state vibration was generated by an electromagnetic shaker which can produce high-frequency harmonic oscillation of the footing. Two accelerometers were located on the surface of the rubber, one fixed near the center and the other at a distance which was gradually increased along a line passing through the center of the foam rubber area. They sensed the vertical component of the Rayleigh wave. When motions in the transducers were in phase, the distance between them was equal to one wavelength and wave velocity was calculated from Equation 3.2. Shear wave velocity  $V_s$  was then calculated as

$$V_s = K_R \cdot V_R \quad (3.3)$$

where  $K_R$  is a constant depending on the value of Poisson's ratio,  $\nu$ . For  $\nu$  equal to 0.325, the value of  $K_R$  is 0.931. Elastic moduli can be evaluated from the measured wave velocities by the following relations (Kolsky, 1953 )

$$G = \rho V_s^2 \quad (3.4)$$

$$E = \frac{(1-2\nu)(1+\nu)}{(1-\nu)} \cdot V_p^2 \quad (3.5)$$

The measured wave velocities and calculated elastic coefficients are presented in Table 3.2.

Table 3.2. Material Properties of Foam Rubber  
(Measured Experimentally)

Unit Weight	Shear Wave Velocity	Rayleigh Wave Vel.	Pressure Wave Vel.	Young's Modulus	Shear Modulus	Poisson's Ratio
$\gamma(\text{lb}/\text{ft}^3)$	$V_s(\text{ft}/\text{sec})$	$V_R(\text{ft}/\text{sec})$	$V_p(\text{ft}/\text{sec})$	$E(\text{lb}/\text{in}^2)$	$G(\text{lb}/\text{in}^2)$	$\nu$
1.5	185.0	172.2	355.0	29.4	11.08	0.325

### 3.5.2. Vertical Vibration of Footings

Footings A and B (Tbl. 3.1) were vibrated vertically under steady-state and pulse loadings. In steady-state tests a harmonic voltage signal from the function generator was amplified by the power amplifier and input to the coil. The frequency of vibration varied from about 20 Hz to 600 Hz. At different frequencies outputs from the load cell and accelerometers were recorded by the Visicorder. All three accelerometers were mounted on the footing, where A1 was placed at the center, A2 at half the footing radius from the center, and A3 at the edge. Linearity of acceleration output versus load amplitude was verified at different frequencies. In the tests where the force amplitude was not constant when frequency of oscillation varied, acceleration amplitudes were originally corrected for a constant force level at different frequencies and then integrated twice with respect to time to produce displacement amplitudes. Figures 3.6 and 3.7 illustrate displacement response curves (amplitude vs frequency) and the values of resonant frequencies and damping ratios derived from experimental data points. Resonant frequencies are estimated from approximate positions of peaks in the plots and damping values are derived from the sharpness of resonant curves(Kolsky, 1953).

Transient pulse shaking of the footings was performed in the same way as for

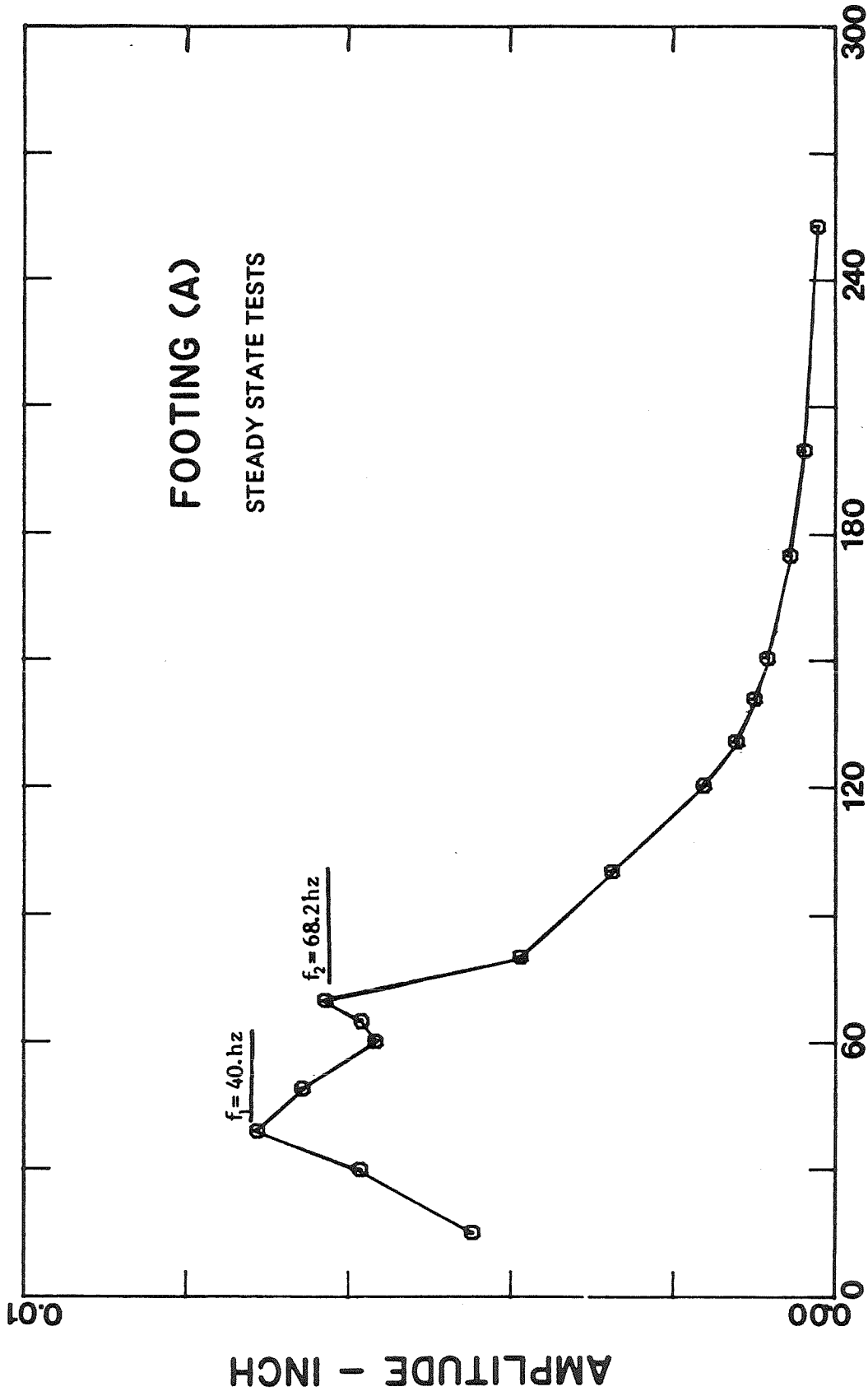


FIG. 3.6 RESPONSE AMPLITUDE (EXPERIMENTAL DATA)



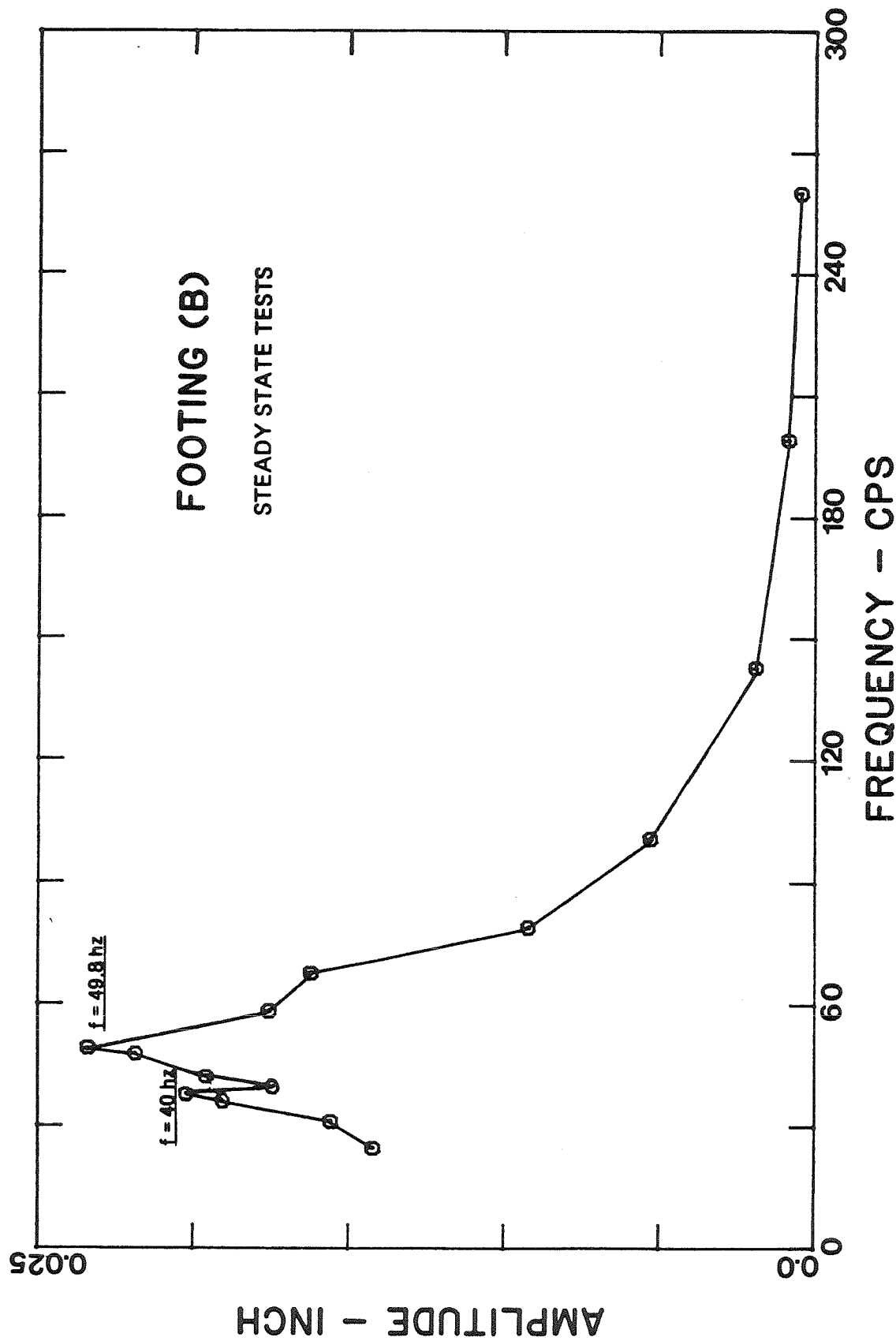


FIG. 3.7 RESPONSE AMPLITUDE (EXPERIMENTAL DATA)

the pressure wave velocity measurements, but with only one accelerometer mounted at the center of footing. Natural frequencies of the vibration and average damping ratios calculated from logarithmic decrement of the amplitudes were derived from free oscillation plots of the footings (see Figs. 3.8a,b).

### 3.6. COMPARISON OF THEORETICAL AND EXPERIMENTAL RESULTS

Theoretical curves for the displacement magnification factor versus dimensionless frequency, and curves for dimensionless frequency and magnification factor at vertical vibration resonance in terms of mass ratio are provided by Richart, et al (1970). Mass ratio  $B_z$  varies from 0 to 5 in these curves. Thus, for footing B with  $B_z > 5$  the damped single degree of freedom analog with frequency-dependent stiffness and damping coefficients should be analysed (see Chapter 1). However, Lysmer (1965) showed that a simplified model of the half-space problem with constant coefficients yields solutions in remarkable agreement with exact ones. He chose the spring constant  $K_z$  equal to the static value

$$K_z = \frac{4Gr_o}{1-\nu} \quad (3.6)$$

(where  $r_o$  is the radius of the footing)

and found the best fit for the damping term  $C_z$  in the range ( $0 < a_o < 1.0$ ) to be

$$C_z = \frac{3.4r_o^2}{(1-\nu)} \sqrt{\rho G} \quad (3.7)$$

Thus, the equation of motion for Lysmer's analog is

$$m\ddot{z} + \frac{3.4r_o^2}{(1-\nu)} \sqrt{\rho G} \dot{z} + \frac{4Gr_o}{(1-\nu)} z = Q \quad (3.8)$$

where  $z$  is the vertical displacement of the rigid footing and  $Q$  is the vertical concentrated oscillating force on the footing.

Using the above model and the values of footing radii and elastic constants in tables 3.1 and 3.2 theoretical response curves for the two footings

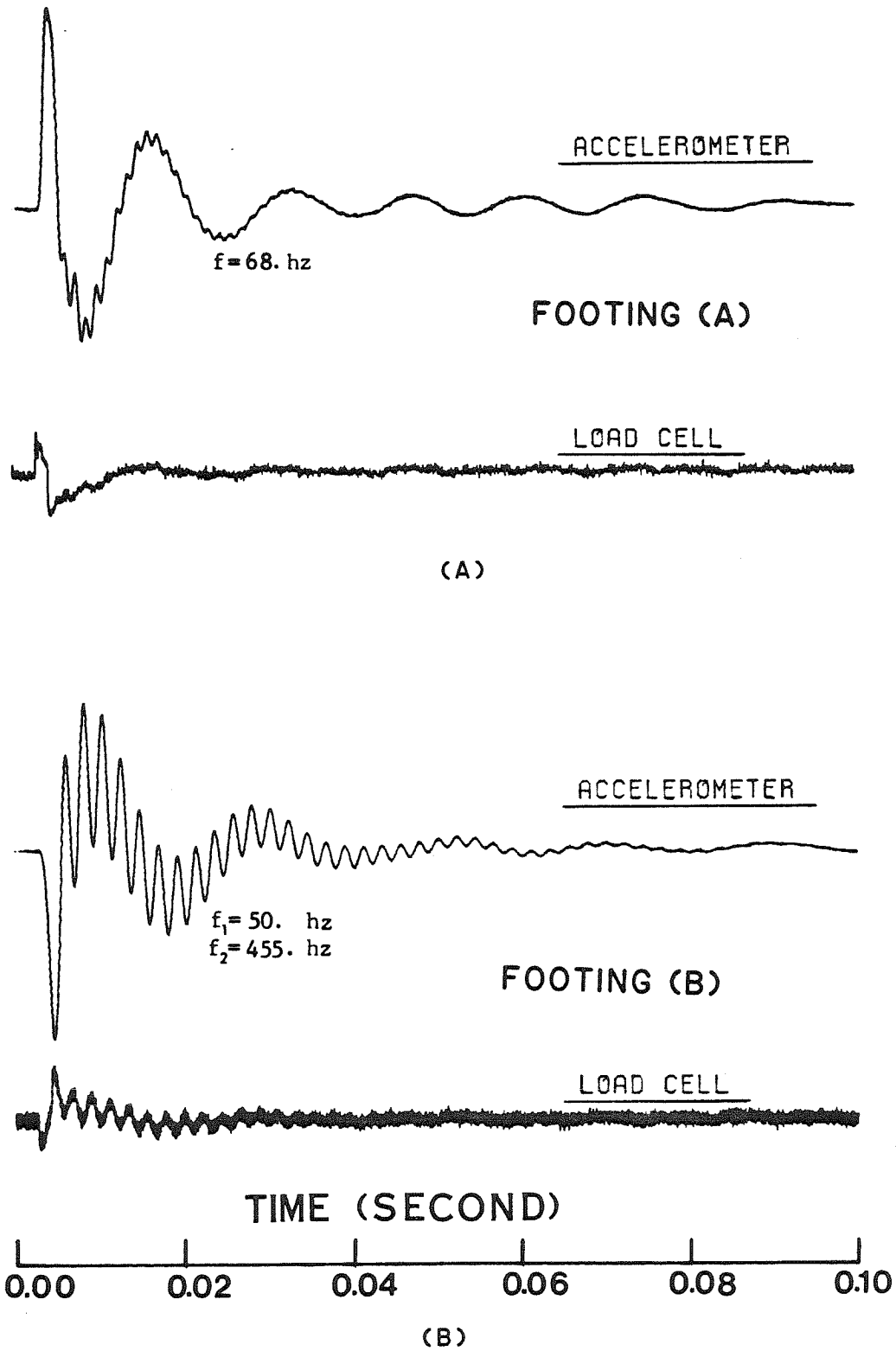


FIG. 3.8 (A AND B) FREE OSCILLATION OF FOOTINGS

(magnification factor  $M$  vs dimensionless frequency  $a_0$ ), are plotted in Figures 3.9a,b. The experimental points are added to these curves which show a reasonable agreement between the theoretical and experimental results particularly as the frequency increases beyond or decreases below the resonant frequency .

Table 3.3 Resonant Frequencies and Damping Ratios  
(Experimental and Theoretical Data)

Method of Derivation	Footing	$f_n$ Resonant Freq. (Hz)	$\xi$ Damping Ratio
Experimental Free Vibration	A	68.0	0.20
	B	50.0	0.22
Experimental Steady-state Vibration	A	68.2	
	B	49.8	0.29
Theoretical Lysmer Analog	A	63.0	0.195
	B	52.8	0.16

Table 3.3 collects the experimental and theoretical values of resonant frequencies and damping ratios for an easy comparison of these parameters. It is seen that there is a close agreement between theoretical and experimental values of resonant frequencies for the two footings. However, the larger damping values for the experimental results explains the greater amplitude difference of the response curves near resonance. A possible reason for discrepancy in damping values is the material damping of the foam which is not included in theoretical damping values.

There are two important aspects of the free vibration and steady-state test results which need some explanation. These are described as follows:

(1) In magnification factor-frequency plots for footing A existence of a second peak at 40 Hz is evidence of profound effect of lateral boundaries at low frequencies of vibration. Kolsky (1953), in a rigorous treatment of the wave propagation problem in rods showed that when wavelengths of vibration increase as frequency decreases, numerous reflections of the waves from boundaries causes

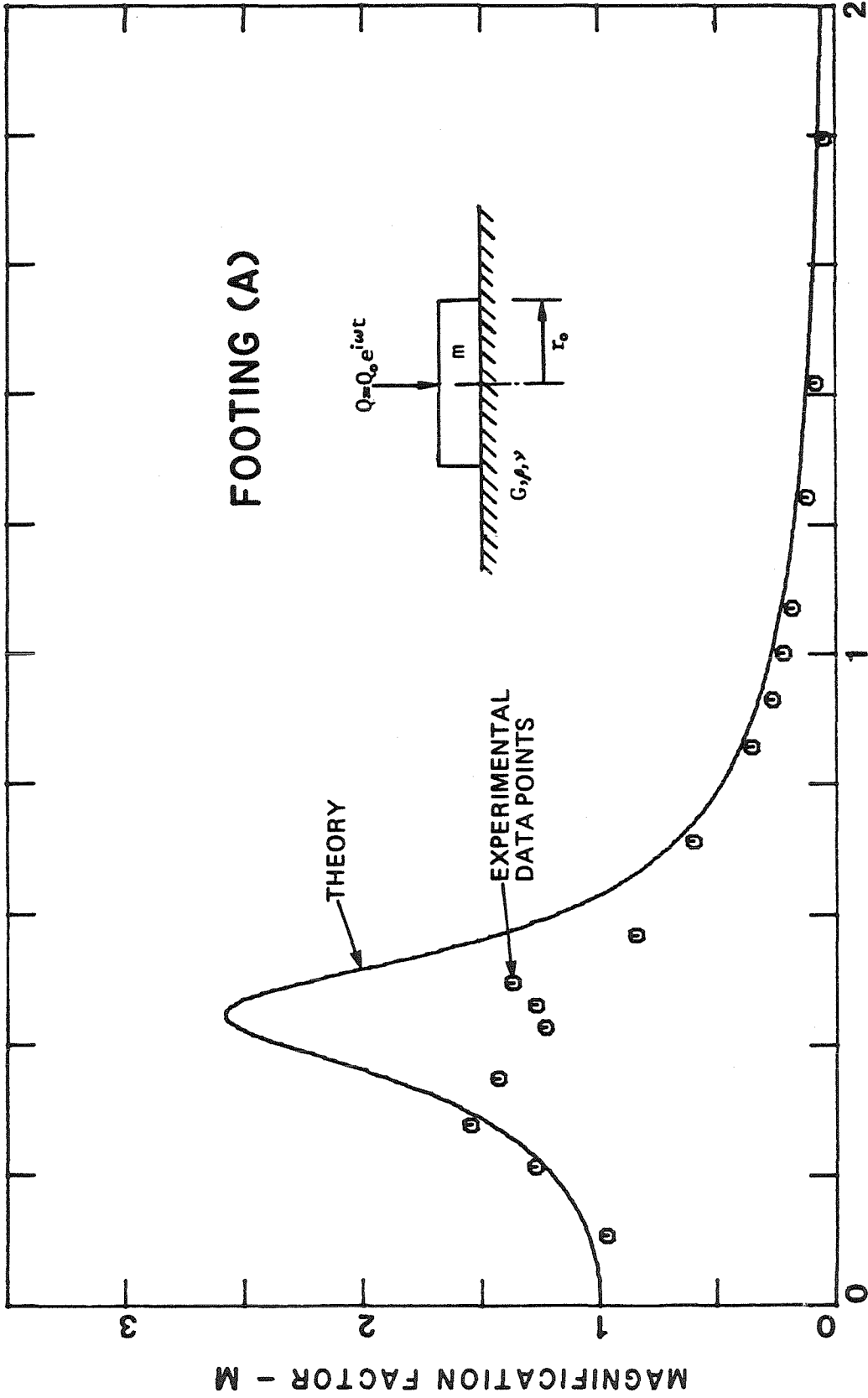


FIG. 3.9 a COMPARISON OF THEORETICAL AND EXPERIMENTAL DATA

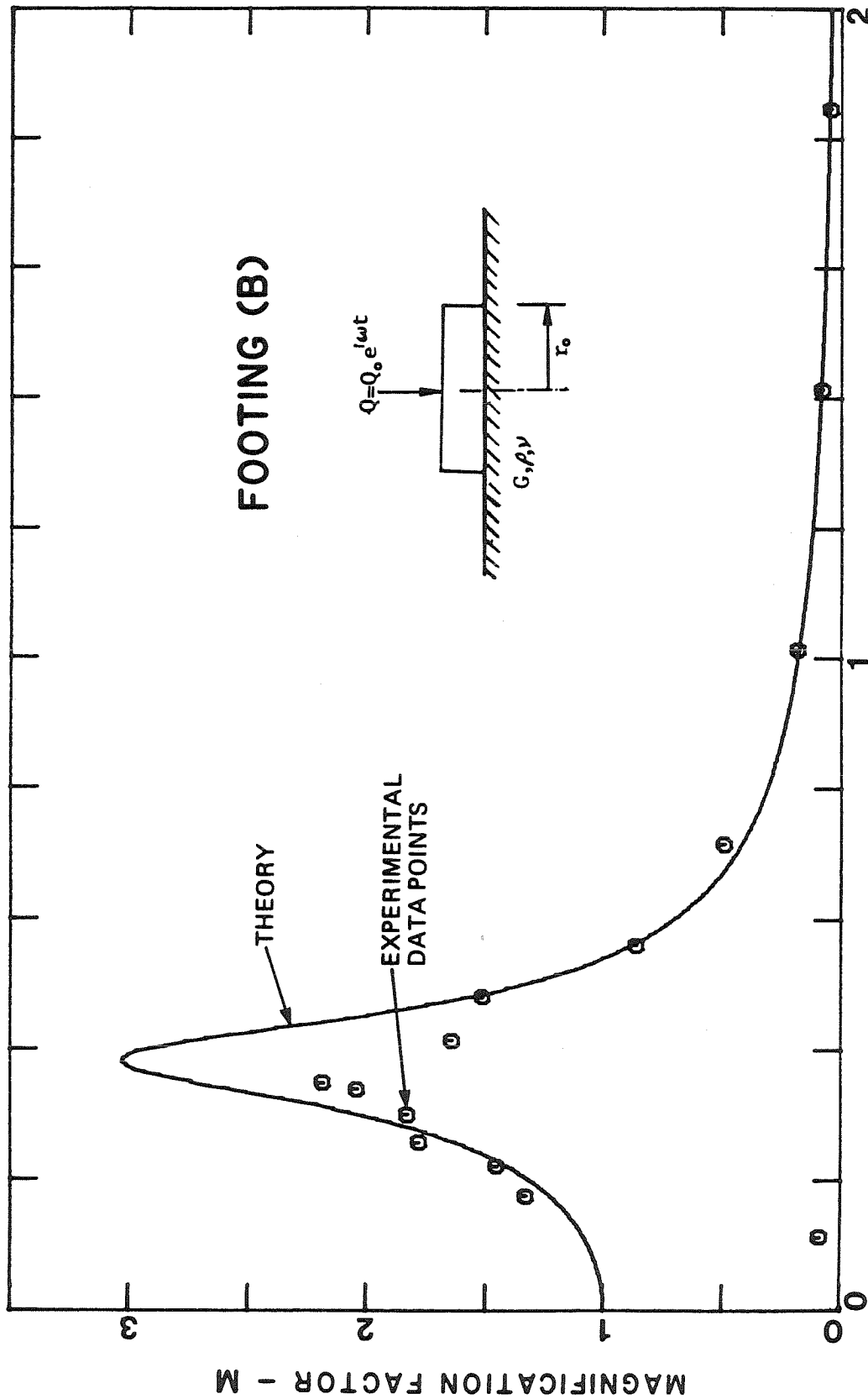


FIG. 3.9 b COMPARISON OF THEORETICAL AND EXPERIMENTAL DATA

the whole wave energy to propagate with one single speed called the rod velocity, equal to  $\sqrt{\frac{E}{\rho}}$ . Assuming that the whole mass of the foam rubber behaves as a fixed-free rod vibrating longitudinally, then the fundamental frequency of the vibration,  $f_n$ , is

$$f_n = \frac{V_p}{4l} = \frac{355.0}{4 \times 2.0} = 44.4 \text{ Hz} \quad (3.9)$$

where  $l$  is the height of foam rubber mass.

This value is in reasonable agreement with the lower frequency observed in steady-state experiments for the footings.

(2) Referring to Figure 3.8b a higher harmonic with smaller amplitude than the fundamental mode is present in the acceleration response of footing B. This suggests that the system of coil, load cell, footing, and foam rubber constitute a two mass oscillator with two degrees of freedom. Mass  $m_1$ , the coil plus one third of the load cell, is elastically supported by spring  $k_1$ , i.e. the load cell. The footing and the rest of the load cell constitute the second mass,  $m_2$ , resting on the spring  $k_2$ , i.e. the elastic half-space (Fig 3.10). From Table 3.1,  $m_1$  is calculated as 0.236 lb and  $m_2$  is found to be 0.148 lb for footing A and 0.337 lb for footing B. Stiffness of the load cell ( $k = 3000$  lbf/in), and its damping ratio ( $\xi = .04$ ) were evaluated from free vibration of the coil and load cell mounted on a rigid base. The spring stiffness  $k_2$  for the foam rubber according to the simplified Lysmer's analog is

$$K_2 = \frac{4Gr_o}{(1-\nu)} = \frac{4 \times 11.08 \times 2.51}{(1-0.325)} = 164.8 \text{ lbf/in} \quad (3.10)$$

Damping ratio  $\xi$  for the footing-rubber system can be found from Equation 3.7. The solution for the undamped response of this system is well known and

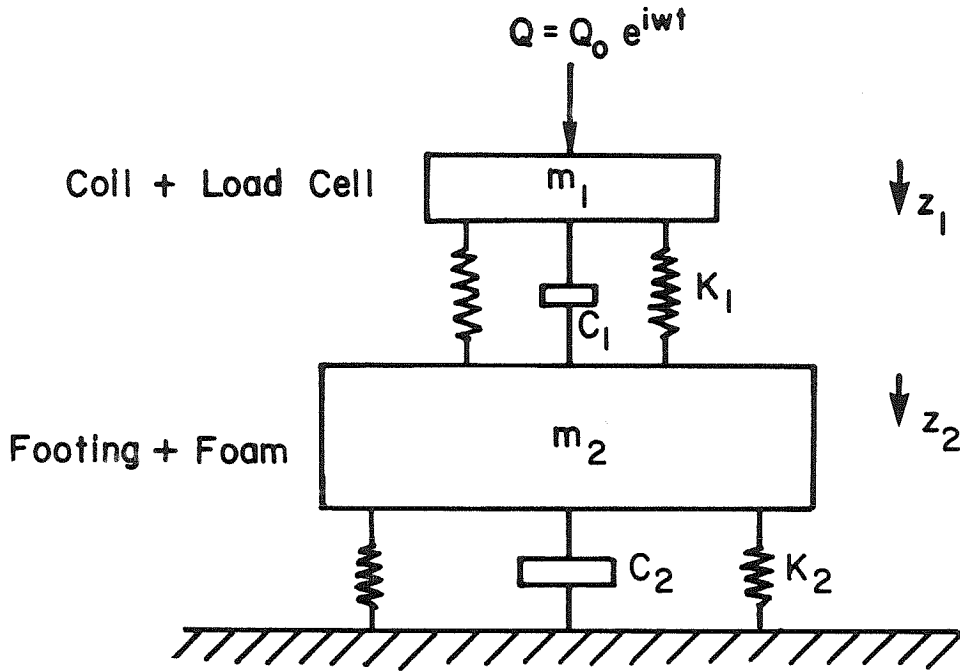


Fig. 3.10. Two mass foundation.

can be written as

$$\begin{Bmatrix} z_1(t) \\ z_2(t) \end{Bmatrix} = \begin{Bmatrix} z_{11} \\ z_{21} \end{Bmatrix} \sin \omega_1 t + \begin{Bmatrix} z_{12} \\ z_{22} \end{Bmatrix} \sin \omega_2 t \quad (3.11)$$

Where  $z_1$  and  $z_2$  are vertical displacements of the masses  $m_1$  and  $m_2$ . In the displacement  $z_{ij}$ , the first subscript identifies the amplitudes of mass  $m_1$  or  $m_2$  while the second subscript indicates the frequency and mode with which the amplitude  $z_{ij}$  is associated. The two natural frequencies of the system are

$$\omega_{1,2}^2 = \frac{1}{2} \left( \frac{K_{11}}{m_1} + \frac{K_{22}}{m_2} \right) \mp \sqrt{\frac{1}{4} \left( \frac{K_{11}}{m_1} - \frac{K_{22}}{m_2} \right)^2 + \frac{K_{12}^2}{m_1 m_2}} \quad (3.12)$$

in which

$$\begin{aligned} k_{11} &= k_1, & k_{12} &= k_{21} = -k_1, \text{ and} \\ k_{22} &= k_1 + k_2, \end{aligned} \quad (3.13)$$

Substituting for the stiffness and mass values in equation 3.12, the frequencies  $f_1$  and  $f_2$  are found to be

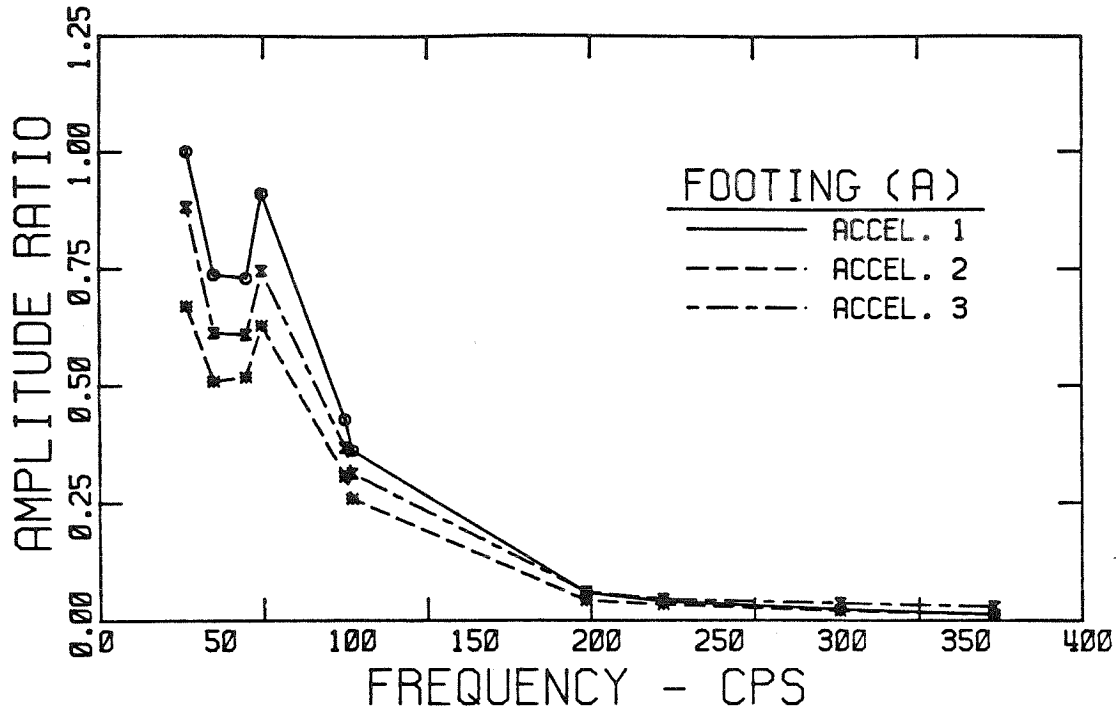


$$\begin{aligned} f_1 &= \frac{1}{2\pi} \omega_1 = 52.8 \text{ Hz} \\ f_2 &= \frac{1}{2\pi} \omega_2 = 462.0 \text{ Hz} \end{aligned} \tag{3.14}$$

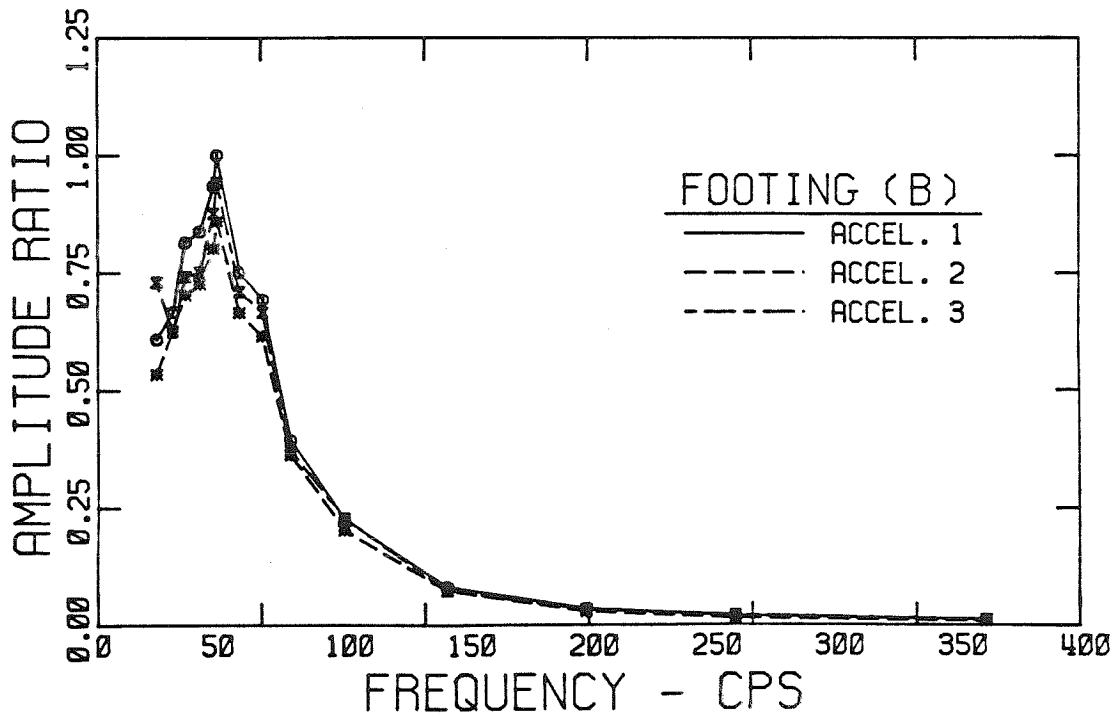
These values are in close agreement with experimental values shown in Figure 3.8b, which proves the validity of the assumed two degree of freedom model.

Rigidities of the footings were checked by plotting response curves of the three accelerometers on the surface relative to the amplitude of accelerometer no. 1 at the center (Fig. 3.11a,b). It is obvious that footing A slightly bends during vibration where accelerometers 2 and 3 at the middle and at the edge have smaller amplitudes compared with accelerometer 1 at the center, but footing B is fairly rigid and therefore yields closer experimental results to the predictions of elastic half-space theory for the vibration of a rigid surface footing.

Thus, even though the footing-foam rubber system chosen for these experiments could not perfectly simulate the vibration problem of a rigid footing on the surface of an elastic half-space medium, it did contribute a great amount of information as an aid to understanding the physics of the problem.



(a)



(b)

FIG. 3.11a&b. Relative Acceleration of Different Points on the Footings

*REFERENCES*

- [1] Arnold, R.N., Bycroft, G.N., and Warburton, G.B., "Forced Vibration of a Body on an Infinite Elastic Solid", ASME Journal of Applied Mechanics, Sept. 1955, PP.391-400
- [2] Kolsky, H., "Stress Waves in Solids", Clarendon Press, Oxford, Great Britain, 1953.
- [3] Lysmer, J., "Vertical Motion of Rigid Footings", Ph.D. dissertation, Dept. of Civil Eng., Univ. of Michigan, Aug. 1965.
- [4] Richart, F.E., Jr., J.R. Hall, Jr., and R.D. Woods, "Vibrations of Soils and Foundations", Prentice-Hall, Inc., Englewood Cliffs, NJ, 1970.

## CHAPTER 4

### SOIL

#### 4.1. INTRODUCTION

The response of a soil-structure system under dynamic loads strongly depends on the actual properties of the soil. In any analytical or numerical analysis for the determination of stress and strain distribution in the foundation-soil system, soil properties are taken into account by a stress-strain matrix. If soil is assumed as a linearly elastic isotropic material the coefficients of the constitutive equations relating stress components to strains, may be defined by two elastic constants. Nonlinear but reversible soil behavior can be approximated in one approach by use of equivalent elastic constants which vary as functions of stress or strain level. This is valid if permanent accumulative strains do not develop in the soil mass.

Strains in soils beneath a well-designed machine foundation generally should be smaller than  $10^{-6}$  to prevent any discomfort to the people working near the machinery and to ensure safe operation of the machinery and nearby equipment. In strong ground shaking during earthquakes, or in large stress loadings during severe storms, strains in the soil beneath buildings or other structures generally should be smaller than  $10^{-5}$ ; otherwise, the motions of the structure would be so large as to damage the structure or associated mechanical/piping systems. In such cases failure of the soil is not of primary concern and even though some permanent displacements do occur it is customary to assume the soil to be a linearly viscoelastic material, or as a nonlinear material whose dynamic properties vary with the amplitude of deformations. Thus, because of the development of small strains in many dynamic soil mechanics problems, measurement and application of elastic moduli in analysis of stresses and strains has more meaning compared with the large deformation problems of soil statics.

Dynamic behavior of soils and soil-supported structures are usually defined by equivalent linear elastic moduli and viscous damping at strain amplitudes less than  $10^{-4}$  as the reference conditions. Nonlinear inelastic soil response is introduced by multiplying the small-amplitude soil properties by reduction factors accounting for large-strain effects (SW-AJA, 1972).

In a common approach, in the stress-strain loop resulting from symmetrical cyclic shear-loading of a soil sample (Fig. 4.1), the secant shear modulus  $G$  is taken to be the slope of a line passing through the extreme points on the hysteresis loop (Seed and Idriss, 1970). Damping ratio  $D$  is defined as  $A_L/4\pi A_T$ , in which  $A_L$  is the area of the loop and  $A_T$  is the area of triangle  $OA\gamma_2$  or  $OB\gamma_1$  for the loops with different levels of maximum strain. As mentioned in Chapter 1 damping in dry sands occurs mainly because of internal friction and the stress-strain behavior of the soil is unaffected by the loading rate. In partial and fully saturated soils, water movements in the pores and the resulting viscous drag between water and solid introduces extra viscous damping in the soil mass. Hall (1962) applied Biot's theory of wave propagation in a poro-elastic medium to evaluate damping in granular saturated soils and concluded that in general the hysteresis contribution is more important.

Empirical rules and experimental curves relating soil moduli and damping coefficient to strain amplitude have been derived by many investigators (Seed and Idriss, 1970; Hardin and Drnevich, 1972; Richart, 1975; etc.). These curves are usually used in current analytical and numerical methods to calculate strains and stresses in a soil mass under dynamic loads. Nevertheless, whenever possible, in the course of a project or a research program, a complete series of tests to evaluate the desired soil properties is recommended.

Conventional geotechnical tests, such as direct shear and compaction tests, were performed for the soil used in this investigation. A special effort was

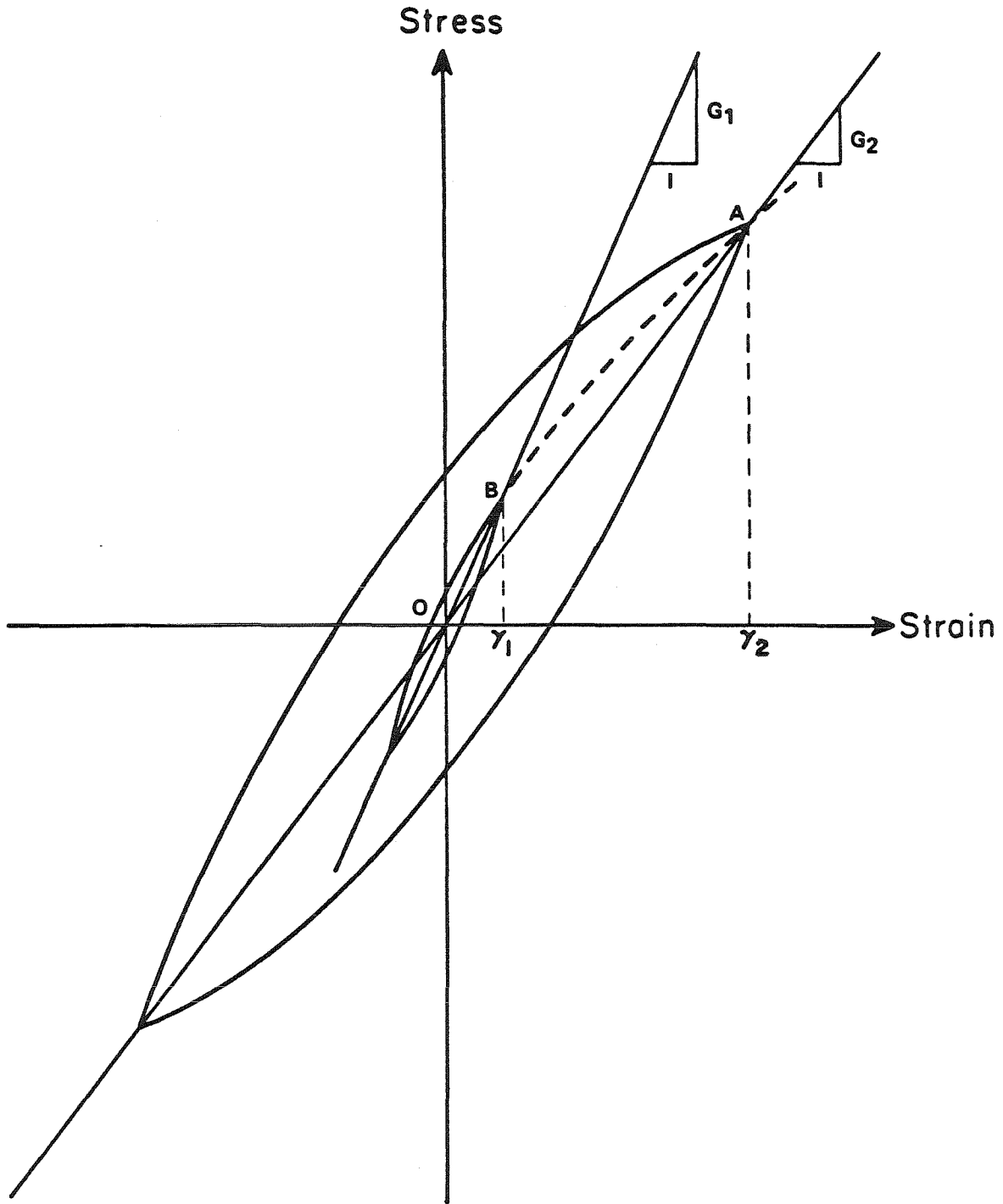


FIG. 4.1 HYSTERETIC STRESS - STRAIN RELATIONSHIPS AT DIFFERENT STRAIN AMPLITUDES (SEED & IDRIS, 1970)

undertaken to measure the dynamic properties of the soil. Results of these tests and brief descriptions of the test procedures are discussed next.

#### 4.2. GENERAL PROPERTIES OF SOIL

The type of soil used was Nevada 120 silica sand (Nevada Fine Sand - NFS). This sand is a uniformly-graded, fine-grained soil with a grain-size distribution as shown in Figure 4.2. In all of the tests the soil was dry and prepared in a dense state with a density of about 104 to 106 pcf equivalent to a relative density of 83% to 91.7%. Other features of this soil are:

- a. Specific gravity of the sand was 2.67.
- b. The friction angle of the dense sand was about 35°.
- c. Minimum dry unit weight of the loose soil was 88 pcf and its maximum dry density at 10.2% water content was 108 pcf.

#### 4.3. DYNAMIC SOIL PROPERTIES

The shear modulus and damping coefficient in the linearized model are influenced by a number of parameters. In the case of sands, strain amplitude  $\gamma$ , effective mean principal stress  $\bar{\sigma}_o$ , void ratio  $e$ , and number of cycles of loadings  $N_L$  are the major parameters affecting the dynamic soil behavior (Hardin and Drnevich, 1972).

Some soil properties are best measured or studied in the field, others in laboratory, and some can be measured both in laboratory and in situ (Woods, 1978). Effect of large amplitude strains and other parameters on dynamic soil properties can best be studied in a laboratory under controlled environment. In the centrifuge tests usually remolded soil is used. Thus, in this case the major difficulty in laboratory testing of soil properties lies in producing the same density and stress environment in the specimen as in the soil in the centrifuge. Stress distributions in homogeneous soil masses in centrifuge tests are

GRAVEL	SAND			SILT			CLAY
	COARSE	MEDIUM	FINE	COARSE	MEDIUM	FINE	

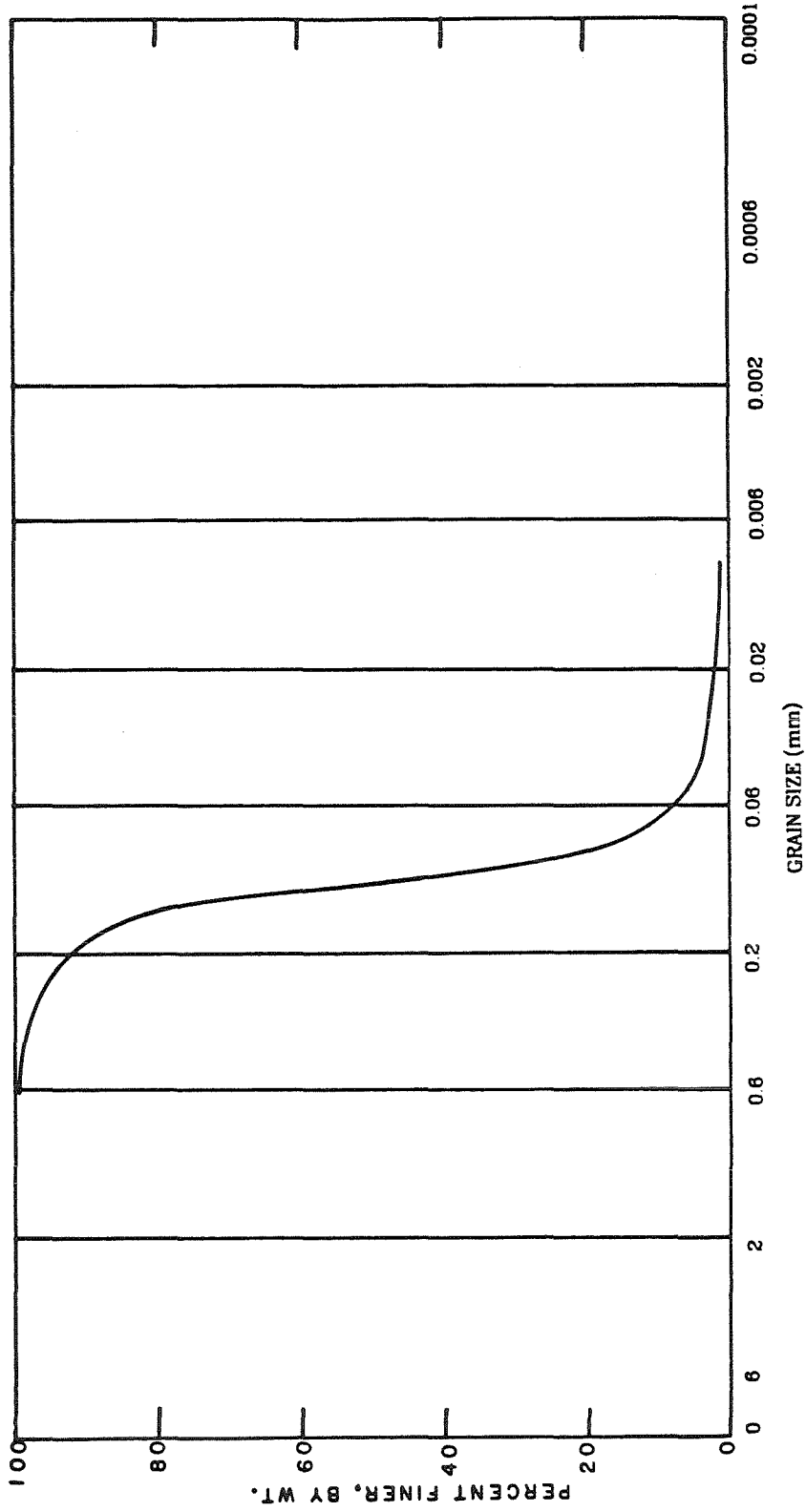


FIG. 4.2 GRAIN SIZE DISTRIBUTION CURVE FOR NFS

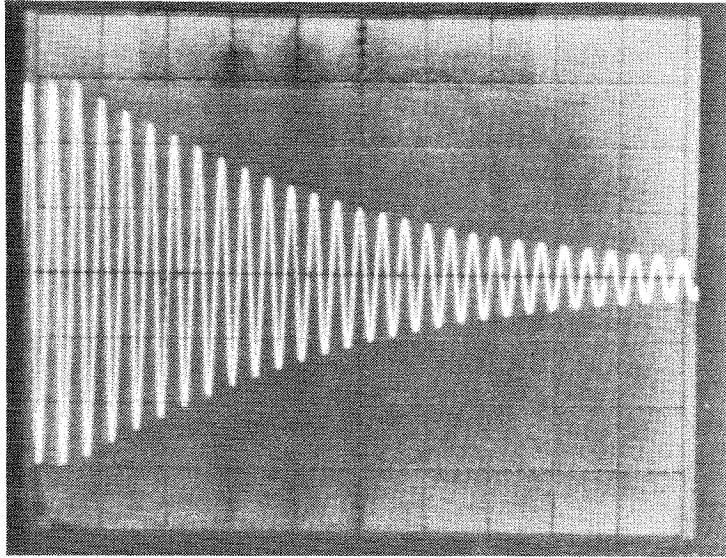


reasonably predictable and can be duplicated in laboratory testing of soil properties. Therefore, with a careful preparation of the soil sample in laboratory and controlling the applied stresses on the sample during the test, it is possible to derive with reasonable accuracy the soil properties, needed for a later analysis of centrifuge test results.

In this study resonant column and ultrasonic pulse tests were performed on the dry NFS to determine small strain shear modulus, Poisson's ratio, and damping ratio of the soil. The results of these tests along with the reduction factors incorporating the effect of large amplitude strains, can be used in any theoretical analysis on this soil employing a nonlinear reversible constitutive model.

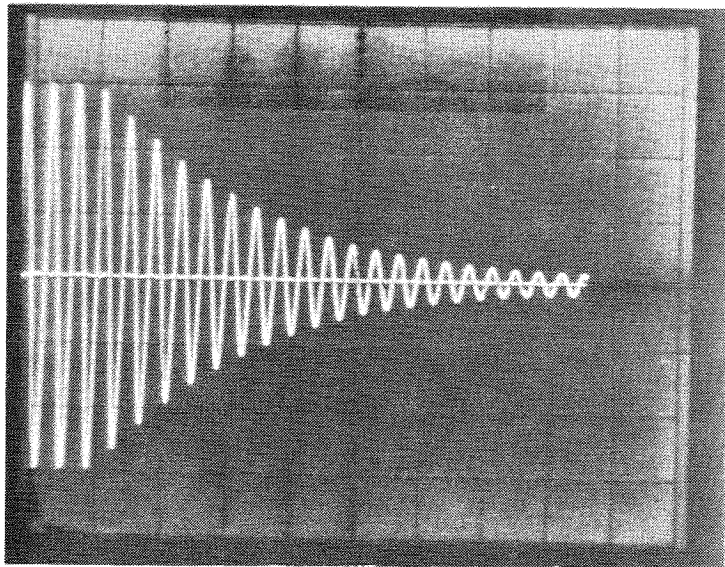
#### 4.3.1. Resonant Column Tests

Resonant column tests are relatively nondestructive for strains below  $10^{-4}$ ; thus, many measurements can be performed on the same specimen under different stress conditions. In these tests a vertical cylindrical specimen of soil, i.e., a soil column, will be vibrated in its longitudinal or torsional mode of vibration by electromagnetic forces induced at one end of the specimen. The frequency of input vibration can be changed until the first mode resonant frequency of the soil column is found. The derived resonant frequency, geometry and end restraint conditions of the sample, provide the necessary information to calculate the velocity of the elastic waves in the soil. Young's and shear moduli are then calculated from values of compression and shear velocities and the density of the soil (Richart, Hall, and Woods, 1970). Damping in the specimen is determined from the magnification factor at resonance or from the decay in amplitude of the free oscillating system after power to the driving coil is cut off at resonance (see Fig. 4.3)



(a) AVERAGE SHEAR STRAIN OF  $0.5 \times 10^{-4}$ , FREQ. = 150 HZ

(DENSITY = 96.3 pcf, CONFINING PRESSURE = 25.0 PSI)



(b) AVERAGE SHEAR STRAIN OF  $1.5 \times 10^{-3}$ , FREQ. = 140 HZ

**FIGURE 4.3: FREE OSCILLATION OF THE SPECIMEN 3 IN  
RESONANT COLUMN TESTS**

Two platens are attached to the ends of specimen. Different boundary conditions exist at the ends of the column depending on the kind of the device used. The whole vibration apparatus, mounted on the upper platen (the active end), and the specimen are placed in a triaxial chamber. For sands the cylindrical specimen is contained within a rubber membrane and a confining pressure is applied which can be varied during the test. The pressure is mainly used to study variation of dynamic soil properties under different levels of confining stresses, however, it also serves to maintain the shape of the sample during the test. A signal generator, a power amplifier, a digital voltmeter, a digital counter, a storage oscilloscope, and an accelerometer comprise the electronic equipment used in the test (see Fig. 4.4).

A "Hardin" resonant column apparatus was used in this investigation. The soil specimen with fixed-free end conditions could only be excited in its torsional mode of vibration (see Fig. 4.5). Tests were performed on three samples of dry NFS with different void ratios (Tbl. 4.1). Samples 1 and 2 were prepared in a dense state with similar void ratios, while sample 3 was looser than the other two. At different confining pressures the lowest mode resonant frequency of the soil column-apparatus system, was measured for different average shear strains ranging from  $10^{-4}$  to  $10^{-3}$ . A computer program was used to calculate the following parameters (Drnevich, Hardin, and Shippy, 1978):

$$(1) \text{ Mass density of the soil } (\rho), \rho = \frac{4W}{\pi d^2 l g} \quad (4.1)$$

$$(2) \text{ Mass moment of inertia of the specimen } (J), J = \frac{\pi \rho d^4 l}{32} \quad (4.2)$$

$$(3) \text{ Shear modulus } (G), G = 4\pi^2 \rho (f_n l)^2 \quad (4.3)$$

$$(4) \text{ Modulus ratio } (G/ G_{\max}),$$

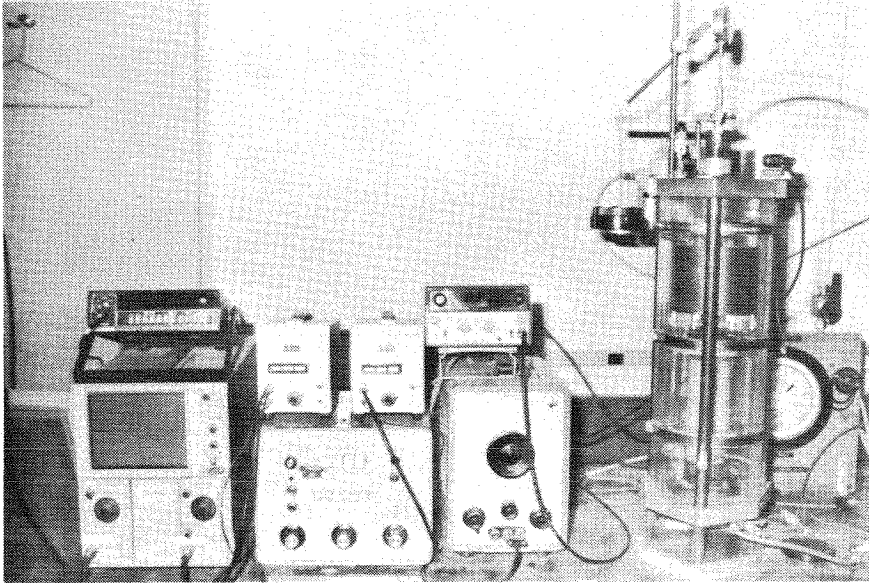


FIGURE 4.4: RESONANT COLUMN APPARATUS

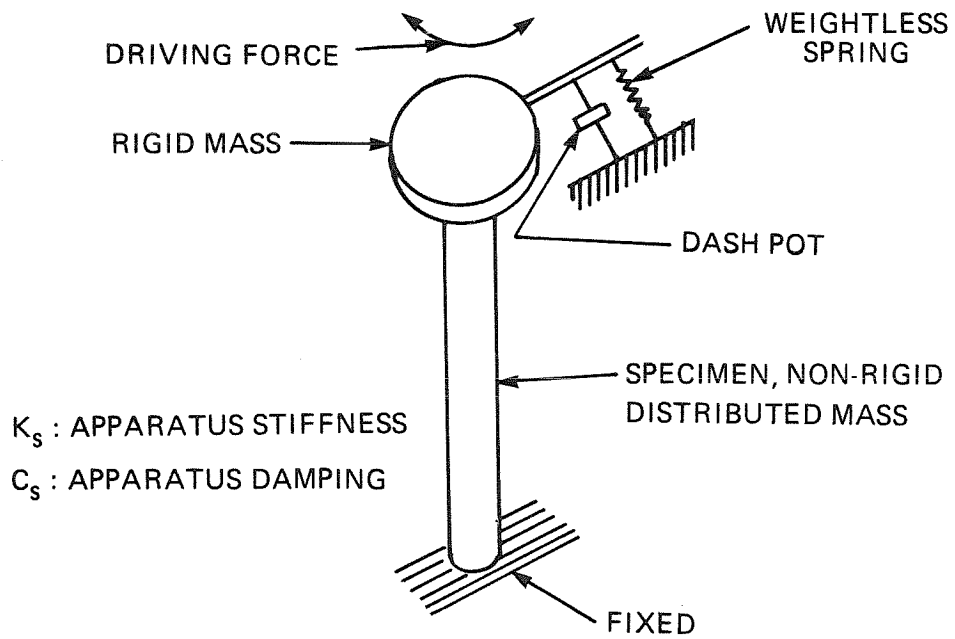


FIGURE 4.5: SCHEMATIC OF RESONANT COLUMN  
END CONDITIONS (HARDIN, 1965)

$$(5) \text{ Shear wave velocity } (V_s), V_s = \sqrt{\frac{G}{\rho}} \quad (4.4)$$

$$(6) \text{ Angular displacement } (\Theta), \Theta = \frac{a}{(f_n)^2 \times 4\pi^2} \quad (4.5)$$

$$(7) \text{ Average shearing strain } (\gamma), \gamma = \frac{\Theta \times d}{3l} \quad (4.6)$$

$$(8) \text{ Steady state damping ratio } (D), D = 0.5/M \quad (4.7)$$

where in above relations

W = weight of specimen

g = gravitational acceleration

l = length of specimen

d = diameter of specimen

f<sub>n</sub> = resonant frequency of the specimen

a = angular acceleration

M = magnification factor at resonance.

The damping ratio, D\*, in free oscillations of the specimen was calculated from the logarithmic decrement δ as

$$D^* \approx \delta/2\pi \quad (4.8)$$

where δ is calculated from

$$\delta = \frac{1}{n} \ln \frac{A_{n+1}}{A_1} \quad (4.9)$$

in which

A<sub>1</sub> = amplitude of the 1st cycle

A<sub>n+1</sub> = amplitude of the (n+1)th cycle

Note: In the above relations the effect of apparatus damping, stiffness characteristics, and calibration factors are not included.

Table 4.2. contains the values of shear modulus, shear wave velocity, average shearing strain, and steady state damping ratios, for samples 1, 2, and 3 of soil

Table 4.1. Properties and Test Conditions of Samples in Resonant Column Test

Sample No.	Dry Unit Weight, $\gamma_d$ (pcf)	Void Ratio, e	Length, L (in)	Diameter, d (in)	Weight (lb)	Confining Pressure Range (psi)
1	105.6	0.57	5.981	2.467	1.748	2 to 50
2	105.6	0.57	5.980	2.467	1.748	2 to 100
3	96.3	0.70	5.987	2.450	1.574	2 to 100

Note: The above values of sample dimensions and unit weights are the initial values at lowest confining pressure.

Table 4.2 Measured Dynamic Properties at Different Confining Pressures in Resonant Column Tests

Confining Pressure (psi)	Sample No.	Shear Modulus (psf) $\times 10^6$	Shear Wave Velocity (ft/sec)	Average Shear Strain (%) $\times 10^{-4}$	Steady State Damping Ratio (%)
2.0	1	0.855	510	1.25	1.74
	2	0.871	515	1.22	2.83
	3	0.661	470	1.59	1.02
4.0	1	1.110	580	0.97	2.80
	2	1.320	634	0.82	1.89
	3	0.861	536	1.24	1.69
8.0	1	1.570	690	0.69	1.87
	2	1.790	737	0.61	1.20
	3	1.270	651	0.86	4.07
12.5	1	1.820	744	0.61	1.43
	2	2.170	813	0.5	1.02
	3	1.560	722	0.7	1.55
25.0	1	2.540	877	0.44	1.08
	2	3.090	969	0.36	1.02
	3	2.210	857	0.5	0.93
50.0	1	3.750	1012	0.6	1.00
	2	4.090	1113	0.27	1.04
	3	3.040	1004	0.37	0.88
100.0	1				
	2	5.490	1287	0.2	1.13
	3	4.170	1171	0.27	0.79

at different values of confining pressures, for strains less than  $10^{-4}$ .

Damping ratios derived from free oscillation of the specimen were found to be consistently smaller than their corresponding steady-state counterparts. Since free vibration of the specimen was not recorded for all cases steady-state damping ratios will be used in later analyses where needed. Figure 4.6a shows the variation of damping ratio as a function of shear strain at two different confining pressures for samples 1 and 2. The damping ratio versus shear strain relationship for sample 3 is shown in figure 4.6b. The nonlinear variation of shear modulus with shear strain is shown in Figure 4.7a and 4.7b for the samples 2 and 3. The resonant column test does not yield reliable results for strains more than about  $10^{-4}$ . Thus, the stress-strain curves are extrapolated beyond the strain limit of  $10^{-4}$  by comparing them with experimental curves derived elsewhere (Seed and Idriss, 1970). Variation of shear modulus and damping ratio as a function of confining pressure for strains less than  $10^{-6}$  is presented in Figures 4.8 and 4.9 for samples 1, 2, and 3. As it is expected the denser samples have higher shear moduli. In Figure 4.8a the shear modulus versus confining pressure for strains around  $10^{-5}$  is also depicted. It is seen that for higher values of strain, the slope of the log-log line relating shear modulus and confining pressure  $\bar{\sigma}_o$  increases. Hardin and Drnevich (1972) also noted this and explained that the power of  $\bar{\sigma}_o$  with which the modulus varies increases from about 0.5 at zero strain amplitude to 1.0 at large strain amplitudes. In the tests on sample 1, slope of the above-mentioned log-log line varied from 0.43 to 0.47 for average shear strains of  $10^{-6}$  to  $10^{-5}$  respectively.

The following conclusions from the results of the resonant column tests on the NFS are derived:

- (1) The variation of shear modulus with power 0.43 to 0.47 of the confining pressure is in close agreement with average value of 0.5 derived for

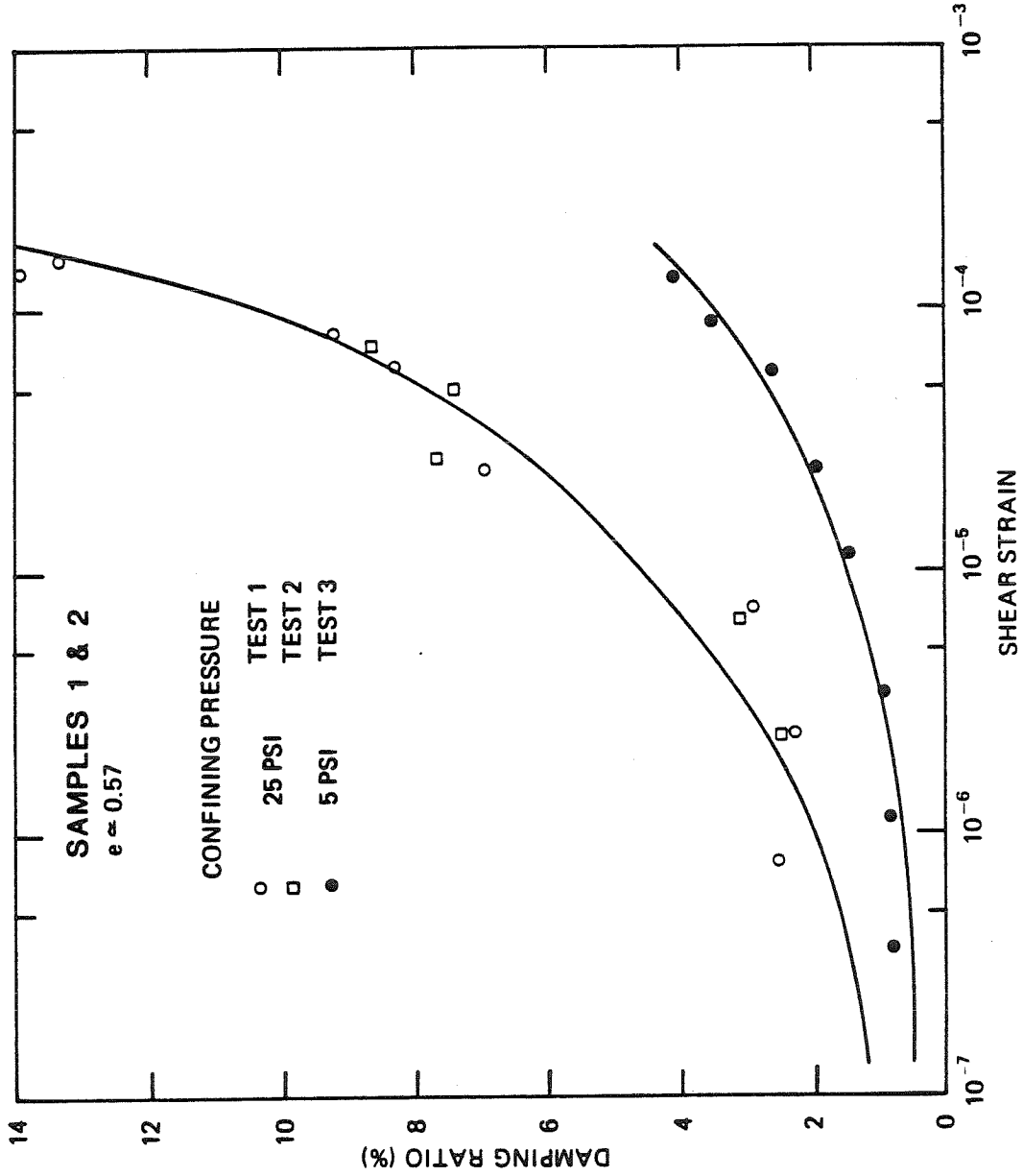


FIGURE 4.6 a : DAMPING RATIO VERSUS SHEAR STRAIN



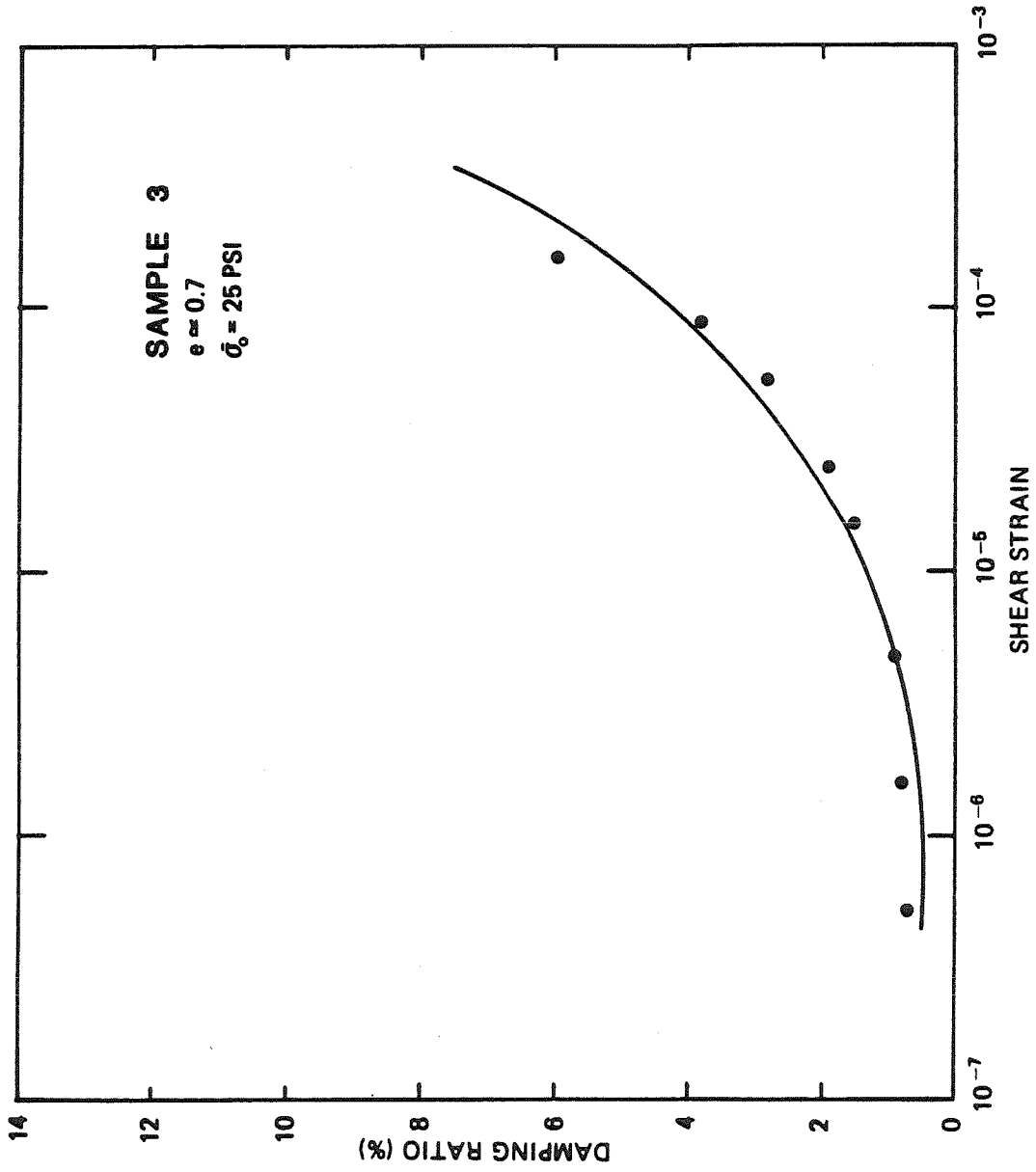


FIGURE 4.6 b : DAMPING RATIO VERSUS SHEAR STRAIN

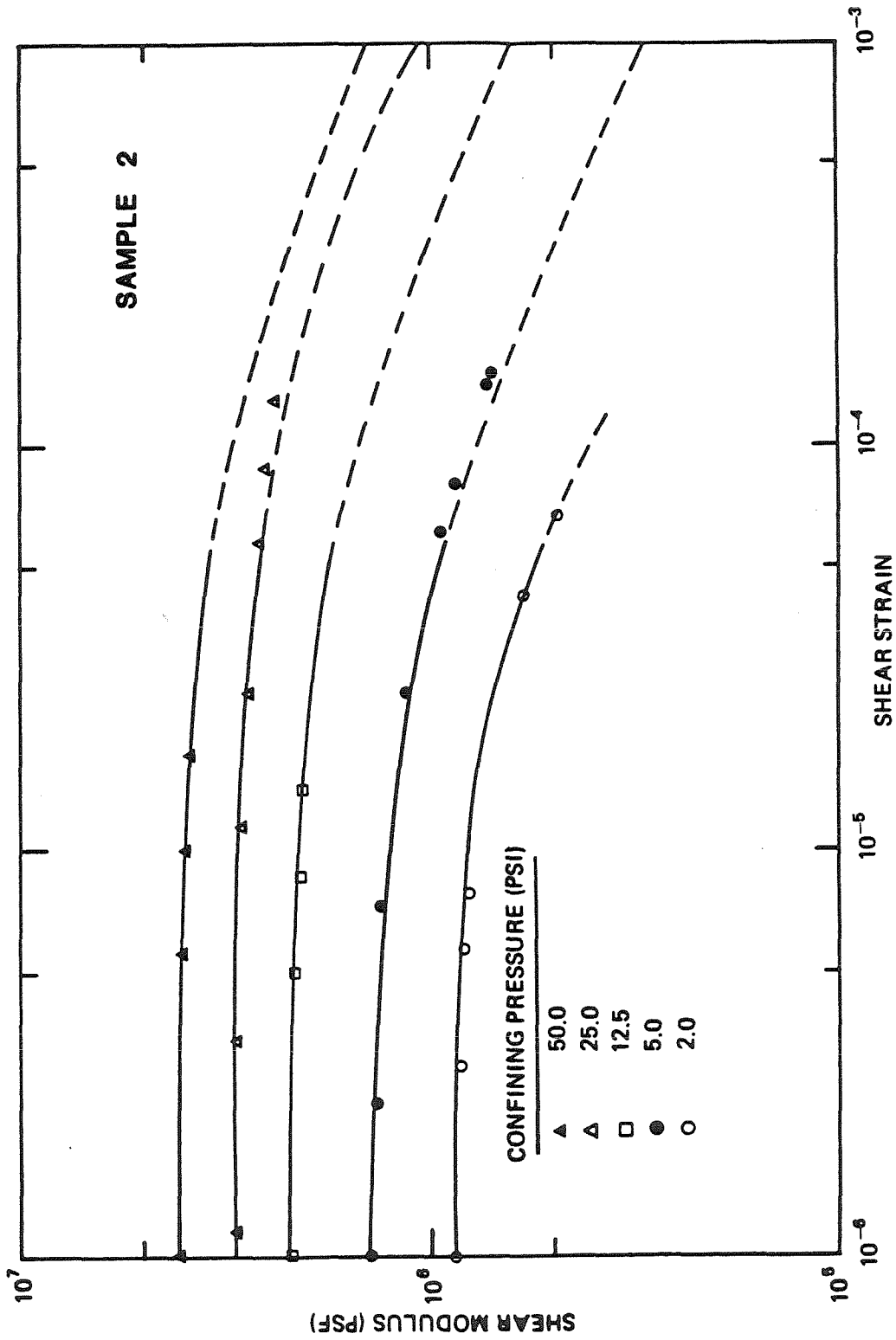


FIGURE 4.7 a: SHEAR MODULUS VERSUS SHEAR STRAIN-SAMPLE 2 ( $\nu = 0.57$ )

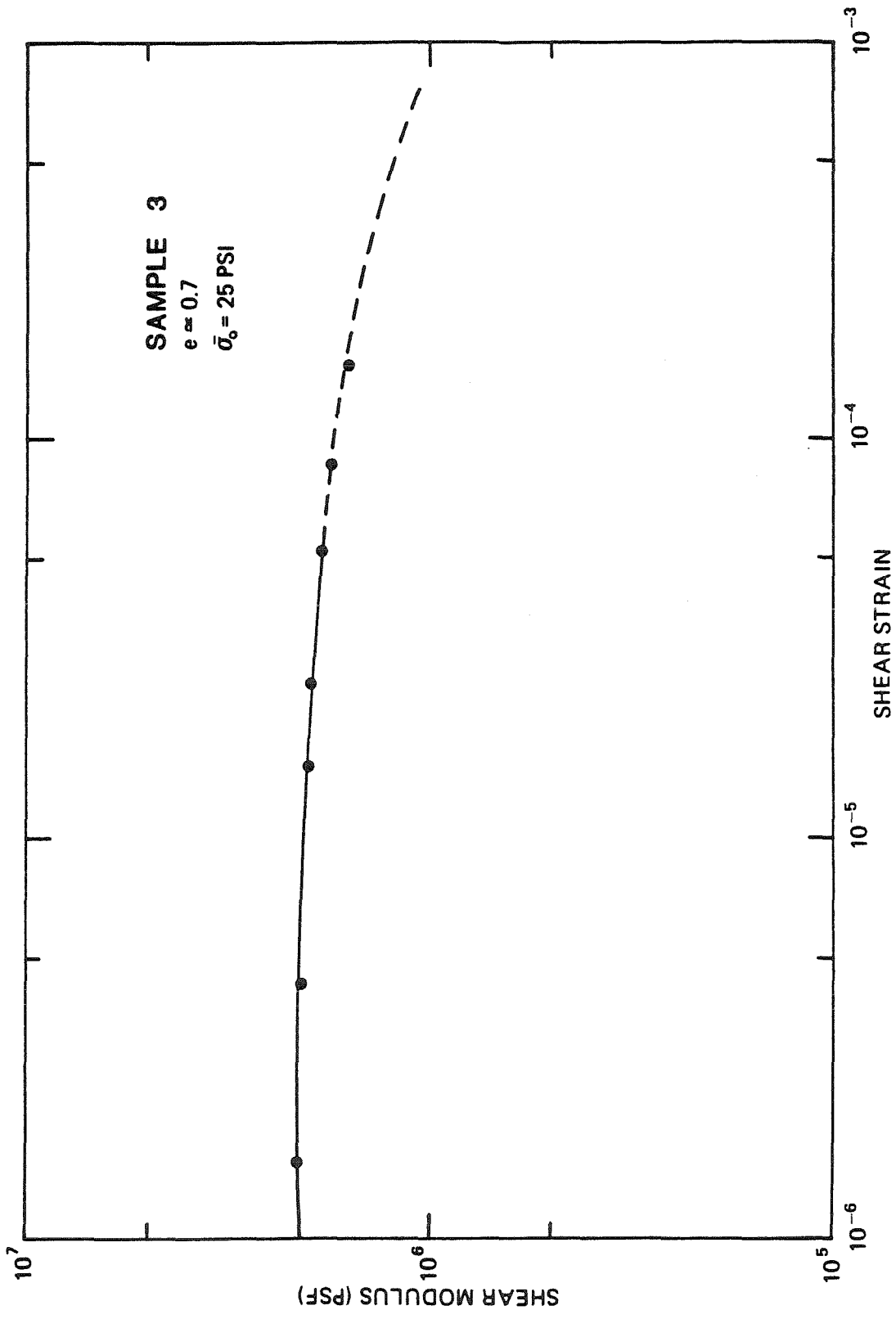


FIGURE 4.7 b : SHEAR MODULUS VERSUS SHEAR STRAIN

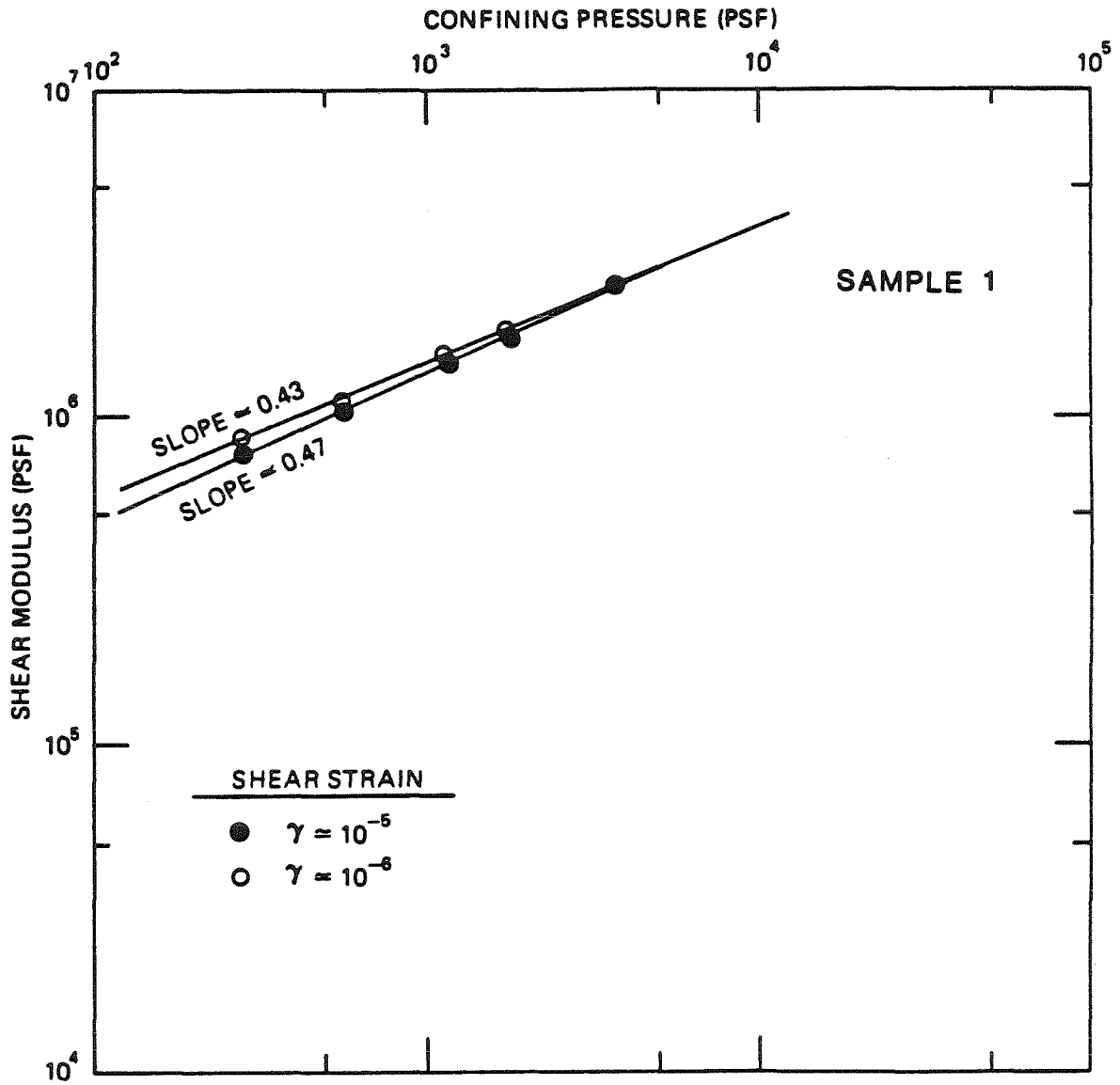


FIGURE 4.8a: SHEAR MODULUS VERSUS CONFINING PRESSURE-SAMPLE 1 ( $e = 0.57$ )

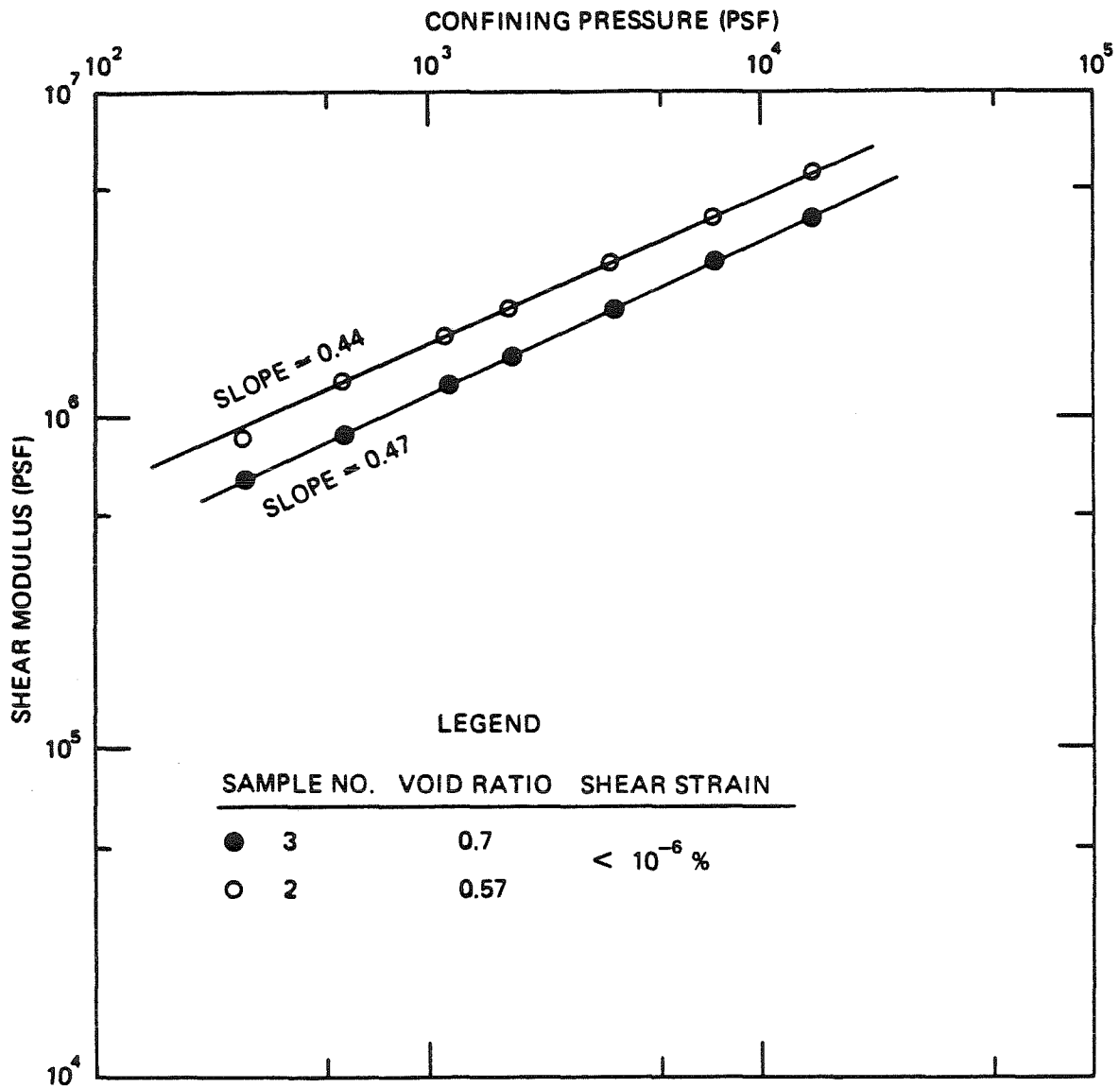


FIGURE 4.8 b: SHEAR MODULUS VERSUS CONFINING PRESSURE-SAMPLES 2 & 3

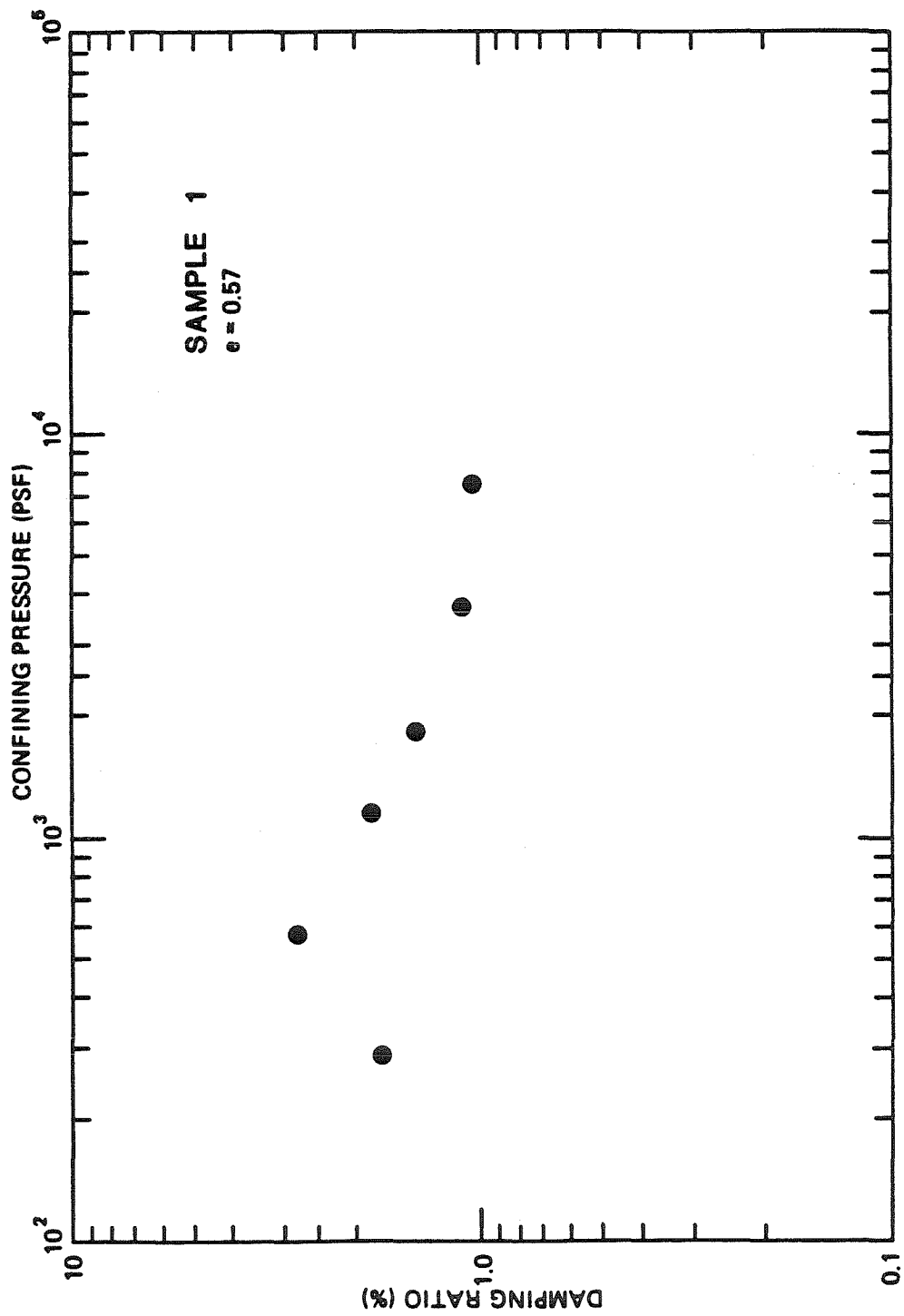


FIGURE 4.9a : EFFECTS OF CONFINING PRESSURE ON DAMPING RATIO ( $\gamma < 10^{-6}$ )

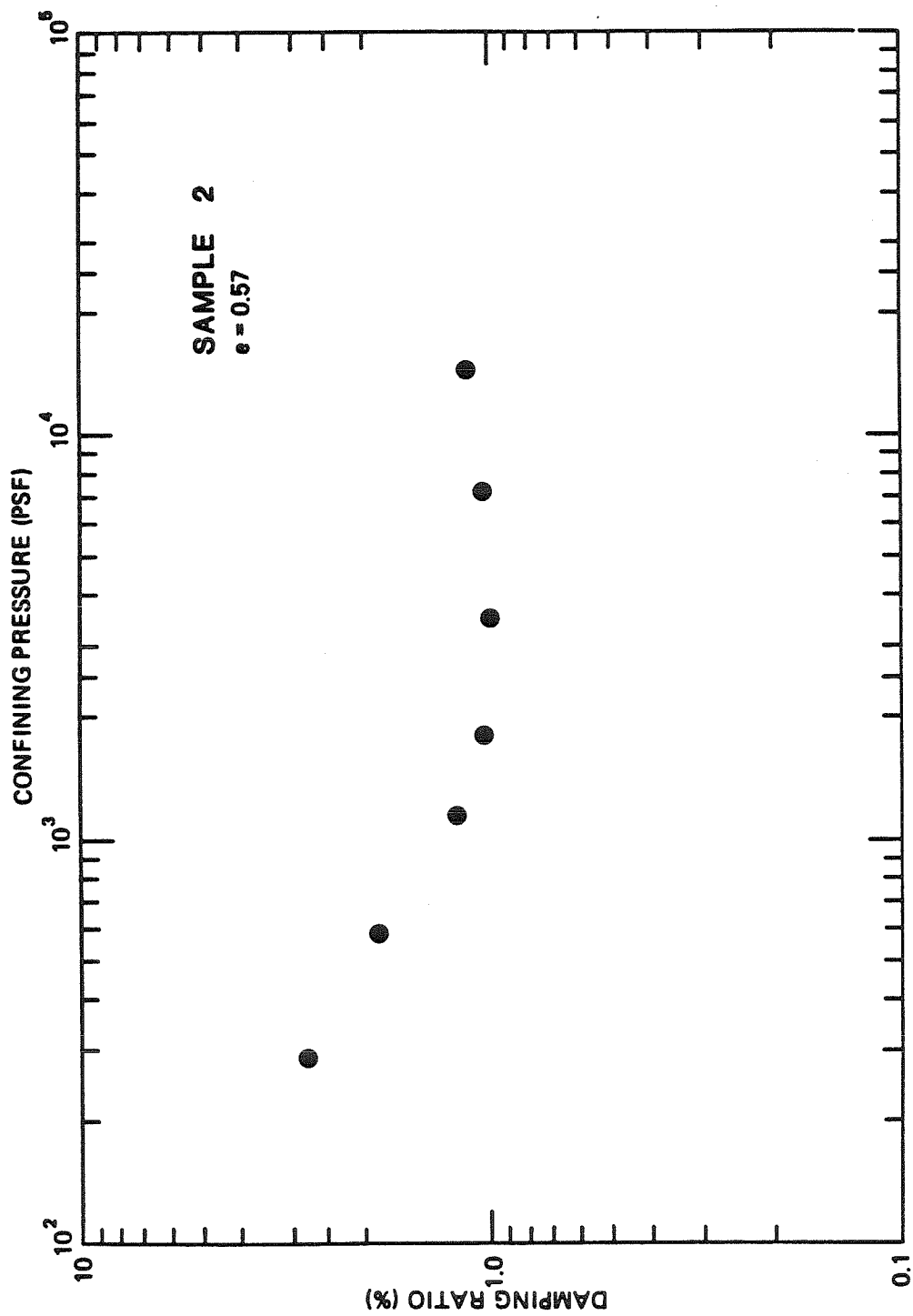


FIGURE 4.9b: EFFECTS OF CONFINING PRESSURE ON DAMPING RATIO ( $\gamma < 10^{-6}$ )

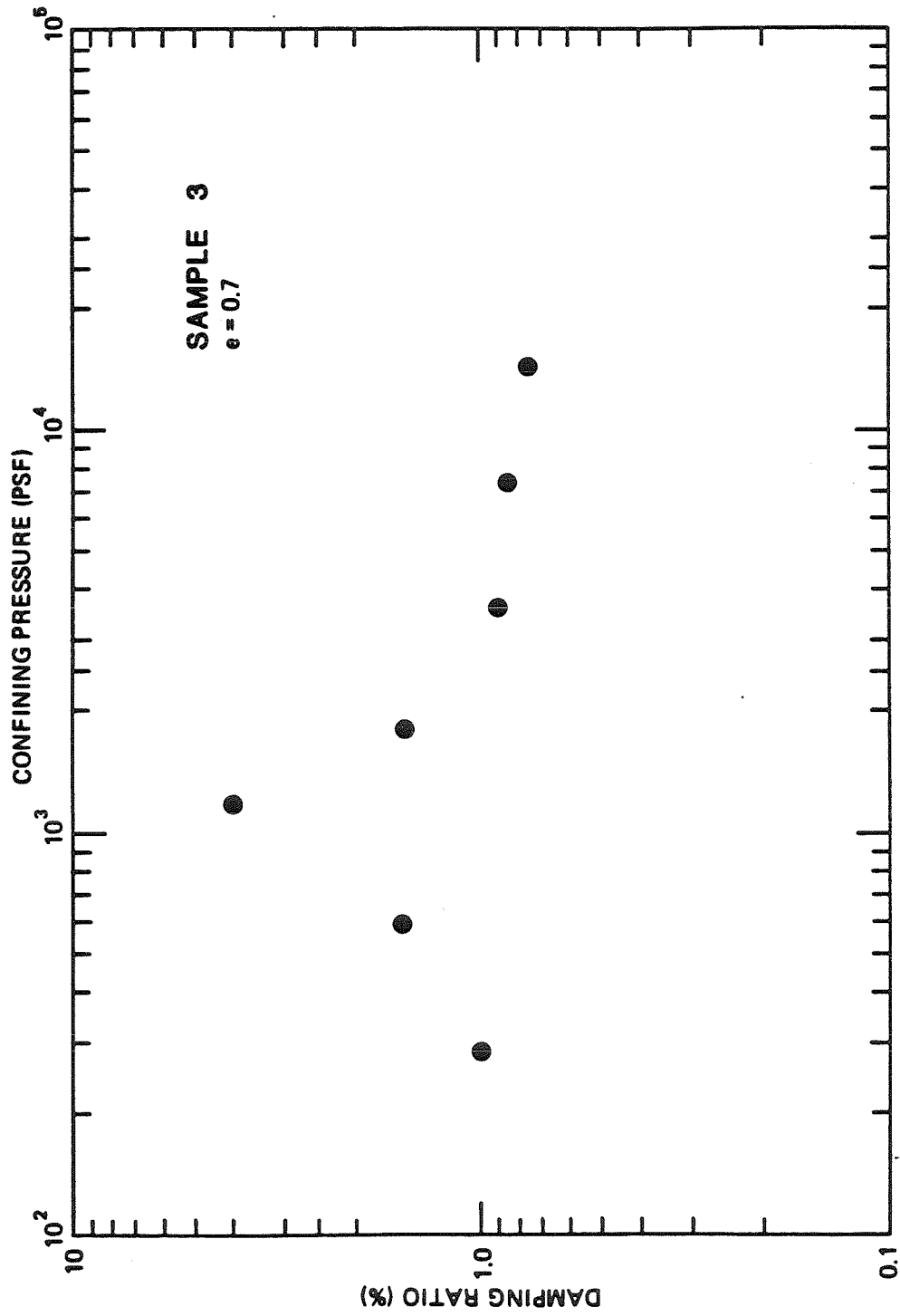


FIGURE 4.9c : EFFECTS OF CONFINING PRESSURE ON DAMPING RATIO (  $\gamma < 10^{-6}$  )



other dry sands.

- (2) The data points for damping ratio versus confining pressure generally show that the damping decreases as the confining pressure is increased. However, in some cases the damping increases when the confining pressure is increased. A comparison between Figures 4.6a and 4.6b shows that the variation of damping with void ratio is not as small as expected.
- (3) Variation of shear modulus and damping ratio with shear strain amplitude and the values of small strain ( $\gamma < 10^{-6}$ ) shear modulus are in good agreement with the results derived for other sands, summarized in a report by Seed and Idriss (1970).

#### 4.3.2. Ultrasonic Pulse Tests

The ultrasonic pulse velocity measurement technique can be used as a quick, nondestructive method to evaluate soil parameters appropriate for dynamic analysis at strain ranges smaller than tests presently available.

Ultrasonic and acoustic wave propagations in solids have been used by many researchers in physics, geology and geophysics to evaluate elastic and damping properties of different materials, such as metals and rocks (Mason and McSkimin, 1947; McSkimin, 1950; Mason, 1958; Birch, 1960; and Simmons, 1965). Measurement of elastic soil moduli under large cyclic confining pressures have been reported by Warren and Anderson (1973); Talwani, Nur, and Kovach (1973). In addition, the method has been used in determination of dynamic soil properties in the range of confining pressures and input frequencies pertinent to soil mechanics problems (Lawrence, 1964; Stephenson, 1978).

In these tests a short cylindrical specimen is placed between two caps each containing one transducer. A pulse voltage is applied to the driving transducer

producing a mechanical vibration. The disturbance is then transmitted through the specimen to a second transducer (receiver) which converts the mechanical signal to an electrical one, amplifying and displaying it on an oscilloscope. Shear and compression wave velocities of the sample are measured from the length of the sample, and the travel time of the pulse between the two ends of the sample. The most critical factors affecting the quality of the test results are the right choice of transducers, dimensions of the specimen, and the characteristics of the pulse generated (Stephenson, 1978; Tosaya, 1982). The requirements for the elastic waves to propagate in the medium without too many reflections, mode conversions, and loss of first-arrival amplitude can be summarized as:

- (1) Effect of Specimen Size: The sample length-to-diameter ratio should be less than 5 to avoid reductions in first-arrival amplitudes caused by delays resulted from numerous reflections of the propagating waves from the sidewalls. Pulse wave length should be much smaller than sample diameter to limit the intensity of the secondary waves and to prevent the wave energy from propagating with the bar velocity rather than longitudinal wave velocity.
- (2) Effect of Finite Medium: For the pressure waves to propagate in an infinite medium the effects of the specimen size should be minimum. This criterion sets an upper limit for the wave length of the ultrasonic pulse in the specimen. Thus for a material with known velocity a minimum frequency limit for the transducer is determined from

$$f_{\min} = \frac{1}{T_{\max}} = \frac{V}{\lambda_{\max}} \quad (4.10)$$

where

$\lambda_{\max}$  = Maximum wavelength compatible with assuming an infinite medium

$f_{\min}$  = Minimum frequency corresponding to  $\lambda_{\max}$

$T_{\max}$  = Maximum period corresponding to  $f_{\min}$  and  $\lambda_{\max}$

V = Velocity of wave propagation

In the experiments on the NFS the pressure and shear (P and S) wave velocities were measured at 2 MHz and 1 MHz respectively. The upper limit for the compressional velocities was close to 4560 ft/sec, measured at a maximum confining pressure of 60 psi and a void ratio about 0.57. These numbers correspond to a maximum compressional wave length of only 0.03 inch compared with sample length and diameter values of 0.33 and 0.58 inch respectively. The maximum shear wave length was also about 0.03 inch.

- (3) Material Grain Size: When wavelengths are comparable with grain size of the material, scattering of the energy by the grains considerably reduces the first-arrival amplitude. To avoid this, the frequency of the transducers should not be greater than a limiting value corresponding to an acceptable minimum value of the wavelength. The minimum shear velocity measured for the lowest confining pressure of 5 psi was about 1545 ft/sec. This corresponds to a wavelength of about 0.02 inch at a maximum frequency of 1 MHz. Almost 90 per cent of the grains in the sand had diameters between 0.002 and 0.008 inch. Thus, scattering of the waves by the grains was not a major problem in the tests.

Two ceramic piezoelectric transducers (lead zirconium titanate, PZT-5A), were used in the tests. The dry soil was compacted in a thick-walled brass cylinder with the endplug/acoustical-transducer assemblies in place. Figure 4.10 contains schematic drawings of the sample/endplug assembly configuration, and the transducers used for the experiments. The entire assembly of the sample, transducers, and endplugs was hydrostatically loaded in a pressure vessel. A schematic diagram of the confining-pressure system is pro-

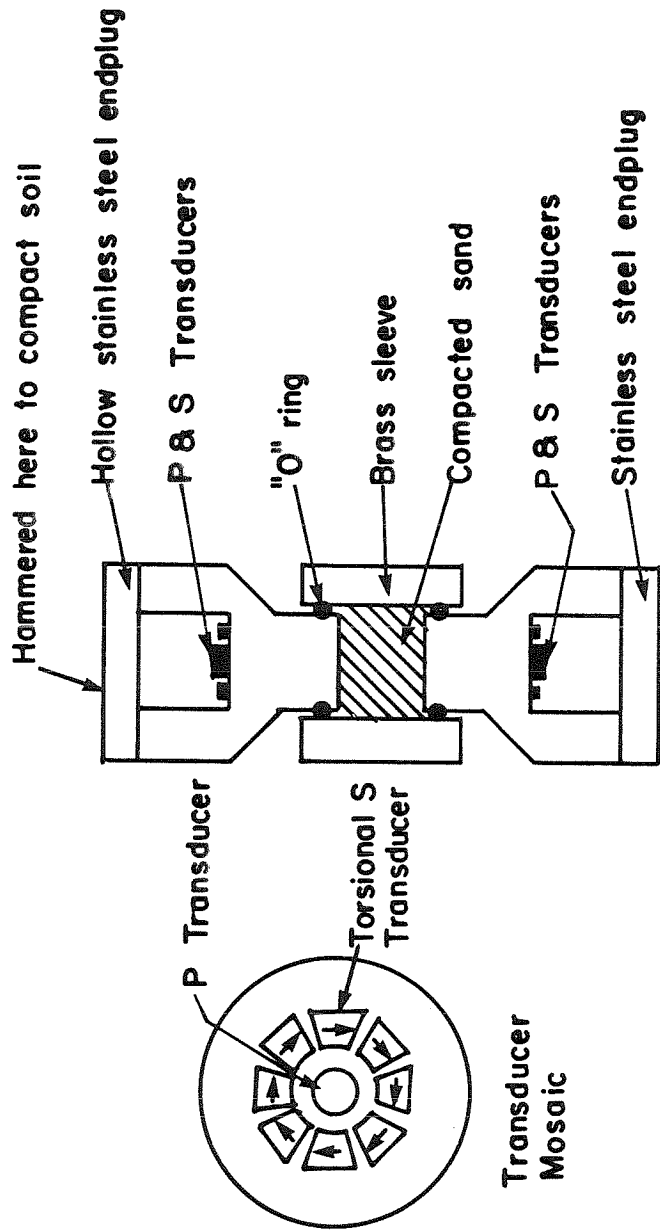


FIGURE 4.10: ENDPLUG / ACOUSTICAL-TRANSDUCER ASSEMBLY

vided in Figure 4.11. Velocities and amplitudes were measured by an ultrasonic-frequency pulse-transmission technique (e.g. Birch, 1960) which was controlled as diagrammed in Figure 4.11. Readings were taken at 5 psi increments of confining pressure from 5 to 60 psi and 10 psi decrements from 60 to 10 psi for hysteresis. The arrival time of the received signals were fairly clear because of the sharp rise time of the signals as they are seen in Figure 4.12. Travel-time resolution was  $\pm 0.025$  microsecond for both pressure and shear wave measurements. Velocities were calculated from sample length and travel-times of the pulse in transmission. Elastic moduli were then calculated from these velocities and the mass density of the soil (see Eqns. 3.4 and 3.5). Table 4.3 contains the values of calculated compression and shear wave velocities,  $V_p$  and  $V_s$ , velocity ratios  $V_p/V_s$ , Poisson's ratio, shear, Young's, and bulk modulus for the sand at different values of confining pressure.

Table 4.3 Dynamic Soil Properties (Ultrasonic Pulse Test)

Confining Pressure (psi)	$V_p$ ft/sec	$V_s$ ft/sec	$V_p/V_s$	Poisson's Ratio	Shear Modulus (psf) $\times 10^6$	Young's Modulus (psf) $\times 10^6$	Bulk Modulus (psf) $\times 10^6$
5.0	2690	1542	1.75	.26	7.73	19.50	13.60
10.0	3150	1739	1.82	.28	10.02	25.6	19.62
15.0	3347	1837	1.81	.28	11.27	28.86	21.92
20.0	3576	1936	1.86	.30	12.32	32.03	26.10
25.0	3740	2034	1.84	.29	13.78	35.55	28.19
30.0	3872	2100	1.85	.29	14.41	37.17	30.27
35.0	4068	2165	1.88	.30	15.45	40.17	34.03
40.0	4167	2198	1.89	.31	16.08	42.12	35.91
45.0	4265	2264	1.89	.31	16.91	44.31	37.58
50.0	4364	2330	1.89	.30	17.75	46.14	39.46
55.0	4495	2362	1.89	.31	18.58	48.69	41.55
60.0	4560	2395	1.90	.31	19.00	49.78	43.22
50.0	4364	2330	1.89	.30	17.75	46.14	39.46
40.0	4167	2198	1.89	.31	16.08	42.12	35.91
30.0	4167	2264	1.86	.30	16.70	43.43	35.29
20.0	3806	2133	1.79	.27	14.82	37.65	27.56
10.0	3445	1936	1.79	.27	12.32	31.29	22.76
Nevada Sand - Room Dry Void Ratio = 0.57		Dry Unit Weight (pcf) = 106.1			Length of Sample (in) = 0.32		

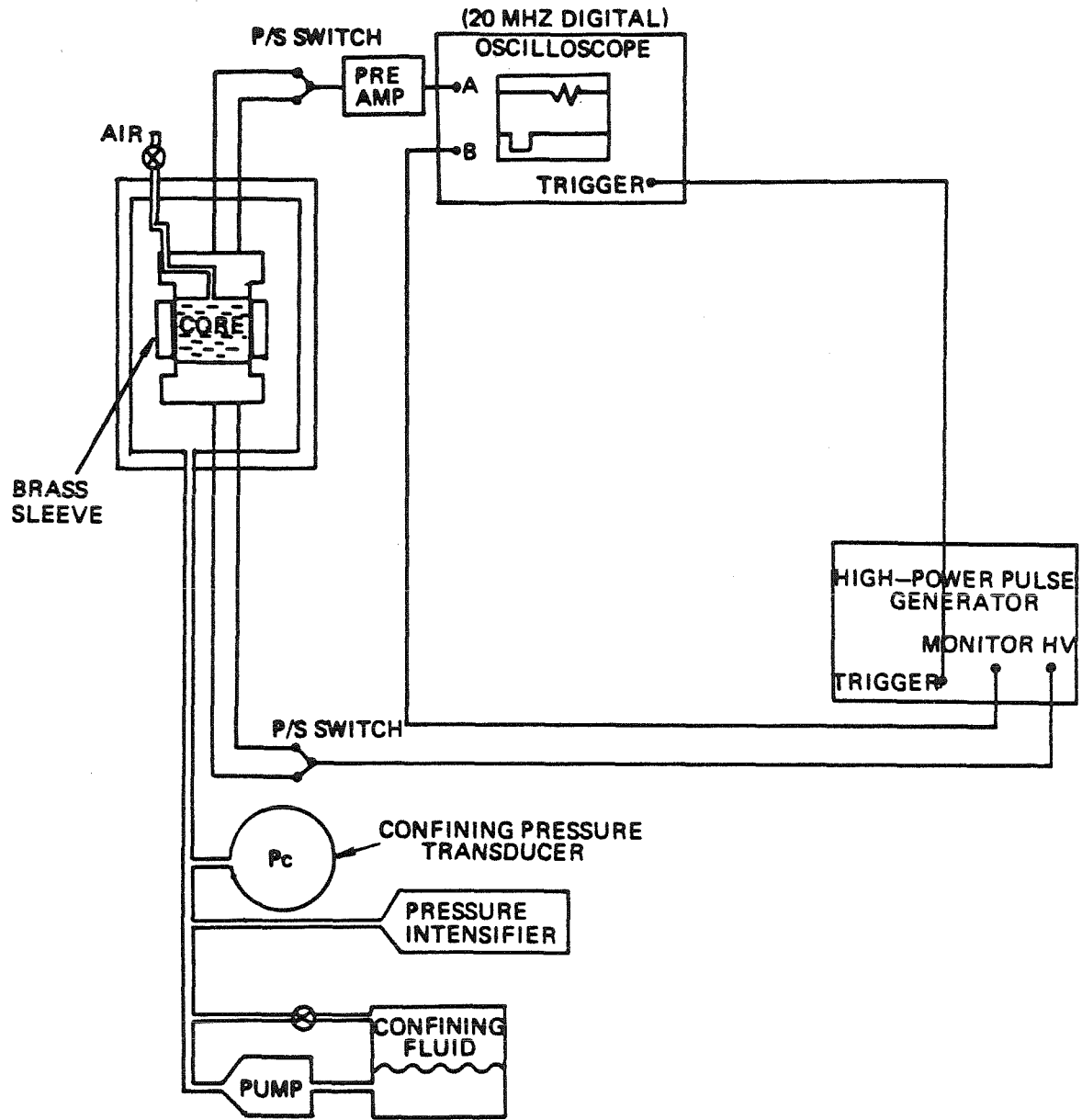
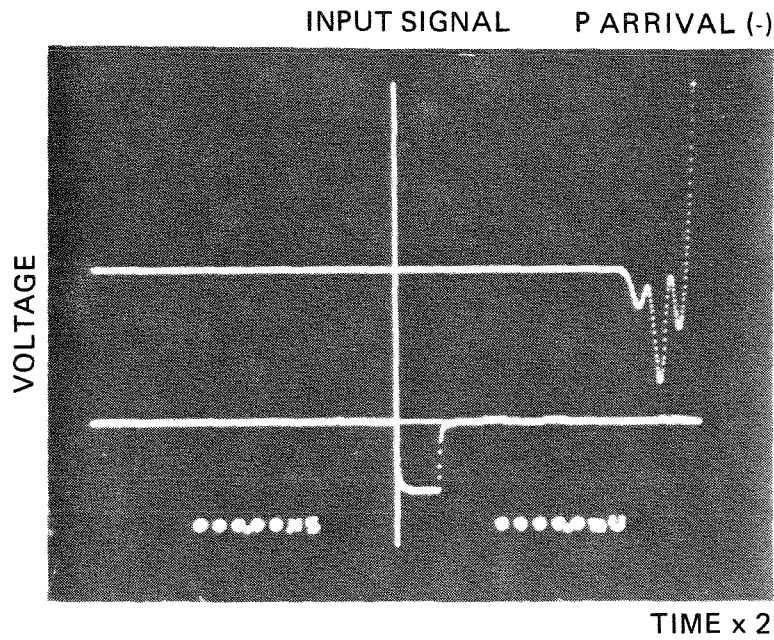
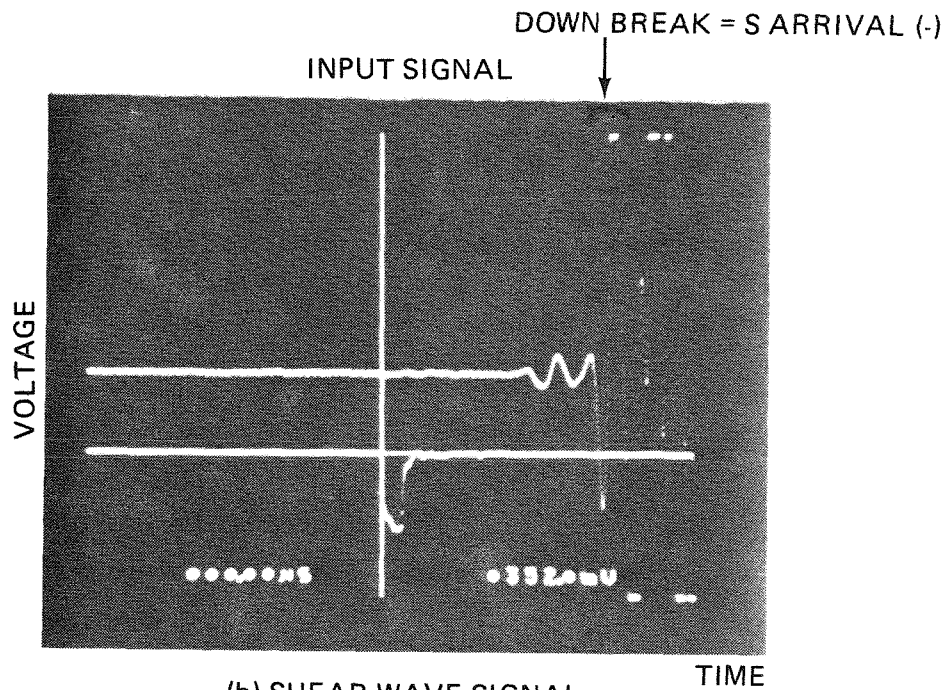


FIG. 4.11 PULSE-TRANSMISSION APPARATUS



(a) PRESSURE - WAVE SIGNAL  
ARRIVAL TIME = 19.10 MS

(ULTRASONIC PULSE TESTS)



(b) SHEAR WAVE SIGNAL  
ARRIVAL TIME = 35.70 MS

FIGURE 4.12 RECEIVED P AND S SIGNALS AT 20 PSI INCREASING PRESSURE CYCLE (VOID RATIO,  $e = 0.57$ )

Values of shear moduli derived by this method are about 5 times bigger than the values derived by resonant column tests. There are a few reasons for this large difference of values. One reason is the difference in preparing the sample causing different void ratios in the samples for the resonant column and ultrasonic pulse tests. Also, the confining pressure equipment in the ultrasonic tests was designed for the very high pressures usually used in testing on rocks. Therefore, control and precise measuring of confining pressure is not as reliable as in resonant column tests. The amplitudes of strains were extremely small in ultrasonic tests and frequencies were very high. These factors can increase stiffness of the soil structure considerably. Figure 4.7a shows that at low shear strain values, shear modulus is almost constant and does not appreciably increase with decrease in shear strain amplitude. This fact suggests that at very low shear strain amplitudes resonant column tests do not effectively measure the real stiffness properties of the soil column.

The values for Poisson's ratio show a reasonable consistency at different confining pressures. Referring to table 4.3 an average value of 0.3 is chosen for Poisson's ratio for subsequent analyses.

#### 4.4. SUMMARY

Shear moduli and damping ratios derived from resonant column tests along with the value of Poisson's ratio measured in ultrasonic pulse tests, provide the dynamic soil properties required for a theoretical method employing a linear viscoelastic or the equivalent linear hysteretic model of the soil. These values are in the range of properties derived by other investigators for dry sands. However, they should be interpreted with care in the case of large amplitude loading in the soil mass.

In the centrifuge experiments performed in this investigation the void ratio of dry NFS was about 0.57 in all the tests. Therefore, test results for the



samples 1 and 2 for small strain conditions can be used in later analysis in Chapter 8. The shear modulus at different levels of confining pressure is derived from table 4.2 or can be evaluated from the log-log curves of modulus versus pressure with the slope of 0.44 derived for this soil. Poisson's ratio as was measured from ultrasonic pulse tests is equal to 0.3 and shear modulus variation with shear strain is determined from the test results in Figure 4.7, for strains less than  $10^{-4}$ . In the linear viscoelastic model employed in the analysis of data in Chapter 8 the nonlinear behavior of soil is not included and the half-space model is assumed to be homogeneous and isotropic. Therefore, a constant value of shear modulus for the entire soil volume is assumed. The value of the modulus is considered for a confining pressure at a depth in soil, representing the average value of modulus over a depth of influence of model vibration. The values of this average confining pressure, soil moduli and damping are derived in Chapter 8.

CHAPTER REFERENCES.

- [1] Birch, F., "The Velocity of Compressional Waves in Rocks to 10 kb," Part 1: J. Geophys. Res., Vol. 65, 1960, pp. 1083-1102.
- [2] Drnevich, V. P., Hardin, B. O., and Shippy, D. J., "Modulus and Damping of Soils by the Resonant-Column Method," Dynamic Geotechnical Testing, ASTM STP 654, American Society for Testing and Materials, 1978, pp. 91-125.
- [3] Hall, J. R., Jr., "Effect of Amplitude on Damping and Wave Propagation in Granular Materials," Ph.D. Dissertation, Univ. of Florida, Aug. 1962, 172 pp.
- [4] Hardin, B. O., and Drnevich, V. P., "Shear Modulus and Damping in Soils: Measurement and Parameter Effects," Proc. Am. Soc. Civ. Engrs, 98, SM6, 1972, pp. 603-624.
- [5] Lawrence, F. V., "The Response of Soils to Dynamic Loadings," Report No. 23: Ultrasonic Shear Wave Velocity in Sand and Clay, Research Report R65-05, U.S. Army Engineer Waterways Experiment Station, Vicksburg, Miss., 1964.
- [6] Mason, Warren, P., "Physical Acoustics and the Properties of Solids," D. Van Nostrand Co., Princeton, N.J., 1958, 402pp.
- [7] Mason, Warren, P., and McSkimin, H. J., "Attenuation and Scattering of High Frequency Sound Waves in Metals and Glasses," J. Acoust. Soc. Am., Vol. 19, 1947, pp. 464-473.
- [8] McSkimin, H. J., "Ultrasonic Measurement Techniques Applicable to Small Solid Specimens," J. Acoust. Soc. Am., 22, 1950, pp. 413-418.
- [9] Richart, F. E., Jr., "Some Effects of Dynamic Soil Properties on Soil- Structure Interaction," Journal of the Geotechnical Engr. Division., Proceedings of the ASCE, Vol. 101, No. GT12, Dec. 1975.
- [10] Richart, F. E., Jr., Hall, J. R., Jr., and Woods, R. D., "Vibrations of Soils and Foundations, Prentice-Hall, Englewood Cliffs, N.J., 1970.
- [11] Seed, H. B., and Idriss, I. M., "Soil Moduli and Damping Factors for Dynamic Response Analysis," Report EERC 70-10, University of California, Berkeley, 1970.
- [12] Simmons, Gene, "Ultrasonics in Geology," Proc. IEEE, 53, sec. 10, 1965, pp. 1337-1346.
- [13] Stephenson, R. W., "Ultrasonic Testing for Determining Dynamic Soil Moduli," Dynamic Geotechnical Testing, ASTM STP 654, American Society for Testing and Materials, 1978, pp. 179-195.
- [14] SW-AJA, "Soil Behavior Under Earthquake Loading Conditions-State of the Art Evaluation of Soil Characteristics for Seismic Response Analysis," Prepared for U.S. Atomic Energy Commission, Jan. 1972.
- [15] Talwani, Pradeep; Nur, Amos; and Kovach, Robert L., "Compressional and Shear Wave Velocities in Granular Materials to 2.5 Kilobars," Department of Geophysics, Stanford University, Stanford, California, Vol. 78, No. 29, 1973.
- [16] Tosaya, Carol, "Acoustical Properties of Clay-Bearing Rocks," Ph.D. Thesis, Stanford University, Dept. of Geophysics, 1982.

- [17] Warren, Nick, and Anderson, Orson L., "Elastic Properties of Granular Materials under Uniaxial Compaction Cycles," Journal of Geophysical Research, University of California, Los Angeles, Vol. 78, No. 29, 1973.
- [18] Woods, R. D., "Measurement of Dynamic Soil Properties-State of Art," Proc. ASCE Specialty Conference on Earthquake Engineering and Soil Dynamics, Pasadena, June 1978.

## CHAPTER 5

### EQUIPMENT AND INSTRUMENTATION

#### 5.1. GENERAL PRESENTATION OF CENTRIFUGE

The centrifuge facility is located in two rooms, one called the "centrifuge room" where the centrifuge is located and the other the "control room" containing all the instruments for test control, data acquisition and reduction systems (Allard, 1983).

As shown in Figure 5.1. the centrifuge room contains:

- the centrifuge
- the centrifuge motor
- the Haskell Engineering and supply Co. Model No. DEN-PR51 hydraulic pump
- The rotating union ( Deublin 1595-40 Deublin 1895-100 ) mounted on top of the centrifuge enclosure at the center axis
- on the left wall are located (a, Fig. 5.1) Sabina Electric and Engineering Model RG2600 XD which controls the power supply of the centrifuge motor
- and (b, Fig.5.1) the on/off power switch

Figure 5.2. shows a view of the "control room" which includes some or all of the following equipment:

- Computer TRS 80
- ADC Analog to Digital Converter
- DAC Digital to Analog Converter
- Visicorder Honeywell Model 1858
- Hewlett-Packard X-Y plotter
- Digital Frequency Counter Heathkit 1M2410
- Controller MTS 406
- Oscilloscope Tektronix 5103N
- B&K Precision 3020 sweep/function generator (called signal generator) on the front wall
- RPM counter box (c), and Centrifuge speed regulator (d), on the front wall next to the RPM counter
- manual command for the hydraulic pump

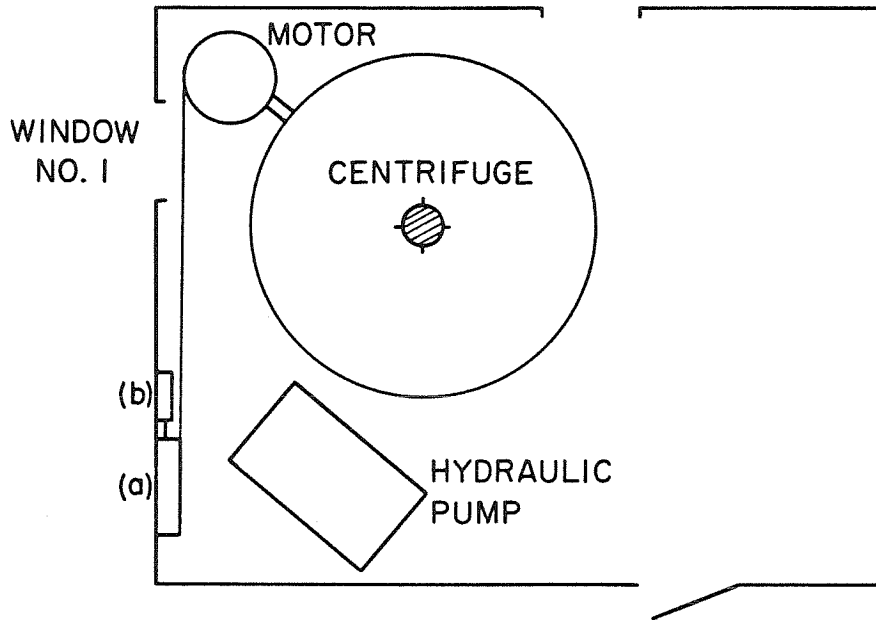


FIG. 5.1 PLAN OF THE CENTRIFUGE ROOM

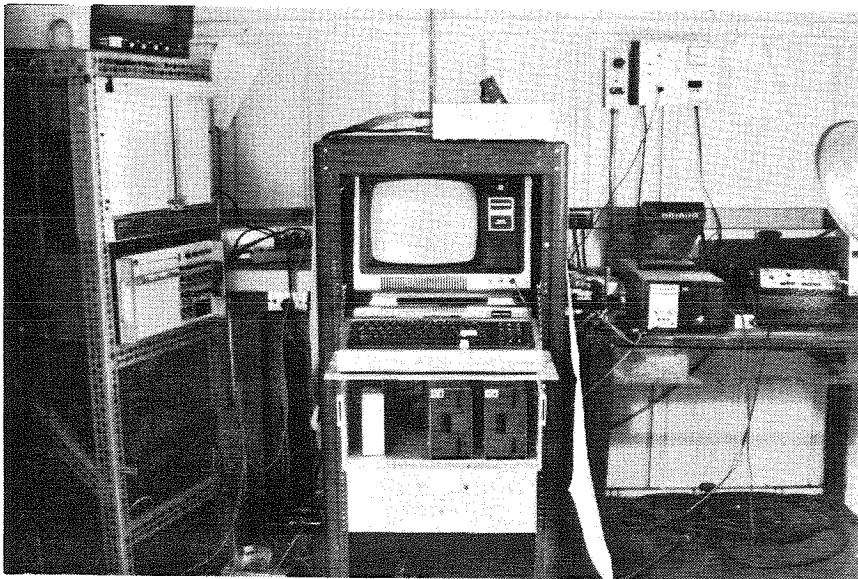


FIG. 5.2 THE CENTRIFUGE CONTROL ROOM

## 5.2. EQUIPMENT

### 5.2.1 *The Centrifuge*

The centrifuge (Fig. 5.3) is a model A1030 Genisco G-accelerator, which consists of an 80-inch diameter aluminum-alloy arm which rotates in the horizontal plane and is rated at 10,000 g-pounds payload capacity. At each end of the arm is located an 18 x 22 inch magnesium frame (Fig. 5.4) capable of carrying a 200-pound payload to 50g or 60 pounds to 175g. The acceleration range at the approximately 40- inch radius of the basket is from 1 to 175g.

The machine is driven by means of a Sabina Electric and Engineering Type RG 2600 Single phase Full Wave Regenerative Static D.C. Drive with a 5 HP, 1725 rpm, 230v, 3-phase, constant torque, double-ended electric drive motor. For accurate determination of the rotational speed, there is located on the main drive shaft a 600 tooth gear wheel, which, via a magnetic pickoff, produces 600 pulses per revolution. The pulses are read by an electronic counter which converts them to an LED display of RPM accurate to 0.1 rpm. The drift and wow of the system at any given setting is 0.05%. The acceleration arm is housed in an extruded aluminum enclosure, with all the controls and instrumentation, in the interests of safety, located remotely.

Electrical power and signals to and from the rotating arm or frame are conducted through 44 sliprings of various capacities in the 10 to 30 amp range. Experiments in the centrifuge can be observed by means of a television camera mounted on the arm close to the axis and a TV monitor in the "control room".

### 5.2.2. **Loading Equipment**

Depending on the loading system or the vibration generating equipment three different groups of dynamic tests were performed. The first two were active dynamic tests which involved direct vibratory loading of the model. The third one included passive dynamic tests in which the soil around the model was submitted to dynamic loading. The model responded to the soil shaking as, for

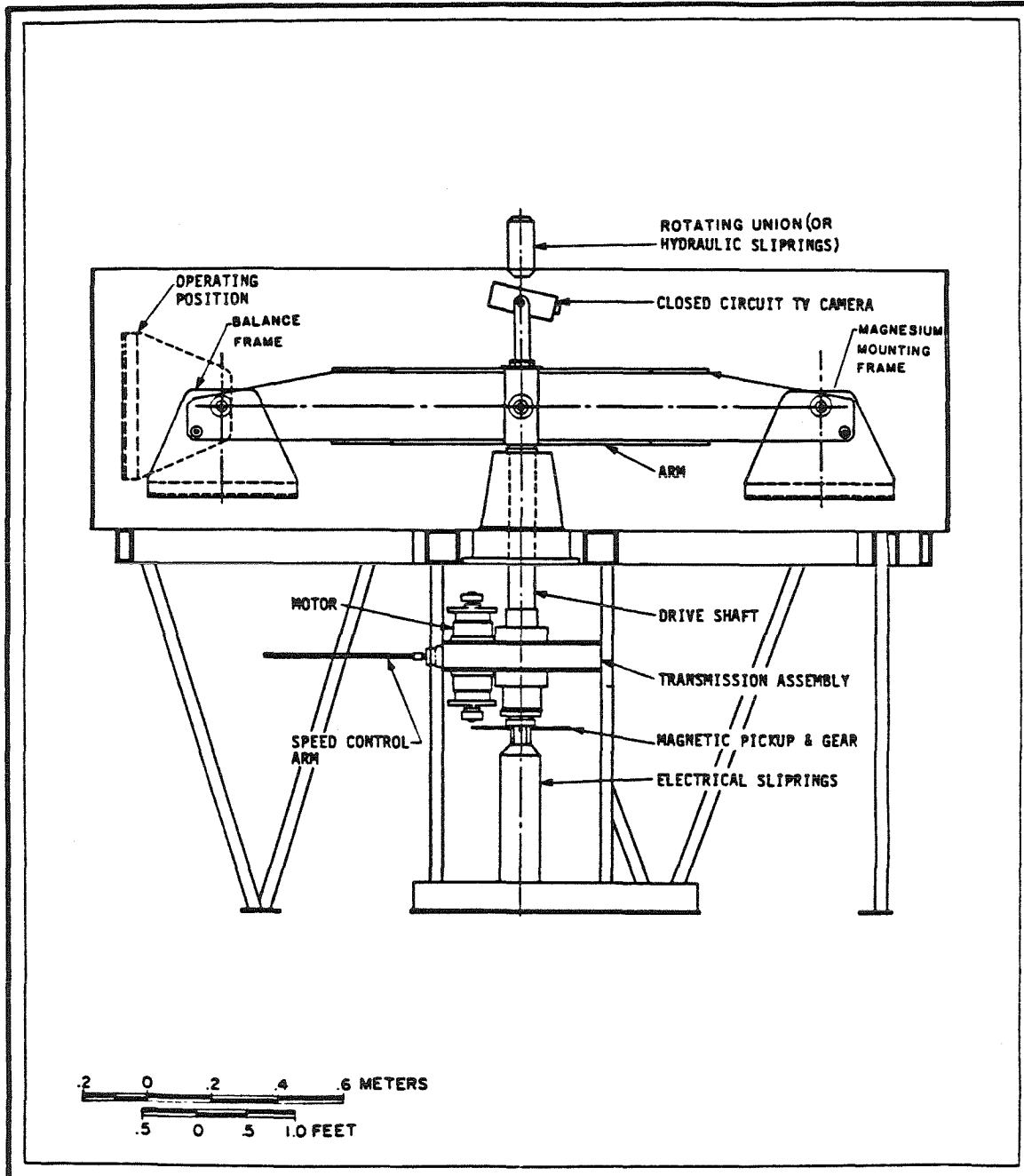


FIG. 5.3 SIDE VIEW OF CALTECH CENTRIFUGE

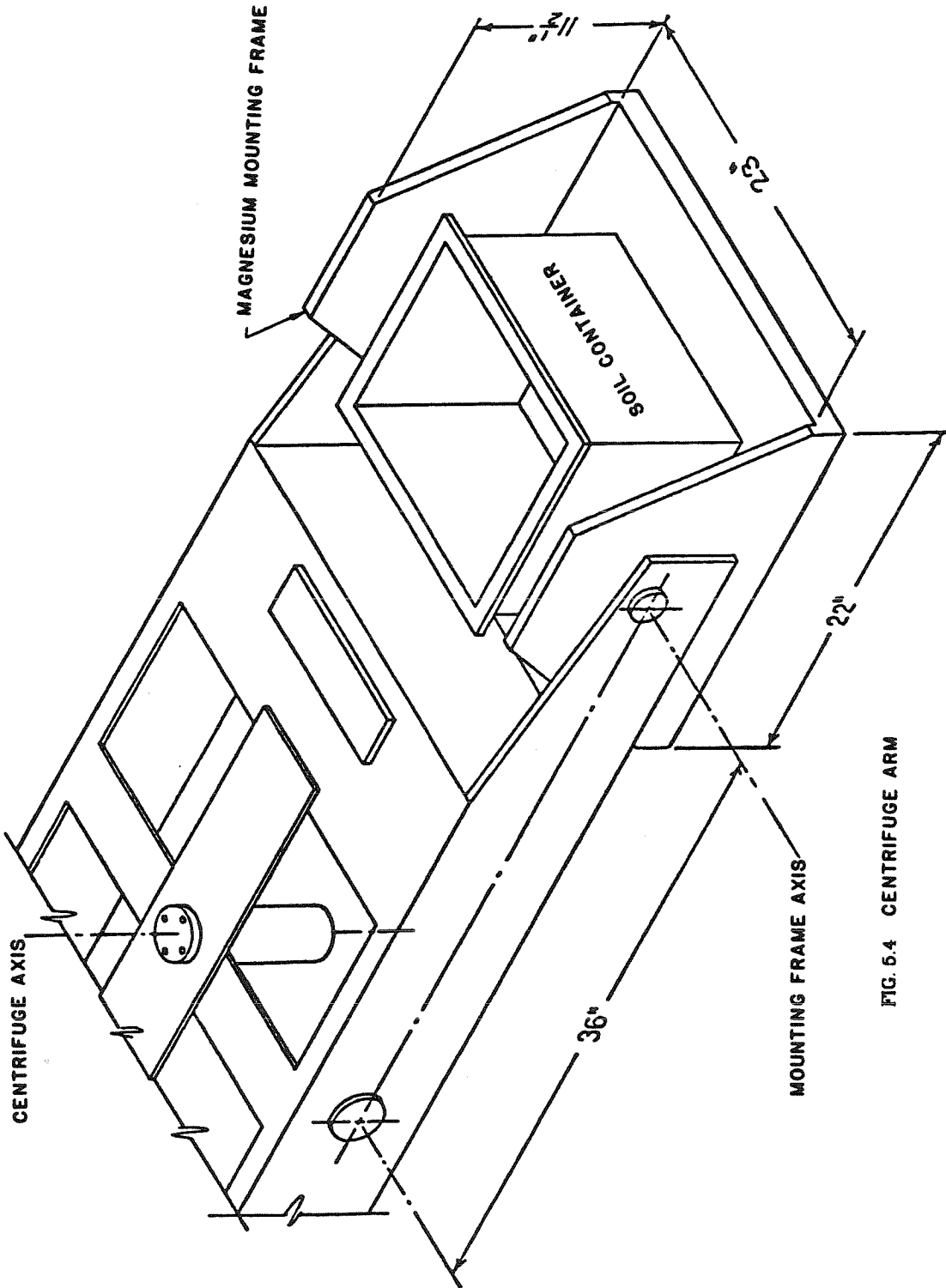


FIG. 5.4 CENTRIFUGE ARM



example, in a real earthquake. The loading systems for these groups of tests are explained next.

#### 5.2.2.1. *Explosion Generating Loading System*

A rigid rectangular model tower with circular footing was perturbed with a small explosive charge detonated on one side near the top. To do this, a small cavity was drilled near the tower top on its wider side on the center axis of the area. Two threaded holes were then drilled from the shorter sides to the explosive nest (the cavity). A few grains of explosive powder were packed into the cavity and a small mass was pushed onto it, covering the powder. The inertial force of the mass leaving the cavity during explosion exerts an impulsive reaction force on the tower and initiates the subsequent oscillation. The explosive was gun powder as used in toy cap guns. Since the powder was not a pure explosive, the energy released from a particular weight was not the same in different tests and varied considerably from test to test.

Two copper wires passed through two nylon screws were run to the explosive nest from the sides. The wires tips in the cavity, inside the powder, were almost at a touching distance. The other ends of the wires were connected to a high voltage capacitor through a relay (Fig. 5.5). The capacitor and the relay were mounted next to each other on a plate fixed on the centrifuge arm near the center axis. The relay was controlled remotely from the "control room" during the test. Once it was closed, the capacitor discharged and an electrical spark between the wires tips inside the cavity detonated the explosive powder.

#### 5.2.2.2. *Counterrotating Eccentric Mass Shaker*

A miniature counterrotating mass shaker was designed and constructed in the soil mechanics laboratory especially for steady-state forced vibration tests in this study. Because of its small size, reasonable force amplitude output, and

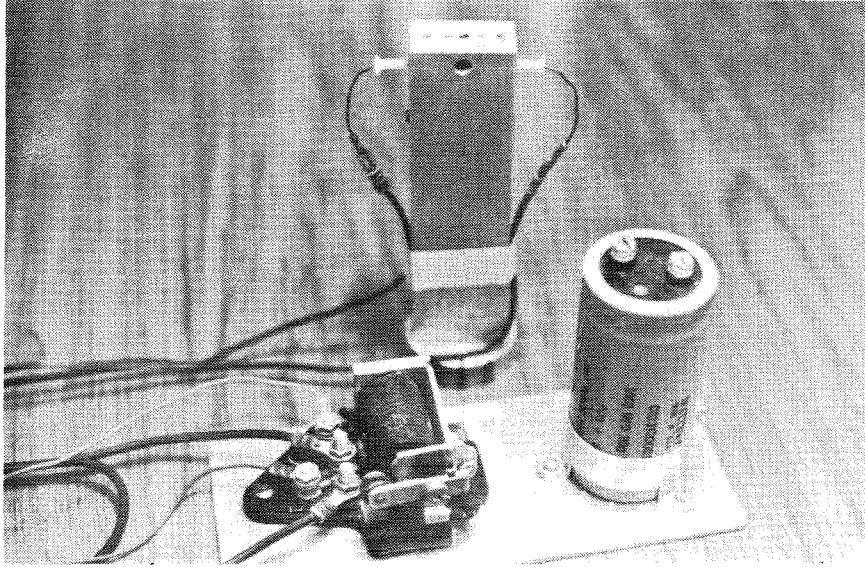


**FIGURE 5.5: RELAY, CAPACITOR, AND THE TOWER**

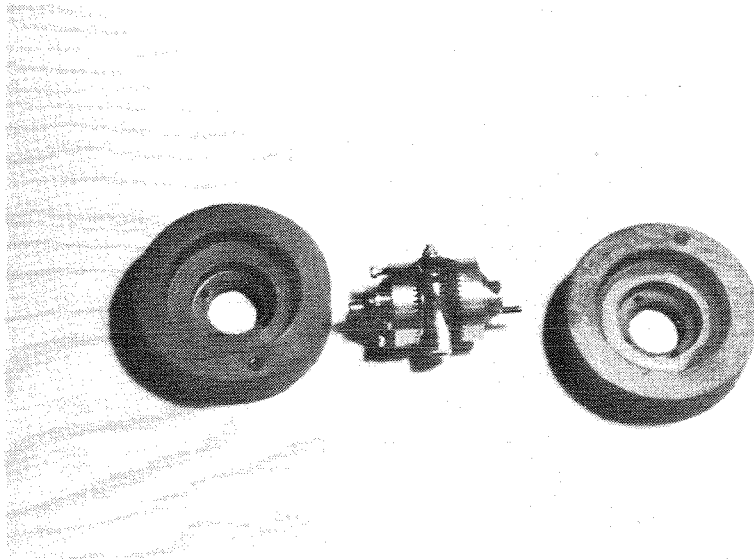


**FIGURE 5.6: COMPONENTS OF THE AIR-DRIVEN SHAKER**

high value of frequency response, it is an ideal loading equipment for any dynamic test in centrifuge.

For a model test at 50g centrifugal acceleration, a shaking frequency ranging from 0 to 15 Hz in a prototype requires a shaker capable of delivering forces at frequencies up to 750 Hz (45000 RPM) in the model. Electromagnetic shakers with constant amplitude force output require a very high current input at high frequencies. In addition electromagnetic shakers or mechanical ones with electric motors usually superimpose an electrical noise on the output signal of transducers hindering the data reduction process of data. To avoid the above-mentioned problems, compressed air was used as the source of energy to run the shaker, thereby obtaining high amplitude force and a frequency response free of noise.

The main part of the shaker is a three gear arrangement, two of them in parallel and the third one fitting in the gap between them normal to their plane of rotation. Two flywheels made from phenolic, a light and strong composite material, are assembled on the parallel gears and have counterrotating motion (Fig. 5.6). Compressed air flows with very high velocity from two nozzles on the sides of the shaker pushing forward circular cups machined on the circumference of one of the flywheels. Two light and transparent nylon tubes connect the nozzles to the air supply. The eccentric masses are two small screws in threaded holes drilled across the thickness of the flywheels near the edge. Screws of different lengths provide various eccentric masses to adjust the force of vibration independently of the speed. The maximum frequency output of the shaker in 50g centrifugal acceleration was about 45000 RPM and its output force amplitude varied from very small values up to few pounds depending on the amount of eccentric mass and speed of the shaker. Other properties of the shaker are summarized in Table 5.1. The moment of inertia and position of the center of gravity for the shaker were found experimentally (see Section 5.2.3).

Table 5.1 Properties of the Air-Driven Shaker

Diameter (in)	Height (in)	Eccentricity (in)	Height of Center of Gravity (in)	Weight (lbf)	Mass Moment of Inertia, (lb-in <sup>2</sup> )
1.73	1.38	0.74	0.67	0.23	0.08

Note: In above table mass moment of inertia is calculated with respect to center of gravity of the shaker.

In the "control room" a flexible tube ( $T_1$ , Fig. 5.7) is hooked at one end to the air source (S, Fig. 5.7). At the other end the flexible tubing ( $T_1$ ) is connected to a Norgren (No. 11008118) pressure regulator and an Ashcroft (Amp 8317) pressure gauge with 0.25 lb subdivisions.

From those instruments a second flexible tube ( $T_2$ ) goes through the wall to the centrifuge room where it can be attached to a rotating union (Deublin 1595-60) mounted on the top of the centrifuge enclosure at the center axis. Inside the centrifuge container the rotating union outlet is connected to the shaker using a thin transparent flexible tube ( $T'_2$ , Fig. 5.7).

In order to control the frequency of the shaker a frequency counter (Heathkit digital frequency counter IM2410) is used. On top of the shaker there are six silver strips of foil. Above the foil there is an LED which is always on, and a photocell. As each strip passes underneath the LED, the LED light is reflected to the photocell. Therefore, the photocell receiving the LED light will send a small increase of voltage to a comparator. Each time the comparator receives a voltage signal it sends a 5 V pulse through one of the slipring lines which is directly connected to the frequency counter in the "control" room. The frequency counter will count 6 units per revolution (there are 6 strips of foil) so dividing

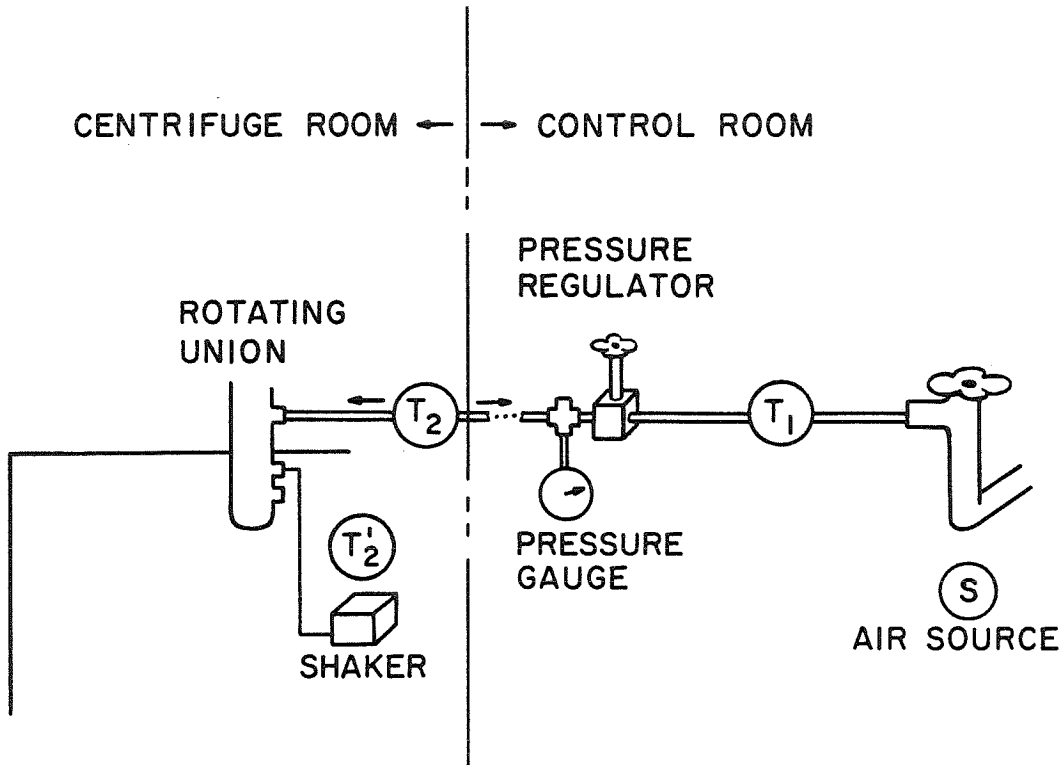
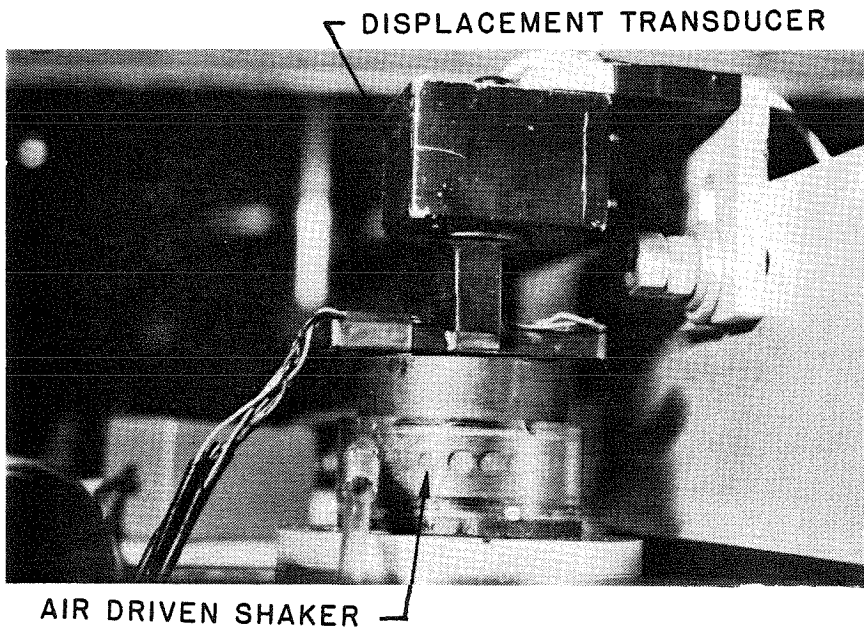


FIG. 5.7 ACTIVE LOADING TEST USING THE AIR DRIVEN SHAKER



by 6, the number given by the frequency counter, the frequency of the shaker in Hertz is obtained.

### 5.2.2.3 The Continuous Earthquake Generating Mechanism

#### 5.2.2.3a *The bucket frame and shaking system*

A special mounting frame (Fig. 5.8) is used. On each side of it, there is one row of four vertical cylindrical rods to support the test container, and at the center of the rectangular base is located the hydraulic double chamber piston with a servo-valve underneath it.

To suspend the soil container on its mounting frame the four horizontal bars on top of the container are screwed to the vertical rods of the mounting frame, (see Fig. 5.9). This prevents all back and forth and up and down movements of the bucket relative to its support, and permits only side to side movement. This movement is caused by the double chamber hydraulic piston. A space is reserved in the thick metallic base of the container to allow room for the piston. Therefore all the piston movements will be reproduced by the bucket. Two rows of four pinned beams connect the base of the container to the four horizontal bars that are attached to the mounting frame so that the container moves according to the piston displacement. A Moog control valve, subject to signals from the MTS controller (see Section 5.2.2.3b) regulates the flow of hydraulic fluid into the piston. In turn, the MTS controller is driven by the signal generator which may deliver a selected signal (sine, square wave or pulse, random noise, etc). With an adequate supply of hydraulic fluid, a continuous shaking from side to side of the soil container is obtained.

The electro-hydraulic system that gives continuous controlled shaking of the bucket, is constituted from the following parts:

The Haskell Engineering and Supply Co. Model DEN.PR51 pump which is driven by a 10 hp motor and has a line capacity of 3000 psi at a maximum rate

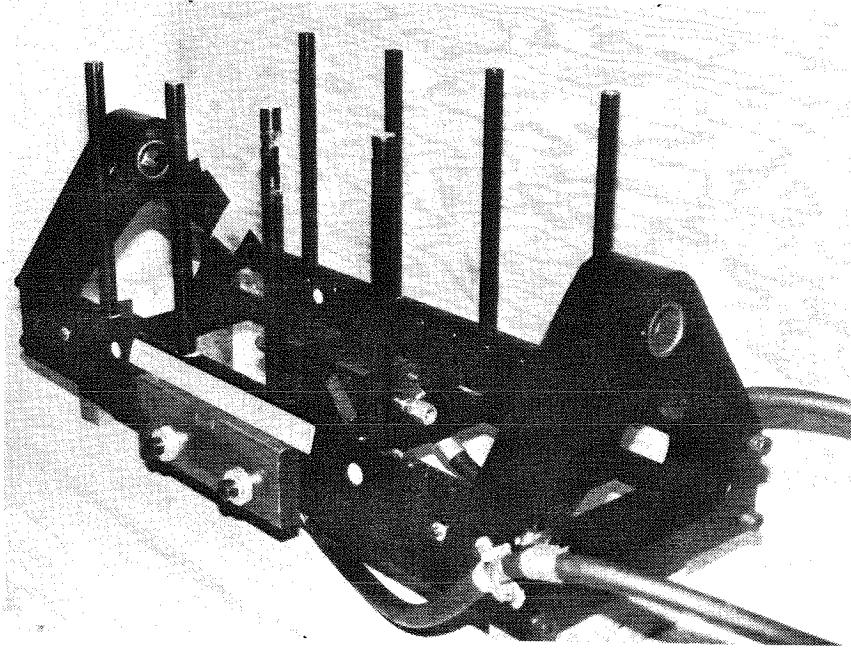


**FIGURE 5.8: THE SPECIAL MOUNTING FRAME OF THE CONTINUOUS EARTHQUAKE GENERATING MECHANISM**

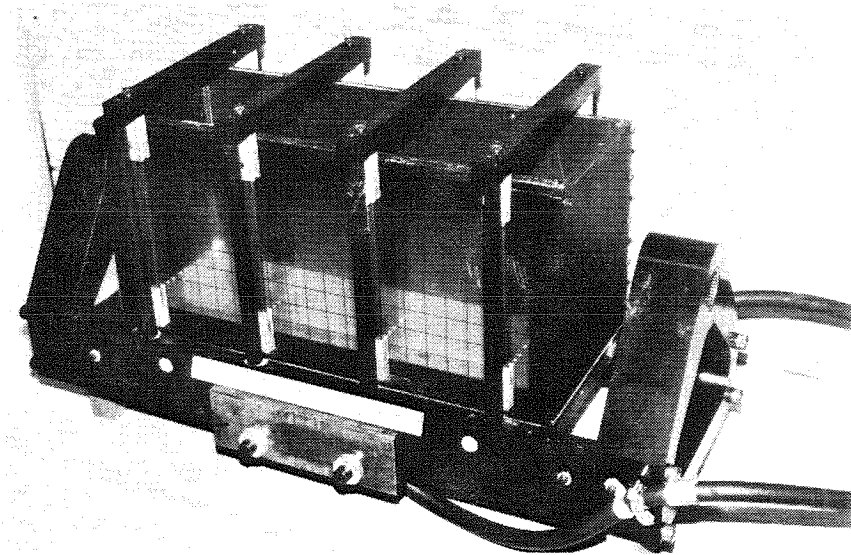


**FIGURE 5.9: THE SOIL CONTAINER SUSPENDED ON ITS MOUNTING FRAME**

of 5 gallons per minute. This pump supplies hydraulic pressure to the entire system.

The flow capacity of the pump is not enough for the experiments. To start the piston, a flow rate on the order of 1 gallon in 1/2 second is needed. So accumulators which are pressurized reservoirs are used. They can deliver a few gallons of hydraulic fluid very quickly.

Two small accumulators (ZEMARC standard Bladder accumulators) of 1 gallon each are fixed underneath the centrifuge arm inside the enclosure, (see Fig. 5.10). These two accumulators deliver the hydraulic fluid directly to the servo valve and piston. They constitute a large reservoir of hydraulic fluid that can be delivered to the servo valve very rapidly. In addition, the connecting lines from accumulator to valve are very short, so that line flexibility and dissipation are minimized. A 5 gallon accumulator outside the centrifuge delivers oil to the accumulators inside the centrifuge through the rotating union (Deublin 1895-100) mounted on the top of centrifuge enclosure. The output from the small accumulators is directly connected to the servo valve and the piston. A second line from servo valve returns the oil through the rotating union to the hydraulic pump.

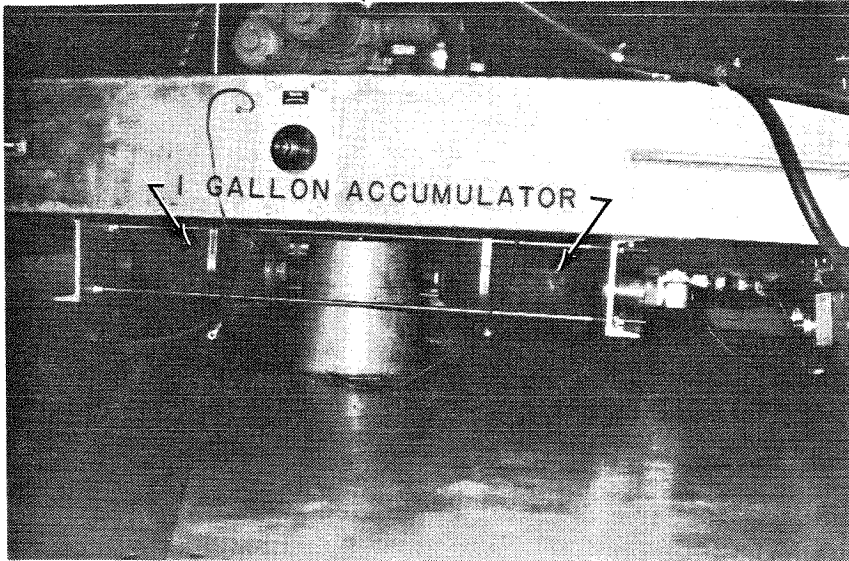
Immediately before starting the test the hydraulic pump is turned on to precharge the accumulators to 3000 psi so they are full of hydraulic fluid ready to go. Then, on command, the computer (Section 5.5.2) will give the signal to start the test. The servo valve receiving the signal opens the side connected to (3 Fig. 5.11). That lowers the pressure and therefore the hydraulic fluid rushes from the two accumulators to the servo valve, permitting a rapid response of the piston to take place.

#### 5.2.2.3b *The Controller MTS 406*

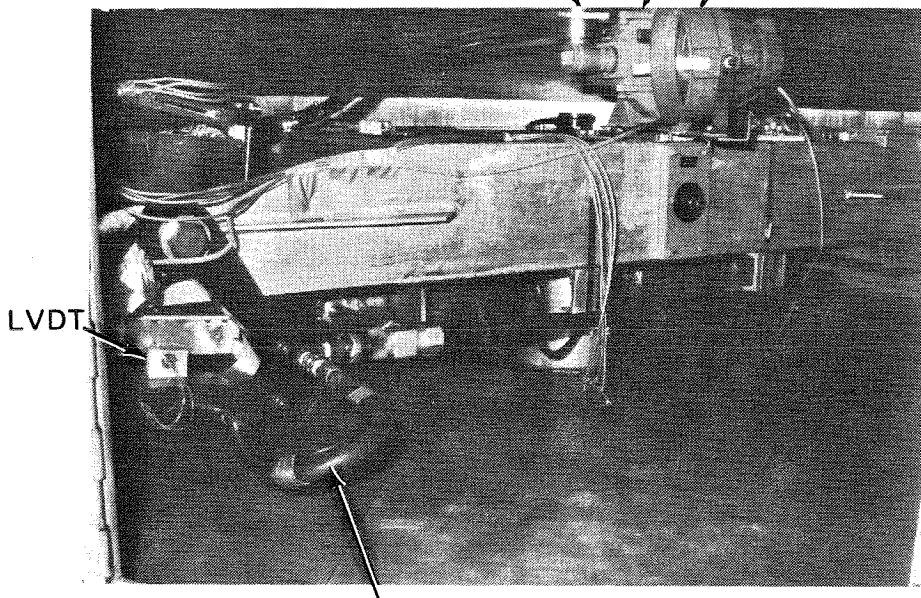
The controller is used to drive a servo valve in dynamic tests whether air or



ROTATION UNION



ROTATING UNION  
HIGH SPEED CAMERA  
AND LIGHT



HYDRAULIC FLUID: INPUT TO THE SERVOVALVE

FIGURE 5.10: THE HYDRAULIC SYSTEM

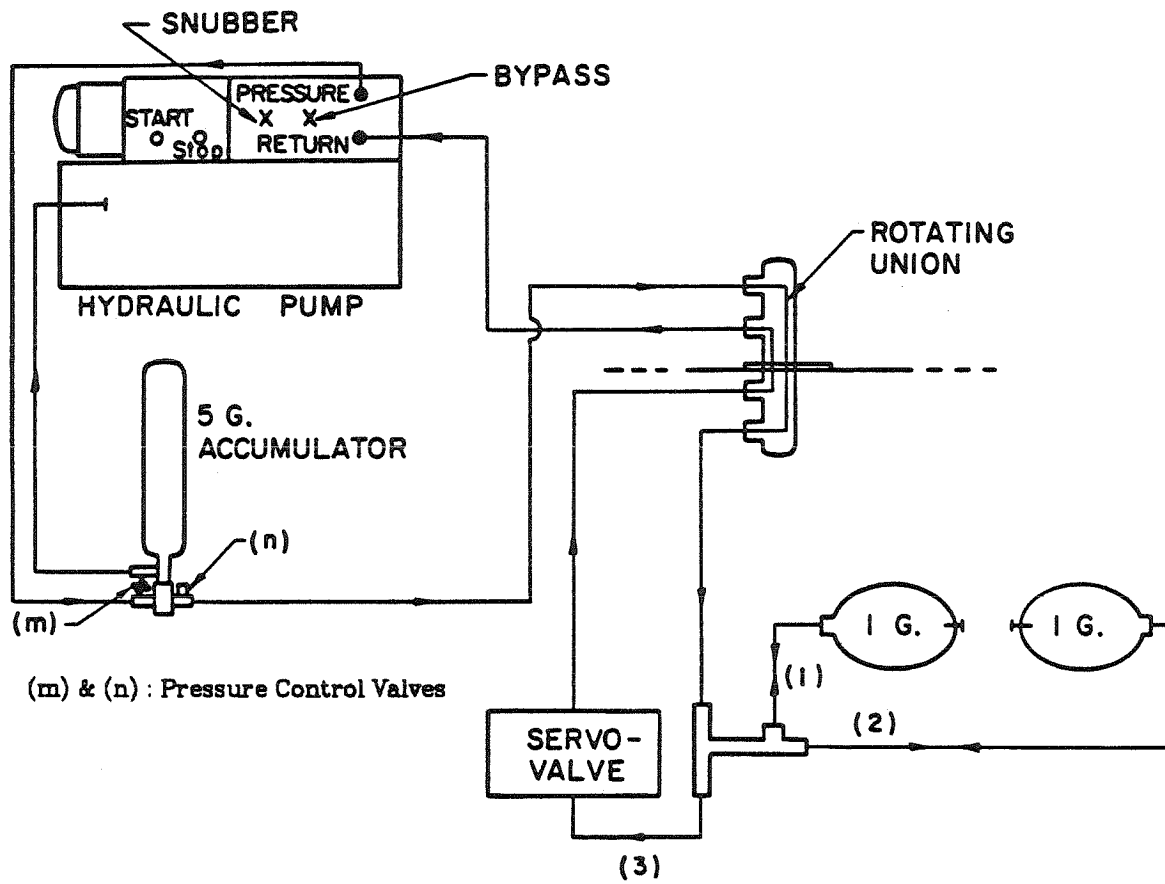


FIG. 5.11 THE HYDRAULIC LOOP

hydraulic fluid is used as medium.

In a test, the servo valve is required to follow a certain displacement function. This function is the one that has to be generated for the electrical signal applied to the servo valve.

An electrical analog signal generator (B&K Precision 3020 Sweep/Function Generator) was used under the control of the computer to generate the signal. The output of the signal generator is connected to the controller. A line with a relay connects the signal generator to the controller. This relay is controlled by the computer. When the computer program says "go" the relay is closed and the signal passes from the signal generator to the controller. When the computer program says "stop" the relay is opened and the signal cannot pass any more.

The controller will send to the servo-valve the signal, given by the signal generator or the computer, through a slipring. The servo valve is supposed to open and close according to this signal (voltage applied).

It is possible to have a feedback mechanism using a linear variable differential transformer (LVDT) (Fig. 5.10). This tells the controller how the valve is effectively moving, and if the displacement is not what it was supposed to be, corrections can be made by the controller.

The MTS controller can receive any type of signal, sine wave, square wave, symmetric or nonsymmetric wave, random noise (using a noise generator) etc. Figure 5.12 depicts the test set up for generation of electrical input signal to the controller.

### 5.2.3. Model Structures

Four rigid model towers were used in all the transient and steady-state forced vibration tests. Two of the towers had rectangular cross sections, one a solid piece of aluminium, and the other a hollow aluminum box. The hollow tower was built from a piece of aluminum channel, with a front panel screwed to

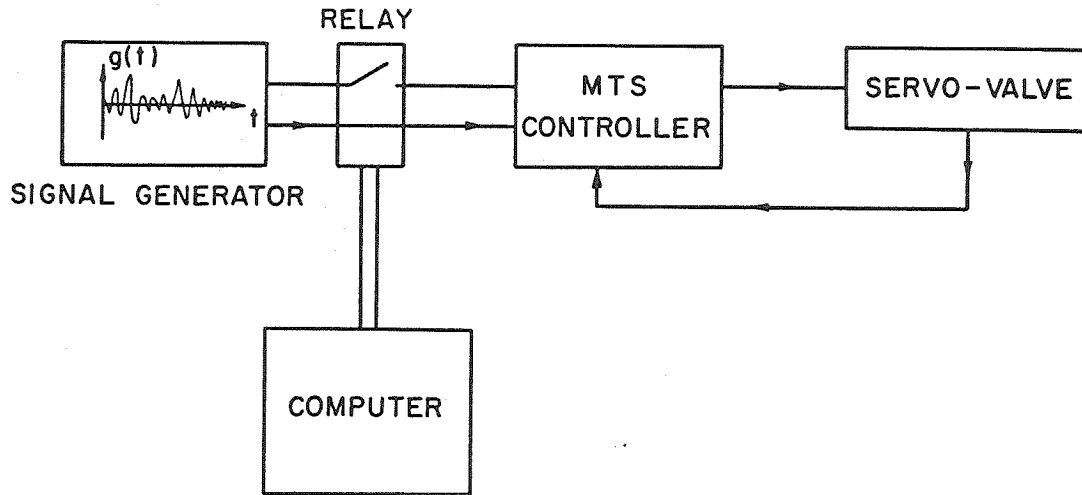


Fig. 5.12. USE OF AN ELECTRICAL SIGNAL TO DRIVE THE SERVO-VALVE

it. Two small plates were screwed to the top and the bottom of the tower. The other two rigid towers were hollow cylinders machined from aluminum pipes to the required diameter and wall thickness. The two ends of the cylinders were covered with rigid circular plates. Two very short towers (circular disks) were also used in order to study sliding and vertical modes of vibration. In addition, three more rigid hollow cylindrical aluminum towers, with linear dimensions in the ratio of 1:2:3 (Fig. 5.13), were used in the "modelling of models" tests, previously referred to in Chapters 1 and 2.

The values of the moment of inertia for the towers were determined experimentally by hanging the towers from a bifilar suspension of known dimensions, and measuring the natural frequency of rotation. The calculated values of moment of inertia for the models were less than 1 per cent different from the experimental values. The properties of the rigid towers are given in Table 5.2. In this table to each model tower an identification number is assigned for future reference. Bases of different sizes and geometries could be fitted on to the

Table 5.2 Physical Properties of the Towers

Tower Shapes →	Rectangular Towers		Cylindrical Towers						
	Tower (1)	Tower (2)	Tower (3)	Tower (4)	Tower (5)	Tower (6)	Tower (7)	Tower (Disk-8)	Tower (Disk-9)
Height (in)	8.00	6.32	7.00	5.25	2.50	5.00	7.50	0.66	0.95
Diameter (Length) (in)	1.83	1.78	3.00	3.00	1.25	2.50	3.75	2.00	3.00
Wall Thickness (Width) (in)	1.00	0.76	0.20	0.20	0.125	0.250	0.375		
Height of Center of Gravity (in)	2.98	3.23	3.33	2.47	1.25	2.5	3.75	0.53	0.58
Weight (lbf)	0.96	0.41	1.49	1.20	0.13	1.00	3.40	0.36	1.36
Mass Moment of Inertia (lb-in <sup>2</sup> )	2.99	1.28	9.84	5.17	0.101	3.23	24.6	0.80	0.84

Note:<sup>(1)</sup> The mass moment of inertia is calculated with respect to the rocking rotational axis of tower, passing through the center of gravity.

towers 1 and 2 and extra mass could be screwed onto the tops of all models to increase the mass and moment of inertia if required. The tower 2 was designed such that by removing the front plate it was possible to add extra mass at any arbitrary elevation thereby varying the moment of inertia without any change in the total mass of the tower. In this way, a fairly extensive variation of the important tower parameters could be undertaken, and these were chosen to correspond approximately with typical scaled values from real structures, although the structures themselves were modeled as being perfectly rigid. In the case of tower 1 for each different footing extra masses were added to the tower top keeping the ratio  $\frac{\sqrt{M}}{I}$  constant (where M is the mass and I is the moment of inertia of the tower). The reason for this will be discussed in Chapter 8. For the tower 2 it was possible to change the footings while keeping all other parameters constant. Figure 5.14 shows the collection of all towers, masses, and footings used in this study. Properties of the complete model structures, used in each particular test, will be given in Chapter 6 "Test Procedure and Data Reduction".

#### 5.2.4. SOIL CONTAINERS

Essentially only two soil containers were needed for all the tests. However, in the first group of tests two cylindrical vessels other than the containers in the rest of the experiments were used. The following buckets were used in the tests:

(A) Group 1 tests, "Explosion Generated Free Oscillation":

- Two cylindrical steel vessels: one 8.5" high and 8" diameter, with 0.4" wall thickness. The other 10" high and 15" diameter with 0.15" wall thickness and fortified with two rings one near the top and other at the midheight.

(B) Group 2 tests, "Steady-State Forced Vibration":

- One cylindrical aluminum bucket with an horizontal upper ring, 12" high and 12" diameter, and a 0.3" wall thickness.

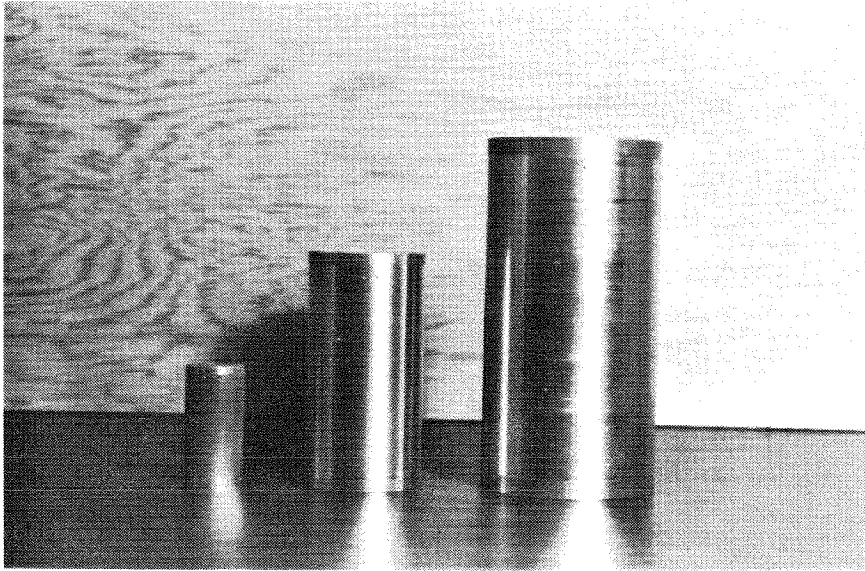


**FIGURE 5.13: TOWERS IN "MODELLING OF MODELS" TESTS**

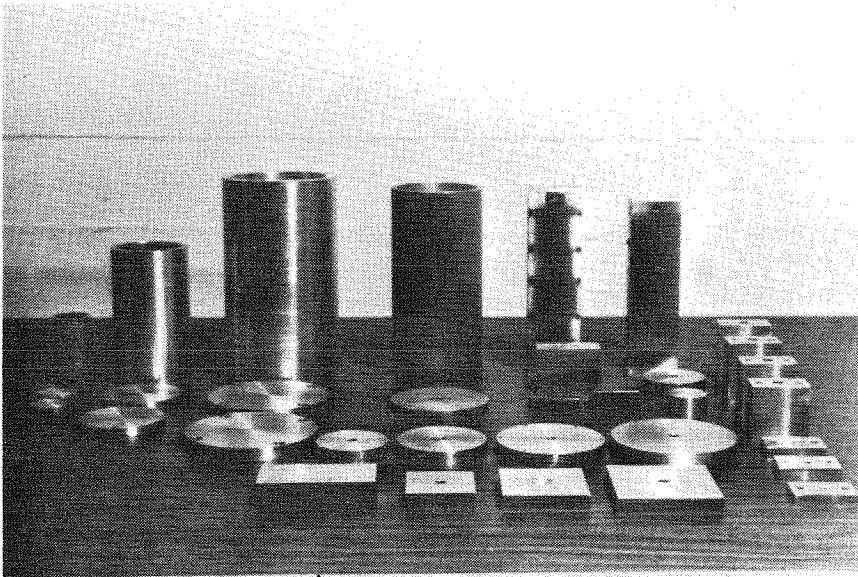


**FIGURE 5.14: COLLECTION OF TOWERS, FOOTINGS AND MASSES USED IN TESTS**

(C) Group 3 tests, "Transient Shaking of the Soil Container":

- One rectangular container 22" x 7" x 10" with a front glass wall.

### 5.3. INSTRUMENTATION

#### 5.3.1. Description of the Different Devices

##### *Accelerometers*

The accelerometers used in this investigation are Entran Devices Inc. Model EGA-125F-500D miniature accelerometer. The accelerometers employ a fully active Wheatstone Bridge consisting of semiconductor strain gages. The strain gages are bonded to a simple cantilever beam which is end-loaded with a mass (Fig. 5.15). Under acceleration, the force on the cantilever is created by the  $g$  effect on the mass ( $F = ma$ ). The accelerated mass creates a force which in turn provides a bending moment to the beam. The moment creates a strain (proportional to the acceleration) which results in a bridge unbalance. With an applied voltage, this unbalance produces a millivolt deviation at the bridge output, which is proportional to the acceleration.

A very attractive feature of this type of accelerometer is its very small size. The entire unit (minus the leads) weighs only 0.02 oz. The accelerometer unit is 0.270" long by 0.145" wide by 0.105" high and is mounted on a 0.270" x 0.37" x 0.040" flange as shown in Figure 5.16. The bold-faced arrow indicates the sensitive axis. The accelerometers are attached to a model with two 0-80 hex screws. The accelerometer has a range of 500g with a nominal sensitivity of about 0.5 mV/g (varies slightly from this with each particular unit), an input impedance of about 1150 ohms, an output impedance of about 550 ohms, and a resonant frequency of 3000 Hz. In addition, the unit is damped to 0.7 of critical using a viscous fluid medium. This helps to eliminate resonance and allows a useful frequency range of DC to 1000Hz. The excitation voltage is 15 v DC.



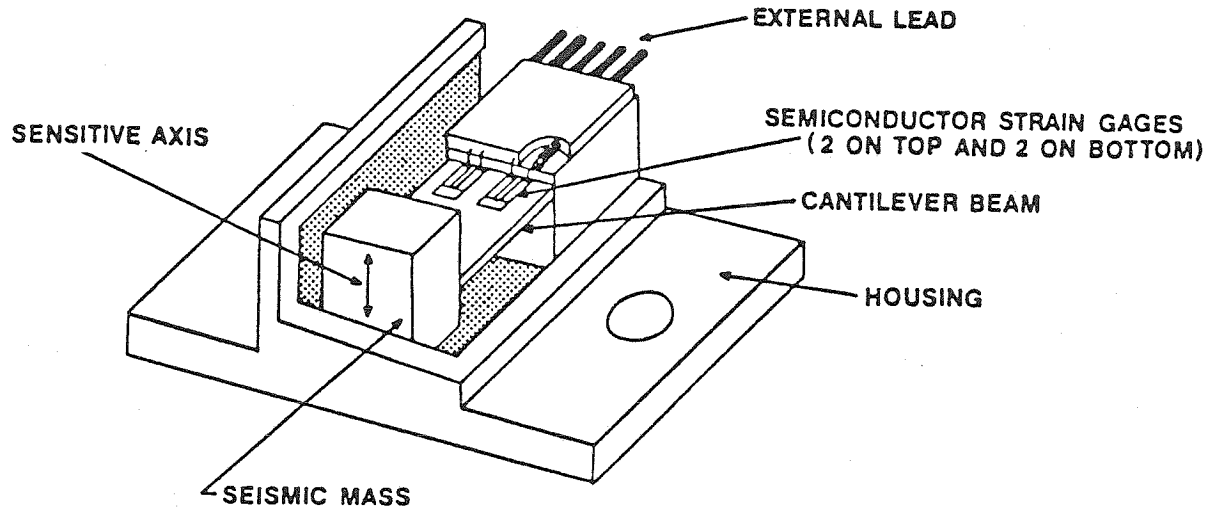


FIG. 5.15 ACCELEROMETER CUTAWAY (FROM ENTRAN DEVICES)

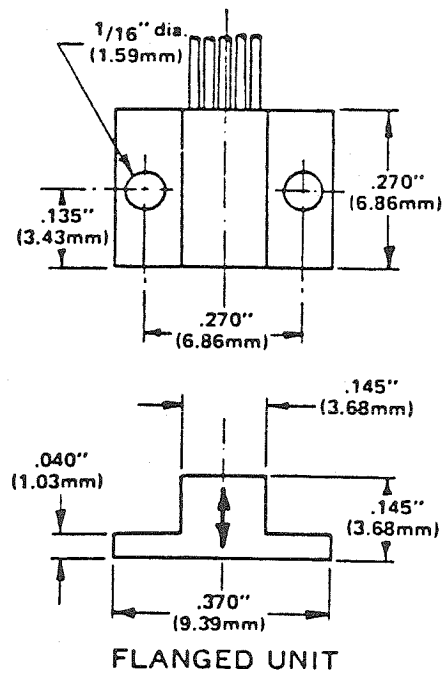


FIG. 5.16 ACCELEROMETER DIMENSIONS (FROM ENTRAN DEVICES)

### *Pressure Transducers*

The pressure transducers are Entran Devices Inc. Model EPF-200-50 Flatline Pressure Transducers. The transducer consists of a semiconductor strain gaged circular diaphragm less than 0.2" in diameter constructed of 17-4 PH stainless steel. This is a piezo-resistive pressure transducer with a fully active semiconductor bridge. Similarly, as with the accelerometer, a load on the diaphragm will create a strain (proportional to the pressure) which results in a bridge unbalance. With an applied voltage, this unbalance produces a millivolt deviation at the bridge output, which is proportional to the pressure.

The transducer is very small (Fig. 5.17) and thin being only 0.040" thick. It has a range of 0 to 50 psis with a nominal sensitivity of about 1.5 mV/psi (varies slightly from this with each particular unit), an input impedance of about 750 ohms, an output impedance of about 250 ohms and a resonant of 50 KHz. The excitation voltage is 6 V DC.

Stress measurements in soils have often proved to be unreliable or unrealistic. Many factors affect pressure transducer measurements in soils, which should be considered with care in order to minimize the measurement errors (Weiler and Kulhawy, 1982). One of the important factors in the case of pressure measurements on the structures in contact with soil, such as retaining walls, shallow foundations, etc. is the extent of transducer protrusion from the structure surface. It is important to provide a housing for the transducer inside or recessed into the base of the model in order not to create perturbations of the soil and disturb the stress field around the transducer. For the above reason transducers were placed inside housings recessed into the aluminum rigid bases, flush with the surface. Figure 5.18 shows one of the footings with the transducers mounted on its surface.

To study the complete dynamic/static pressure distributions over the contact area between the soil and the footing, 5 rigid circular disks with different

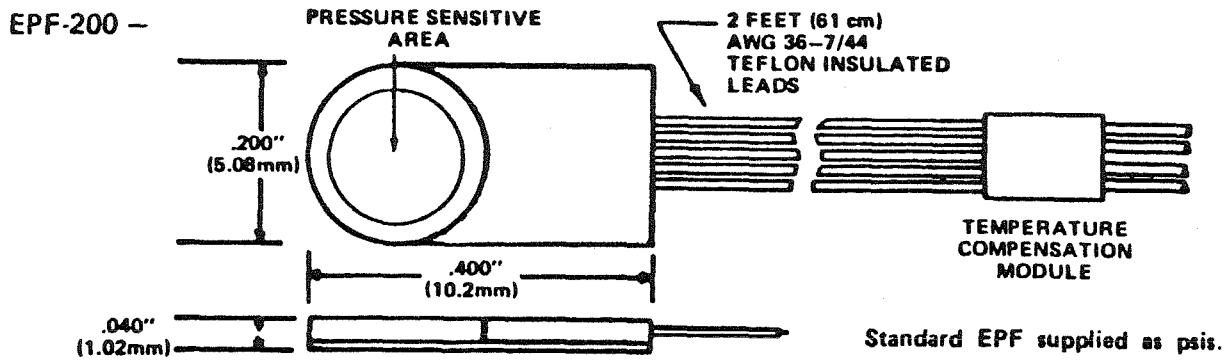


FIG. 5.17. PRESSURE TRANSDUCER (FROM ENTRAN DEVICES)

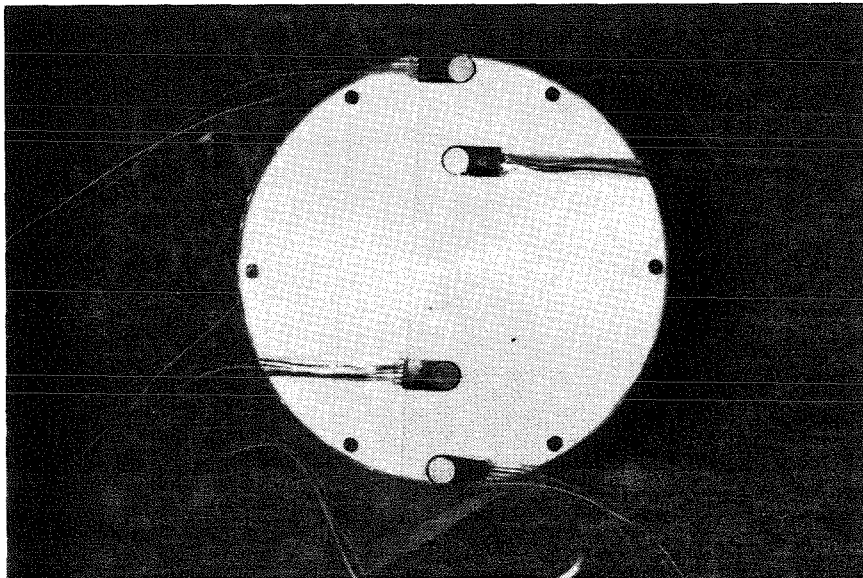


FIG. 5.18. PRESSURE TRANSDUCERS MOUNTED ALONG FOOTING DIAMETER

patterns of transducer locations were built (Fig. 5.19). The footings were all 3 inches in diameter and 0.4 inch thick. They were mounted at the base of the cylindrical tower 4 in different tests. Figure patterns A, B, and C of transducer locations were designed to determine pressure variation with the angle  $\theta$  around the footing and the other two to measure the pressure variation along the footing diameter normal to the rotational axis of rocking vibration.

#### *Displacement Transducers*

The Position Sensing Detector PIN-SC/10D obtained from United Detector Technology, Inc., was used in the tests. It is a dual axis position sensor that provides x and y axis information on the position of a light spot on the detector surface. This device senses the centroid of the light spot and provides continuous analog output as the light spot moves from the null point to the limit of the active area.

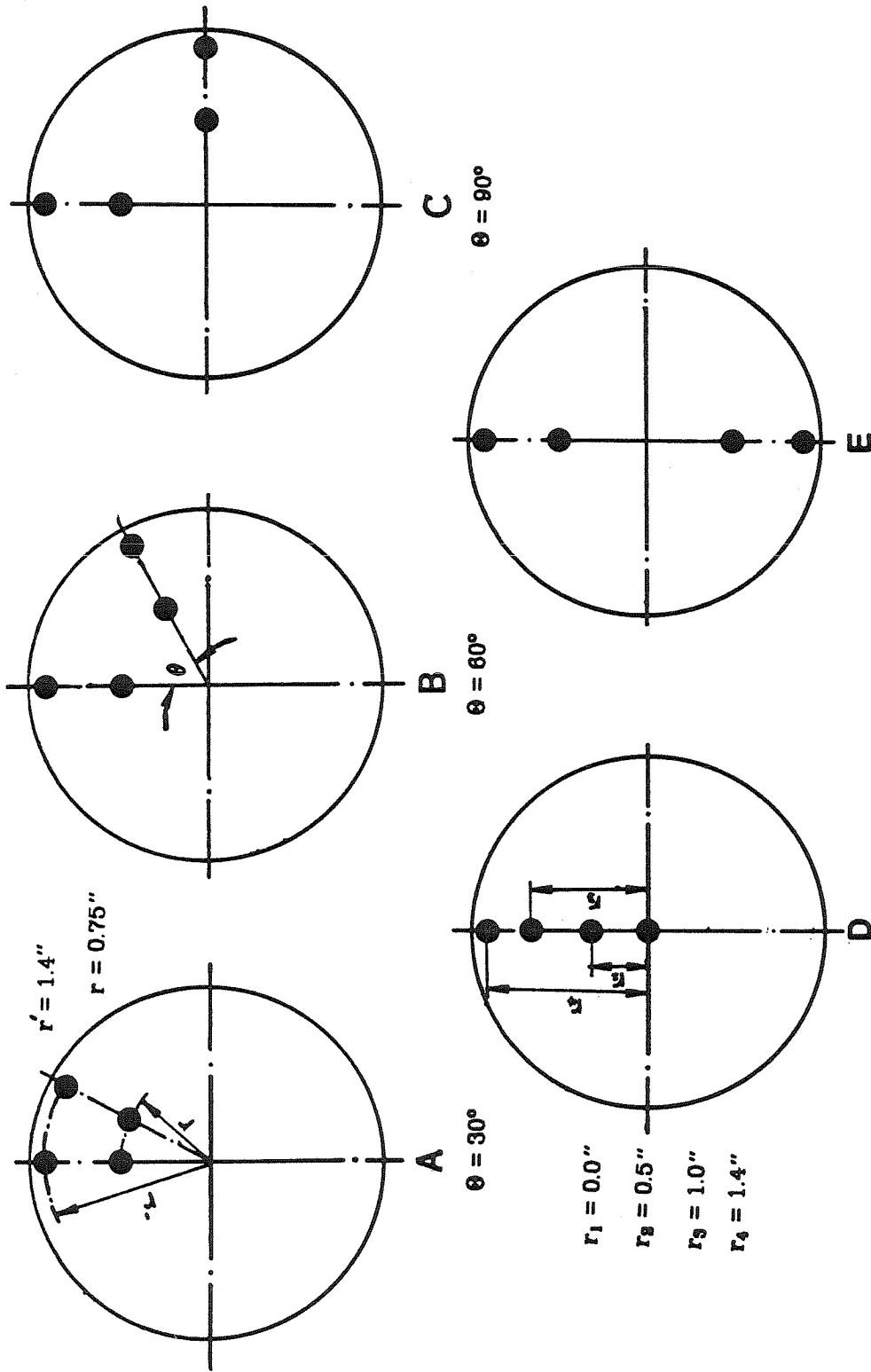
### 5.3.2. The Circuitry

#### *General Presentation*

As was seen in the description of the different instruments different excitation voltages were needed. So several power supplies were used to provide input voltage to the different instruments. During the tests these instruments took appropriate measurements and transmitted the data they got via an electrical signal called the "signal source".

Efforts to minimize the electrical noise in transducers outputs included the installation of a signal amplifier mounted on the acceleration arm in order to increase the signal to noise ratio as close to the signal source as possible. Coming out of the amplifier the amplified signals pass through the sliprings to the data acquisition system.

The signals were amplified with one LF3512 amplifier (Fig. 5.20). The



NOTE: RADIAL DISTANCE OF TRANSDUCERS ARE THE SAME FOR PATTERNS A, B, C, AND E

FIGURE 5.19: PATTERNS OF PRESSURE TRANSDUCER HOUSINGS ON FOOTINGS

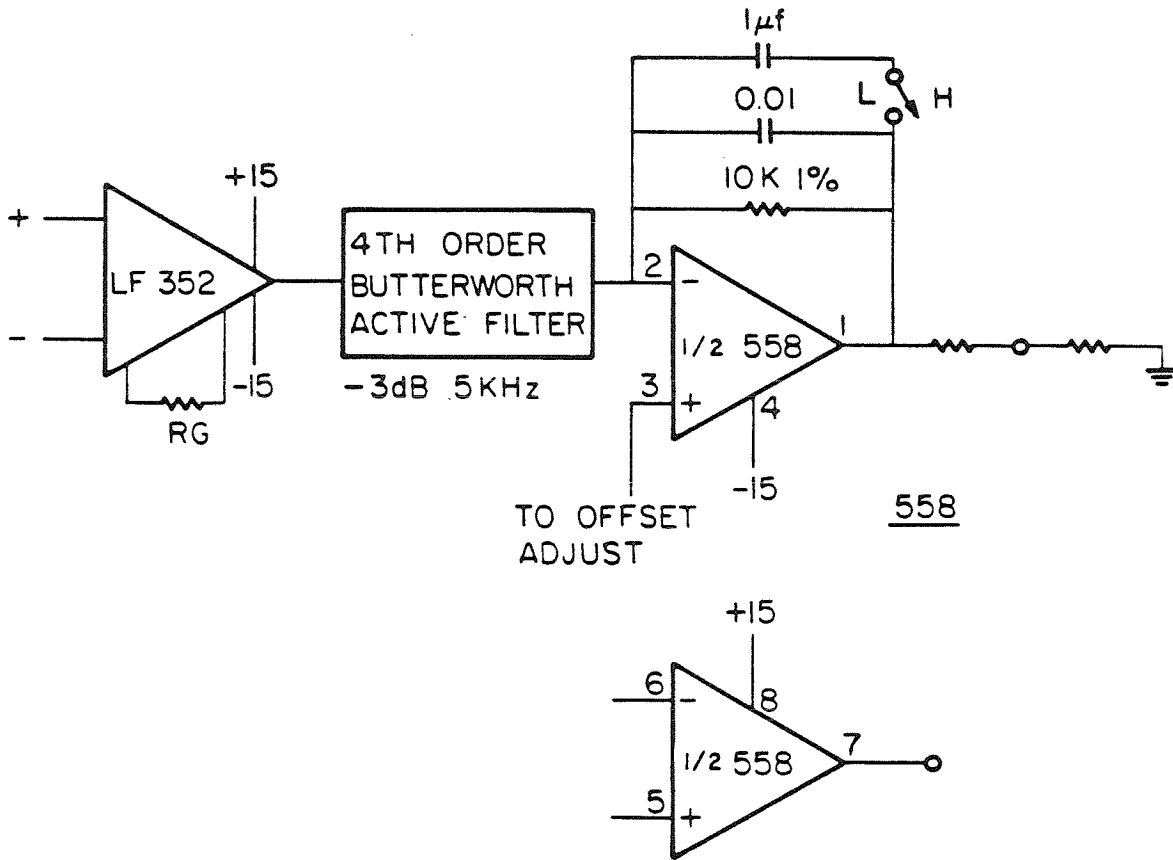


FIG. 5.20 AMPLIFIERS FOR PRESSURE TRANSDUCERS AND ACCELEROMETERS

amplifier had 16 channels with variable amplification factors. The displacement transducer PIN-SC/10D and the frequency counter had their own amplifiers. Output signals of the accelerometers, displacement transducers and pressure transducers were suitably amplified and filtered to minimize the high frequency noise inherent with centrifuge testing. The accelerometer circuit is shown in Figure 5.21. The pressure transducer circuit is similar to that of the accelerometer.

#### 5.4. CALIBRATION OF TRANSDUCERS

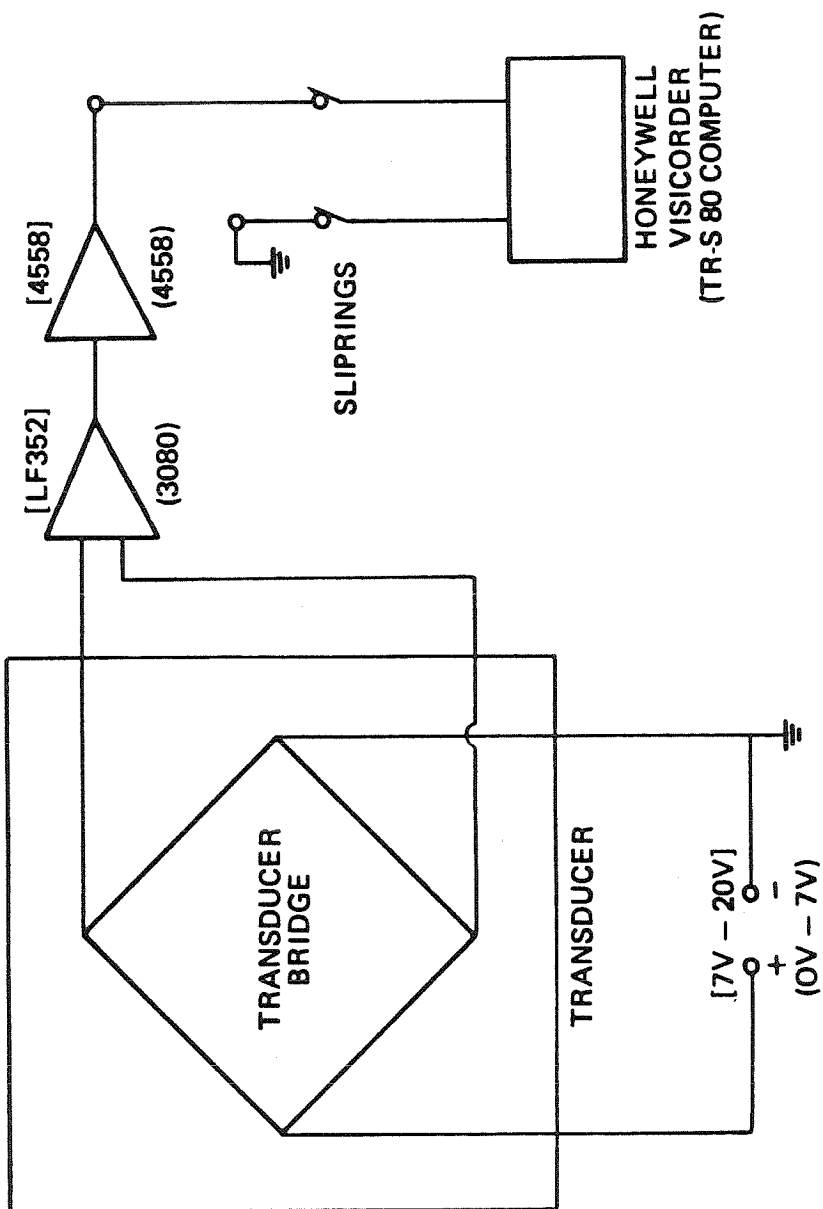
All pre-test calibrations were normally carried out using the entire electronic circuitry, i.e. the calibration signals were routed through the terminals, amplifier channels, filters, sliprings and data acquisition and reduction systems, which were used during the actual testing. Outputs of transducers were read on the computer or directly on a voltmeter. All transducers are linear and therefore require, each, two calibration factors (slope, and intercept). Table 5.3 presents the calibration factors, serial numbers, and classification labels used for the transducers in this investigation.

##### *Accelerometers*

They were placed with the sensitive axis facing downward on the floor of the centrifuge bucket which is at a radius of 41 inches from the centrifuge axis. Then by taking the centrifuge up to different accelerations 10, 20, 30g, etc., and recording the different outputs the calibration factors can be determined.

##### *Pressure Transducers*

These transducers were placed on the bottom of the centrifuge bucket at a radius of 41 inches from the centrifuge axis, and a layer of soil or water in a plastic bag placed on top of them. Then the output for the centrifuge stationary (1g) and spinning at 10, 20, 30g, etc was measured. The increase in g accelera-



[ACCELEROMETER]                      [CIRCUIT]  
FIG. 5.21  
(PRESSURE TRANSDUCER)



Table 5.3 Calibration Factors of Transducers

Transducer Type	Serial Number	Classification Label	Slope	Y-intercept
Accelerometer	SN7E9E-E9-9	A1	0.549	-0.358
Accelerometer	SN9595-A6-3	A2	0.516	-0.925
Accelerometer	2X1X-A8-3	A3	0.487	-0.766
Accelerometer	SN9J9J-A3-1	A4	0.514	-0.664
Pressure Cell	28J6C7-D7-2	P1	1.58	0.0
Pressure Cell	12J9J-D5-3	P2	1.51	0.0
Pressure Cell	12J9J-D4-2	P3	1.47	0.0
Pressure Cell	12J9J-D3-1	P4	1.40	0.0
Displacement Transducer	PIN-SC/10D	D1	$0.332 \times 10^{-3}$	$-0.11 \times 10^{-2}$
Displacement Transducer	PIN-SC/10D	D2	$0.337 \times 10^{-3}$	$-0.13 \times 10^{-2}$

Note: In above table the Y-Intercept is in millivolt and the slopes of the calibration lines for accelerometers, pressure and displacement transducers are in units of mv/g, mv/psi, and in/mv, respectively.

tion to N g's causes an increase in the soil or water unit weight by N and thus an increase in pressure, the pressure simply being the weight density of the soil or water (at the particular acceleration level) times the height. The calibration factors were determined using the resulting pressure-voltage curve.

Note that the calibration factor for a pressure transducer is best determined from a water bag test. Use of this calibration factor when the transducer is in contact with soil will give the pressure acting on the gauge. This pressure may not be the pressure which would be present in the soil in the absence of the gauge. The relative stiffness of gauge and soil is important in assessing the soil pressure. In addition the real soil stresses during unloading cycles will generally

be difficult to interpret from the gauge readings.

### *Displacement Transducers*

They were mounted on a platform moving in both X and Y directions in a horizontal plane. The output voltage from transducers versus the distance from a stationary LED yields the calibration factors.

## **5.5. DATA ACQUISITION AND REDUCTION SYSTEMS**

### **5.5.1. Data Acquisition**

The analog signals of the different instruments (pressure and displacement transducers, accelerometers, etc.) were amplified, passed through the sliprings and came out through coaxial cables in the "control room". There, they could be recorded by the Honeywell Model 1858 CRT Visicorder (see Chap. 3), or by the Analog to Digital Converter acquisition system (ADC), defined in detail in the next section.

*The ADC can accept inputs from 16 channels.*

There are also 3 sets of switches to control the data recording conditions:

- 1st set to give the number of channels being sampled.
- 2nd set to give the number of kilobytes of information being stored.
- 3rd set to set the speed of the data sampling from 10 to 258 microseconds between data samples.

There are several buttons and lights:

- 1) the fast-slow button

Fast position: it will take data as fast as possible up to 100 KHz for one channel of data. Then it will send the data directly to the ADC's own memory. In this case the computer just says "go" and the data are acquired automatically.

The slow position: It doesn't matter what speed is set at the back, in this case it is the computer program that determines the rate of acquisition of the data.

Therefore it is up to controlling program to access the data fast enough so data are not lost.

Normally the ADC is connected to the computer which controls, by the program, the ADC.

The ADC acquires data in the range  $\pm 2V$  and in this range it will give a number between 0 and 4095. (it is a 12 bit ADC) so

-2V corresponds to 0

0V corresponds to 2048

2V corresponds to 4095

It can be seen that 1 mv corresponds approximately to 1 bit of information so if the signal is very small, inferior to 1 mv, it is lost; no data will be acquired. That is why an amplifier is used for the signal coming out from the transducer. If a signal exceeds +2v, it will run out of scale.

### 5.5.2. Data Reduction

For the control of the data input and its reduction a Radio Shack TRS80 Model I computer was used. The required software was designed to match the characteristics of the available hardware. Details of the programs are not discussed here. The process of taking and storing data is:

At a special frequency in steady-state forced vibration tests or just before starting a transient vibration test the controlling program commands the ADC to take data. Then the program allows one to take a part of the data of the ADC and put it in the memory of the computer. Once data are in the computer's memory, computing or reducing the data according to the program is possible, or they can be stored on a disk for later utilization. A speed-up module which is an addition to the computer, speeds up the computer clock by a factor of 2. This allows it to do all operations, except disk operations, twice as fast. All the data stored in the ADC can be extracted part by part, according to the size of

the computer's available memory. This is generally smaller than the one in the ADC.

Because of the large body of data recorded in this study, the stored data on the floppy disks were then transferred to a PRIME500 mini-computer through the RS232 data interface. In this way the speed of data reduction was increased considerably.

*REFERENCES*

- [1] Allard, M. A., "Caltech Centrifuge Manual," Soil Mechanics Laboratory, California Institute of Technology, Pasadena, California, 1983.
- [2] Weiler, Jr., W. A., Kulhawy, F. H., "Factors Affecting Stress Cell Measurements in Soil," Journal of Geotech. Engrg. Div., ASCE, Vol. 108, No. GT12, Dec., 1982, pp. 1529-1548.

## CHAPTER 6

### TEST PROCEDURE AND DATA REDUCTION

#### 6.1. GENERAL STEPS OF EXPERIMENT SET UP

In every test performed the following general procedure in preparing the experiment was carried out.

To begin with, the soil container was mounted on the arm. For the test group 1 (the explosion-generated free oscillation) the rectangular bottom plates of the cylindrical vessels were bolted to the magnesium platform at the active end of the arm, where the experiment took place. The cylindrical bucket for the second group of tests (steady-state forced vibration tests) was fixed in place by four chains hooked to the bucket rim and bolted to the magnesium platform (Fig. 6.1). In the case of the third test group (transient shaking of the soil container) the magnesium platform had to be removed and substituted with the special frame of the test bucket (see Chap. 5), and then the bucket was fixed on the frame.

Dry Nevada Fine Sand was then placed in the centrifuge bucket to a predetermined depth and density. For the medium to dense conditions applied in this study the soil was compacted with a 2 lb weight in layers of one or two inch thickness. The number of blows for the compaction of each layer was about 40 times, determined from the compaction tests performed on the soil. This way a dry unit weight of about 103 to 106 pcf was obtained in different tests.

The next step was to balance the arm adding exactly the same weight present at the active end of the arm, including the weight of the model and other equipment, as a counterbalance, to the other end of the arm. Then the centrifuge was brought up to speed and run at the  $g$ -level used in the test for about one hour allowing the soil to settle and stabilize before setting up the model and beginning the test. Depth of the soil was measured next and knowing the

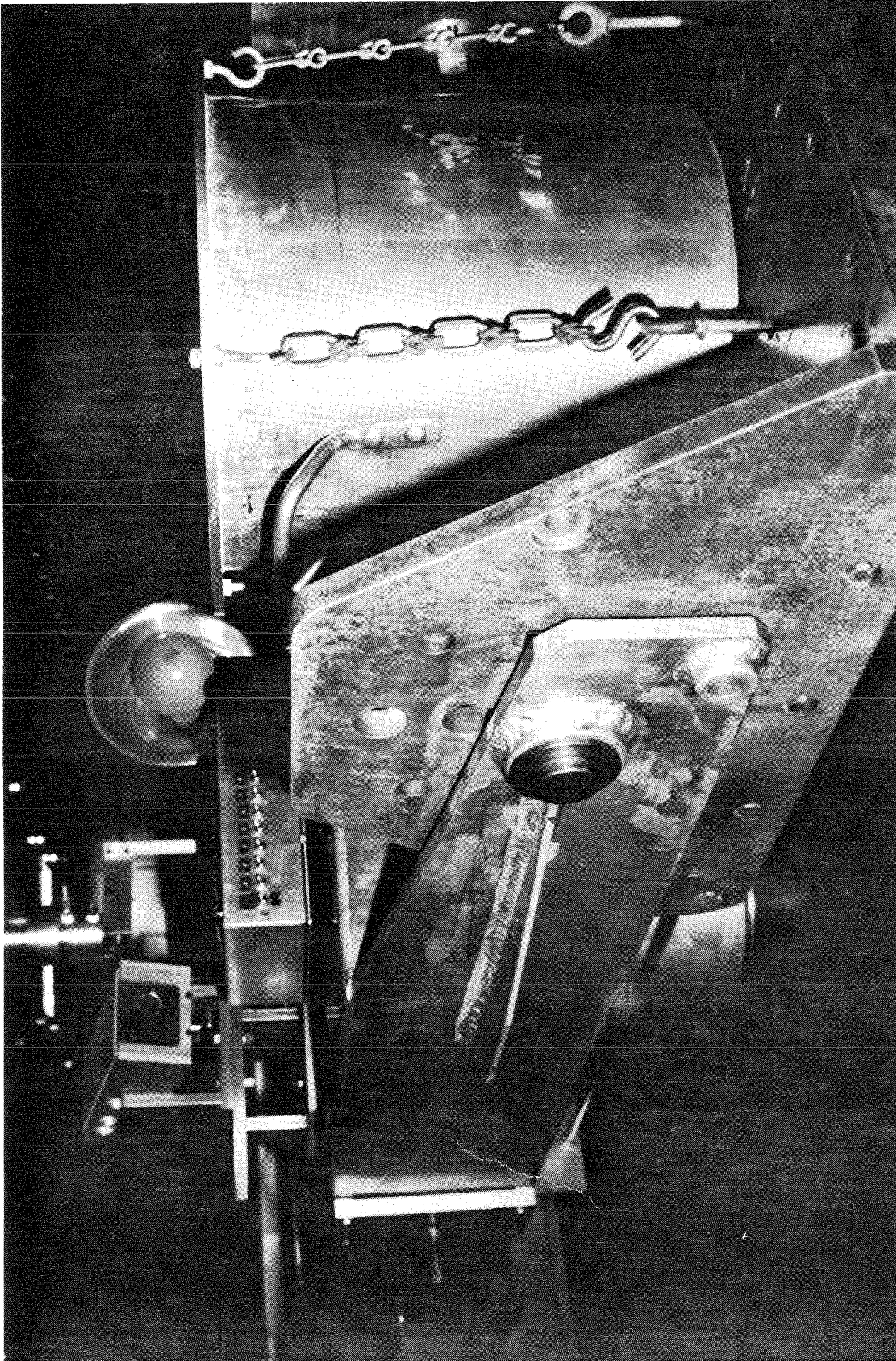


**FIGURE 6.1: A VIEW OF CENTRIFUGE ARM WITH CYLINDRICAL BUCKET FOR TEST GROUP 2**

volume and the weight of the soil in the container, the soil density was determined. The soil densities and depths for each group of tests are given in the next section.

The soil surface was leveled and smoothed especially at the center where the footing was to be located. Next, the model structure with appropriate parameters, and transducers required for each special test was securely placed on the sand (see Fig. 6.5). The tower was checked carefully to be level by placing a miniature leveling bubble on the footing and on the tower top. In the tests with embedded foundation, after locating the tower on the soil surface, more sand was placed around the tower and was compacted carefully to the required density and depth of embedment. Figure 6.2 shows tower 4 placed in the sand at different depths of embedment, prepared for a steady-state forced vibration test.

In all the tests transducer readings were recorded at the following stages of the experiment:

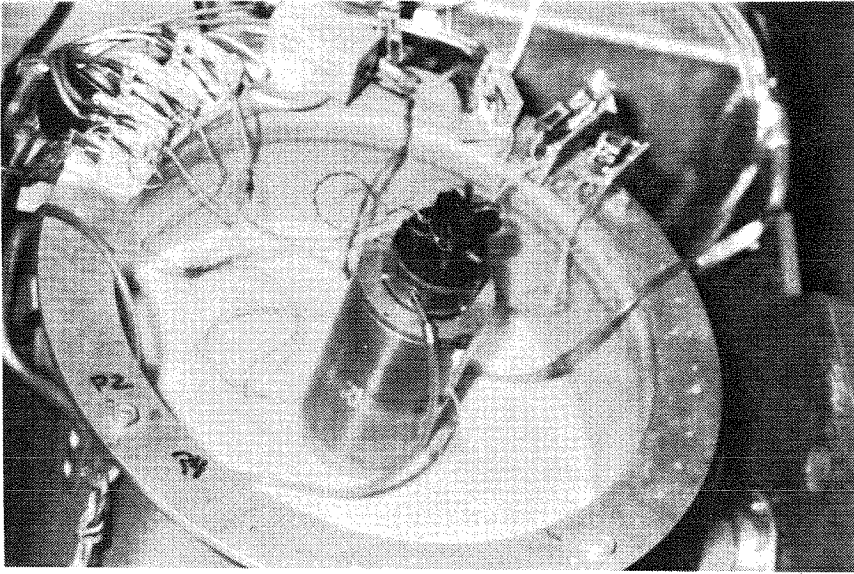
- (i) At 1g acceleration level before and after starting the test
- (ii) At the acceleration level predetermined for the main test, just before and after the shaking, and during the dynamic test.
- (iii) At some other intermediate acceleration values before and after the dynamic test

In this way any change in the offset of the transducer outputs was detected to help in controlling the test process, and in determining the static contact pressures underneath the footing and the permanent displacements of the tower because of tilting and/or slipping on the sand surface.

Some other features common to all the tests were:

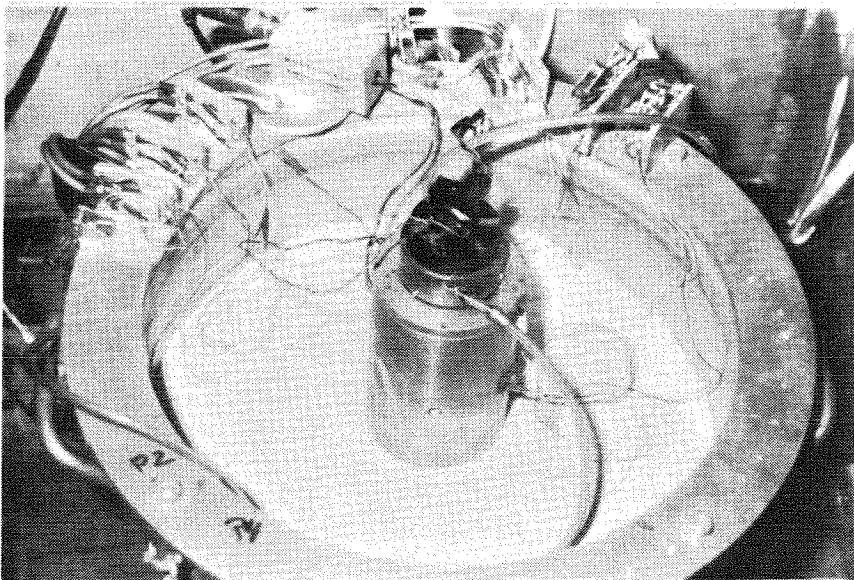
- (1) In order to simulate more closely the contact conditions between the footing and the soil, sand was glued to the footing surface resulting in an





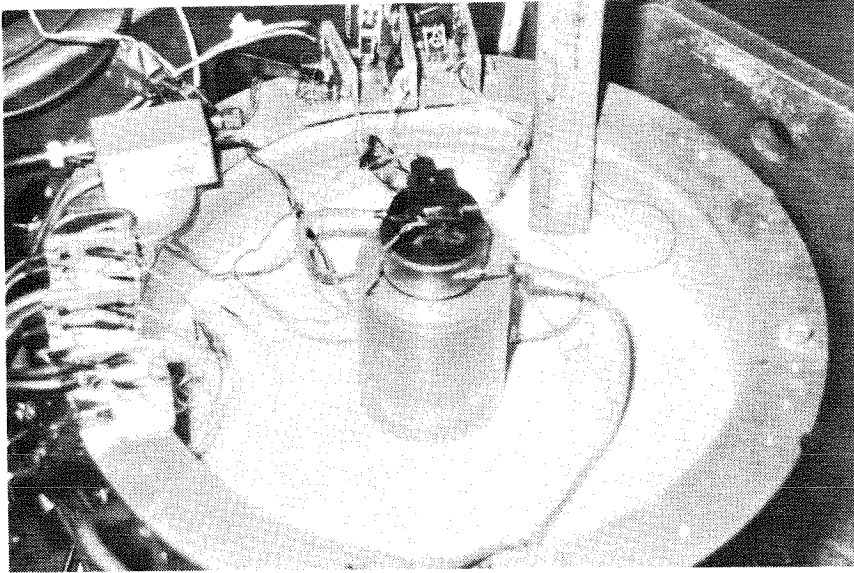
(a)  $d_e = 0$

$d_e$ : DEPTH OF EMBEDMENT  
R: FOOTING RADIUS

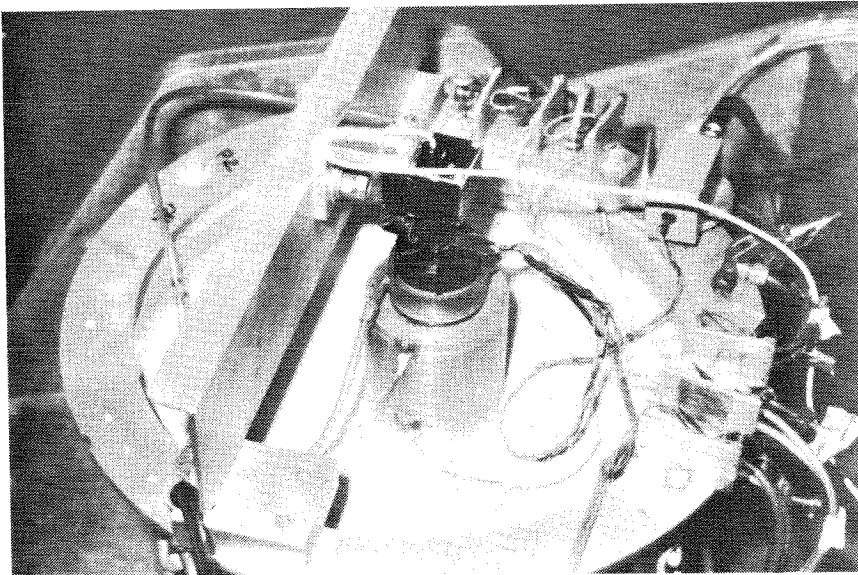


(b)  $d_e = R/2$

**FIGURE 6.2: MODEL TOWER EMBEDDED AT DIFFERENT DEPTHS IN SAND**



(C)  $d_e = R$



(d)  $d_e = 3R/2$

**FIGURE 6.2: (CONTINUED)**

increase in contact friction.

(2) The required centrifugal acceleration for the test was calculated from the centrifuge rotational speed and the distance from the axis of rotation to the soil surface plus radius of the model footing. Therefore, properties of the soil, affected by the confining pressure were exactly scaled to the required prototype values at a depth equal to the footing radius. The reason for this choice of the arm distance will be discussed in Chapter 7.

Using different sizes of soil buckets in these experiments, brings up the question regarding the effect of soil container boundaries on the dynamic behavior of the foundation-soil system. Ratio of the width or diameter of the smallest bucket over the diameter of the largest footing was equal to 2 and the diameter of largest bucket was 8 times larger than the smallest footing size. Only a few tests with the similar models and soil conditions were performed in the different buckets which will be discussed later. The procedure in running each dynamic test was different depending on the type of the loading. The next section of this chapter will amplify each special test method used.

## 6.2. SPECIAL TESTING METHODS

### 6.2.1. *Explosion Generated Free Oscillation Tests*

After the tower was primed with a few grains of explosive, and placed on the sand, the capacitor was charged while the relay was open, and the copper wires coming out from the explosive nest were connected to the capacitor through the relay. Next the package was spun up to speed to a predetermined centrifugal acceleration and then by closing the relay the explosive was detonated. Traces of the subsequent vibration of the tower were recorded, from which the frequency of oscillation and damping ratio at that modelling scale could be measured.

Experiments were performed on models constituted from the rigid solid rectangular tower (tower 1) and different rigid circular footings as the base of rectangular tower. Table 6.1 summarizes properties of the models I and II (solid tower with different size circular footings and added masses at top) and other pertinent test information.

Note that for the Model I the air-driven shaker was attached at the top (Fig. 6.3), so that the free oscillation test results could be compared directly with the results of steady-state forced vibration tests. Because of difficulties in working with explosives the tests were not carried on for all the model towers with different possible parameters. Many problems were faced in using the cap gun powder as an explosive. The energy released from the powder was very small and variable from test to test. Moreover, closure of the relay, and the subsequent electrical spark, produced a high frequency and large amplitude electrical noise which rendered some problems in data reduction. Therefore, these tests were performed as a limited effort aimed at studying some critical aspects of the vibration of rigid structures, such as detecting lift-off of the foundation, by measuring the contact pressure near the edge of the base.

Usually two accelerometers and one pressure transducer were used in the tests. Accelerometer A1 was placed near the tower top, at 5.75 inches elevation from the footing surface, measuring horizontal acceleration associated with the rocking-sliding motion of the tower. The other accelerometer (A2) was located on the footing surface, at the edge, measuring vertical acceleration during rocking. The pressure transducer (P1) was located underneath the footing, at the edge, exactly at the point below accelerometer A2. The output of transducers after amplifying and passing through the sliprings was recorded on the Visicorder at a rate of 50 to 100 in/sec depending on the particular test.

A small amplitude oscillation was observed in the tower before and after the

Table 6.1 Properties of the Models in Group 1 of Tests

Test Number	Weight W (lb)	Mass Moment of Inertia $I_{c.g.}$ (lb-in <sup>2</sup> )	Height of Center of Gravity $h_{c.g.}$ (in)	Mass Moment of Inertia w.r.t. Base $I_b$ (lb-in <sup>2</sup> )	$\frac{\sqrt{M}}{I_b}$ (lb <sup>-1/2</sup> -in <sup>-2</sup> )	Footing Diameter D (in)	g Level
1,2,3	1.413	8.29	3.54	26.0	$45.72 \times 10^{-3}$	3.0	69.5
4,5,6	1.13	4.58	3.03	14.95	$71.10 \times 10^{-3}$	2.0	63.0

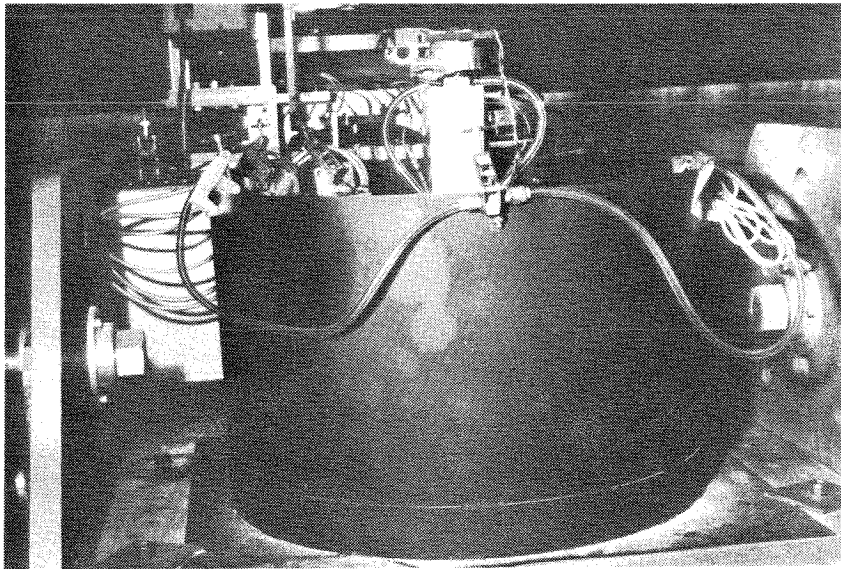


FIG. 6.3 THE TOWER AND SOIL CONTAINER IN TEST GROUP 1

explosion during spinning the centrifuge. An initial guess suggested that the tower was oscillating in response to random gusting and air turbulence inside the centrifuge chamber. Therefore, it was expected that the tower would oscillate at its natural frequency and that the frequency would vary as the centrifuge speed changed (Morris, 1981). However, this was not the case since the frequency of oscillation remained unchanged above 30g centrifugal acceleration. In order to discover the source of the vibration, the tower was placed on the sand, prepared in the 8 inch diameter steel bucket (see Section 5.2.4), and then the bucket and the tower were covered by a plastic container shielding the whole test set up from the wind. The centrifuge arm was also instrumented to detect any vibration in the arm. After spinning the centrifuge the following facts were observed:

1) The tower oscillation even after the test set up was isolated from air flow in the centrifuge chamber did not disappear; thus, it could not be a wind-induced vibration.

2) The ratio of the top horizontal acceleration to the vertical acceleration of the footing edge was the same as the ratio between the tower height and the footing radius, thereby proving that the tower was in fact oscillating (in the rocking mode) and the observed signal was not an electrical noise.

3) A similar oscillation with very small amplitude was detected in the centrifuge arm, which also did not change in frequency above 30g centrifugal acceleration.

4) The frequency of oscillation increased linearly with the increase of centrifuge speed; i.e. it changed as the square root of the g-level below the 30g acceleration limit (Fig. 6.4).

It was concluded that the probable source of the oscillation was the centrifuge motor which was located underneath the centrifuge chamber and hanging from it.

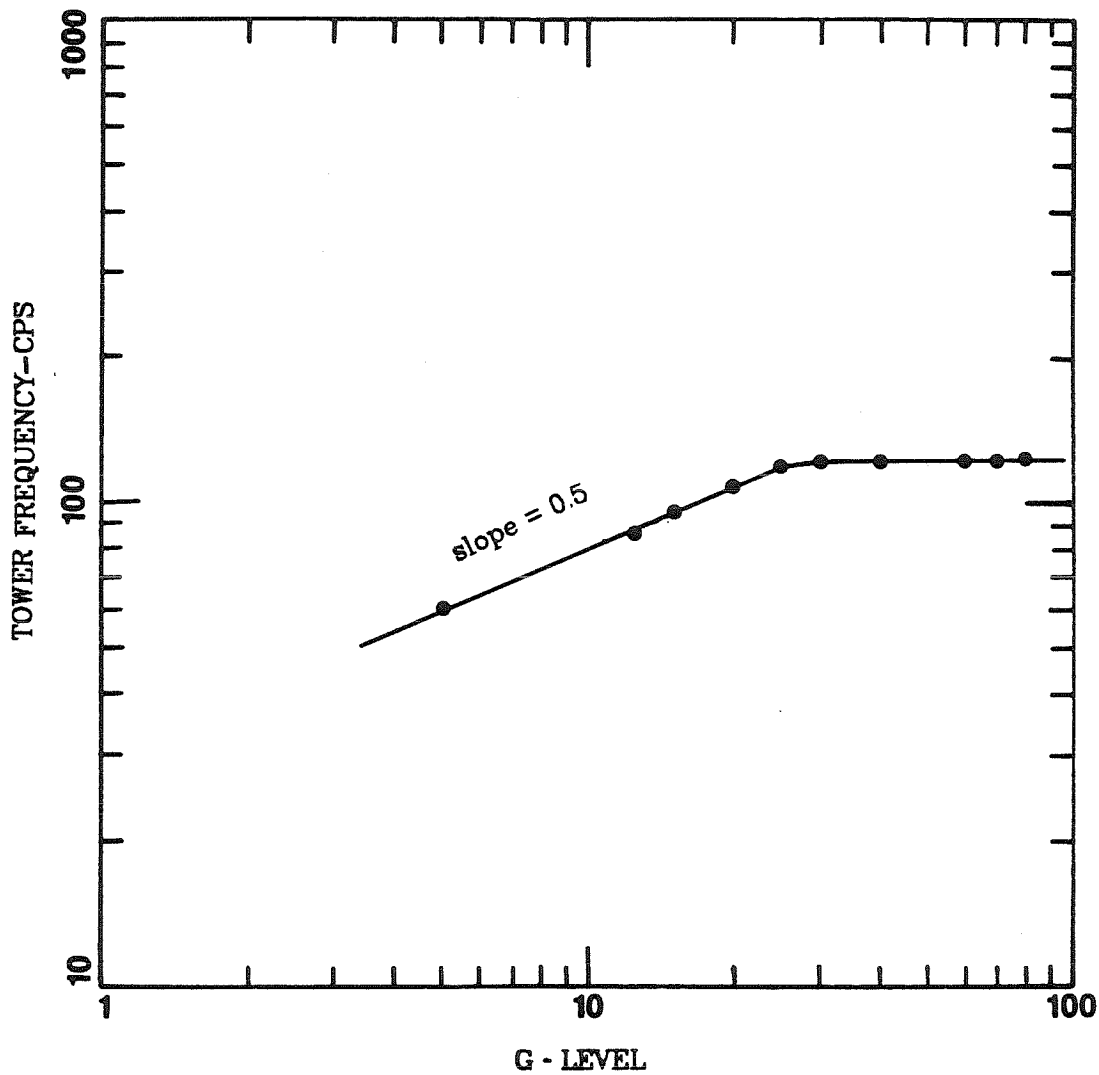


**FIGURE 6.4: VARIATION OF TOWER OSCILLATION FREQUENCY (DUE TO CENTRIFUGE ARM VIBRATION) WITH CENTRIFUGAL ACCELERATION**

### 6.2.2. Steady-State Forced Vibration Tests Using Air-Driven Shaker

These tests constitute the main body of the experiments in this investigation. Almost all the tests were performed to study the rocking-sliding mode of vibration, where the rocking oscillation was the major component of the motion. The effect of different foundation-soil parameters on the dynamic behavior of the rigid towers was studied by varying one particular parameter in each test series, while the others were left unchanged. These parameters included: (1) soil depth ( $d_s$ ); (2) footing shape and size ( $D$ ); (3) centrifugal acceleration ( $g$ -level) whose variation implies the modelling of similar prototype structures of different dimensions; (4) force level of the shaker which varies with change of the eccentric weight,  $w_e$ , in shaker; (5) moment of inertia of the model structure ( $I$ ); (6) the ratio  $\frac{\sqrt{M}}{I_b}$  (see Chap. 8); (7) Depth of embedment ( $d_e$ ). Table 6.2 summarizes model and soil properties in each of the above parametric studies.

In addition more experiments were performed to study:

- (i) Static and dynamic pressure distributions over the contact area
- (ii) Vertical mode of vibration of a rigid footing
- (iii) Rocking-sliding mode of vibration with emphasis on sliding motion of the model

After the sand was prepared in the bucket, the tower with the air-driven shaker (the counterrotating mass shaker) and the transducers, was placed on the soil surface. For rocking vibration of the tower the shaker was mounted on the top (see Fig. 6.3) and for sliding vibration it was mounted inside a hollow cylindrical tower (tower 4) on the base. Usually 2 to 3 accelerometers, 1 to 4 pressure transducers, and 1 displacement transducer, measuring  $x$  and  $y$  displacement components, were used to describe the complete dynamic behavior of the tower. Figure 6.5 shows a view of the centrifuge arm, transducers, amplifier, and a model structure (tower 1), with the air-driven shaker mounted on its top.



Soil-Structure Parameters	Test Number	Tower Number	W (lbf)	I <sub>C.G.</sub> <sup>2</sup> (lb-in <sup>2</sup> )	h <sub>C.G.</sub> (in)	I <sub>b</sub> (lb-in <sup>2</sup> )	$\sqrt{h} / I_b$ (lb <sup>-1/2</sup> -in <sup>-2</sup> )	D (in)	d <sub>s</sub> (in)	W <sub>e</sub> (lb)x10 <sup>-4</sup>	
Soil Depth	1,2,3,4,5	2	0.97	9.13	3.60	21.70	0.045	3.0	Section 7.2.2	0.84	
	25,26,27,28,29	3	1.75	14.32	4.0	42.37	0.031	3.0	Section 7.2.2	1.14	
Footings Shape and Size	Circular	10,11,12	Section 7.2.3	Section 7.2.3	Section 7.2.3	Section 7.2.3	0.041	Section 7.2.3	8.0	0.84	
		5,6,7	2	0.97	Section 7.2.3	Section 7.2.3	21.7	0.045	Section 7.2.3	8.0	0.84
	Square	41,43,44	2 (with added mass)	1.85	11.08	3.75	37.10	0.036	Section 7.2.3	8.0	1.14
		40,42,45	2 (with added mass)	1.85	11.08	3.75	37.10	0.036	Section 7.2.3	8.0	1.14
g - Level	Rectangular	46,47,48	2 (with added mass)	1.85	11.08	3.75	37.10	0.036	Section 7.2.3	8.0	1.14
		36,37,38,39	4 (with added mass)	2.13	10.87	2.34	22.56	0.065	3.0	8.0	1.14
Eccentric Mass of Shaker	44,50,51,52,53	2 (with added mass)	1.85	11.08	3.75	37.50	0.036	2.5	8.0	Section 7.2.5	
	31,55,56,57	4 (with added mass)	1.75	9.08	2.75	22.33	0.059	3.0	8.0	Section 7.2.5	
I <sub>b</sub>	29,31,62	Section 7.2.6	1.75	Section 7.2.6	Section 7.2.6	Section 7.2.6	Section 7.2.6	3.0	8.0	1.14	
	29,30,31,41	Section 7.2.7	Section 7.2.7	Section 7.2.7	Section 7.2.7	Section 7.2.7	Section 7.2.7	3.0	8.0	1.14	
Depth of Embedment	64,65,66,67	4	1.47	7.85	3.10	22.0	0.055	3.0	Section 7.2.8	2.5	

Table 6.2. Soil-Foundation Parameters in Steady-State Vibration Tests

Note: In all the experiments, model foundations were placed on soil except for the tests 64 to 67 where foundation was embedded at different depths in soil (see Chapter 7). Centrifugal acceleration was 50 g except for tests 36 to 39.

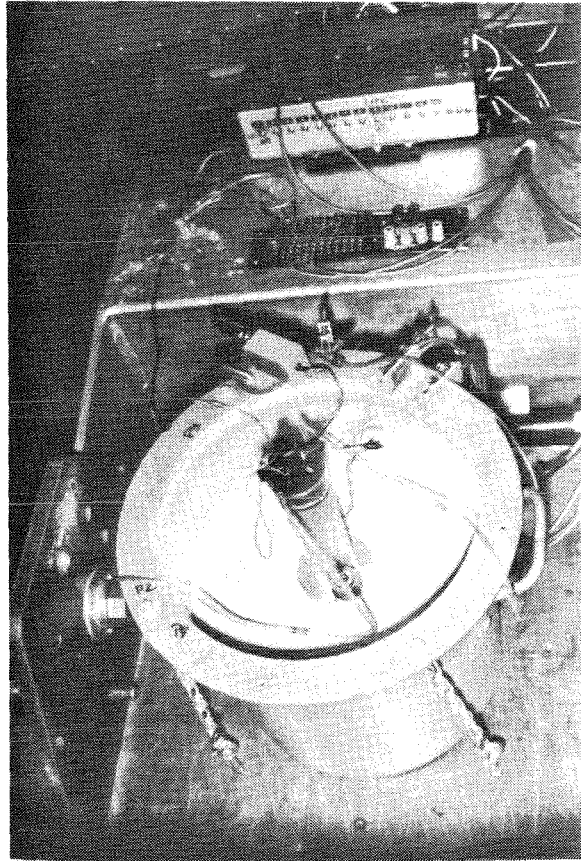


**FIGURE 6.5: TOWER WITH THE AIR SHAKER AND  
TRANSDUCERS PLACED ON SAND**

placed on the soil surface.

The LED for the displacement transducer and the one for the shaker frequency counter were both mounted on a light plastic bar fixed on the top of the shaker (see Fig. 5.7). The displacement transducer was mounted above the shaker looking down at the LED to measure horizontal components of the tower motion in rocking and/or sliding mode. For the vertical mode the shaker and the displacement transducer were mounted on the footing surface on a special frame designed to deliver vertical load to the footing (Fig. 6.6). Accelerometers were placed at the footing edge, at the top and at the midheight of the tower. For a single footing model only one accelerometer was placed on the footing surface, measuring horizontal or vertical acceleration of motion, depending on the mode of vibration. Pressure transducers were mounted according to the patterns shown in Chapter 5, Figure 5.19. Positions of transducers, associated channel number of the recording system for each transducer, and other pertinent information related to the tests are summarized in Table 6.3.

After the air tubes going to the shaker sides were connected to the air source through the rotating union, the centrifuge was spun up to the required acceleration. To start the test the air source was opened and pressure increased gradually. The higher the pressure the faster the shaker went (up to 45,000 RPM - 750Hz). The shaking machine was run through a range of frequencies while the tower motions were observed on an oscilloscope and at the same time were recorded at different frequencies of the oscillation. The signals were recorded by the data acquisition system (ADC) which converted the analog transducer outputs to digital signals and stored them in the random access memory. The stored data in ADC was then accessed by the TRS80 computer and stored on disks.

Around resonance some difficulties in controlling the shaking frequency were

Test No.	Tower No.	Channel 1		Channel 2		Channel 3		Channel 4		Channel 5		Channel 6		Channel 7		Channel 8	
		TRAN (in)	AMP	TRAN (in)	AMP	TRAN (in)	AMP	TRAN (in)	AMP	TRAN (in)	AMP	TRAN (in)	AMP	TRAN (in)	AMP	TRAN (in)	AMP
1 to 5	2	A2	6.48 50	A3	3.40 100	A4	0.2 100	P1	0.0 50	P2	0.60 50	P3	1.0 50	P4	1.4 50		
6	2																
7	2	A2	6.48 50	A4	0.80 100			P2	0.40 50	P3	0.80 50	P4	1.18 50			D2	9.1 10
10	1		+0.44		-0.44		-0.80		+0.80		0.28		0.90		0.27	D2	0.90
11	1	P1	+0.56 10	P2	-0.56 10	P3	-1.15 50	P4	+1.15 50	A2	0.11 50	D1	0.66 10	A3	3.03 100	D2	0.93 10
12	1		+1.0		+0.50		-1.40		+1.40		0.97		0.97		2.88		
19	1		0.66		0.66		0.11		0.11		3.03						
20	1	D1	0.96 10	D2	0.96 10	A2	6.11 50	A3	6.11 120	A4	3.03 180	P3	0.0 10				
21	1		0.90		0.90		0.28		0.28		3.17						
25	3	A3	0.88 50														
26, 27	3																
28	3	P1	+0.75 10	P2	-0.75 10	P3	-1.40 10	P4	+1.40 10	A3	0.86 50	D1	0.36 10	D2	0.36 10		
29	3											A4	0.68 50				
30, 31	4	P1	+0.76 10	P2	-0.76 10	P3	-1.40 10	P4	+1.40 10	A3	0.12 50	D1	7.63 10	D2	7.63 10		
32 to 38	4	P1	+0.76 10	P2	0.76** 10	P3	+1.40 10	P4	1.40** 10	A3	0.12 50	D1	7.63 10	D2	7.63 10		
40 to 48	2	D1	0.1 10	D2	0.1 10	A3	0.46 50										
49	2	A3	0.48 50	A4	3.40 100												
50 to 53	2	D1	0.1 10	D2	0.1 10	A3	0.46 50	A4	3.40 100								
54	4	A3	0.12 50	A4	2.65 100												
55 to 57	4	D1	7.63 10	D2	7.63 10	A3	0.18 50	A4	2.65 100								
58	6	D1	1.63 10	D2	1.63 10												
60	4	D1	5.27 10	D2	5.27 10	P1	+1.40 50	P2	-1.40 50	P3	-0.75 50	P4	+0.75 50	A4	6.12 100	A3	2.65 100
61	9	P1	0.0 50	P2	0.47 50	P3	0.83 50	P4	1.40 50								
62	1	A4	6.11 50	A2	3.03 100	D1	0.76 10	D2	0.76 10								
63	3	A4	0.88 50	A2	3.50 100												
64 to 67	4	A4	6.12 50	A2	2.65 100	D1	7.63 10	D2	7.63 10	P1	0.0 10	P2	0.47 10	P3	0.93 10	P4	1.40 10

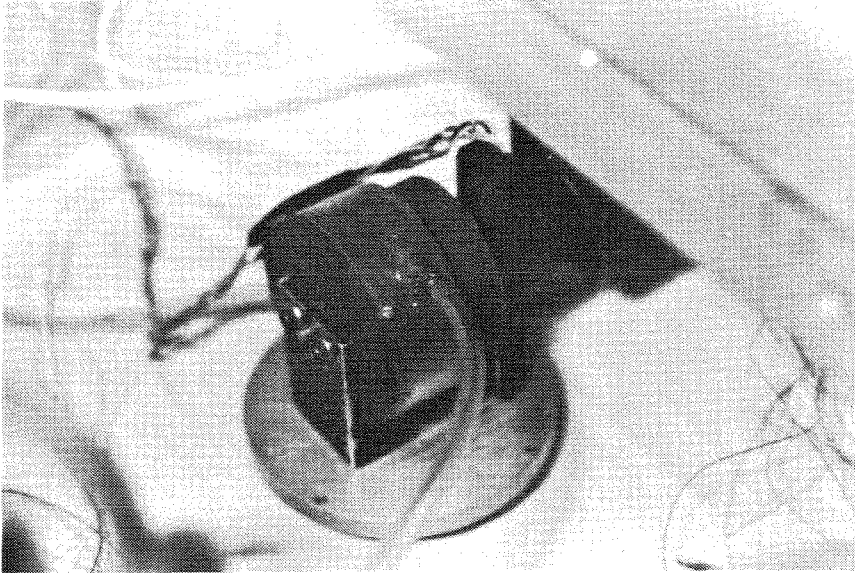
Table 6.3. Transducers Positions, Recording Channel Numbers, and Amplification Factors in Steady State Vibration Tests

Table 6.3. Continued

\* Accelerometer was placed on soil surface about 5.0 inches from the footing center.

\*\* Pressure Transducers were mounted according to pattern C (see Chapter 5).

Note: In above table "TRAN" stands for transducer, and "AMP" for amplification. "s" is the elevation of accelerometer on tower or radial distance of the pressure transducer from the footing center. Negative radial distance means that transducers were located on both sides of the rocking rotational axis.



**FIGURE 6.6: SHAKER ON A FOOTING FOR VERTICAL VIBRATION TEST**

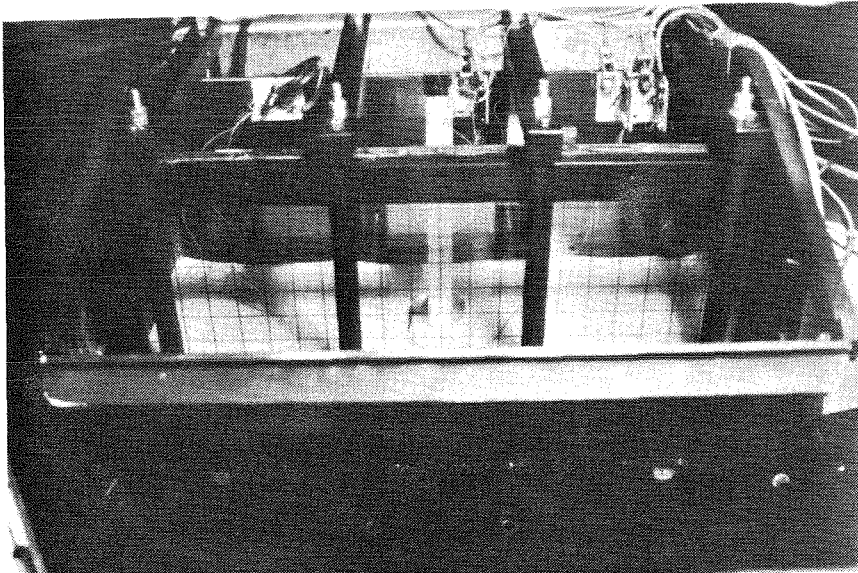


**FIGURE 6.7: TOWER PLACED ON SAND IN TRANSIENT SHAKING OF THE SOIL CONTAINER**

observed; these are explained as:

*- Interaction between the motion of the shaker and the model tower:*

If the motion of tower is small compared to the eccentricity ( $r$ ) of the counter-rotating masses  $m$ , then the motion of  $m$  can be taken as circular, and the acceleration of the tower center of mass in direction of tower motion is  $r \omega^2 \sin \omega t$  (where  $\omega$  is the angular velocity of the mass  $m$ ). There is thus an exciting force  $m r \omega^2 \sin \omega t$  acting on the tower producing the rocking-sliding motion of the tower in the direction of the force. If the tower motion is not small (near resonance) then mass  $m$  under the influence of tower acceleration cannot apply a horizontal harmonic force on the tower. In order for the shaker to pass the resonant frequency of the tower a large amount of energy should be input to it which forces the tower to vibrate with the frequency of the shaker. Once this happens the shaker frequency increases very quickly and the amplitude of the tower motion decreases considerably.

*- Nonlinear behavior of the soil-structure system:*

Under applied loads soil behaves nonlinearly, and inelastically. In machine foundations and relatively small amplitude dynamic loading of foundations, nonlinear reversible soil models with hysteretic damping are used if the permanent deformations can be assumed negligible. The response spectra (amplitude versus frequency curve) for the behavior of a nonlinear material obeying Duffing's equation (Timoshenko, Young, and Weaver 1974), represent mathematical models of the *drop-jump phenomenon* observed in experiments upon nonlinear mechanical systems subjected to harmonic forcing functions. This phenomenon was observed during some of the tests on dynamic behavior of the rigid towers, which did not allow attaining the actual maximum amplitude of the tower motion at resonance. Therefore, acquiring data for a complete response curve of the tower especially around resonance requires a discontinuous variation of forcing frequency, such as increasing frequency gradually from a low value and then decreasing it from a high value above the critical frequency where the drop-jump phenomenon happens.

### 6.2.3. Transient Shaking of the Soil Container

Once the sand was prepared in the bucket and the model tower with transducers attached to it placed on the soil (Fig. 6.7), the centrifuge was brought up to the speed required for the test. A computer program was then loaded on TRS80 computer which listed the test procedure step by step in the following order:

- (1) Turn on the MTS controller, and the noise or the signal generator.
- (2) Start charging the accumulators up to 3000 psi oil pressure depending on the g-level for the test, soil weight, and the intensity of shaking desired.
- (3) Choose the time length for the input transient signal for the desired duration of shaking of the soil container.

When ready for the test, a command by the computer starts acquiring data and

then immediately the test starts. The computer controls a relay between the signal generator and MTS controller. Once the relay is closed, the signal passes from signal generator to the controller and the test starts. After the time interval chosen in step 3 is passed, computer opens the relay and the shaking stops.

"Modelling of models" tests were also performed with the hydraulic shaking system. In these tests a random voltage of very short duration compared with the period of the tower oscillation was input to the controller which forced the bucket to shake for a while and then stop in a short time. Subsequent free oscillation of the tower was recorded on the Visicorder. The models were tested in three different  $g$  levels in the ratio of their length dimensions, i.e., 1:2:3. Models 5, 6, and 7 were used for "modelling of models" tests. Table 6.4 presents the physical properties and other test information related to this group of tests. Usually only accelerometers were used in these tests to measure the horizontal acceleration of the tower and of the soil. The accelerometer in the soil was placed on the rigid floor of the bucket with no soil in it and then soil was placed on the floor to the required depth.

### 6.3. DATA REDUCTION

Depending on the type of recording equipment used, i.e. the Visicorder analog recorder or the ADC and TRS80 computer the following steps in reducing the data were undertaken:

#### (A) *The Visicorder*

(I) For the free oscillation tests if the frequency content of the signal could not be determined visually and measured by hand, the record was digitized on a Benson-Lehner 099D data reducer unit. The procedure for digitizing is described elsewhere (Ortiz, 1982).

(II) The results from the tests were obtained by processing the digitized data with the FORTRAN program DATA. The program was run on a VAX-11/780



Table 6.4. Physical Properties of Models and Other Test Information  
(Transient Shaking of Soil Container)

Test Number	Tower	W (lbf)	h <sub>C.G.</sub> (in)	I <sub>C.G.</sub> (lb-in <sup>2</sup> )	Footing Diameter (in)	Soil Depth (in)	g-level
1	1	See Table 6.1 Tests 4 to 6			2.00	2	50
2,3	2	See Tables 6.2 & 7.2 Test 6			2.00	2	50
4	3	See Table 6.2 Tests 25 to 29			3.00	6	50
5	4	See Table 6.2 Tests 64 to 67			3.00	6	50
6	5	0.132	1.280	0.105	1.25	7	52.5
7	6	1.060	2.550	3.370	2.50	7	26.3
8	7	3.570	3.840	25.440	3.75	7	17.5

Note: In above tests listed in the table soil dry unit weight was about 105.5 pcf.

Computer System. The inputs to the program are the digitized data points and other experimental data such as, centrifuge speed, distance from centrifuge axis to a soil depth equal to radius of the footing below the model base, geometrical properties of the model, calibration factors, etc. The program then performs the following steps:

- (1) The raw digitized data are checked for any decreasing time value which should be excluded from the data points.
- (2) All the traces are corrected for base line rotation and translation.
- (3) The data are scaled to prototype dimensions using calibration factors.
- (4) The data are then plotted and printed.
- (5) Fourier spectra of the data are derived, smoothed, and plotted.

(B) *The ADC and TRS80 Computer*

Some preliminary data processing was usually done during the tests whenever possible as a check for quality of the data recorded. This included displaying the data on the computer screen and plotting them on a Hewlett-Packard X-Y plotter.

The subsequent data reduction was partially performed on the TRS80 computer, but because of the large volume of data a more efficient data storage and file organization procedure was needed. In addition reducing such a great amount of data required a much faster computer system. Therefore data were transferred to a PRIME500 mini-computer using the special FORTRAN routines TRANSFER and MAGTRAN written for TRS80 and PRIME500 computer respectively.

The following steps in data reduction were carried on:

(I) Transient Data: They were printed, plotted, and if necessary, their Fourier transforms were calculated.

(II) Steady-State Forced Vibration Data: The procedure for reducing these data included:

(1) The data for each test, for all the channels and frequencies were plotted first. Using test information input to the plotting program, the time dimensions of the data were scaled to prototype values and the time length of each record was plotted to the right of the signal trace. In this way frequencies of oscillation could be calculated by hand and compared with the frequency values registered from the frequency counter during the test. Appendix B includes the plotted output for a typical test. The abbreviated name shown to the left of each plot is the computer filename under which the data were stored. The letters and the numbers in each name have special meanings. For example the name "T10F1C2" means test 10, frequency 1 (the first frequency at which data were taken), channel 2; and "T1110C5" stands for test 11, frequency 10, channel 5; etc.

(2) If some of the signals were very noisy after plotting the data they were filtered using a low and high pass digital filter called "modified Ohmsby filter" (Beck, 1983), and then the filtered data were stored and plotted again. Before filtering, a Fourier transform analysis of the data determined the frequency limits for the low and high pass filters. Mainly signals were contaminated by high frequency noise which is a characteristic of centrifuge testing.

(3) The raw data were sine-fitted for the best sine wave fitting the data points in a least square sense. A program called "SINEFIT" was written in Fortran and run on both TRS80 and PRIME500 computers. Input to the program included time spacings between the digitized data points and the frequency of each signal in prototype scale. The output of the sine fit included the average value of the data, the amplitude, and the phase of the sine wave.

(4) A plotting routine was then used to plot the raw amplitudes (derived from the sine fits) of the signals for all the channels of data against frequencies of oscillation (in prototype scale), repeated for all the tests.

*REFERENCES*

- [1] Beck, L. J., "Modified Ohmsby Filter", Class Notes, Earthquake Engineering Laboratory, California Institute of Technology, Pasadena, California, 1983.
- [2] Morris, D. V., "Dynamic Soil-Structure Interaction Modelled Experimentally on a Geotechnical Centrifuge," Canadian Geotechnical Journal, Vol. 18, No. 1, Feb. 1981, pp. 40-51.
- [3] Ortiz, L. A., "Dynamic Centrifuge Testing of Cantilever Retaining Walls," Ph.D. Thesis, Soil Mechanics Laboratory, SML 82-02, California Institute of Technology, Pasadena, 1982.
- [4] Timoshenko, S., Young, D. H., and Weaver, W., Jr., "Vibration Problems in Engineering," 4th ed., Wiley, New York, 1974.

## CHAPTER 7

### EXPERIMENTAL RESULTS

This chapter presents the experimental results obtained in different groups of tests on the model towers in the centrifuge. The main volume of data and derived experimental results are related to steady-state vibration tests studying the effect of different soil-footing parameters on the dynamic characteristics of the model structure. The first section describes the transient vibration tests with explosion-induced excitation. In Section 7.2. results of the steady-state vibration tests and the parametric studies are presented and discussed. Transient passive excitation of the model towers produced by shaking the whole bucket, is reported in Section 7.3. Comparisons between some of the results obtained on similar models under approximately comparable soil conditions in transient vibration tests and steady-state shaking tests are given in this chapter. Different physical phenomena observed during the tests such as: lift-off of foundation, yielding of the soil underneath the footing and subsequent settlement and tilting of the tower, variation of contact pressure distribution during vibration, etc. are explained and clarified. The results are summarized in tables and plots representing the data and are discussed in each case.

#### 7.1. EXPLOSION - GENERATED FREE OSCILLATION

As was mentioned in chapter 6 these experiments were performed on the rigid solid rectangular tower with two different size circular foundations resting on the soil surface. Tower oscillation in the tests was usually short in duration and very small in amplitude. Extra amounts of explosive to deliver longer vibration times with higher amplitudes caused new problems in data processing because of extreme electrical and high frequency mechanical noise superimposed on the main signal. Natural frequency of tower oscillation was measured

by counting the number of cycles and dividing it by the time length of the record. Damping ratio was found by calculating the logarithmic decrement of the oscillation (see Chap. 3). The frequency of oscillation measured by hand is not precise enough because of the few number of large amplitude cycles and the noise contamination in the signal.

Fourier analysis of the digitized data proved to be very helpful in determining the exact free oscillation frequency of the tower and the overall frequency content of the signals. Because of the above-mentioned noise in the signals, and the short duration of tower oscillation, on each model three experiments under comparatively similar conditions were performed to check the reliability of the repeating pattern of the results. Tests 1, 2, and 3 were performed on the tower with the 3 inch diameter footing and extra attachments on the tower top (model I in this group of tests, see Table 6.1). The air-driven shaker used in steady-state vibration tests was mounted on the tower top so that a comparison between dynamic properties of the tower, derived from transient and steady-state vibration tests was possible. Figures 7.1 and 7.2 present the time history and the Fourier spectrum of the recorded acceleration at the tower top for tests 1, 2, and 3. The modelling laws have been used to convert all values into equivalent prototype values. Therefore all the frequencies, time values, and force or displacement amplitudes are in prototype scale in the tables and plots presented for the data. Results of the tests on model II (tower and the 2 inch diameter footing with no attachment, Table 6.1) are presented in Figures 7.3 and 7.4 for test 4, Figures 7.5 and 7.6 for test 5, and Figures 7.7 and 7.8 for test 6. In these tests a pressure transducer was also mounted on the footing surface, at the edge, to detect any lift off and to obtain cleaner and more readable records of data because of the high frequency filtering property of pressure transducers. Note that the pressure-time history plots in Figures 7.3 to 7.8 do

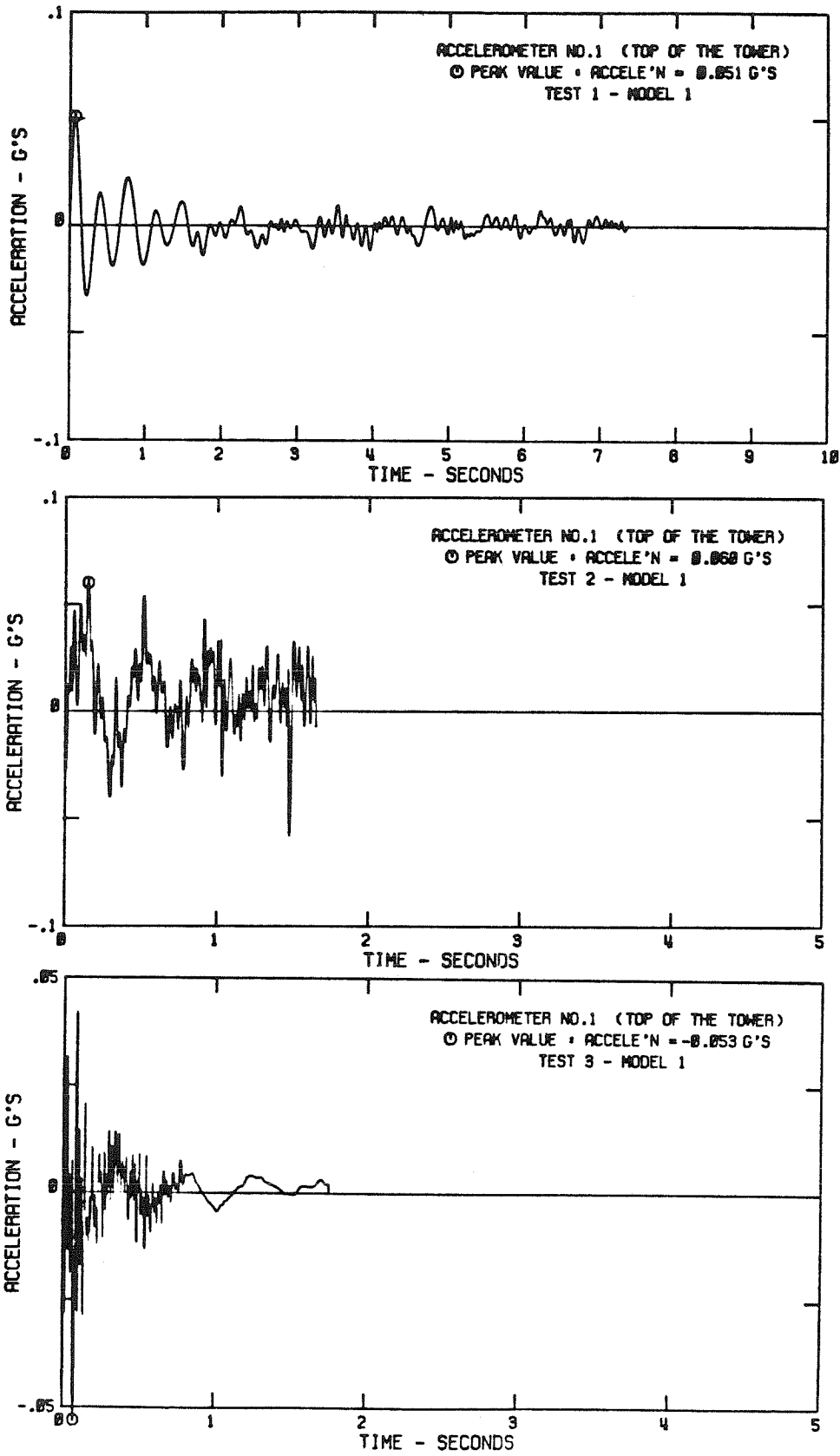


FIG. 7.1 TOWER ACCELERATION IN EXPLOSION-GENERATED FREE VIBRATION TESTS, (TESTS 1,2,3)

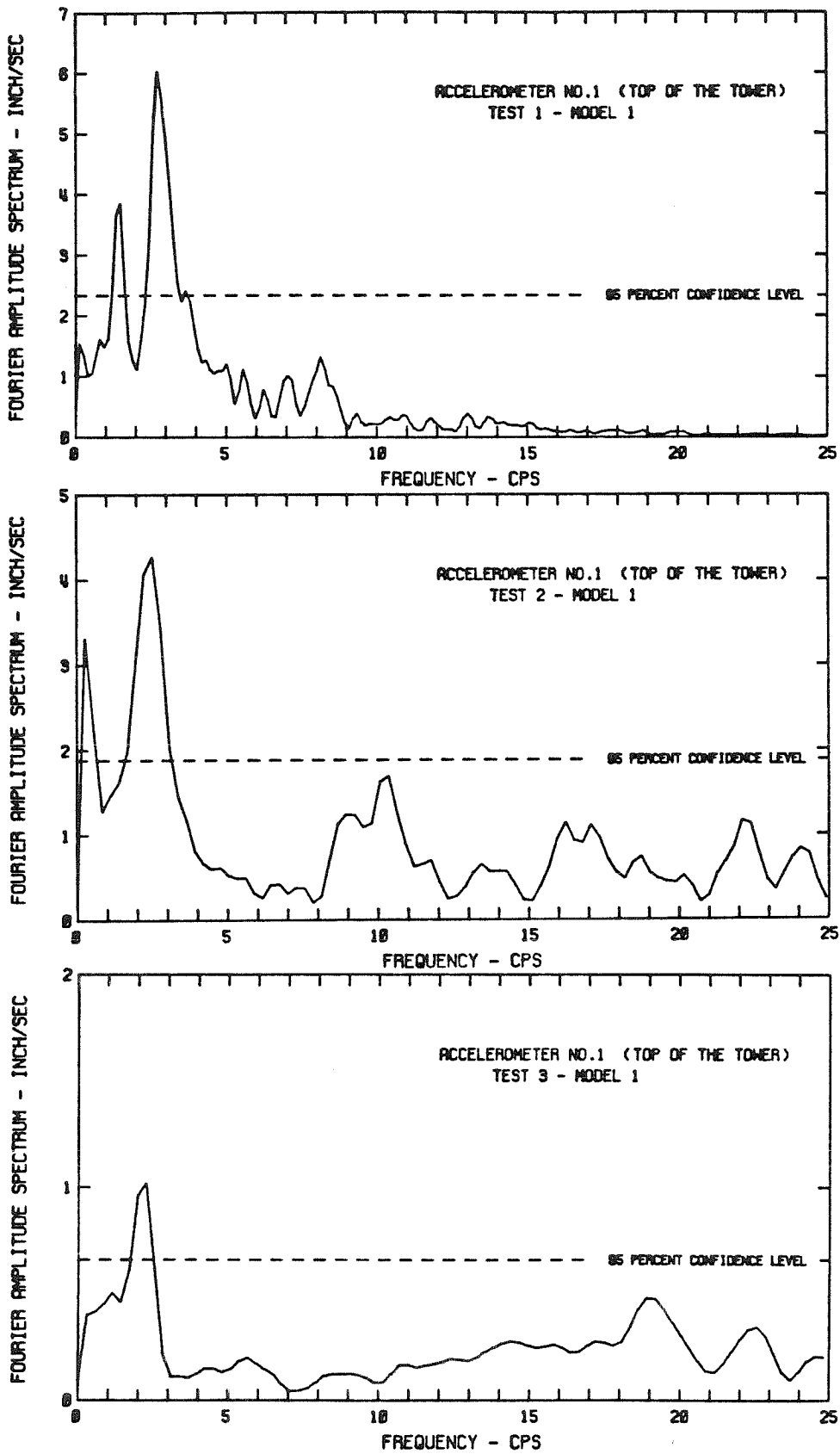


FIG. 7.2 FOURIER SPECTRUM OF THE ACCELERATION SIGNALS (TESTS 1,2,3)



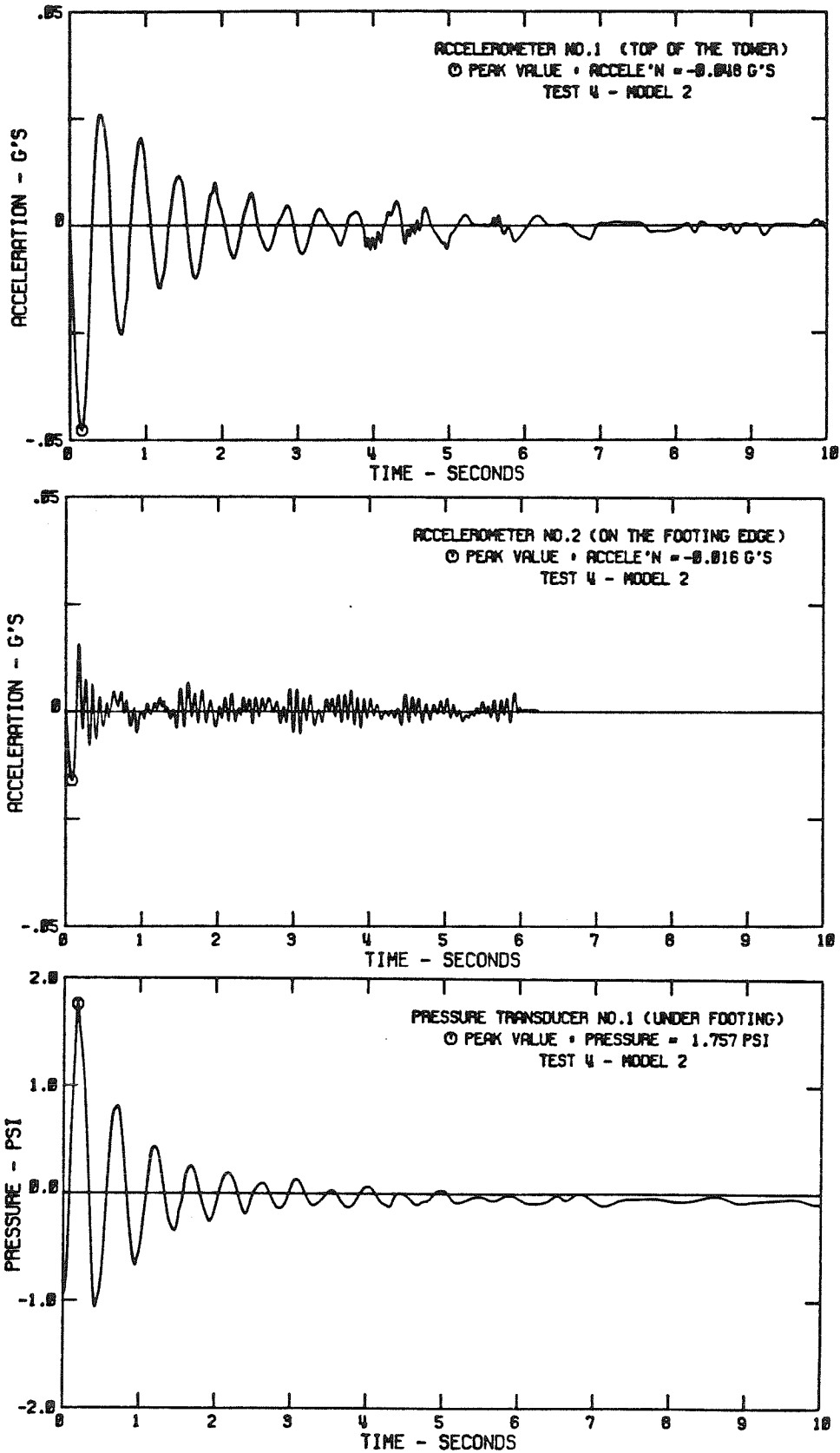


FIG. 7.3 TOWER ACCELERATION AND CONTACT PRESSURE SIGNALS (TEST 4)

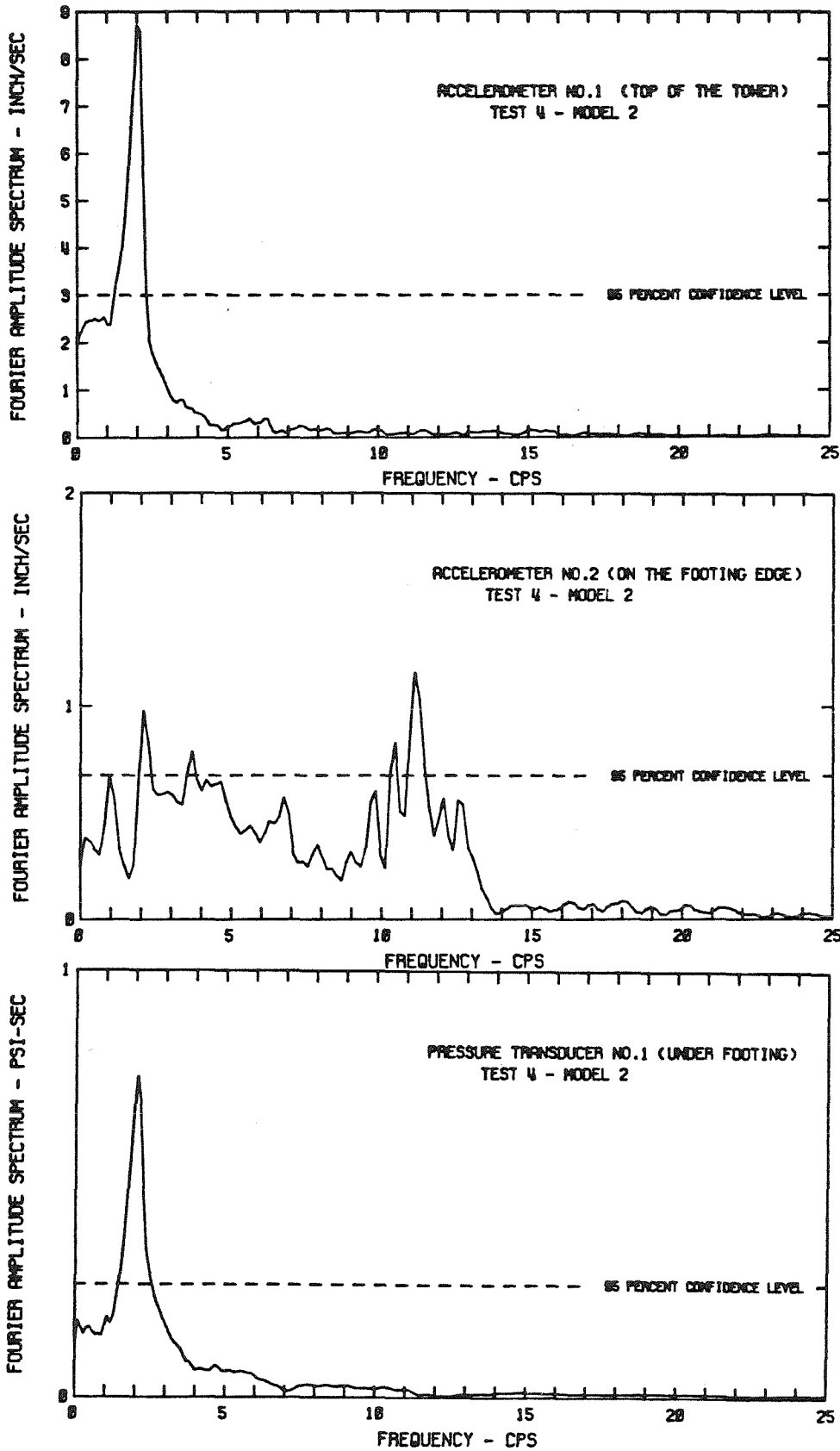


FIG. 7.4 FOURIER SPECTRUM OF THE ACCELERATION AND PRESSURE SIGNALS

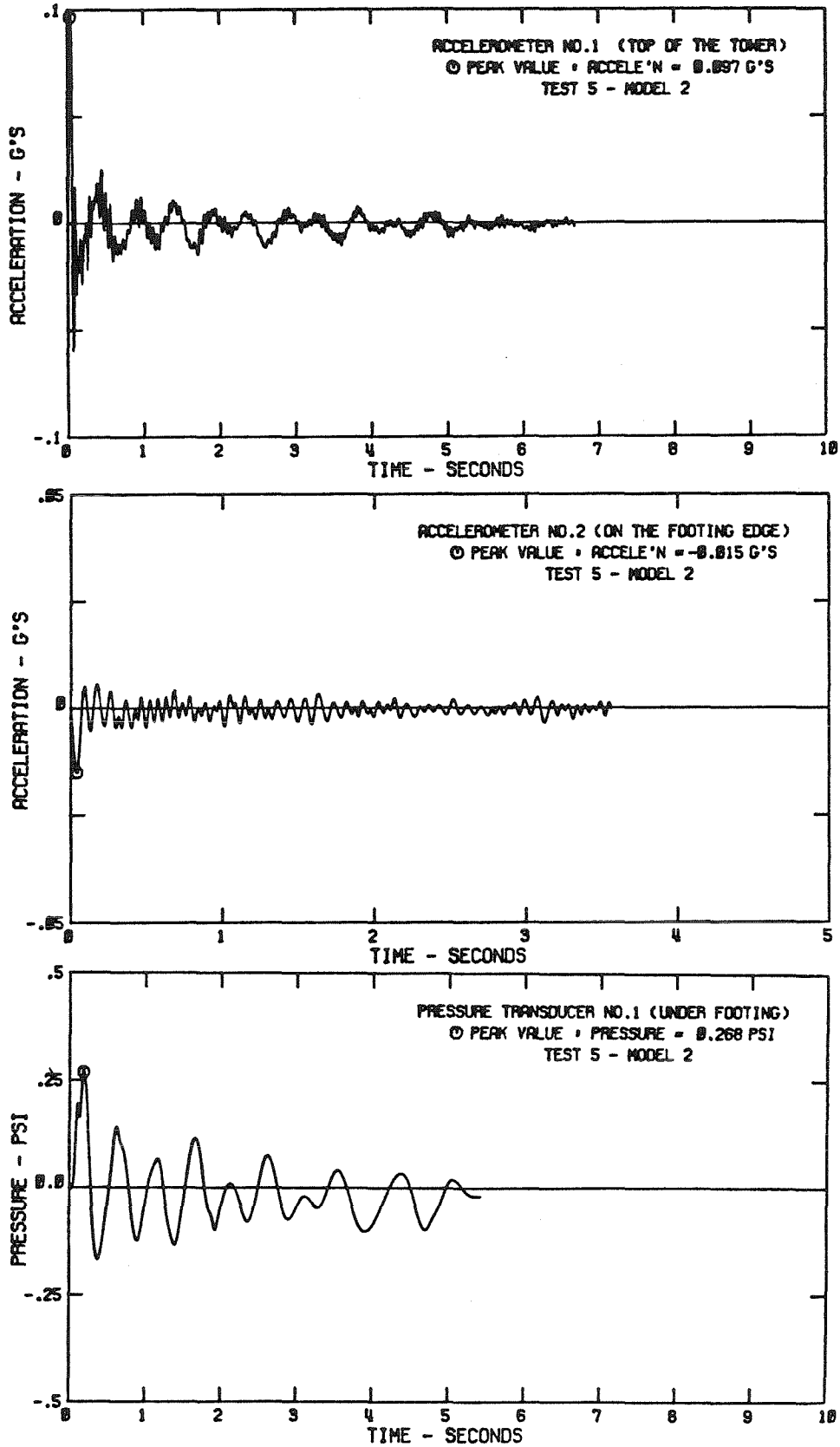


FIG. 7.5 TOWER ACCELERATION AND CONTACT PRESSURE SIGNALS (TEST 5)

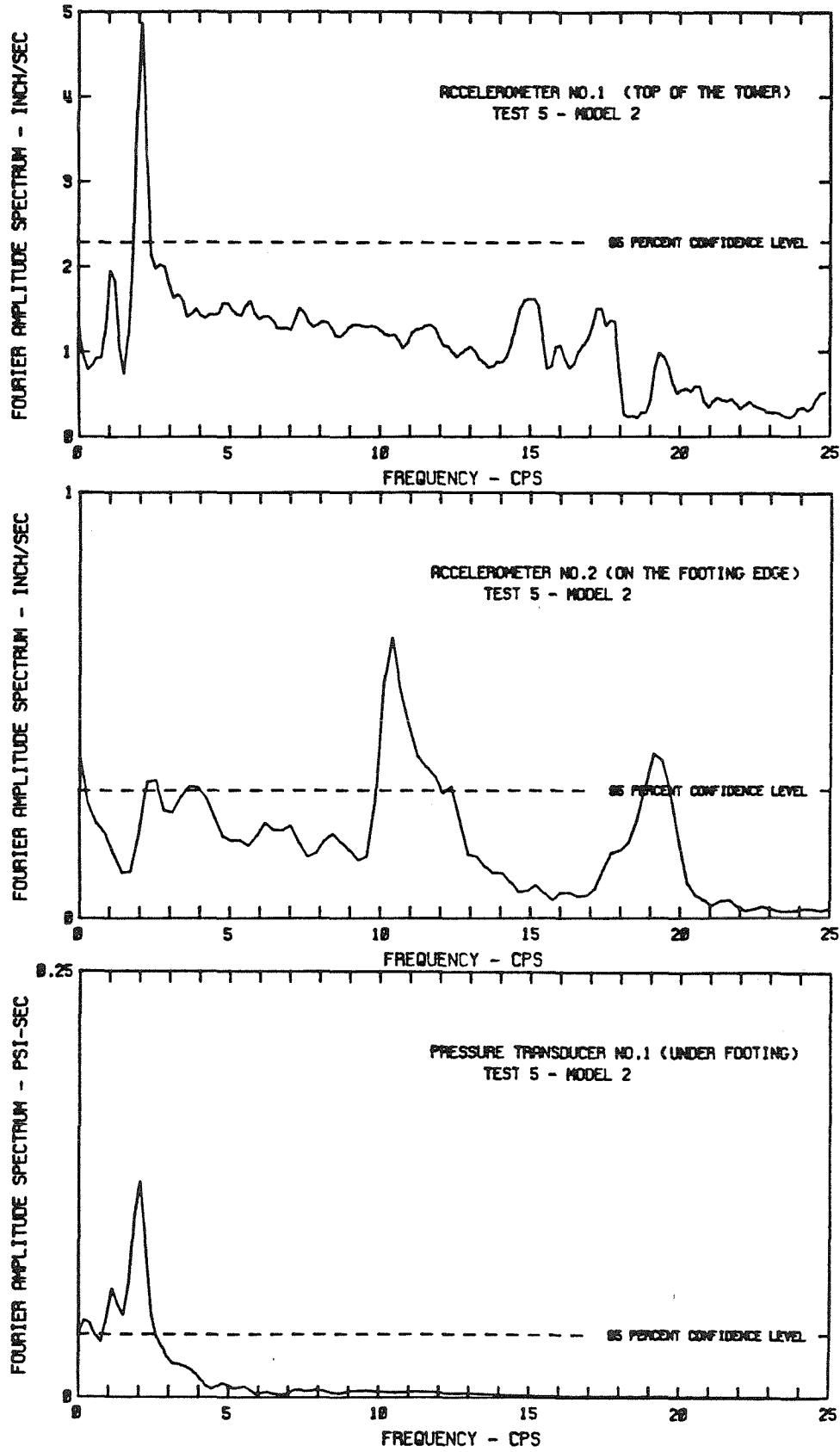


FIG. 7.6 FOURIER SPECTRUM OF THE ACCELERATION AND PRESSURE SIGNALS

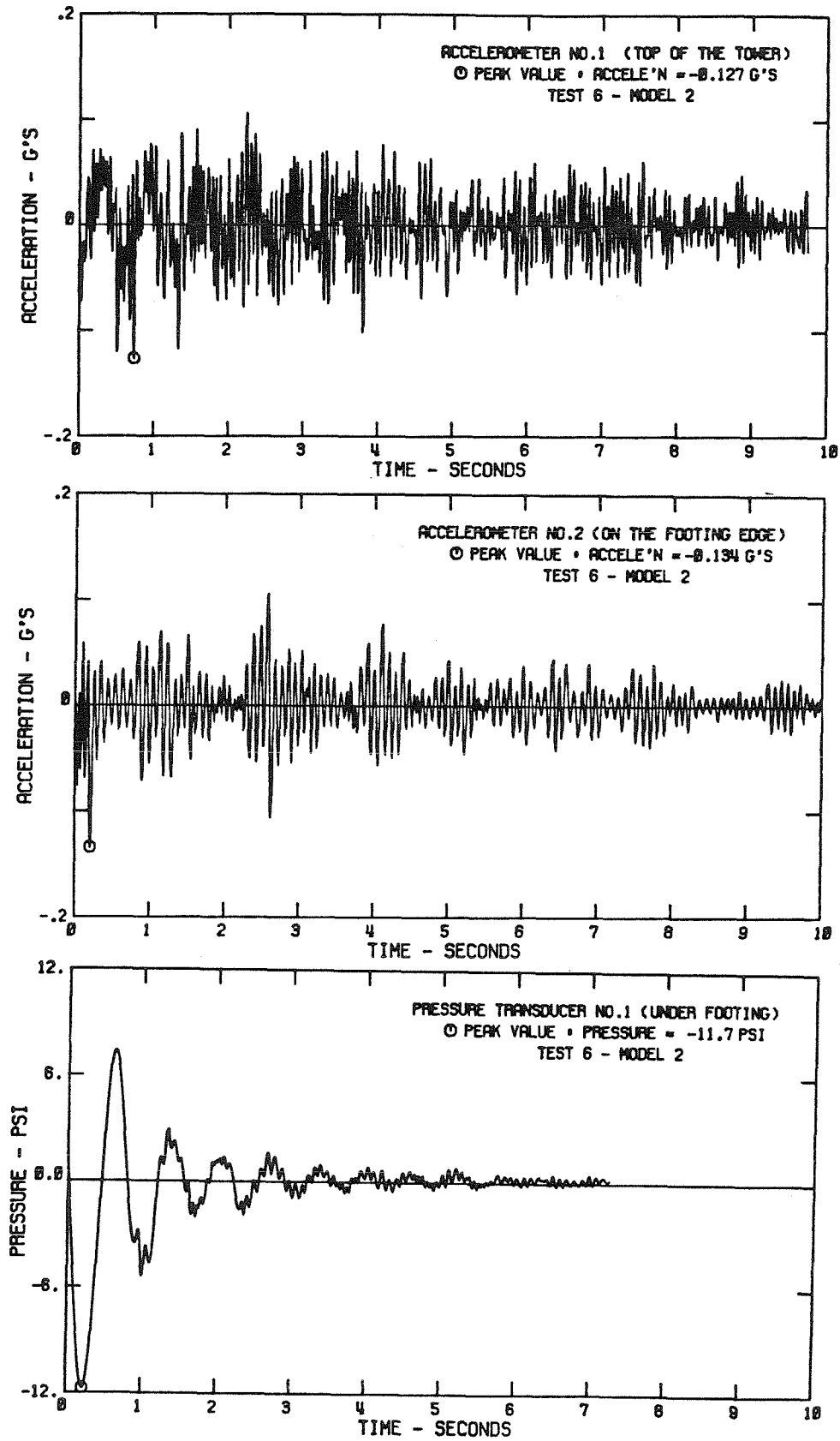


FIG. 7.7 TOWER ACCELERATION AND CONTACT PRESSURE SIGNALS (TEST 6)

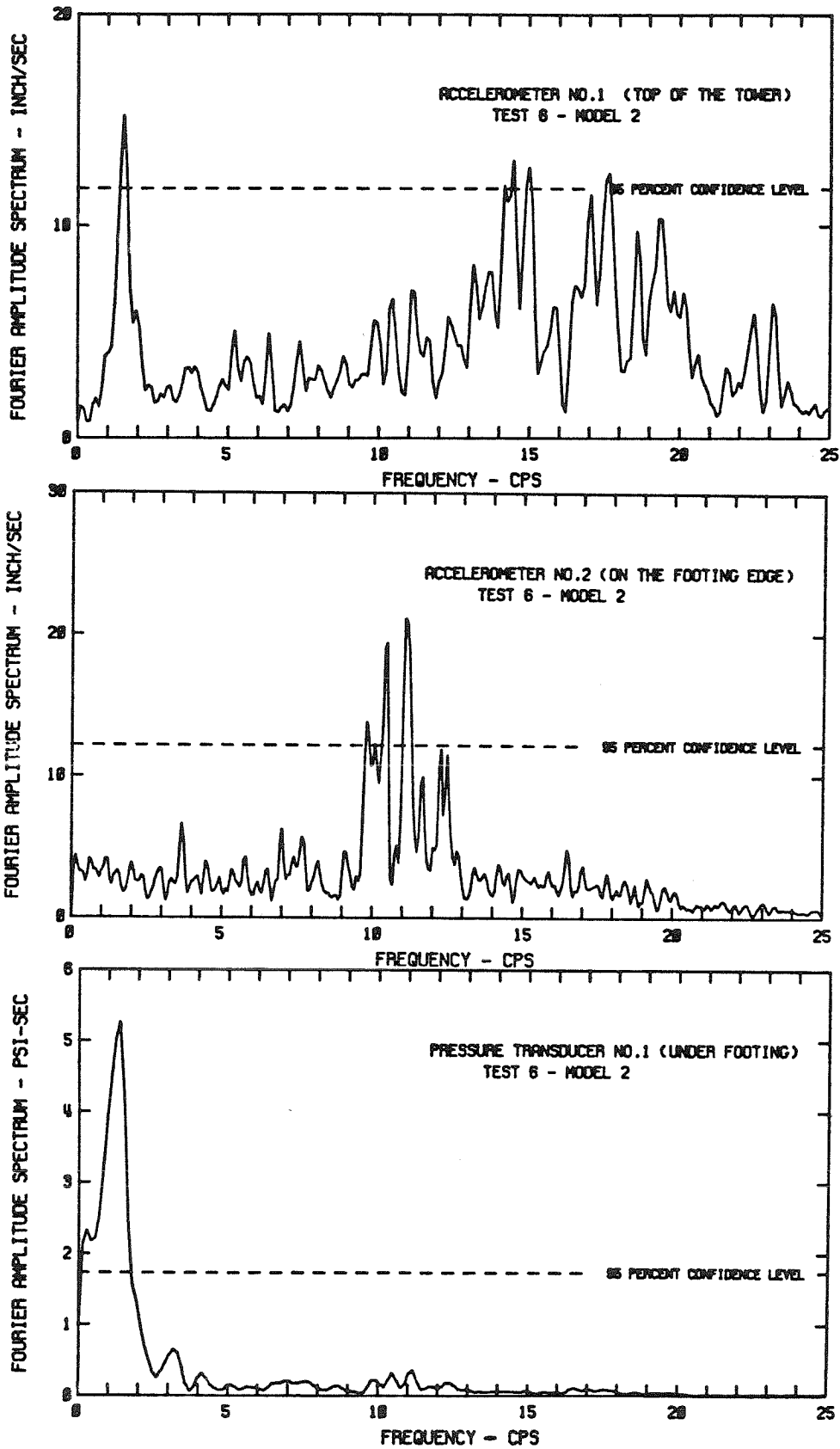


FIG. 7.8 FOURIER SPECTRUM OF THE ACCELERATION AND PRESSURE SIGNALS

not include static (steady-state) component of pressure and only excess dynamic pressure component is plotted. However, it was observed that static component of the contact pressure changed very little during the dynamic tests. This means that the supporting soil did not yield and consequently permanent deformations did not occur. The average value of free oscillation frequency and damping ratio for the three tests on Model I (Tests 1, 2, and 3) are 2.45 Hz and 5% respectively. The frequency and damping values for the Model II are 2.0 Hz and 5%.

Several interesting aspects of these results are described here:

- (1) As is seen from all figures cited above, maximum acceleration amplitude is very small (about 0.05g) which probably means a more or less linear reversible behavior of the soil under the small strains developed. The pressure signal (Fig's. 7.3, 7.4, and 7.5) is smooth and continuous which suggests there has been no separation between footing and soil even at the edge during rocking. Therefore, in these tests existence of full contact between footing and soil during test is consistent with theoretical models which assume rigid contact during oscillation.
- (2) Tests 1, 2, and 3 on Model I give approximately a comparable value for the free oscillation frequency of the tower. Similarly tests 4 and 5 yield very close values for the frequency of oscillation of the Model II. However a considerable reduction in free vibration frequency of the tower is observed in test 6 compared with the results derived in tests 4 and 5. The reason for this discrepancy can be explained by comparing the amplitude of acceleration at the tower top. Acceleration amplitude in test 6 is more than twice the value observed in the other tests, thus the foundation soil will behave in a more nonlinear and inelastic fashion

and because of the softening and large amplitude oscillations the tower resonant frequency decreases considerably. In addition note that the pressure amplitude at the edge of footing-soil contact area is about 4 times the pressure developed in test 4 and 25 times the pressure in test 5. The considerable increase of contact pressure might have been resulted partially because of tilting of the model structure toward the side pressure transducer was mounted.

- (3) Model II which has smaller footing, has a lower natural frequency than model I. Therefore, overall increase in the size of foundation of the structure will result in an increase in frequency of fundamental mode of vibration.
- (4) Time domain records for the vertical acceleration signal of the footing edge (Fig's. 7.3, 7.5 and 7.7) do not show a significant amplitude. Fourier spectra for these signals (Fig's. 7.4, 7.6, and 7.8) show peaks at other frequencies higher than the fundamental rocking frequency of vibration. It is suspected that these higher frequency peaks are generated by vertical oscillations of the tower, which may have been originated at the very start of the explosion, and by reflections of the energy waves from the bucket boundaries. The dominant higher frequency peak observed in all the Fourier spectra plots is about 11.0 Hz.
- (5) In some of the Fourier spectra plots a third peak at a frequency about 1.75 Hz (120.0 Hz model scale) exists which is produced by the spurious mechanical vibration of the centrifuge arm explained in detail in Chapter 6.



## **7.2. STEADY - STATE FORCED VIBRATION TESTS**

Forced vibration experiments were conducted to determine the natural frequencies and damping ratios of the excitable modes in the soil-structure system and to derive response amplitude curves of the rigid model structure, describing the significant dynamic characteristics of the system. A thorough determination of dynamic properties of the system at the fundamental resonant frequency in the principal test direction (direction of applied horizontal load on top of the tower) was made. These tests were conducted to study effect of different parameters of the soil-structure system on the dynamic behavior of the rigid towers and foundations listed previously in Table 6.2. The results of these tests will be presented and discussed in the following subsections. Before introducing the test data and the related results basic steps in analysis and methodology of their presentation will be discussed in the next section.

### **7.2.1 Presentation and Analysis Method of the Results**

The experimental results were derived by plotting and sine-fitting the data which produced the amplitude and the phase information of each transducer signal over the entire range of frequencies sampled during each test. The derived amplitude data were plotted versus frequency of oscillation for all the signals. With an average of 5 transducers used in each test and about 70 tests performed, a total of 350 response curves was derived. The reason for plotting response curves for all transducers was to provide enough information for the difficult process involved in the interpretation of the data, which resulted from nonlinear inelastic behavior of the soil-structure system. Because of the large volume of the data, among these response curves, only the ones for studying the effects of embedment of the foundation, change of the eccentric mass of the

shaker, and some other ones containing particularly interesting information such as nonlinear and inelastic behavior of the foundation-soil system, and pressure distribution variation with frequency and amplitude of vibration are presented here. The complete set of response curves for the typical data recorded in a test (e.g. Test 64, Appendix B) is presented in Figures 7.9 to 7.16. These plots include two acceleration, two displacement, and four pressure response amplitudes. Figures 7.11 and 7.12 show the response amplitudes of the displacement transducers mounted on the top of the tower in the main direction (parallel to the tower rocking-sliding motion, channel 3, transducer D1) and in the direction normal to the main (channel 4, transducer D2). Mainly displacement response curves were used in determination of resonant frequency and damping characteristics of the models in different tests. However, other transducer data were also analyzed for frequency and damping properties to verify the derived test results.

The y-axis of the plots is expressed in terms of displacement, pressure, or acceleration amplitude per frequency squared. However, frequency squared shows the force generated by an eccentric mass shaker having a unit "mass times eccentric distance" factor in any arbitrary units. Therefore the y-axis shows the amplitude per unit force of an imaginary shaker of unit mass-times-eccentricity product. The response curve for any other eccentric mass is just derived by scaling the plot by a constant factor. This is only approximately true because of the more nonlinear behavior of the system as the eccentric mass in the shaker is increased. In these plots the unit for the vertical axis labeled as "Amplitude / Force" is in "in-sec<sup>2</sup>" for displacement data; "psi-sec<sup>2</sup>" for pressure signals; and "g-sec<sup>2</sup>" in case of accelerations.

Natural frequency and damping properties can be derived approximately from the response curves by locating the position of peak amplitude and

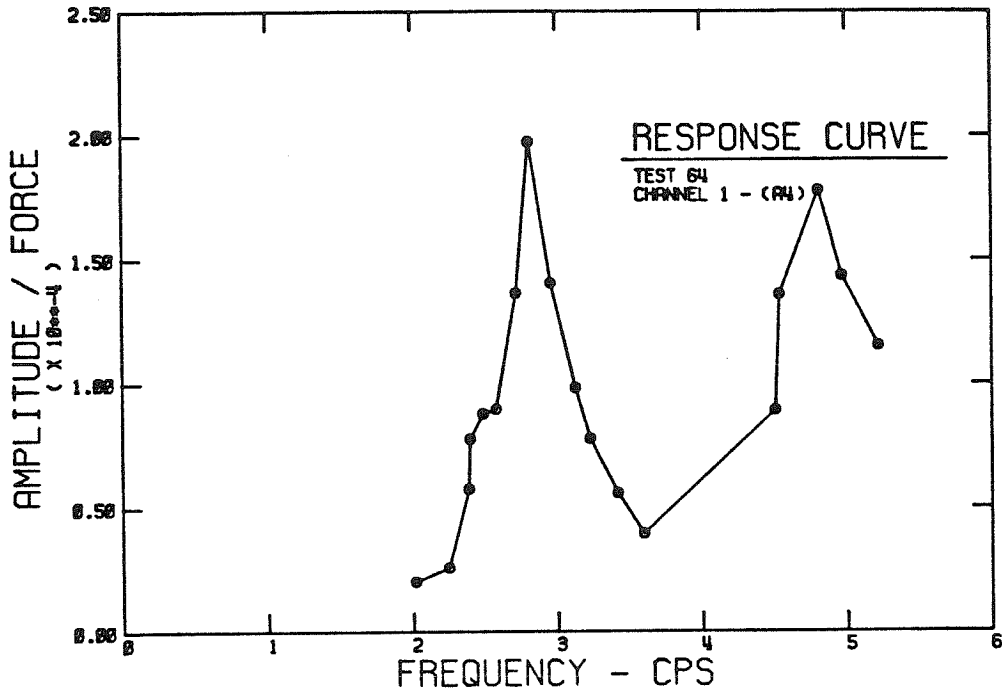


FIG. 7.9 RESPONSE CURVE FOR TOWER TOP ACCELERATION

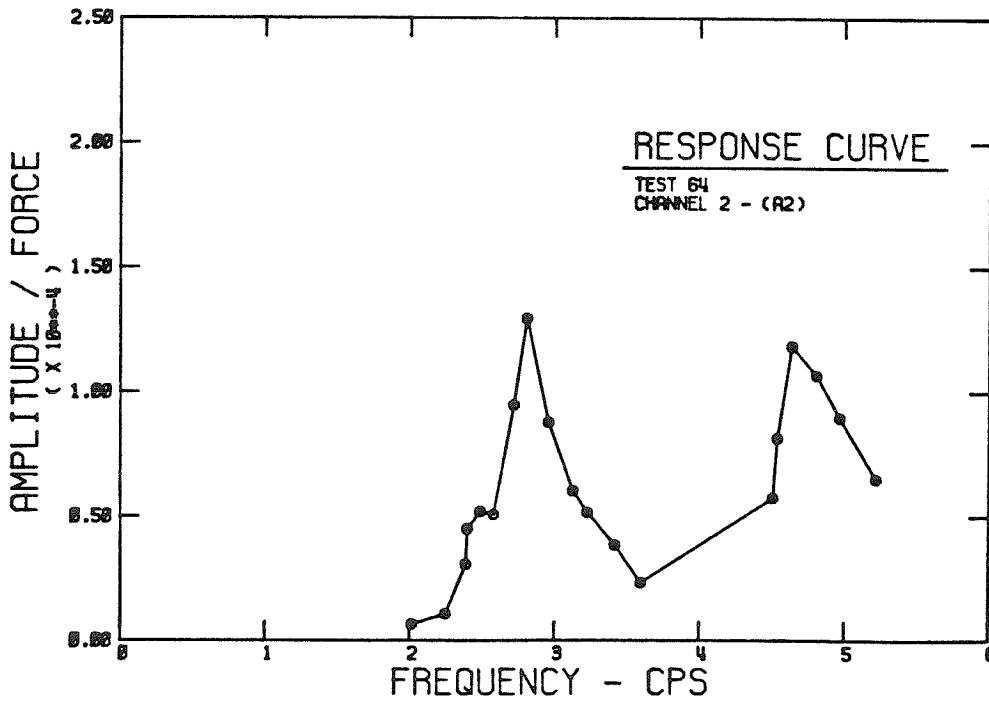


FIG. 7.10 RESPONSE CURVE FOR TOWER ACCELERATION AT ITS MIDHEIGHT

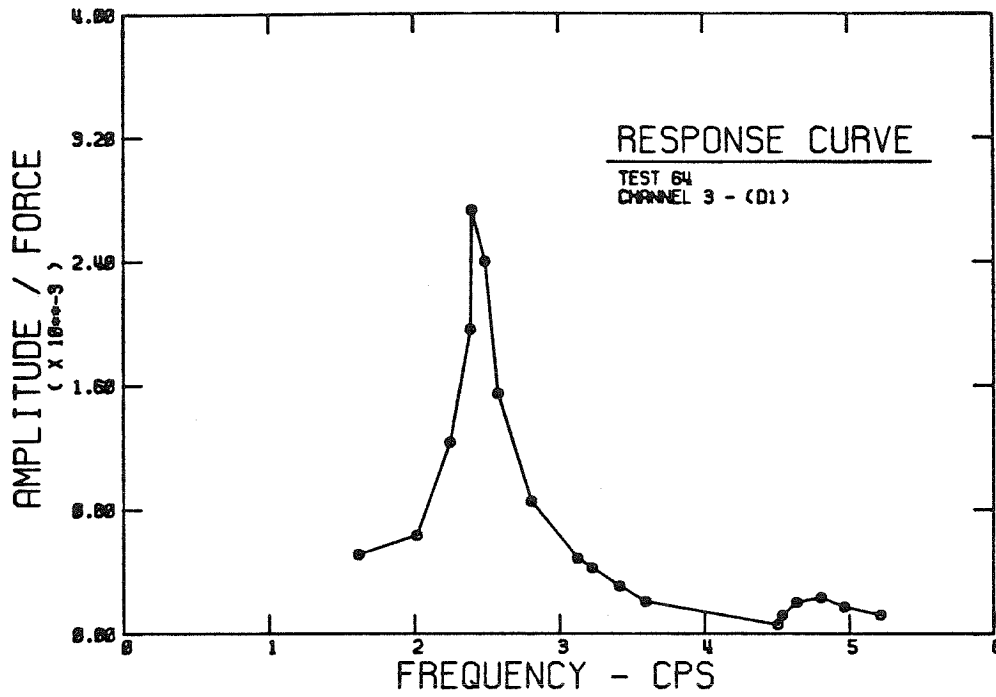


FIG. 7.11 RESPONSE CURVE FOR TOWER TOP DISPLACEMENT (MAIN ROCKING DIRECTION)

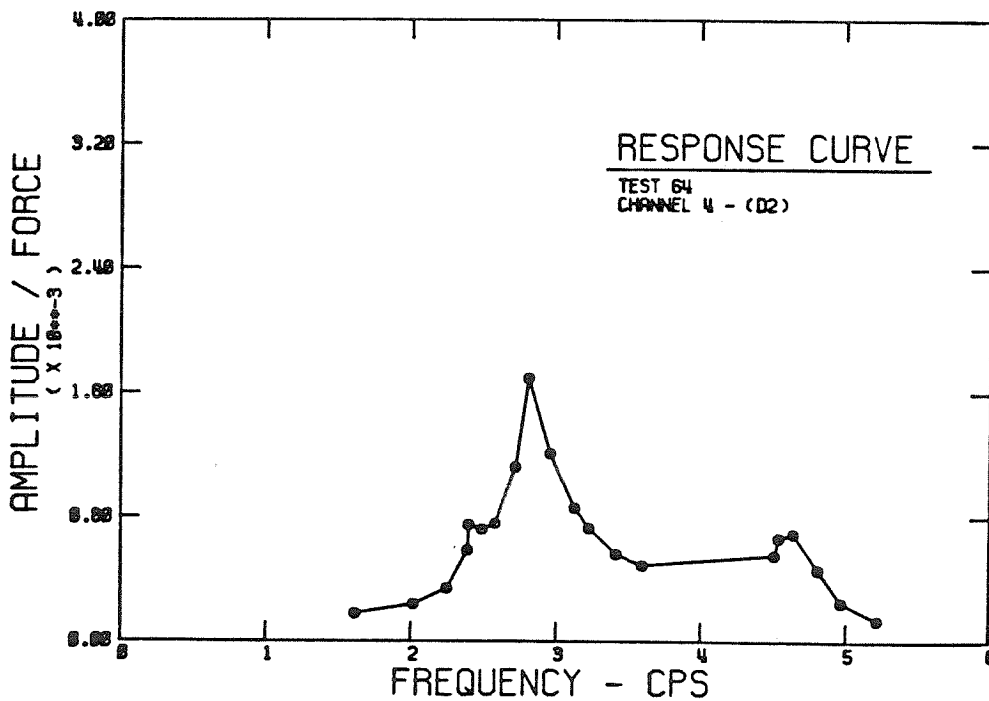


FIG. 7.12 RESPONSE CURVE FOR TOWER TOP DISPLACEMENT (NORMAL TO MAIN DIRECTION)

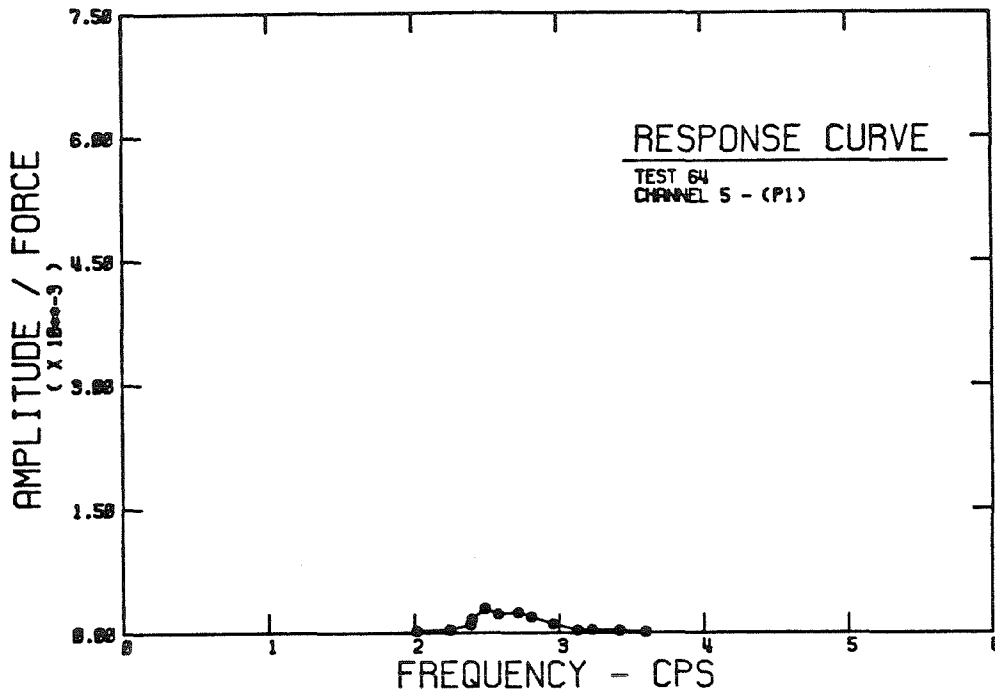


FIG. 7.13 RESPONSE CURVE FOR CONTACT PRESSURE AT FOUNDATION CENTER

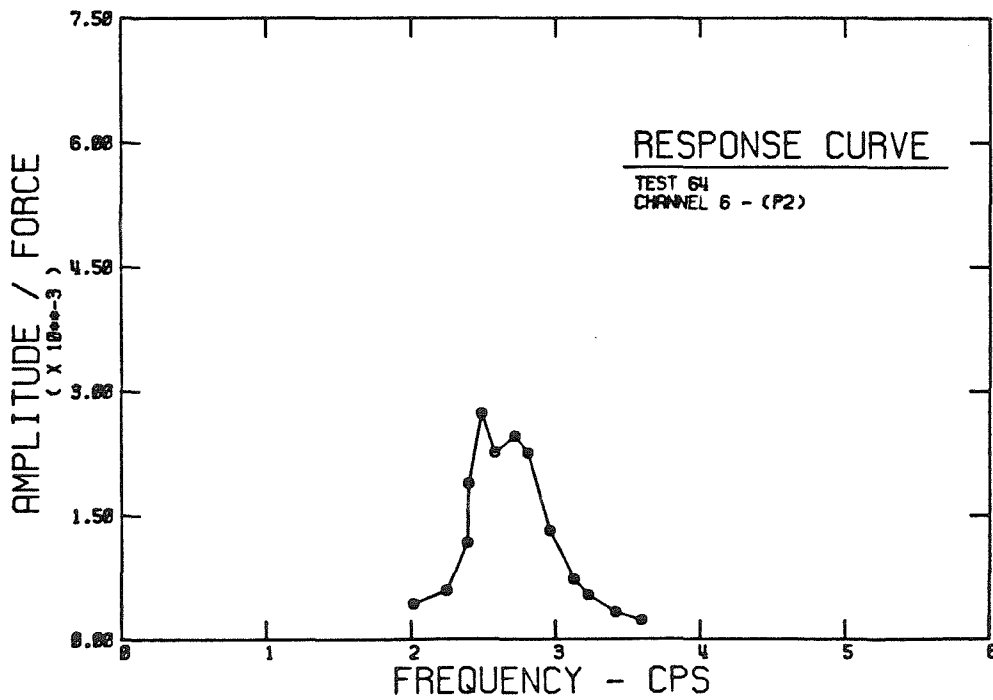


FIG. 7.14 RESPONSE CURVE FOR CONTACT PRESSURE AT 2R/3 DISTANCE FROM EDGE

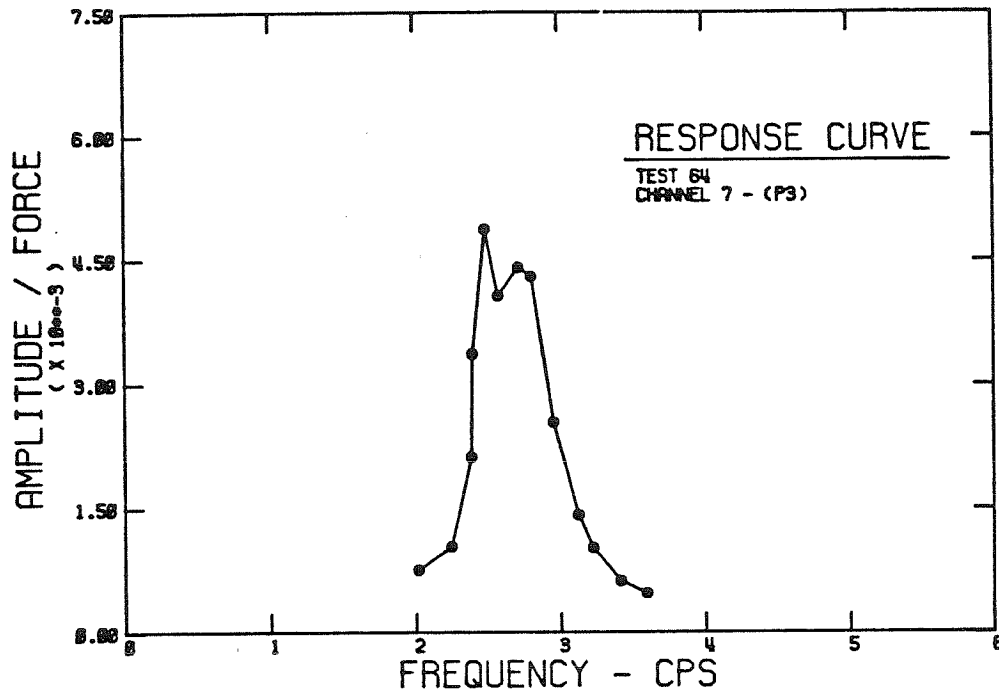


FIG. 7.15 RESPONSE CURVE FOR CONTACT PRESSURE AT R/3 DISTANCE FROM EDGE

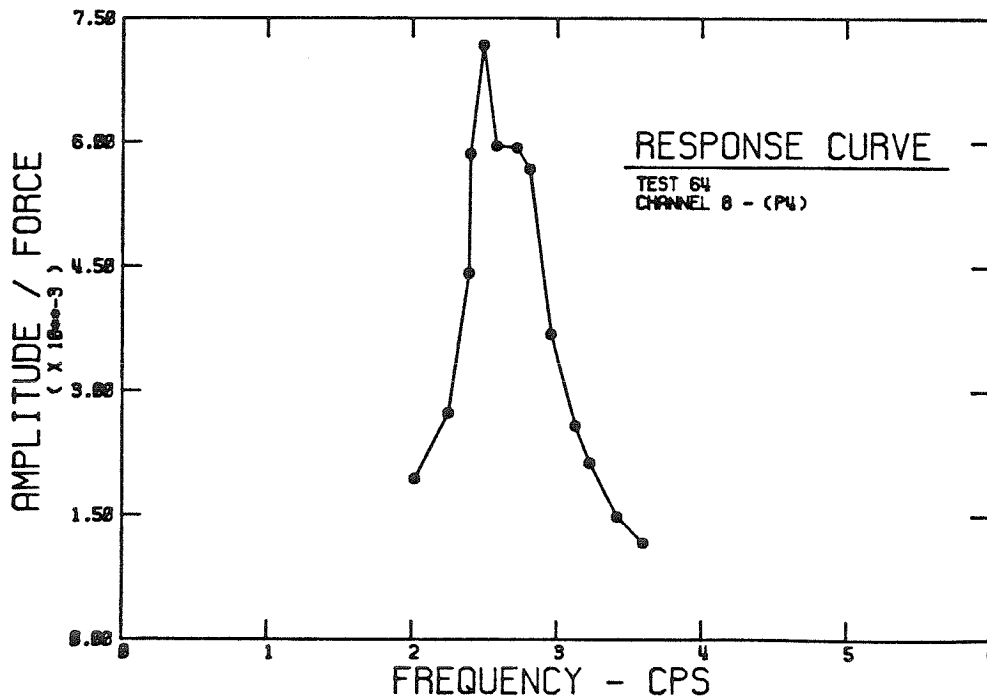


FIG. 7.16 RESPONSE CURVE FOR CONTACT PRESSURE AT FOOTING EDGE

measuring band width of the curve at an amplitude equal to 0.707 of resonant amplitude (see Chapter 3). However because of some common anomalies and scatter in the experimental response amplitude data points this simple method will usually fail in giving accurate results, especially in the case of the damping coefficient. Thus the powerful method of system identification technique (Beck 1978) was applied to obtain the dynamic properties of the foundation-soil system. Each response curve was used to develop an equivalent single degree-of-freedom (SDF) oscillator, from which resonant frequency and damping values were derived. Response of the SDF oscillator (Figure 7.17) to a sinusoidal frequency-dependent exciting force is defined as

$$z = \frac{me\omega^2}{\sqrt{(k - M\omega^2)^2 + (c\omega)^2}} \sin\omega t = Z_0 \sin\omega t \quad (7.1)$$

In nondimensional form, the amplitude  $Z_0$  may be expressed as follows:

$$Z_0 = \frac{A \frac{\omega^2}{\omega_n^2}}{\sqrt{[1 - (\omega/\omega_n)^2]^2 + (2\xi\omega/\omega_n)^2}} \quad (7.2)$$

where

$$A = \frac{me}{M}; \omega_n = 2\pi f_n = \sqrt{\frac{k}{M}}; \xi = \frac{c}{2\sqrt{kM}} \quad (7.3)$$

In the above equations  $m$  represents the unbalanced mass placed at eccentricity  $e$  from the center axis of the shaker;  $M$  is the total mass of the oscillator including  $m$ ; and  $k$ , and  $c$  are spring stiffness, and damping coefficient of the SDF oscillator respectively.

If by variation of amplitude  $A$ , resonant frequency  $f_n$ , and damping ratio  $\xi$  the theoretical response curve for the SDF oscillator coincides with the experimental data points or is fitted to them in a least square sense then the dynamic properties of the SDF oscillator give the best estimate to the experimental values,

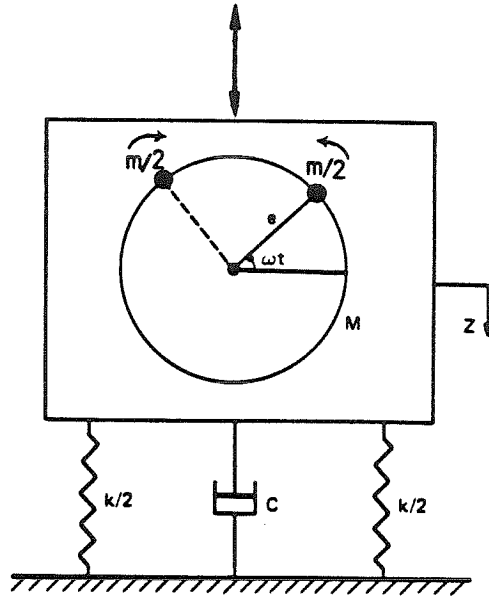


FIG. 7.17 SINGLE DEGREE-OF-FREEDOM OSCILLATOR

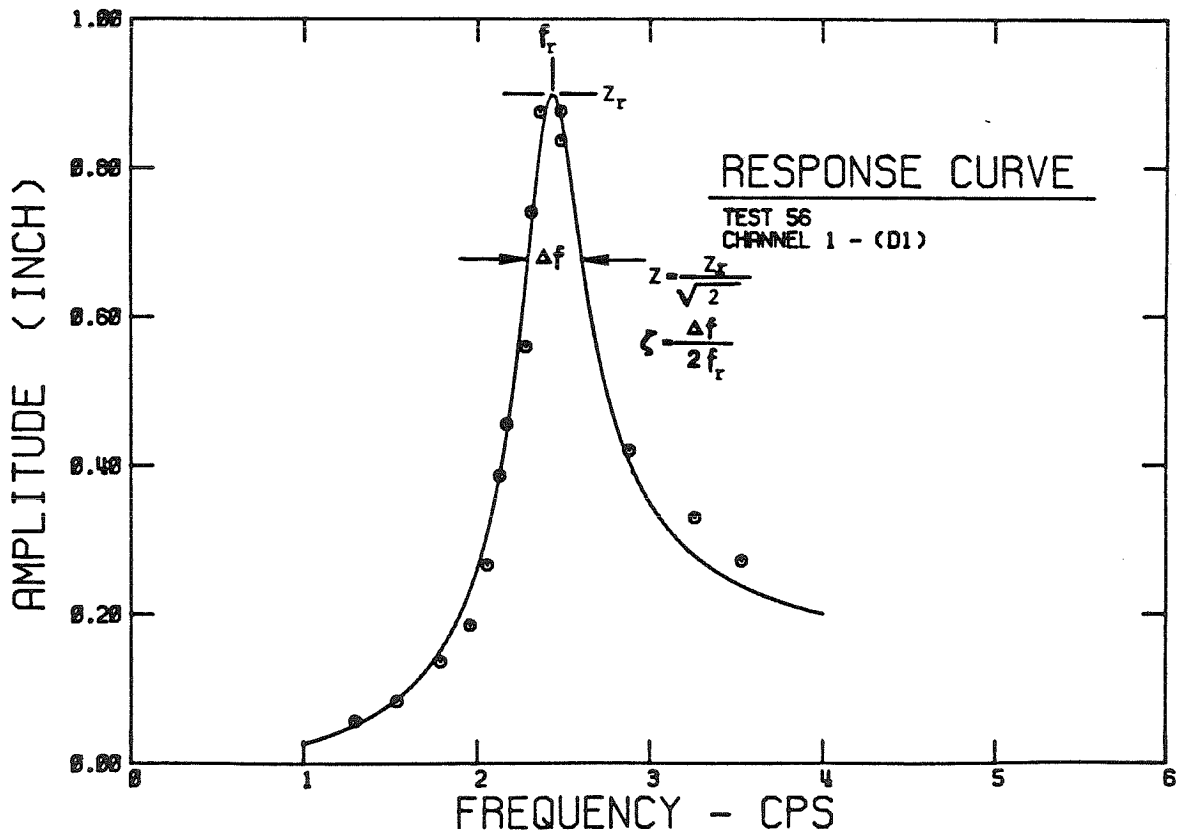


FIG. 7.18 COMPARISON OF RESPONSE OF FITTED OSCILLATOR AND EXPERIMENTAL DATA



for the particular vibration mode of the system being fitted. Expression 7.2 is nonlinear in terms of  $f_n$  and  $\xi$ ; thus, the fitting process requires a two-dimensional iterative minimization scheme in terms of these variables. A computer program originally developed by Beck (1978) and modified by Lin (1982) was adapted to a more efficient structure to analyze the present test data. The program was mainly changed for preprocessing of the input data and preparing the output plots and tables. Each resonant peak in the response curve was treated as an independent mode and was fitted individually. Because of some scatter in data points resulting from inelastic and nonlinear behavior of soil reflected in the data, some of the points had to be excluded from the fitting and in doing this special care was taken to avoid losing any useful information.

Figure 7.18 shows a typical experimental response curve for a surface foundation vibrating in its fundamental rocking-sliding mode (Test 56) and the response of the fitted equivalent oscillator. The experimental points in the figure are only those around the resonant peak which is used in the fitting. This way any error introduced by the contribution of the other response modes will be avoided. Even though response of a linear dynamic system is used to fit the experimental observations from a nonlinear system, in most cases of small to moderate amplitude vibration of the model tower, a reasonable fit was obtained which provides a unified approach in interpretation and evaluation of the data.

In the following sections effect of the different soil-foundation parameters on the fundamental frequency of oscillation for the rocking-sliding mode ( $f_n$ ) and on the damping ratio of the same mode ( $\xi$ ) are presented and discussed. In the presentation of data all the quantities involved are converted to prototype dimensions unless otherwise indicated.

### 7.2.2 Effect of Soil Depth and Side Boundaries

Two series of experiments with two different models (see Tbl. 6.2) were performed to study the effect of finite depth of the soil layer supporting the foundation.

Table 7.1 summarizes the test information and the resulting resonant frequencies and damping ratios of the model towers on different soil depths. Figure 7.19 shows the variation of the fundamental resonant frequency of rocking-sliding motion with the change of soil depth ratio  $d_r$  (equal to  $\frac{d_s}{R}$ , where  $d_s$  is the soil depth and  $R$  is the footing radius). Note that the data point giving the resonant frequency of the tower for zero soil depth (rocking on the rigid floor of the bucket) is not plotted. This is because the limiting condition of the zero soil depth is a singular case which can not be compared with the non-zero soil depth data. As is seen from the experimental values depicted in the figure the effect of the soil depth beyond a limiting minimum value of depth ratio, is negligible and does not significantly affect the natural frequency of tower oscillation. Therefore, the soil effect on dynamic characteristics of the rocking tower is a local effect developed at resonance because of large strain amplitude deformations around the edges of the foundation. This experimental observation is in agreement with the results of other similar experiments in a centrifuge (Morris, 1979). Whitman (1972) has also indicated that presence of a rigid stratum under an elastic half-space has negligible effect on dynamic behavior of a surface foundation if the depth to the stratum is at least twice the width of the foundation. In a theoretical study Kausel (1974) has shown that rotational stiffnesses (rocking and torsional stiffnesses) of rigid footings on the surface of a stratum on a rigid base are the least affected by the presence of the rigid base. His results illustrates that for  $d_r > 1.5$  only a few per cent decrease in resonant

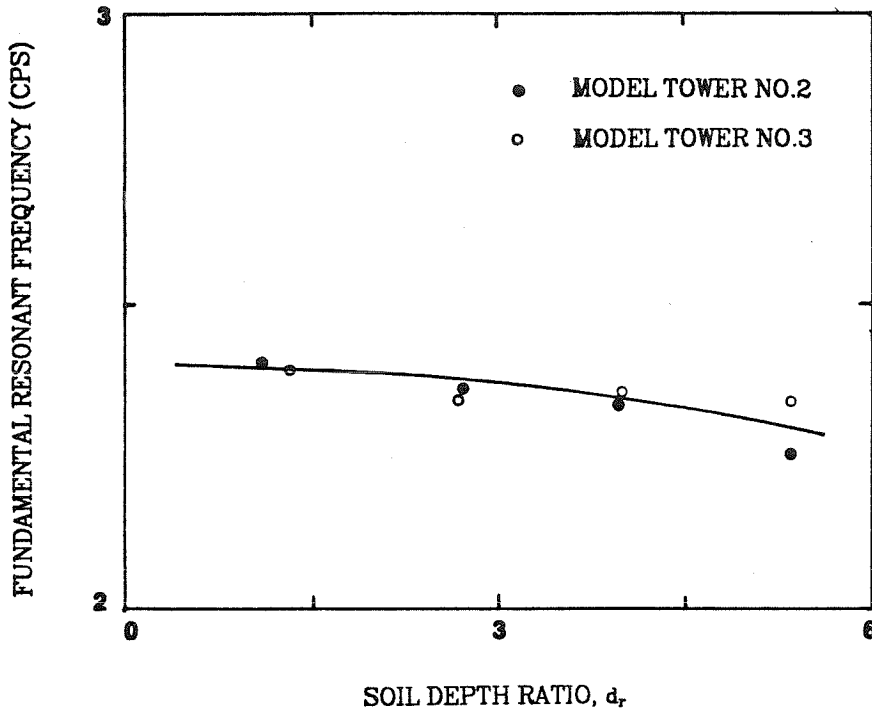


FIG. 7.19 EFFECT OF SOIL DEPTH ON ROCKING-SLIDING RESONANT FREQUENCY

Table 7.1. Fundamental Resonant Frequencies and Damping Ratios for Different Depths of Soil

Model (Tower) No.	Test No.	Soil Depth (ft) $d_s$	Depth Ratio $d_R$	Fundamental Frequency (Hz)	Damping Ratio (%)
2	1	0.0	0.0	1.65	1.2
	2	6.9	1.1	2.41	-
	3	16.7	2.67	2.35	5.0
	4	25.0	4.0	2.35	8.2
	5	33.3	5.33	2.25	-
3	25	0.0	0.00	1.65	1.2
	26	8.3	1.33	2.40	3.0
	27	16.7	2.67	2.37	5.0
	28	25.0	4.00	2.35	6.2
	29	33.3	5.33	2.30	4.4

frequency of the system occurs. The present test results even show smaller depth effect, where up to a depth approximately equal to foundation radius no substantial change in resonant frequency of the tower was observed.

This local effect of soil on fundamental frequency of the system was also observed in the tests of model foundations in different size buckets, which proved that the effect of side boundaries is also negligible in what is happening in the soil around the foundation and the structure supported on it, when the tower is oscillating with large amplitudes in its fundamental rocking-sliding mode of vibration. However, a profound effect of the rigid boundaries of the bucket was observed in the tests in the form of a second higher resonant frequency of the rocking mode of vibration, not far from the first one. Almost all the resulted response curves showed this second rocking mode which according to the theory and experimental observations (Gazetas, 1983; Richart, Hall, and Woods, 1970) is a higher rocking-sliding mode of a rigid surface footing on a homogeneous soil stratum. The modes of vibration of the foundation system are associated with the natural frequencies (in shear and dilation) of the soil layer (the bounded soil mass in the bucket in the centrifuge tests). Figures 7.20 and 7.21 from Test 28 depicting displacement response curves in D1 and D2 directions show clearly this effect of boundary presence, where a second peak is present around 4.0 Hz in both directions. There are other peaks in the response curves whose importance will be discussed later in the text.

A trend of increasing damping ratio with the increase of soil depth is seen from Table 7.1 which reflects an increase in loss of energy in the soil due to both material and radiational damping. The average damping of the soil-foundation system was about 5% in these tests.

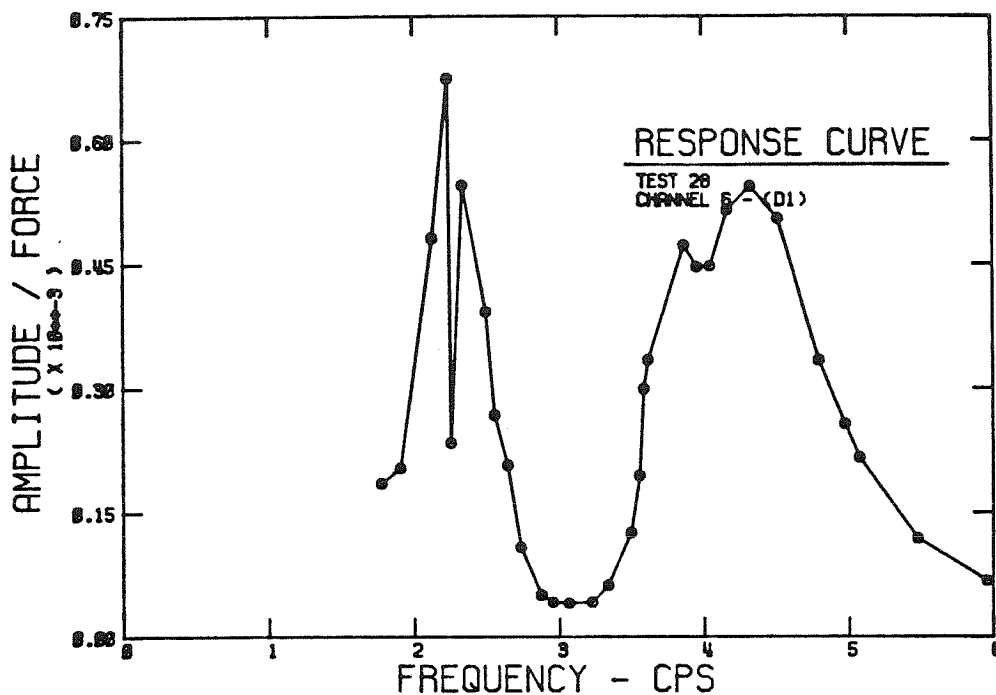


FIG. 7.20 SECOND ROCKING MODE AROUND 4.0 HZ BECAUSE OF BOUNDARY EFFECTS (D1 DIRECTION)

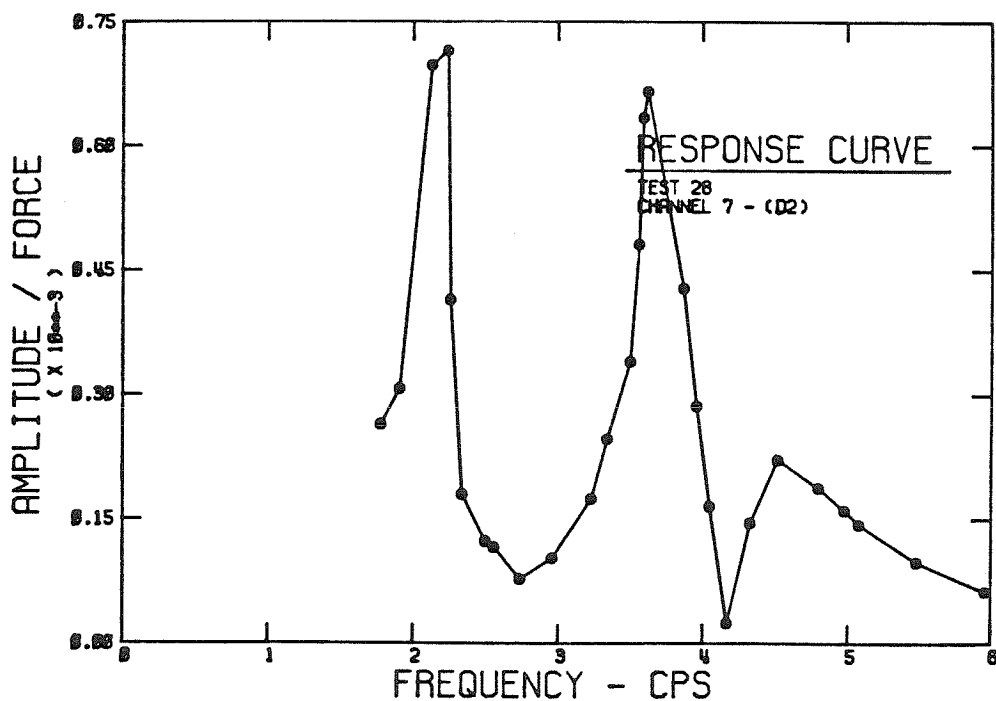


FIG. 7.21 SECOND ROCKING MODE AROUND 4.0 HZ BECAUSE OF BOUNDARY EFFECTS (D2 DIRECTION)

### 7.2.3 Influence of Foundation Size and Shape

Experiments 5, 6, 7 and 41, 43, 44 were performed on similar rigid towers with circular foundation with the only difference that in the latter group of tests a mass was added inside the tower. Tests 10, 11, and 12 were performed on another tower (tower No. 1, Table 6.2), varying the footing size while keeping the ratio  $\frac{\sqrt{M}}{I_b}$  constant. In the other two series of tests (Tests 5, 6, 7 and Tests 41, 43, 44) size of foundation was varied with all other tower parameters kept constant, independent from each other. Table 7.2 and Figure 7.22 summarize the resulting values of natural frequency and damping ratios of tower oscillation and the trend of frequency variation with the change of radius of the footing. A comparison of the results with a simple theory is presented in Chapter 8.

Table 7.3 and Figure 7.23 also present similar results derived for the square footings. In these tests the variables  $M$  and  $I_b$  were independently constant for all the models. The experimental results show that with all properties of the tower remaining constant, resonant frequency of vibration increases with the increase of footing radius. As is seen from Figure 7.22 and 7.23 natural frequency of the square footings with equivalent semi-dimensions are very close to the values for the equivalent circular footings. However, the resonant frequencies of square footings are slightly bigger than the ones for equivalent circular foundations over the entire range of frequencies of interest.

The equivalent semi-dimension for rectangular footings in general has been defined in three ways (Richart, Hall, and Woods, 1970). It is defined, (1) as the radius of a circular footing having the same area as the rectangular one; (2) as the radius of a circular footing with equivalent area moment of inertia as the rectangular one; and (3) as the radius of a circular footing with equal static spring stiffness for a footing on the surface of an idealized semi-infinite solid. In

Table 7.2. Effect of Footing Size on Damping Ratio and Fundamental Resonant Frequency (Circular Footings).

Test No.	D (ft)	W (ton)	I <sub>C.G.</sub> (ton-ft <sup>2</sup> )x10 <sup>3</sup>	h <sub>C.G.</sub> (ft)	f <sub>n</sub> (Hz)	ξ (%)
6	8.3	60.62	8.981	15.5	1.8	10.0
7	10.4	60.62	9.353	15.3	1.90	7.3
5	12.5	60.62	9.908	15.0	2.25	
10	8.3	87.50	9.267	15.9	1.55	
11	10.4	92.48	9.874	15.6	1.70	
12	12.5	91.89	8.980	15.4	2.00	
43	8.3	115.62	12.027	15.8	1.65	
44	10.4	115.62	12.027	15.8	1.90	4.0
41	12.5	115.62	12.027	15.8	2.35	7.5

Table 7.3. Effect of Footing Size on Damping Ratio and Fundamental Resonant Frequency (Square & Rectangular Footings).

Test No.	2c (ft)	2d (ft)	f <sub>n</sub> (Hz)	ξ (%)
(Square Footings)				
42	7.3	7.3	1.70	1.0
45	9.1	9.1	1.90	3.4
40	10.9	10.9	2.42	3.0
(Rectangular Footings)				
46	6.4	12.8	2.04	1.5
45	9.1	9.1	1.90	3.4
47	12.8	6.4	1.43	2.9
48	18.0	4.5	1.17	~ 0.5

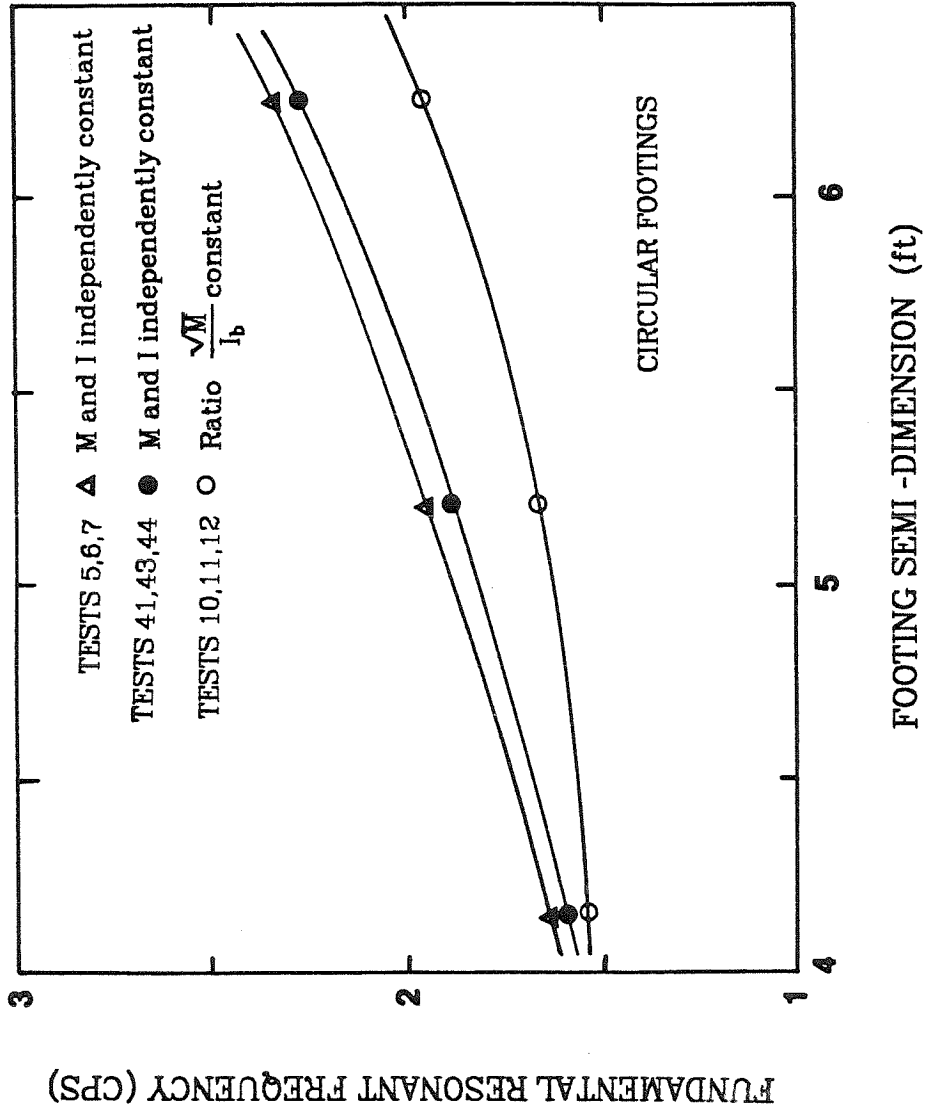


FIG. 7.22 EFFECT OF FOUNDATION SIZE ON ROCKING-SLIDING RESONANT FREQUENCY



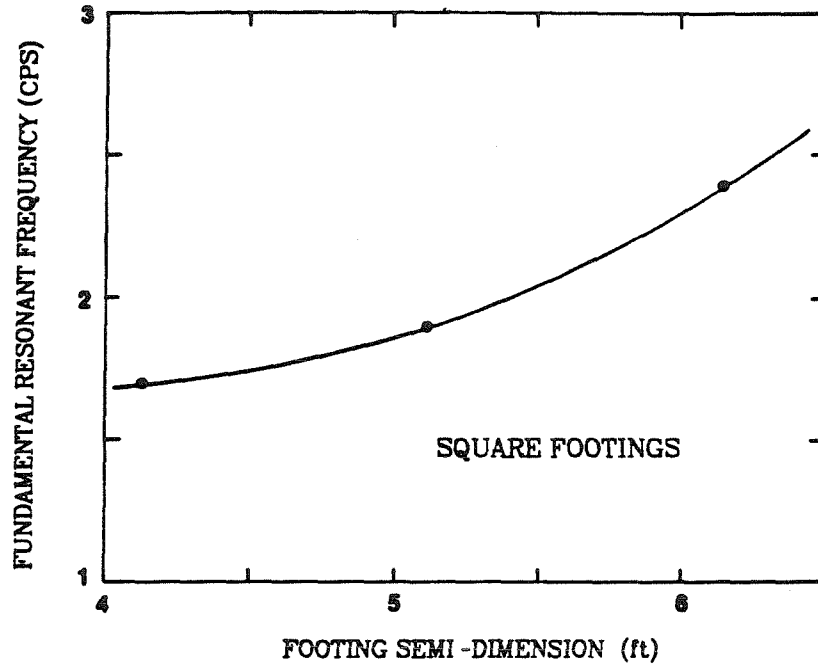


FIG. 7.23 EFFECT OF FOUNDATION SIZE ON ROCKING-SLIDING RESONANT FREQUENCY

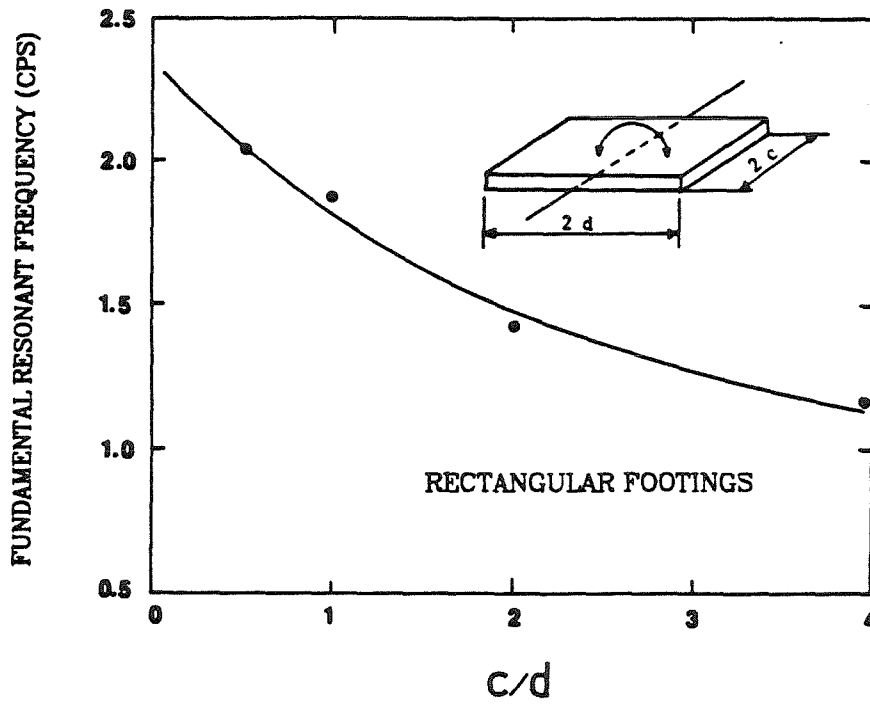


FIG. 7.24 EFFECT OF FOUNDATION SHAPE ON ROCKING-SLIDING RESONANT FREQUENCY

present study equivalent semi-dimensions of the tower bases were calculated according to method 2 from equating the areas of the model foundations.

Figure 7.24 shows the results for a rectangular footing with an area approximately equal to the area of the medium size circular or square footing used in former tests. The length-to-width ratio ( $c/d$ , where  $c$  and  $d$  are the half side lengths) for these rectangular footings was varied over a range of practical interest. It is obvious from this figure that an increase of the ratio of the side length parallel to the rotational axis of rocking to the length of the footing side normal to the rocking axis will result in a considerable decrease in resonant frequency of the foundation. Therefore, as expected narrow footings rocking around an axis parallel to their longer side will have low values of rocking frequencies and can be excited very easily in their rocking mode of vibration with larger amplitudes of motion in comparison to footings rocking around an axis parallel to the shorter side of footing.

#### **7.2.4 Variation of Rocking Resonant Frequency with Centrifugal Acceleration**

The natural frequency of towers varied with the centrifuge acceleration, increasing as the acceleration was increased. It is expected that this variation would be substantial because at each centrifugal acceleration the model structure simulates a prototype structure with different geometrical dimensions. Table 7.4 and Figure 7.25 support this expectation. According to the test results resonant frequency is proportional to  $(Ng)^{0.22}$  where  $Ng$  is the centrifuge simulated gravitational acceleration. The variation of frequency with a power of 0.25 of  $Ng$  has been predicted by theory and also reported by Morris (1981) in an experimental study.

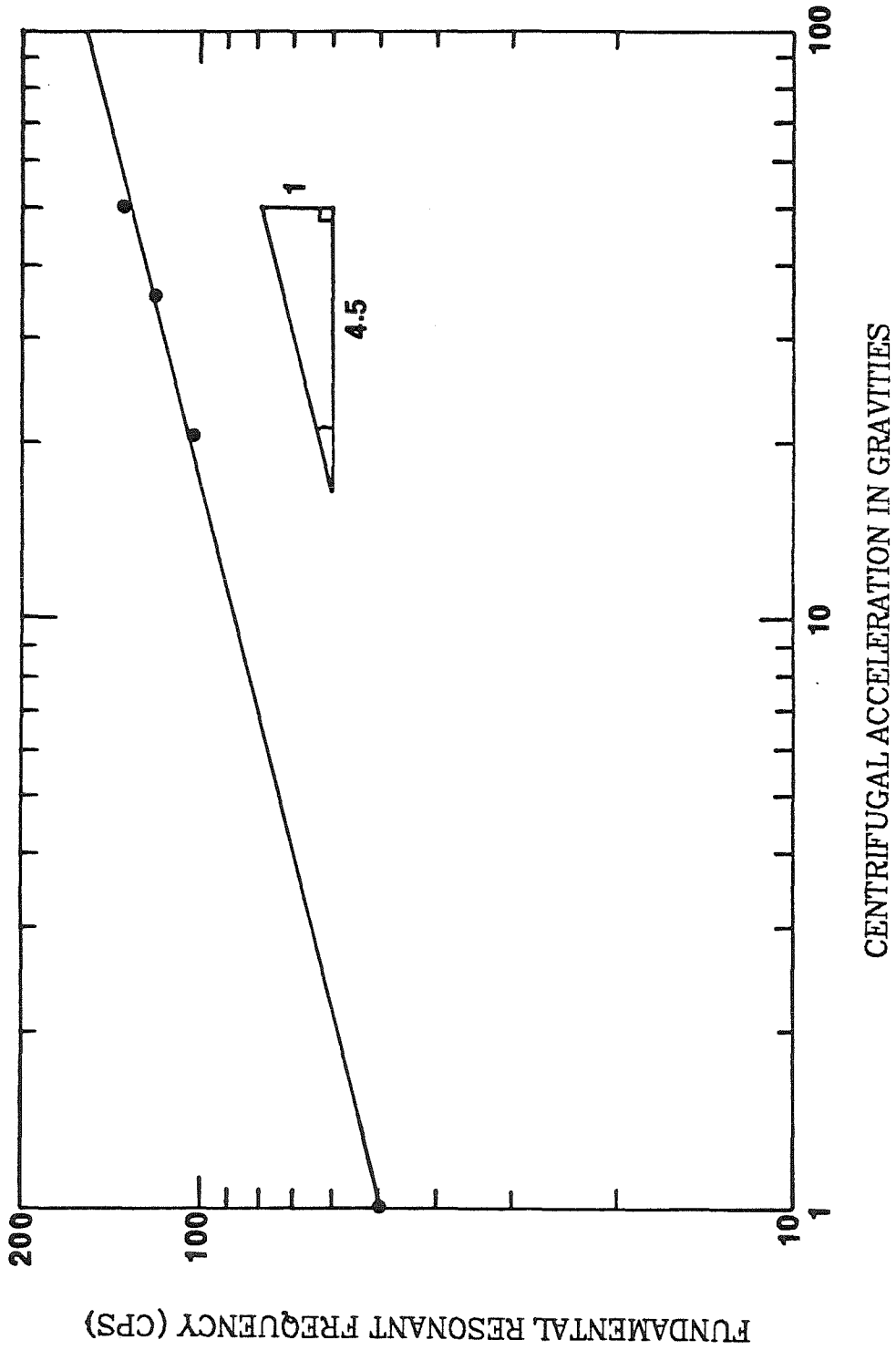


FIG. 7.25 EFFECT OF CENTRIFUGAL ACCELERATION ON ROCKING-SLIDING RESONANT FREQUENCY

### 7.2.5 Variation of Resonant Frequency with Eccentric Mass of Shaker

Increasing eccentric weight,  $w$ , in the shaker will increase the force amplitude at a particular frequency of shaker rotation. This will cause higher shear strain amplitudes in the soil under the foundation which results in more softening and nonlinear behavior of the soil. As a result resonant frequency of the system decreases while damping increases. These predictions were observed in the experiments showing a clear trend of decrease in resonant frequency with increase in the eccentric mass of the shaker. Tables 7.5 and Figure 7.26 show the result of the tests on two different models (Models 2 and 4, Table 6.2) both following the same trend of behavior as the eccentric mass increases. Figure 7.27 depicting the response curves for four tests with different shaker masses gives a better physical picture of this phenomenon. Note that as eccentric mass increases resonant frequency of the fundamental mode of rocking-sliding system decreases while both damping ratio and amplitude of vibration increase substantially. The increase in the shaker force and nonlinear behavior of the soil, due to increase in the eccentric mass, produces a more appreciable rise in amplitude and damping of the system than a decrease in their values resulted from the reduction of resonant frequency (due to yielding and softening of the supporting soil).

It should be noted that when resonant frequency decreases, force amplitude decreases as well; however, because of overall increase of the shaker force, the resulting softening in soil lowers the soil stiffness. The curves in Figure 7.26 are not very steep and the effect of increase in eccentric mass is not very important after a certain limit because of the reduction in the resonant frequency and the force which is proportional to frequency squared. An interesting fact observed in these tests was the increase of sliding amplitude relative to rocking contribu-

Table 7.4. Effect of g-Level on Damping Ratio and Fundamental Resonant Frequency of Towers.

Test No.	g-Level (g)	$f_n$ (Hz)	$\xi$ (%)
37	1.0	50.0	10.0
38	20.6	103.0	4.0
39	35.5	120.0	2.0
36	50.0	132.0	2.0

Table 7.5. Effect of Eccentric Mass of the Shaker on Dynamic Response of Model Towers.

Model No.	Test No.	Eccentric Weight, W (lbf $\times 10^{-4}$ )	$f_n$ (Hz)	$\xi$ (%)
	44	1.144	1.90	4.0
	51	2.384	1.78	3.5
2	50	6.244	1.64	5.4
	52	9.552	1.65	5.7
	53	14.070	1.62	9.1
	31	1.144	2.68	3.5
4	57	2.384	2.67	5.0
	55	6.244	2.33	6.0
	56	9.552	2.30	7.2

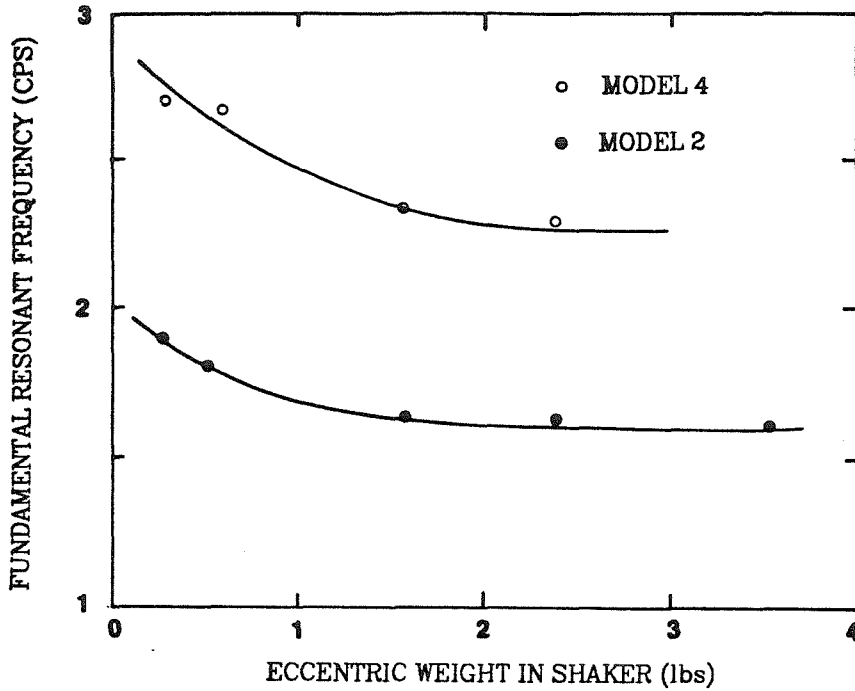


FIG. 7.26 EFFECT OF ECCENTRIC WEIGHT OF SHAKER ON ROCKING-SLIDING RESONANT FREQUENCY

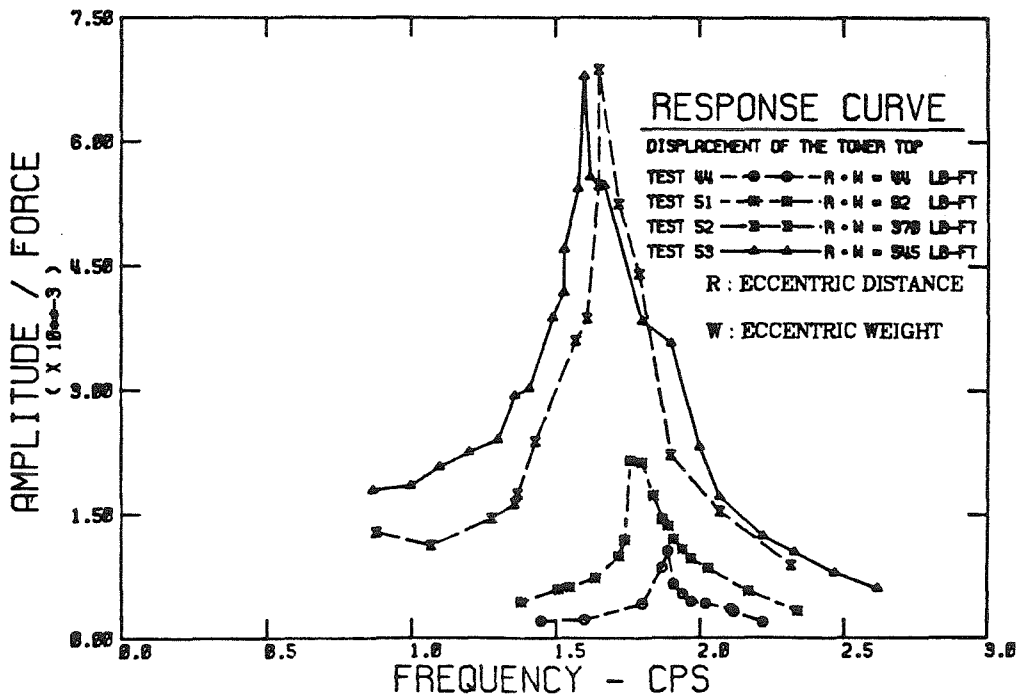


FIG. 7.27 RESPONSE CURVES OF TOWER DISPLACEMENT UNDER DIFFERENT FORCE LEVELS

tion in the total displacement of the model tower. After the experiment, it was noted that the tower had walked under the high amplitude horizontal force on its top, leaving a trace of its path on the soil.

### 7.2.6 Effect of Mass Moment of Inertia ( $I_b$ )

The result shown in Table 7.6 and Figure 7.28 for a decrease of resonant frequency with the increase of mass moment of inertia (about the rocking axis passing thru the center of footing-soil contact area), is well known and has been predicted by elastic half-space theory for dynamic behavior of rigid surface footings in numerous studies. This effect was clearly observed during experiments as is shown in Figure 7.28. Table 7.6 also presents the resonant frequency results along with damping ratio values varying with the mass moment of inertia.

### 7.2.7 Effect of the $\frac{\sqrt{M}}{I_b}$ Ratio

Table 7.7 and Figure 7.29 summarize the influence of this factor on the dynamic properties of the tower. These results are derived from tests on models of equivalent footing size with different inertial properties (different  $\frac{\sqrt{M}}{I_b}$  ratios). The number of tests was insufficient and they were performed on various model towers at different times during the testing schedule. Therefore, conclusive results in this case require more thought and judgement than other cases. However, the trend of frequency variation with the value of  $\frac{\sqrt{M}}{I_b}$  ratio is shown in the figure and will be discussed more in Chapter 8 in a comparison with theoretical prediction.

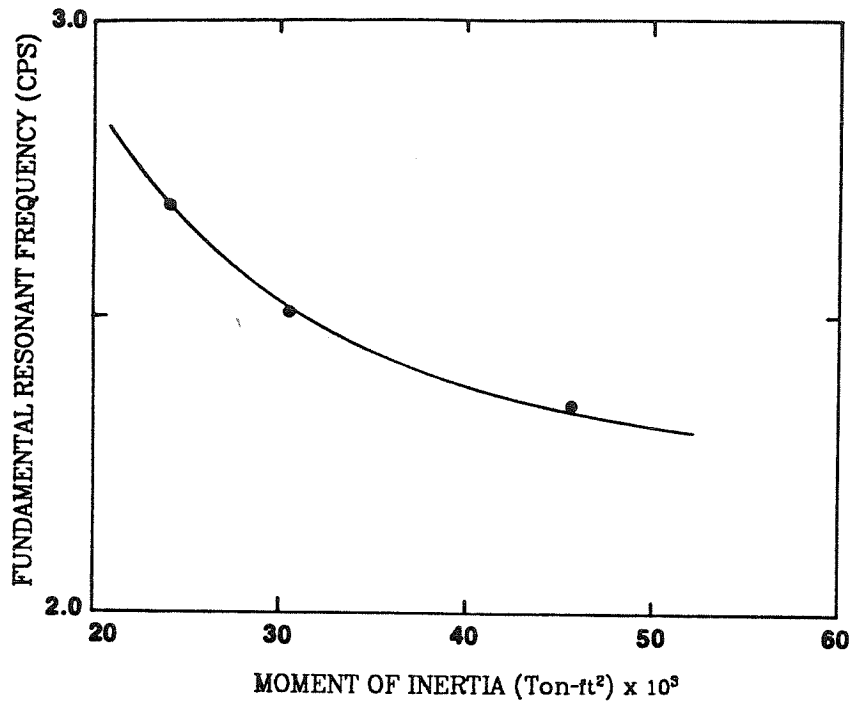


FIG. 7.28 EFFECT OF MASS MOMENT OF INERTIA ON FUNDAMENTAL ROCKING-SLIDING FREQUENCY OF TOWER

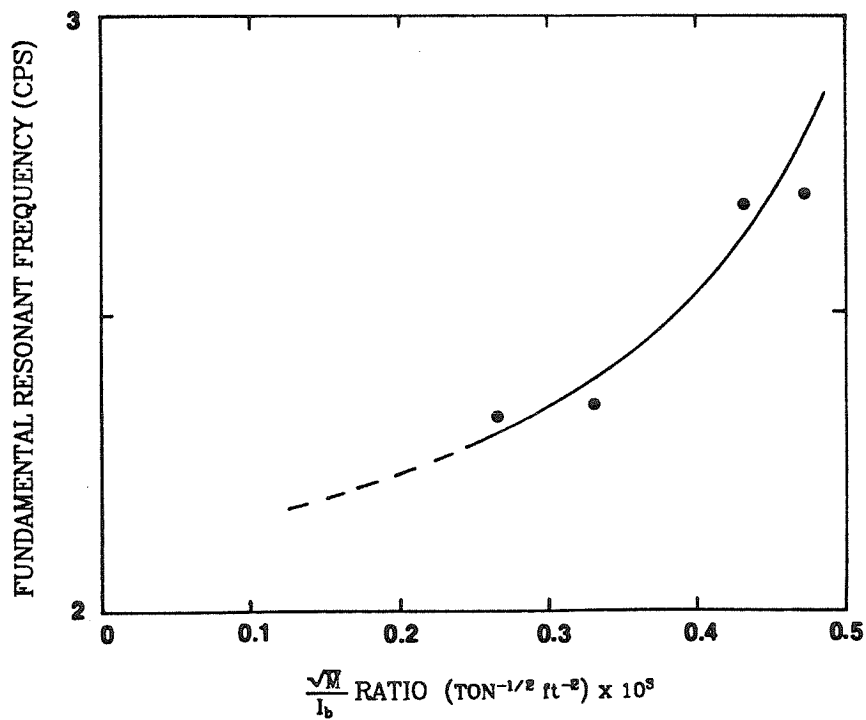


FIG. 7.29 EFFECT OF THE  $\frac{\sqrt{M}}{I_b}$  RATIO ON FUNDAMENTAL ROCKING-SLIDING FREQUENCY OF TOWER



### 7.2.8 Influence of Footing Embedment

Effect of embedment is shown in the results presented in Table 7.8 and Figure 7.30 for the variation of damping ratio and resonant frequency of the model tower with the embedment ratio ( $\delta$ , equal to the ratio of depth of embedment to radius of footing). The results are given for both the direction of applied horizontal force on the tower top and direction normal to it (represented by subscripts 1 and 2 respectively in Table 7.8). It is well known that increasing embedment depth of the foundation will increase the stiffness of the soil-structure system and therefore will result in an increase in natural frequency of the structure. This phenomenon was studied in a series of tests changing depth of embedment from 0 to 1.5 times the radius of the tower base. As shown in the Figure 7.30 increase of the frequency with embedment ratio is not very large. This is because of the high amplitude of the force, large number of load cycles, and particularly ineffective contact between the tower side walls and the soil mass. In most theoretical methods full contact between soil and foundation side boundaries is assumed during oscillation which will influence the results considerably, amplifying the effect of embedment of the foundation. Tension stresses cannot develop between footing side walls and the soil surrounding it; therefore a gap between soil and tower side walls will be formed and filled by loose soil, resulting in the reduced effect of embedment. Stokoe and Richart (1974) in an experimental study on full-scale model circular footings embedded in a dense, dry sand subjected to rocking excitation showed that embedment without adequate lateral support was essentially ineffective. In fact only a 10 to 15 per cent increase in geometrical and resonant frequency was observed at an embedment depth equal to 1.5 times the footing radius. They showed that proper embedment had a significant effect on both total damping and resonant frequency.

Table 7.6 Damping Ratio and Fundamental Resonant Frequency for Models with Different Mass Moment of Inertia.

Test No.	Moment of Inertia, $I_b$ (ton-ft <sup>2</sup> ) $\times 10^3$	$f_n$ (Hz)	$\xi$ (%)
31	24.230	2.68	3.5
62	30.762	2.50	3.3
29	45.974	2.30	4.4

Table 7.7. Damping Ratio and Fundamental Resonant Frequency for Models with Different  $\sqrt{M}/I_b$  Ratios.

Test No.	$\sqrt{M}/I_b$ ( $\times 10^{-3}$ ton <sup>1/2</sup> ft <sup>-2</sup> )	$f_n$ (Hz)	$\xi$ (%)
5	0.331	2.25	4.4
30	0.471	2.70	
31	0.432	2.68	3.5
41	0.264	2.35	

Table 7.8. Damping Ratio and Fundamental Resonant Frequency at Different Depths of Embedment

Test No.	$d_e$ (ft)	$\delta$	$f_{n1}$ (Hz)	$\xi_1$ (%)	$f_{n2}$ (Hz)	$\xi_2$ (%)
64	0.0	0.0	2.45	5.4	2.88	5.7
65	3.13	0.5	2.57	5.8	3.25	3.7
66	6.25	1.0	2.63	5.9	3.55	3.7
67	9.38	1.5	2.67	5.1	3.80	3.6

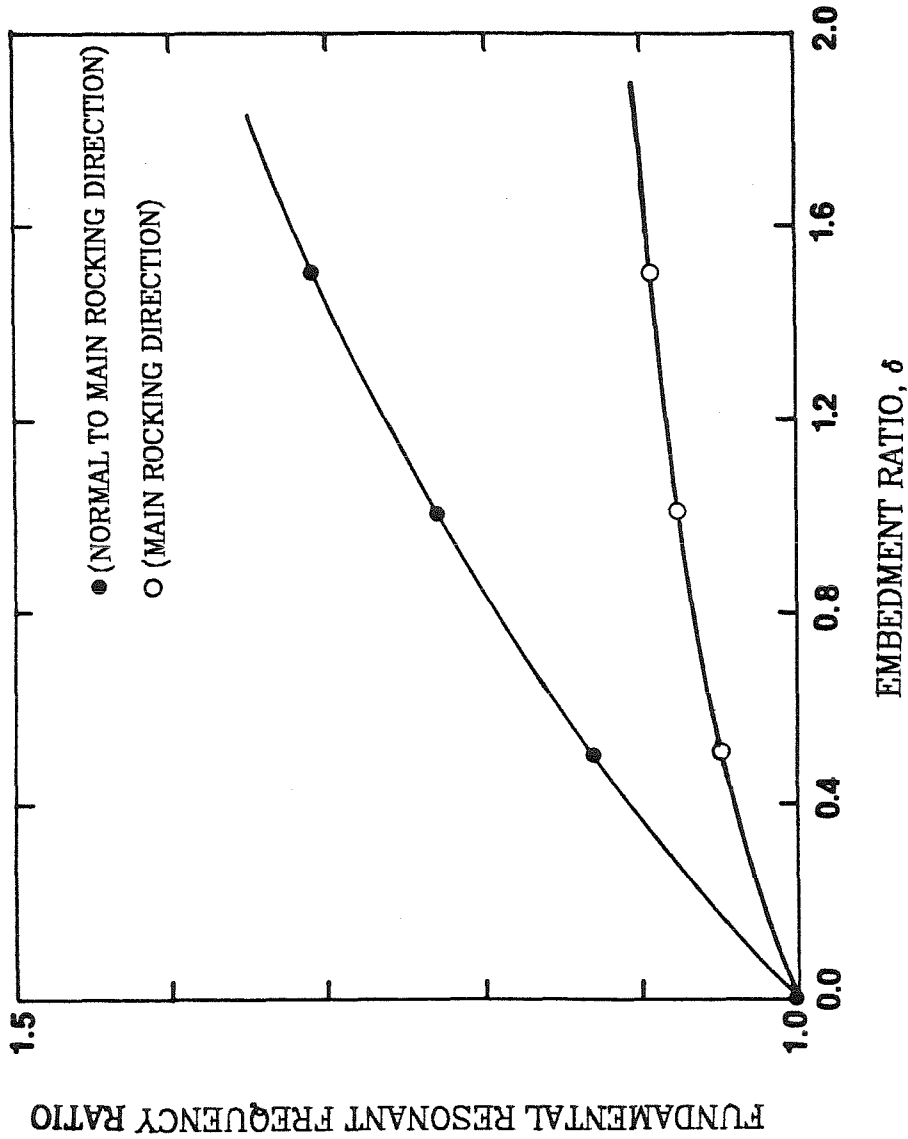


FIG 7.30 EFFECT OF DEPTH OF EMBEDMENT ON FUNDAMENTAL ROCKING-SLIDING FREQUENCY OF TOWER

Figures 7.31 and 7.32 give a clearer physical appreciation of the embedment effect by collecting the response curves for the four different depths of embedment in one place. The following facts and conclusions can be deduced from a careful study of the results shown in the figures and the table presented in this section on the effect of embedment:

- (1) Embedment effect is different in the two directions of main rocking motion and normal to it (D1 and D2 directions). Stiffness of the soil-structure system increases more effectively in the direction normal to main rocking motion. This fact, to which no attention has been paid before, is a result of large amplitude loading in the rocking direction which produces a nonhomogeneous strain pattern and soil-footing contact condition around the tower. In an experiment no matter how much care is spent in mounting the loading system on the model a pure one-dimensional loading in the desired direction can not be obtained. Thus there is always a small amplitude load in a direction normal to the main rocking motion. If the model structure and the soil bucket are completely axisymmetric and the surrounding soil is homogeneous, then it is expected that the non-alignment of the force will only create a motion and a single related resonant frequency in a direction having a small angle with the rocking motion direction initially desired. It was observed, however, in the experiments that two different resonant peaks close to each other in the two above mentioned directions exist in the system. Therefore existence of the two different resonant peaks as is seen in the response curves is a sign of the nonhomogeneity of the soil around the model structure, and inaccuracy of the axisymmetry assumption for the model and soil container. In fact the model structure wobbled around in the horizontal plane of motion along an

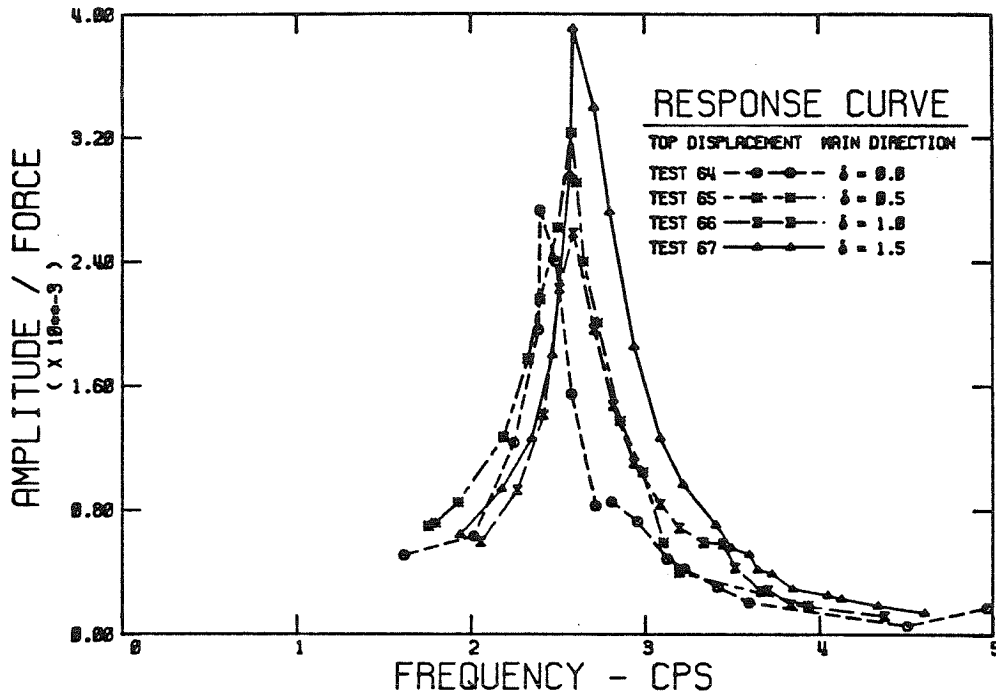


FIG. 7.31 RESPONSE CURVES FOR TOWER DISPLACEMENT AT DIFFERENT DEPTHS OF EMBEDMENT (MAIN ROCKING DIRECTION)

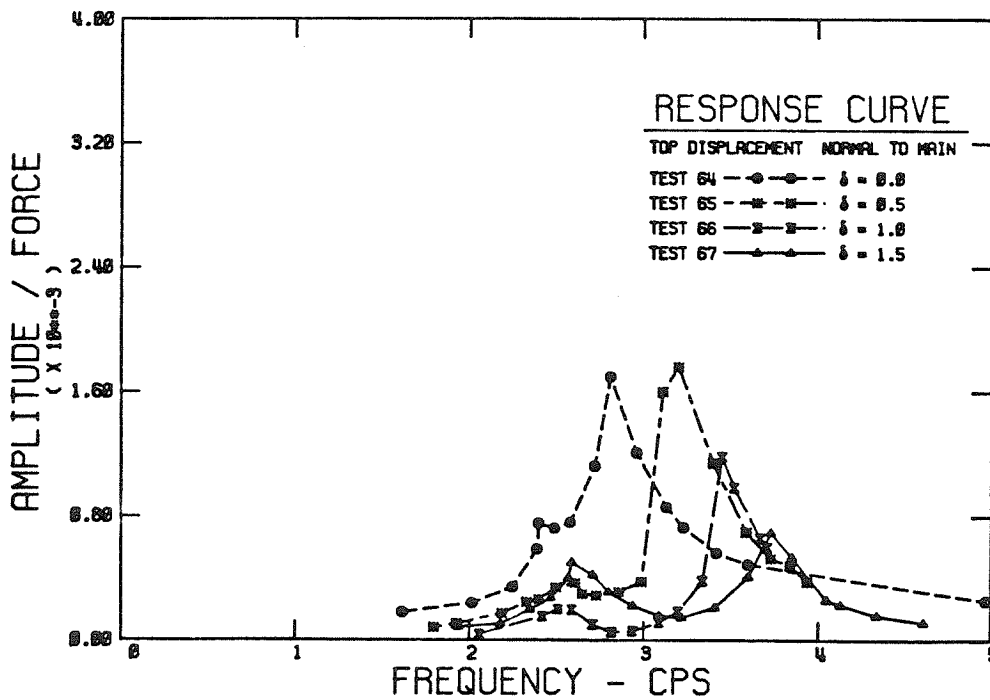


FIG. 7.32 RESPONSE CURVES FOR TOWER DISPLACEMENT AT DIFFERENT DEPTHS OF EMBEDMENT (NORMAL TO MAIN ROCKING DIRECTION)

elliptical path which its shape constantly varied over the frequency range of vibration. Displacement path of the tower top center point during rocking-sliding vibration in Test 64 is shown in Appendix C. Since the strains developed in direction normal to the main rocking motion are much smaller, therefore, less yielding and softening in the soil adjacent to the foundation, and consequently less separation between soil and foundation will occur. This causes a more appreciable increase in resonant frequency of the model in this direction with the increase in depth of embedment. Resonant frequency increases about 30 % from zero embedment to 1.5 times radius depth of embedment for the direction normal to the main direction, while there is only a 10 % increase in resonant frequency in the main rocking direction. As seen from Figure 7.32 the gap between the two resonant peaks in each response curve increases as depth of embedment increases, showing a faster increase in resonant frequency in direction normal to main when embedment ratio increases. Also more nonhomogeneity develops in the soil as the experiment goes on and layers of soil are added around the tower.

- (2) Amplitude of motion overall increases with increase of embedment depth in the main direction, but there is a definite decreasing pattern in the amplitude, in the direction normal to main one, as embedment ratio increases. Once again this is because of much smaller strain amplitudes in direction normal to main one, which results in a more elastic behavior in the soil. Another important factor, explaining the unexpected increase of vibration amplitude in main direction, is negligible variation of total damping with the change of embedment. This will be discussed in next paragraph.

- (3) Damping does not show any particular trend with the change in depth of embedment and overall remains constant for all embedment ratios. The improper footing embedment (ineffective bond between soil and foundation) is the main factor causing the slight variation of damping ratio. The small value of geometrical damping in the soil-foundation system, because of rigid boundaries of the soil bucket, is another reason for the above phenomenon. Therefore, embedment does not change the damping. However, there is a clear difference between the damping ratios in the two rocking directions which shows higher damping values in main direction of rocking presumably because of larger strain amplitudes in the soil in this direction.
- (4) The major increase in stiffness of the embedded foundation occurs from the zero embedment to the first embedment depth of 0.5 times foundation radius. Additional increase in embedment depth has a minor effect on stiffness of the soil-foundation system. This is because confining pressure in the soil at the footing edge, changes from zero to a finite value from no embedment to an initial depth of embedment.

## **7.2.9 Static and Dynamic Pressure Distribution over the Footing-Soil Contact Area**

### **7.2.9.1 *Static Pressure Distribution***

Static pressure distribution along the radius of the rigid circular footings resting on the surface of sand at the center of area inside a cylindrical container was measured for different soil depths. Soil depth was varied from 1.5 to 8.0 inch and contact pressure distributions were measured at 1.6, 4.0, 6.0, and 8.0 inch of soil depth. Figure 7.33 shows these pressure distributions along the

diameter of the foundation assuming an axisymmetric distribution over the entire contact area. In all the tests measuring pressure distributions the radius of the model footing was 1.5 inch. Meyerhof (1951) has suggested that the static stress block (static contact stress distribution) for a rigid surface footing on a cohesionless material, to be a trapezoid which changes to a triangular at ultimate load (Fig. 7.34). As is seen from Figure 7.33 the static pressure distribution measured for the footing on maximum soil depth of 8 inches (excluding the effect of rigid floor of the bucket) approximates the theoretical shapes in Figure 7.34. However, a more rounded vertex is observed, as would be intuitively expected. Both theoretical and observed distributions indicate that because of low confining pressure in the sand under the edges of the footing, it can sustain very little stress, and strength increases towards the center where the sand is more confined. Under large vertical static loads the soil in the proximity of the foundation edge yields and some initial permanent deformation occurs. This initial yielding will affect the dynamic pressure distribution as is seen in later parts of this section. Before presenting the test results for dynamic pressure distribution produced by the rocking moment, it is essential to explain the mechanism of permanent deformation and lift off observed during the tests which directly affects the shape of the stress block under the footing.

#### *7.2.9.2 Mechanism of Yielding, Lift off and Separation During Rocking of The Tower*

Most of the theoretical and experimental research to date has ignored either plastic yielding effects or separation of the footing from the soil. The present experiments in this study showed that in almost every dynamic test the soil around the footing edge yields and the foundation edge separates from the soil. In fact this is caused by the plastic deformations which results in densification



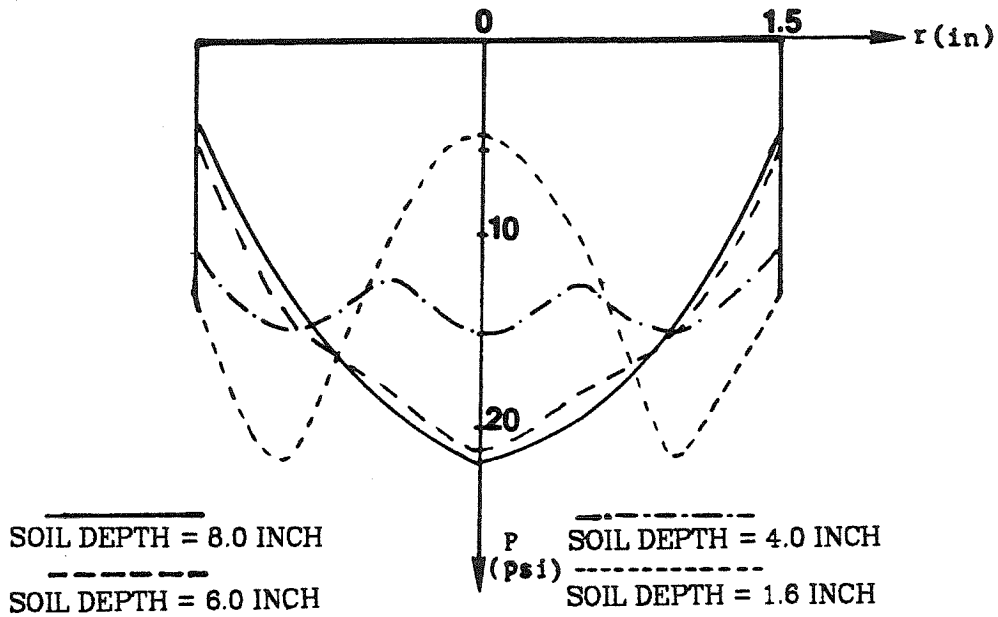


FIG. 7.33 STATIC PRESSURE DISTRIBUTIONS ALONG FOOTING DIAMETER AT DIFFERENT SOIL DEPTHS

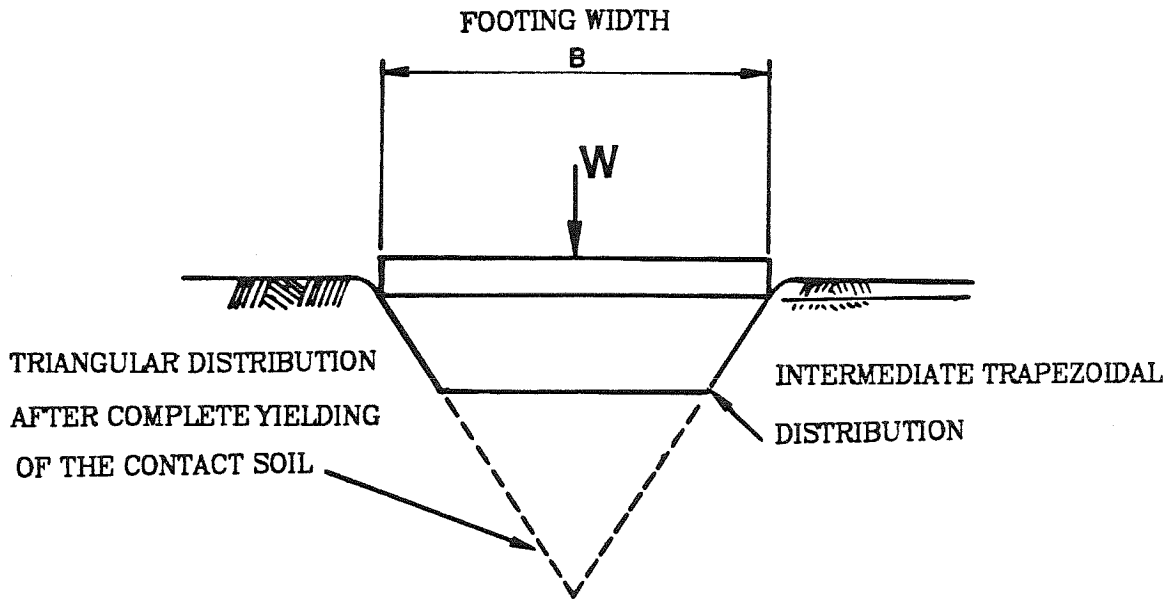


FIG. 7.34 THEORETICAL PREDICTION FOR INITIAL STATIC PRESSURE DISTRIBUTION OF A RIGID STRIP FOOTING ON SURFACE OF A COHESIONLESS SOIL

and settlement of the soil. The addition of the rocking moment, no matter how small, will cause further yielding along the leading edge in addition to the initial statically yielded zone and results in more separation of footing and soil along the trailing edge due to foundation lift off and deformed outer zone. During the rocking vibration, the footing deforms the soil (starting from the edges and moving gradually inwards) into a rounded profile, causing the rigid footing to lose full contact with the soil (Fig. 7.35). The reduced bearing width in successive cycles due to rounding of the foundation will produce increasing settlement of the foundation. Since the vertical load on the footing remains constant during the test, for equilibrium the volume under the contact stress block must stay the same and consequently the shape of the stress block should vary continuously until the contact soil surface assumes a stable configuration. No major change in average pressure distribution was observed at frequencies far from resonance indicating a more linear reversible behavior at these small amplitude vibrations. Lift off and increased yielding at the edges will occur mainly at frequencies close to resonance and therefore the soil-structure system behaves highly nonlinearly at these frequencies because of both plastic deformation and the lift off process. Due to the above mentioned increased non-linearity the resonant frequency of the soil-foundation system decreases and the amplitude of the vibration increases.

At resonance a profound change in configuration of the contact pressure distribution occurs. Pressure amplitude (dynamic plus static) at the foundation edge drops to a small value because of partial separation or to zero in case of full separation, while pressure in the vicinity of the footing center increases an appreciable amount. Figure 7.36 shows the static pressure distribution before and after applying the dynamically varying moment and going through resonance during a test. It is observed that because of reduction in contact width

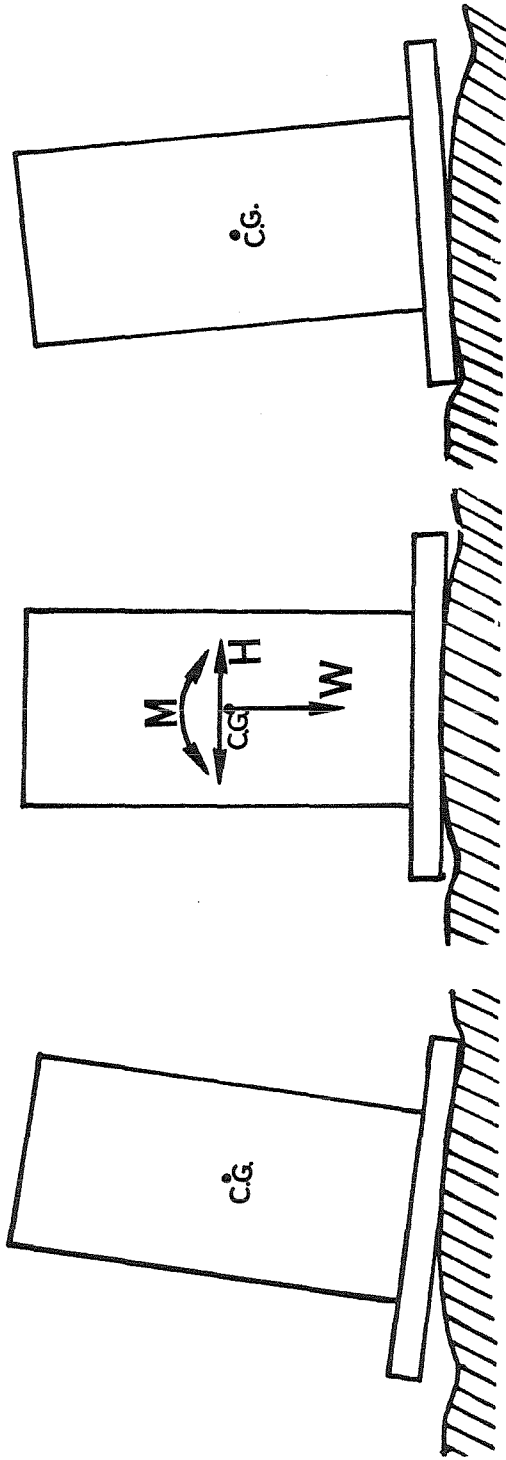


FIG. 7.35 MECHANISM OF FOUNDATION LIFT-OFF AND ROUNDING OF THE CONTACT SOIL SURFACE

the stress block has reverted to a much narrower wedge shape configuration. It was observed that in some tests due to initial yielding under static load, the footing separates from the soil near the edge from beginning of the test. Therefore in such a case going through resonance will cause more yielding and lift off of the foundation.

### 7.2.9.3 *Dynamic Pressure Distribution*

At a constant depth of soil equal to 8 inches, dynamic pressure distributions along the diameter of the footing (Tests 17 and 33), and around the circumference of the circular footing (Tests 14 to 16 and 34 to 36) were measured. For measuring pressure variation around the circumference two pressure transducers P1 and P3 were mounted on the diameter normal to the rocking axis and the other two transducers (P2 and P4) were mounted at similar distances along a diameter at different angles, depending on the test, with respect to the direction of P1 and P3 (see Fig. 5.19 patterns A, B, and C). Approximate pressure distributions were derived by comparing the response curves for the pressure signals over the entire range of frequencies in the test. Two distinct pressure distribution patterns were observed depending on the amplitude of vibration. In the case of low amplitude vibration (practically no plastic deformation in soil) the average dynamic pressure distribution over the frequency domain is plotted in Figure 7.37a. As is seen the dynamic pressure amplitude increases from a minimum value at the footing center to a large amount at the footing edge (see also Fig. 7.40a, Test 64). This configuration of pressure distribution remains unchanged until there is some yielding and lift-off around the edge of the foundation. Figure 7.37b shows a progressive change of dynamic pressure distribution along the footing diameter (normal to rocking axis) as the frequency increases. Note that in this case soil around the footing edge has yielded and

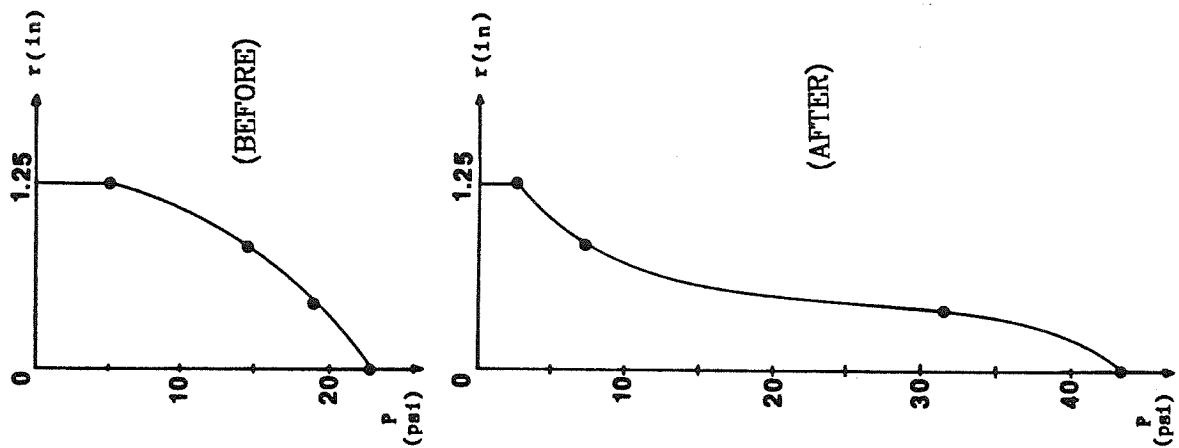


FIG. 7.36 STATIC PRESSURE DISTRIBUTION BEFORE AND AFTER TEST

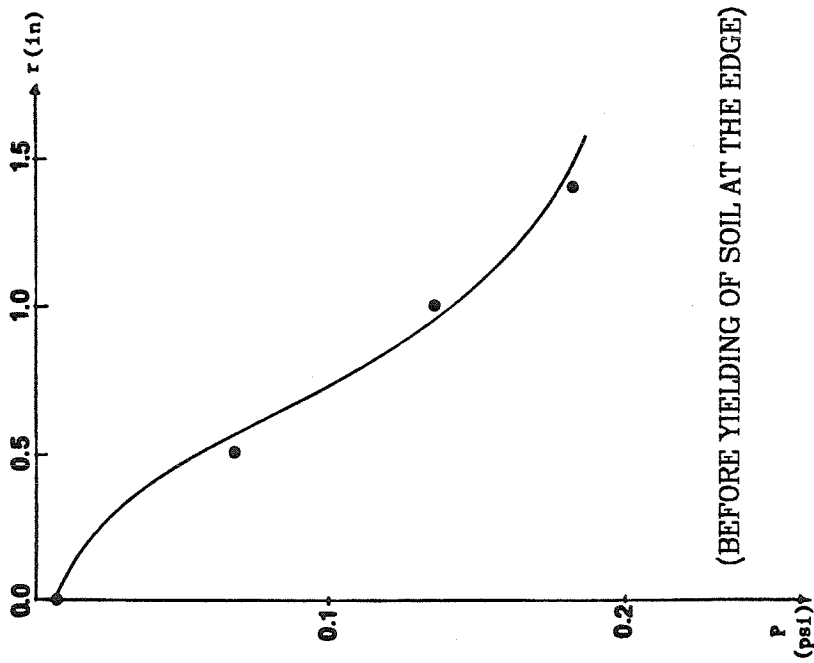


FIG. 7.37a DYNAMIC PRESSURE DISTRIBUTION UNDER ROCKING  
FOUNDATION DIAMETER

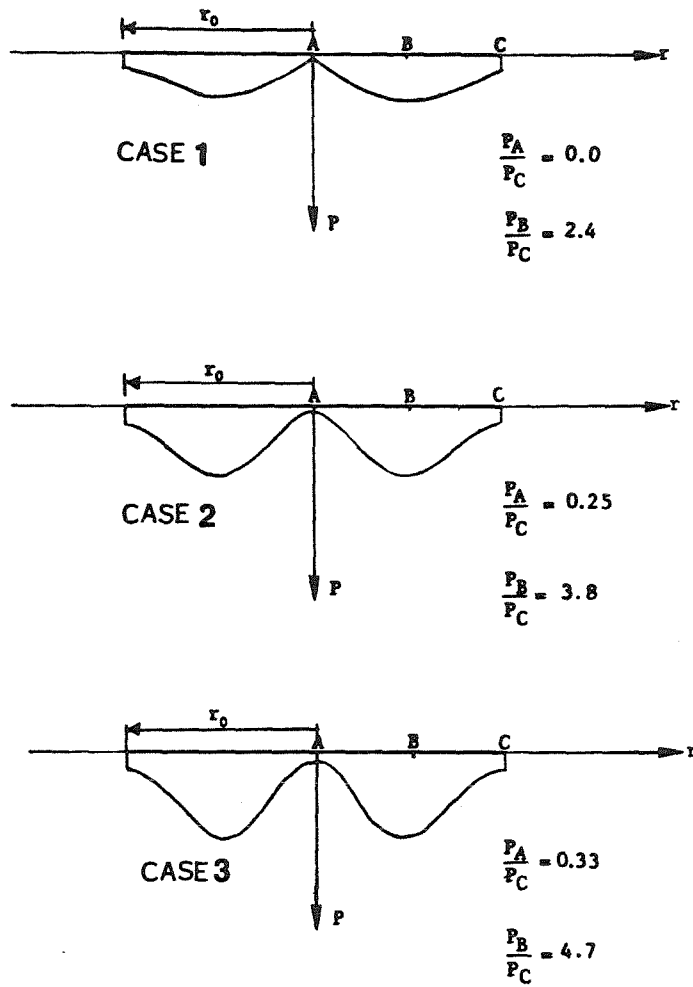


FIG. 7.37b DYNAMIC PRESSURE DISTRIBUTION UNDER ROCKING FOUNDATION ALONG DIAMETER AND AT INCREASING ROCKING AMPLITUDES FROM CASE (1) TO (3) IN FIGURE (AFTER YIELDING OF SOIL AT THE EDGE)

some plastic deformations has occurred in soil. Figures 7.38 and 7.39 show the response curves for the pressure signals after soil has yielded around the footing edge or lift off of foundation has occurred. Thus, because of yielding of soil in contact with foundation around the edge, pressure for transducer P4 at the footing edge is smaller than pressure at P3 position (see Fig. 5.19 pattern D). In Figure 7.38 (Test 17) pressure at the edge is smaller than pressure at the next transducer location toward the footing center at all frequencies of vibration. On the other hand in Test 33 (Fig. 7.39) pressure at the edge is originally bigger and then becomes smaller than pressure measured by P3 around resonance when soil has yielded and lift off has occurred. Figures 7.40a, 7.40b, and 7.40c show variation of pressure distribution with increase of embedment depth by comparing the response amplitudes of pressure signals. It is observed that embedment increases the confining pressure in the sand near the footing edge and therefore results in an increase of soil strength, preventing the foundation lift off and yielding of the soil at the edge. As the depth of embedment increases dynamic pressure amplitude near the edge increases considerably compared to pressure amplitude at points closer to the footing center. This shows that, with embedment, the behavior of the soil-foundation system is approaching the linear elastic half-space model which predicts very large vertical stresses near the footing edge.

Because of many effects such as: tilting of the tower during the test or when spinning the centrifuge to speed; local irregularities in the soil-footing contact surface; nonhomogeneity in the soil, and other factors, the pressure distribution was very sensitive to the test conditions and varied a lot from test to test which to some lesser degree is also the case with real foundations placed on soil. Dynamic pressure distribution as a function of  $\theta$  (angle around the circumference, see Fig. 5.19) under the footing rocking about an axis ( $\theta = 90^\circ$ ) passing

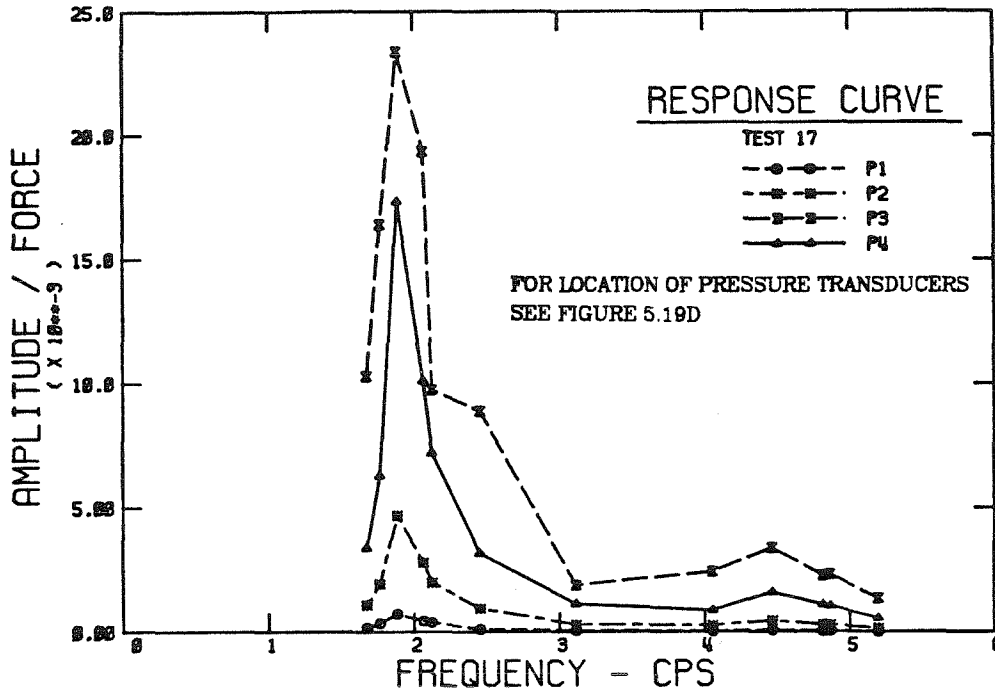


FIG. 7.38 RESPONSE CURVES FOR PRESSURE SIGNALS AFTER YIELDING AROUND THE EDGE DUE TO INITIAL YIELDING BY STATIC LOAD

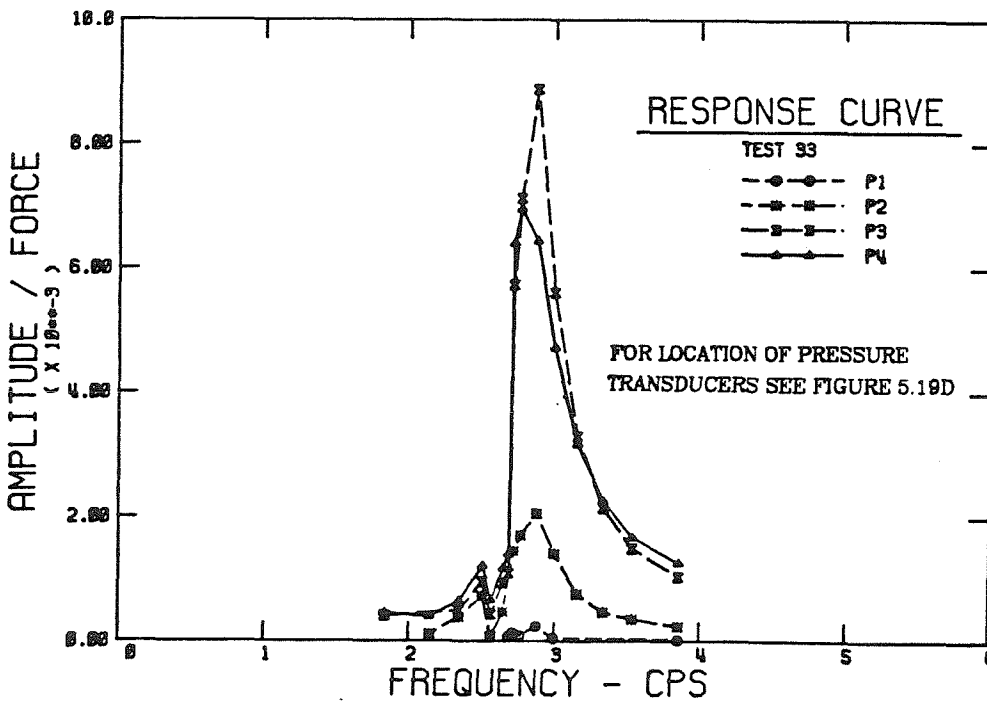


FIG. 7.39 RESPONSE CURVES FOR PRESSURE SIGNALS SHOWING THE PRESSURE DISTRIBUTION PATTERN BEFORE AND AFTER SOIL HAS YIELDED AROUND THE FOUNDATION EDGE (WHEN PASSING THROUGH RESONANCE)



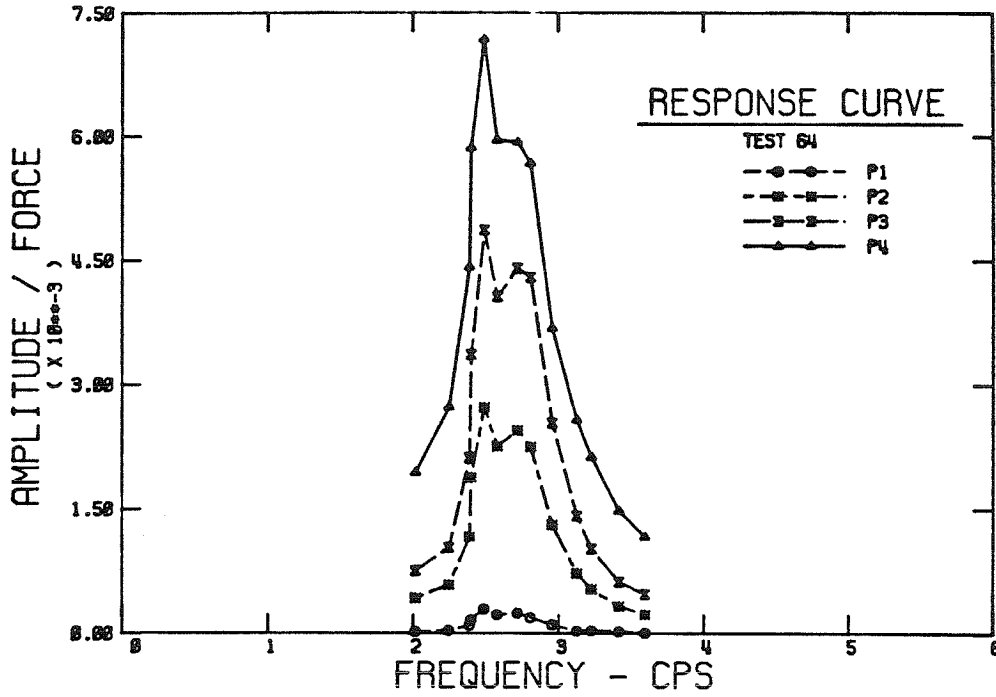


FIG. 7.40a  $\delta = 0.0$

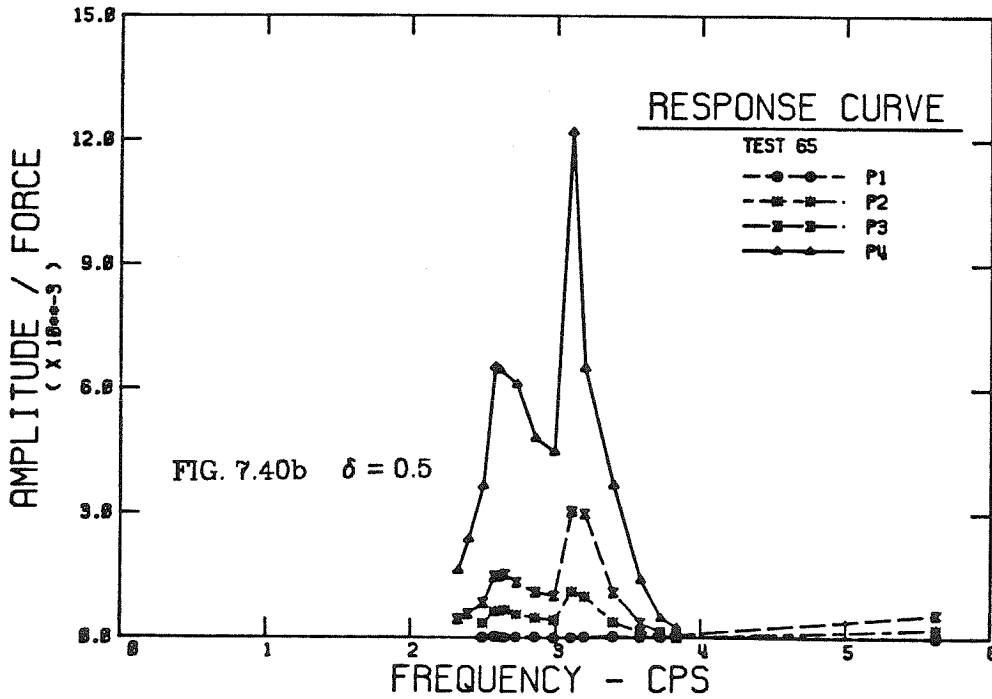


FIG. 7.40b  $\delta = 0.5$

FIG. 7.40 RESPONSE CURVES FOR PRESSURE SIGNALS ALONG DIAMETER AT DIFFERENT EMBEDMENT RATIOS ( $\delta = 0.0, 0.5, 1.0$ ) FOR LOCATION OF PRESSURE TRANSDUCERS SEE FIGURE 5.19D

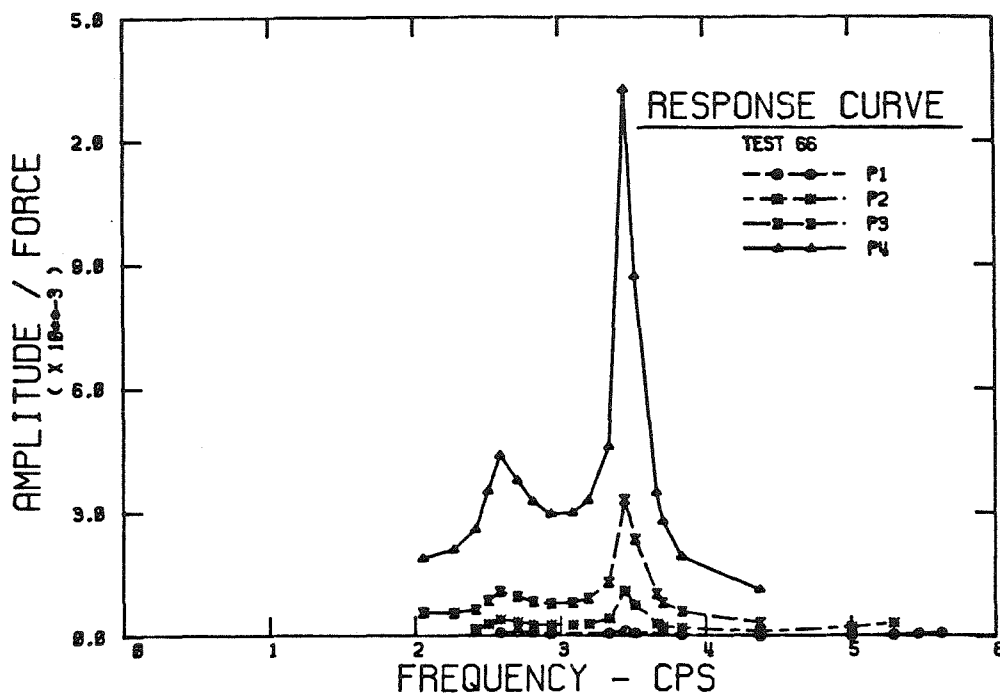


FIG. 7.40c  $\delta = 1.0$

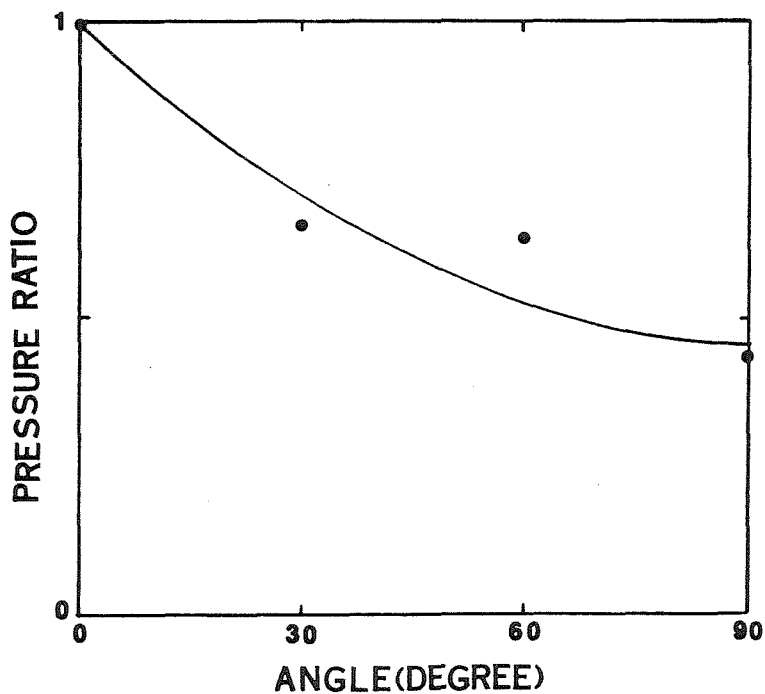


FIG. 7.41 VARIATION OF DYNAMIC PRESSURE AROUND THE FOOTING AT A CONSTANT DISTANCE FROM CENTER

through the center of contact surface is shown in Figure 7.41. Scatter of points is a result of the above mentioned problems. As is seen from the figure dynamic pressure amplitude changes from its maximum value at  $\theta = 90^\circ$  to a minimum value at  $\theta = 0^\circ$ . In conclusion, for determination of complete contact pressure distribution over the area of footing the surface of the foundation should be amply instrumented with many transducers so that with one test, pressure distribution over the contact surface would be known. Pressure distributions measured and presented here are among the most repeatable ones in the tests. Absolute values of pressures are not as reliable as relative values which determine the distribution patterns. The reason for this was discussed in Chapter 5.

#### 7.2.10. Nonlinear Inelastic Behavior of the Soil-Tower System

A phenomenon observed in all the tests was the reduction of resonant frequency of the tower and increase in damping of the vibration after going through many cycles of vibration and particularly through resonance while the test was running. It was observed that resonant frequency was higher when shaker frequency increased monotonically from 0 to an upper limit and it was lower when reducing the frequency back to zero. This was a result of both nonlinear and inelastic behavior of soil under large amplitude loading which results in yielding at the leading edge of the foundation and lift off at the trailing edge during rocking. Figures 7.42 and 7.43 depict the observed nonlinearity effect for two tests on two different models and with two different load levels (having unequal eccentric masses in the shaker). Data points in direction of increasing and decreasing frequency are marked separately and connected to each other by a full and a dashed line for clarity. The reduction of resonant frequency when decreasing the exciting frequency from a high value is apparent from the figures. As is seen from Figure 7.42 the nonlinear-inelastic effect on dynamic

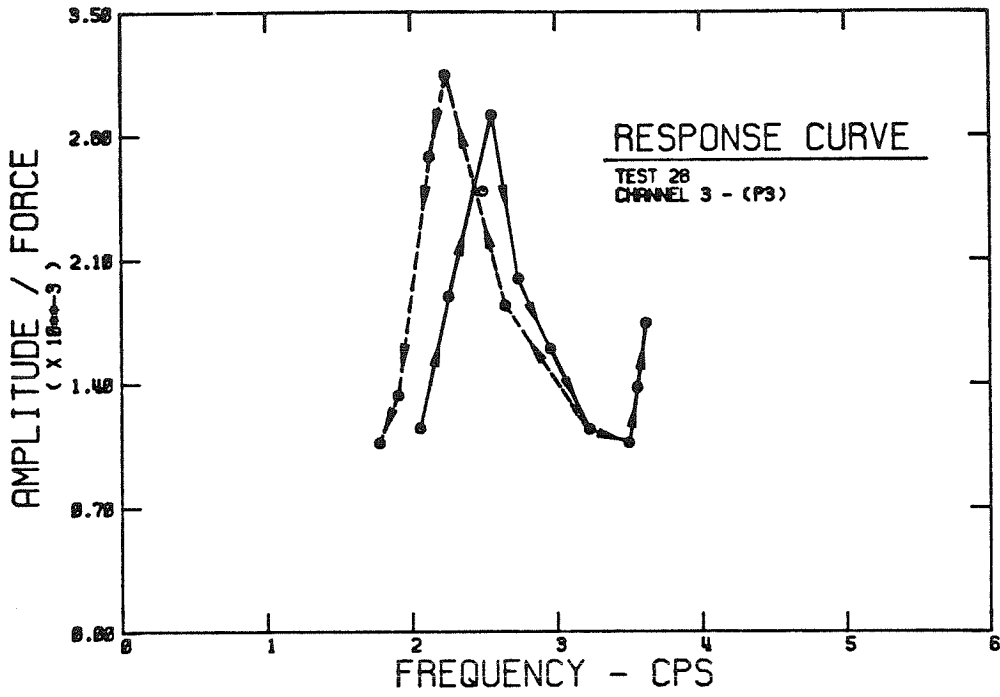
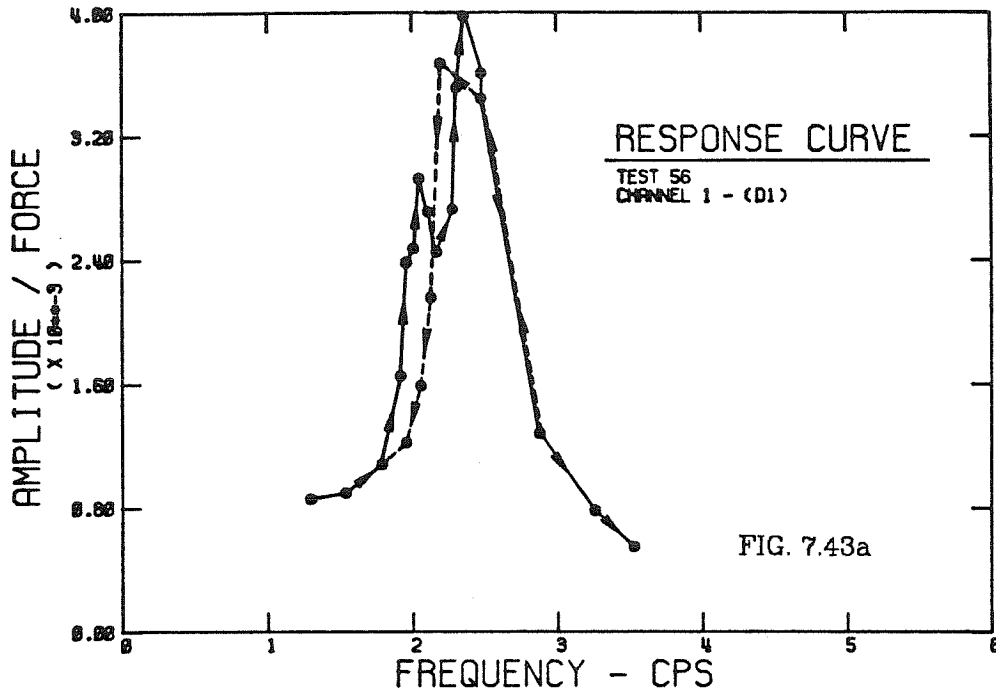


FIG. 7.42 EFFECT OF NONLINEAR AND INELASTIC SOIL BEHAVIOR ON RESONANT FREQUENCY OF THE ROCKING TOWER (PRESSURE RESPONSE CURVE)



(DISPLACEMENT RESPONSE CURVES)

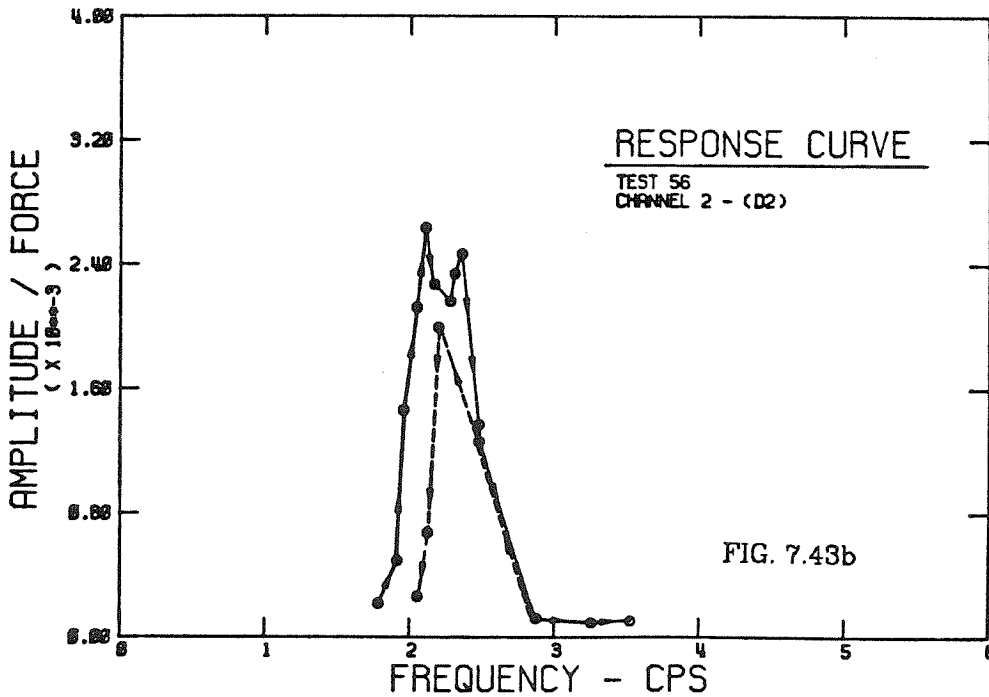


FIG. 7.43a,b EFFECT OF NONLINEAR AND INELASTIC SOIL BEHAVIOR ON RESONANT FREQUENCY OF THE ROCKING TOWER

response of foundation is more visible in a pressure signal because of major change in contact pressure distribution during vibration. Even though the amplitude of the applied moment in Test 56 (Fig. 7.42), at a particular frequency, was more than twice the amplitude in Test 28 (Fig. 7.41), bigger non-linearity effect was observed in test 28. For a rigid surface foundation on a cohesionless soil at low amplitudes of loading usually a dominant lift off process is observed, while with the increase of rocking moment inelastic deformation of the soil (starting from the edges and working inwards) dominates the nonlinear behavior of the soil. Thus the nonlinearity effect in Test 28 is mainly because of the lift off process and not due to the inelastic deformation of the soil in contact with the foundation.

#### 7.2.11. Imperfection of the Axisymmetry and Soil Homogeneity

As was mentioned in the discussion on embedment effect, there existed almost in every test a second peak close to resonant peak in the main rocking direction. Figures 7.44a,b (depicting the response curves for displacement signals in Test 56) show the two peaks existing in both main rocking-vibration direction (measured by Transducer D1), and in the direction normal to that (measured by Transducer D2). Comparing the two figures reveals that the second peak in Figure 7.44a is the resonant peak in the main direction and the first one is the resonant peak in the direction normal to the main. Therefore, even though the tower and the soil container are axisymmetric and the soil has been prepared with extreme care to avoid any nonhomogeneity, the dynamic properties of the system are different in the two D1 and D2 directions, creating the coupled modes of vibration in the two above-mentioned directions. The reason for this as was mentioned before is the imperfection in the model tower in the sense that it is not purely axisymmetric (geometrical and material

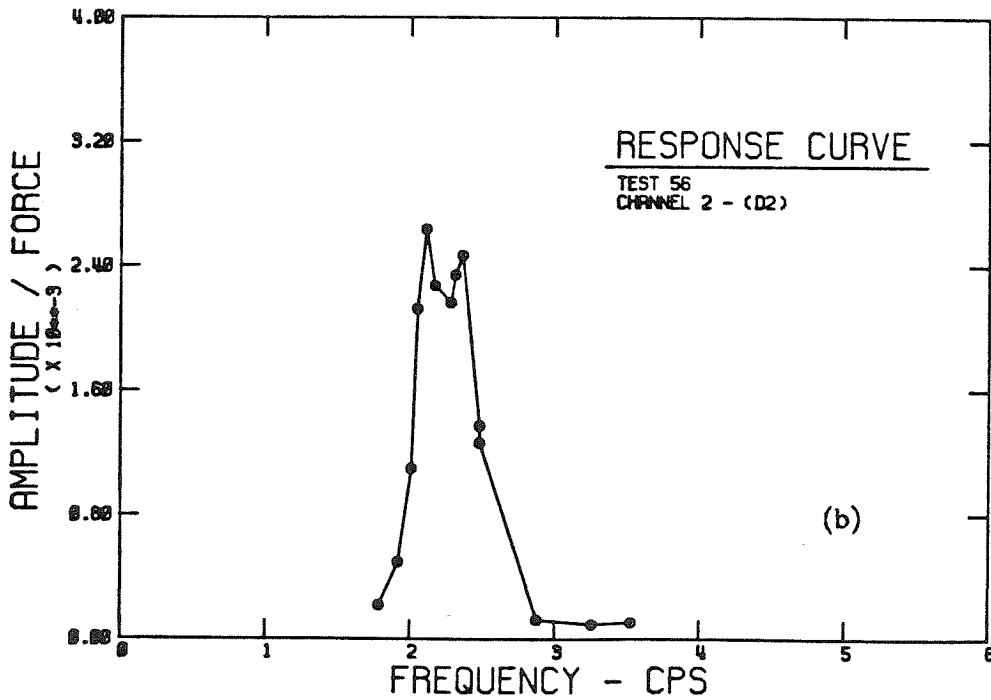
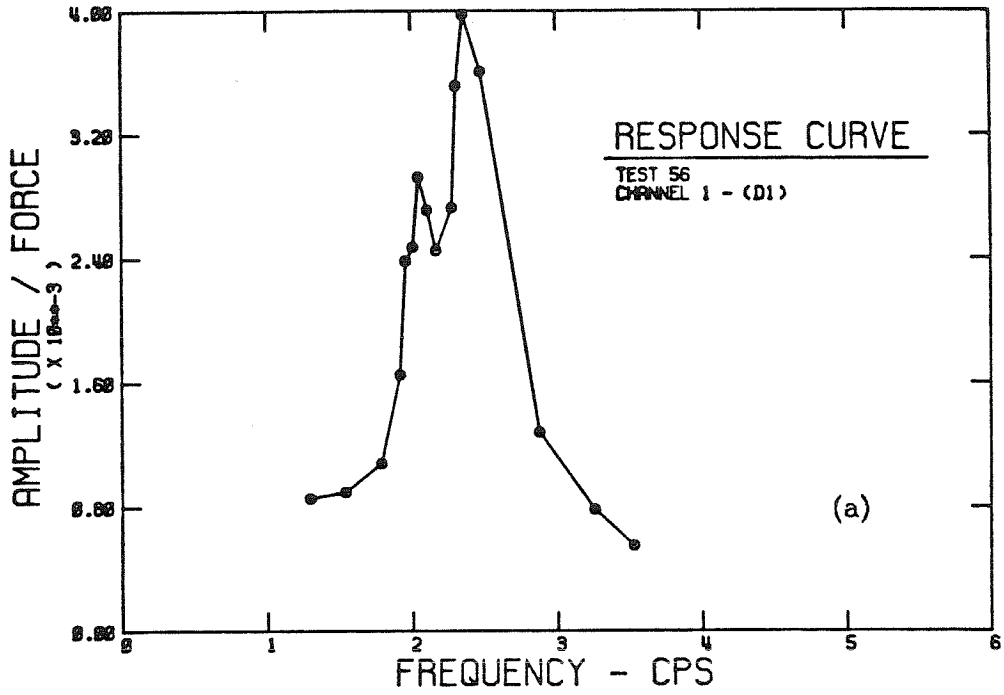


FIG. 7.44a.b EXISTENCE OF TWO RESONANT PEAKS IN RESPONSE BECAUSE OF IMPERFECTION IN SOIL-STRUCTURE SYSTEM (CYLINDRICAL TOWER)

axisymmetry) and that the soil is not absolutely homogeneous. The model tower in Test 56 was a cylindrical tower with the axisymmetric shaker on its top surface. Figures 7.45a,b present response curves for a tower with rectangular cross section and circular foundation (Test 40) and with excitation along the short side of the tower cross section. For this model because of the big difference in the mass moment of inertia of the tower in the two D1 and D2 directions the gap between the two peaks is much bigger and the effect of the three-dimensional nature of the soil-structure system is more obvious. Note that the two-peak phenomenon also exists in the second rocking mode of vibration (produced by the effect of rigid side boundaries of the bucket) as is seen in Figure 7.45.

#### 7.2.12. Determination of Response Modes

Under applied horizontal dynamic force on the tower top, it will always vibrate in a coupled rocking-sliding mode. It is known from theory (Prakash, 1981) that for a rigid block on the soil surface vibrating simultaneously in both rocking and sliding modes, the ratio of the horizontal displacement of the center of gravity to the rocking angle of rotation is defined as

$$\rho = \frac{A_x}{A_\varphi} = \frac{\omega_{nx}^2}{\omega_{nx}^2 - \omega^2} h_{c.g.} \quad (7.4)$$

where  $A_x$  is the maximum sliding amplitude of the the center of gravity of the block, and  $A_\varphi$  is the maximum rocking amplitude,  $h_{c.g.}$  is height of center of gravity from soil surface,  $\omega_{nx}$  is the natural frequency in pure sliding, and  $\omega$  is frequency of the exciting force. If the frequency of excitation  $\omega$  is small in comparison to  $\omega_{nx}$ , then  $\rho = h_{c.g.}$ ; that is, the axis of rotation lies along the central axis of the base area at zero elevation from soil surface. The foundation undergoes only rocking, and sliding is absent.



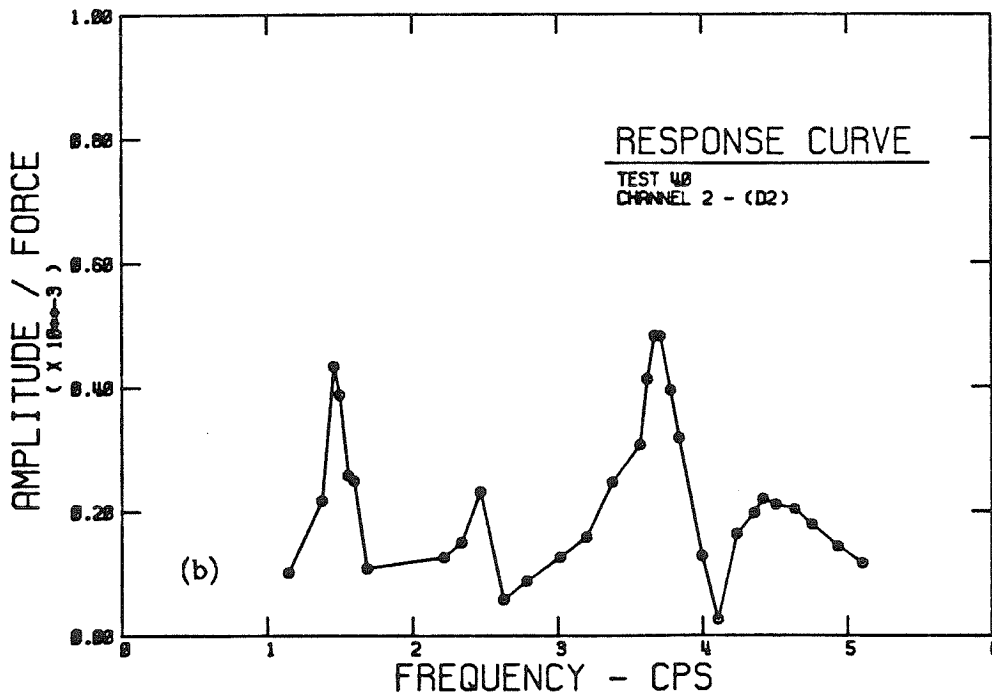
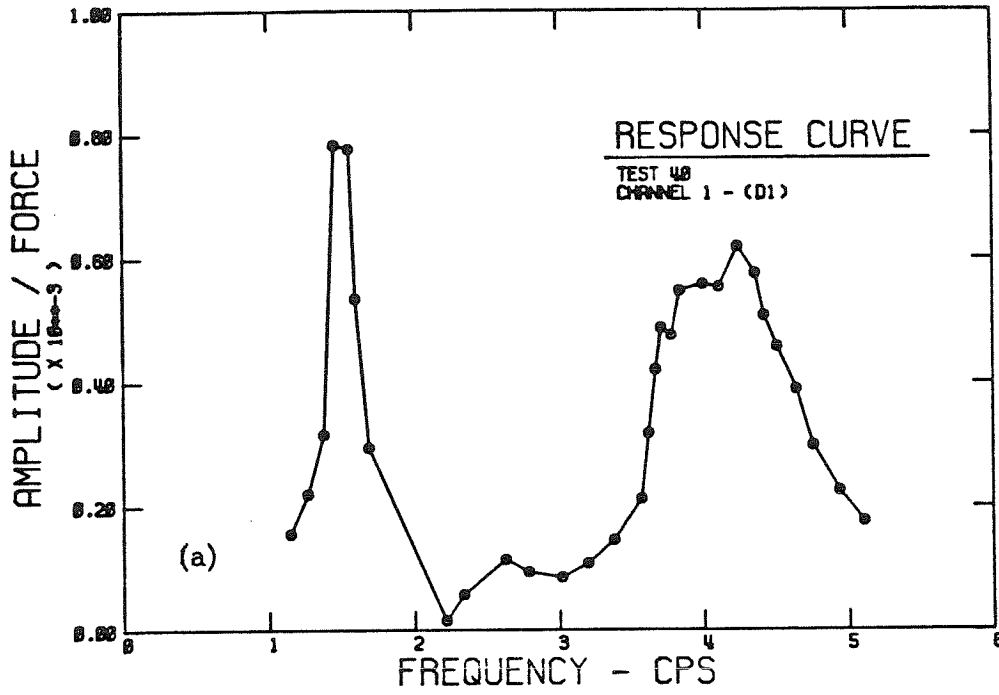


FIG. 7.45a,b EXISTENCE OF TWO RESONANT PEAKS IN RESPONSE BECAUSE OF IMPERFECTION AND NONAXISYMMETRIC SOIL-STRUCTURE SYSTEM

With the above theoretical discussion in mind, using the accelerometer records for the top and middle accelerations of the tower, total horizontal amplitude of the tower, and contribution of both sliding and rocking amplitudes to the horizontal motion of the tower top were calculated. Since pure sliding resonant frequency of vibration for all the models was very high, sliding was expected to make little contribution to the total horizontal motion of the tower top. Figures 7.46 to 7.51 show the contribution of both sliding and rocking amplitudes and the total horizontal amplitude of the tower top itself, all plotted in the form of response curves over the frequency range of interest. Figures 7.46 to 7.48 are from the tests on the same model but on different soil depths and Figures 7.49 to 7.51 are from tests on three different models. Different load levels were also used in some of these tests. In all these experiments, as is seen from the figures, the sliding amplitude over the entire frequency domain is negligible. This verifies the prediction of pure rocking motion about the axis passing through center of the base area in contact with soil. Note that only at resonance sliding amplitude is slightly bigger but it is still very small compared with rocking amplitude. Also comparing Figures 7.46 to 7.48 it is concluded that contribution of sliding amplitude and effect of coupling increases as soil depth increases.

Figures 7.52a,b show the same information as presented in Figures 7.46 to 7.51 for the case of a model with a surface footing (Fig. 7.52a) as compared with the same model embedded in soil (Fig. 7.52b). No major difference is observed between the modal response of the surface and embedded foundation in direction of main rocking motion. However, it is expected that because of low amplitude motion in the direction normal to the main, embedment will increase sliding contribution and the rocking-sliding coupling will be stronger.

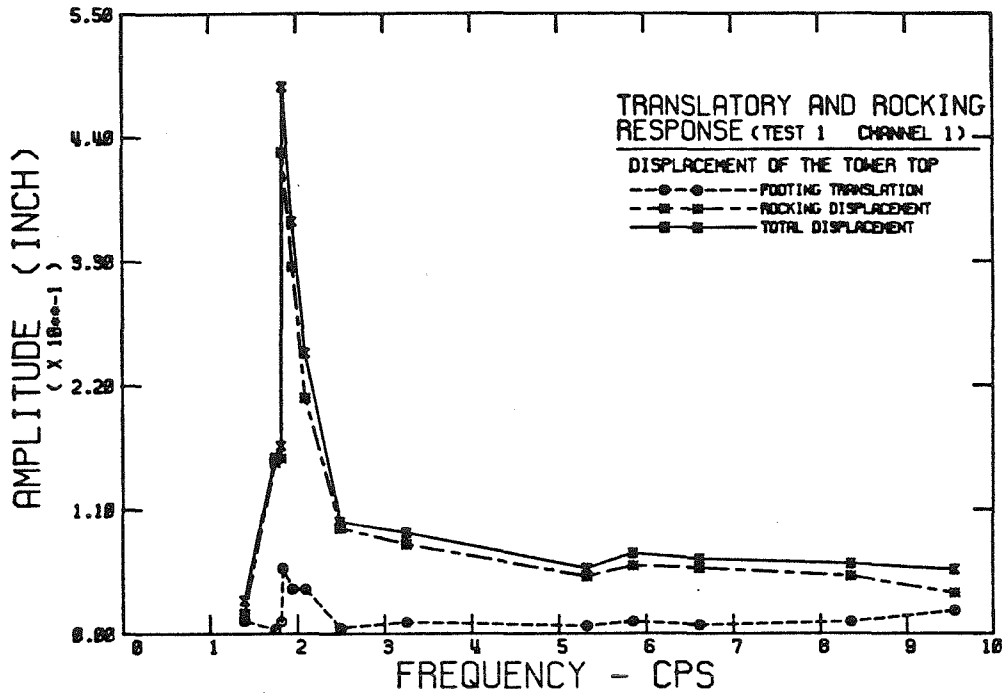


FIG. 7.46 CONTRIBUTION OF SLIDING AND ROCKING MOTIONS TO TOTAL HORIZONTAL DISPLACEMENT OF THE TOWER TOP (SOIL DEPTH= 8.3 FEET, MODEL 2)

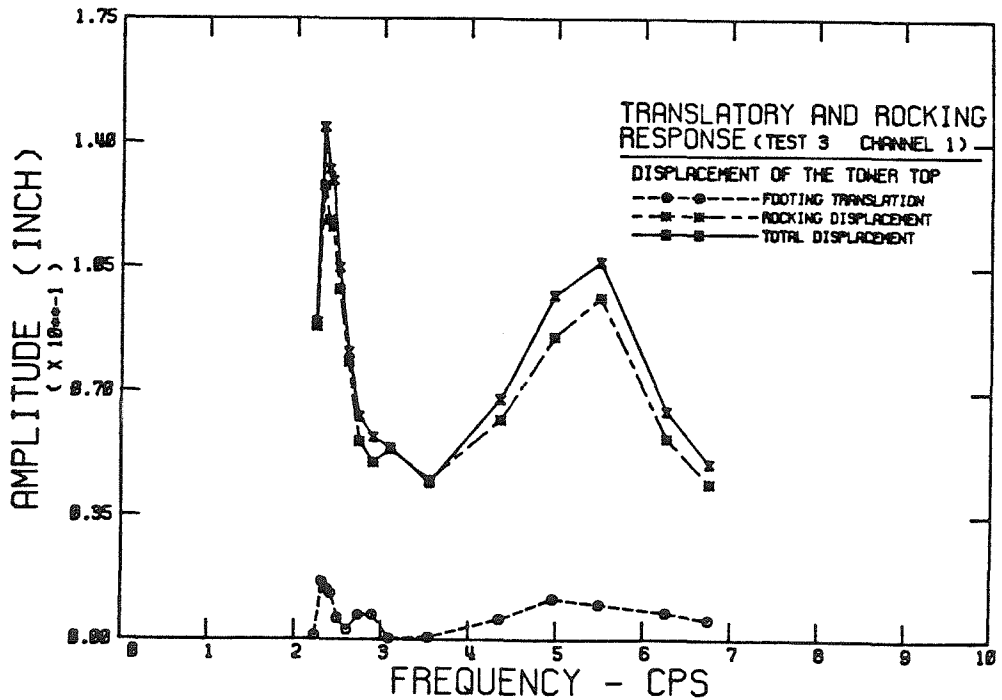


FIG. 7.47 CONTRIBUTION OF SLIDING AND ROCKING MOTIONS TO TOTAL DISPLACEMENT OF THE TOWER TOP (SOIL DEPTH= 16.7 FEET, MODEL 2)

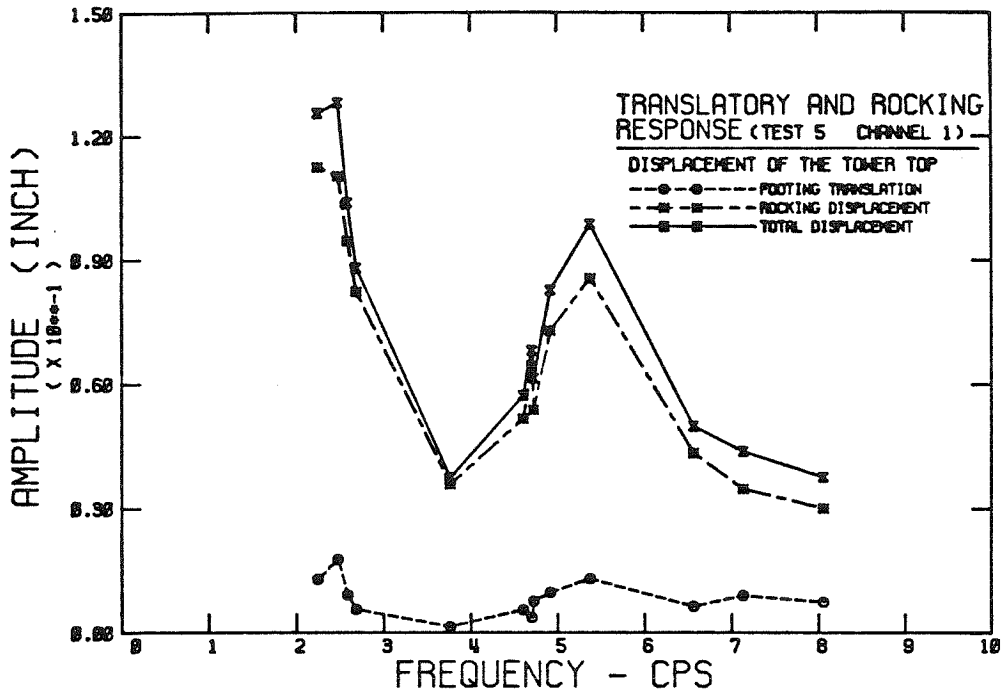


FIG. 7.48 CONTRIBUTION OF SLIDING AND ROCKING MOTIONS TO TOTAL HORIZONTAL DISPLACEMENT OF THE TOWER TOP (SOIL DEPTH= 33.3 FEET, MODEL 2)

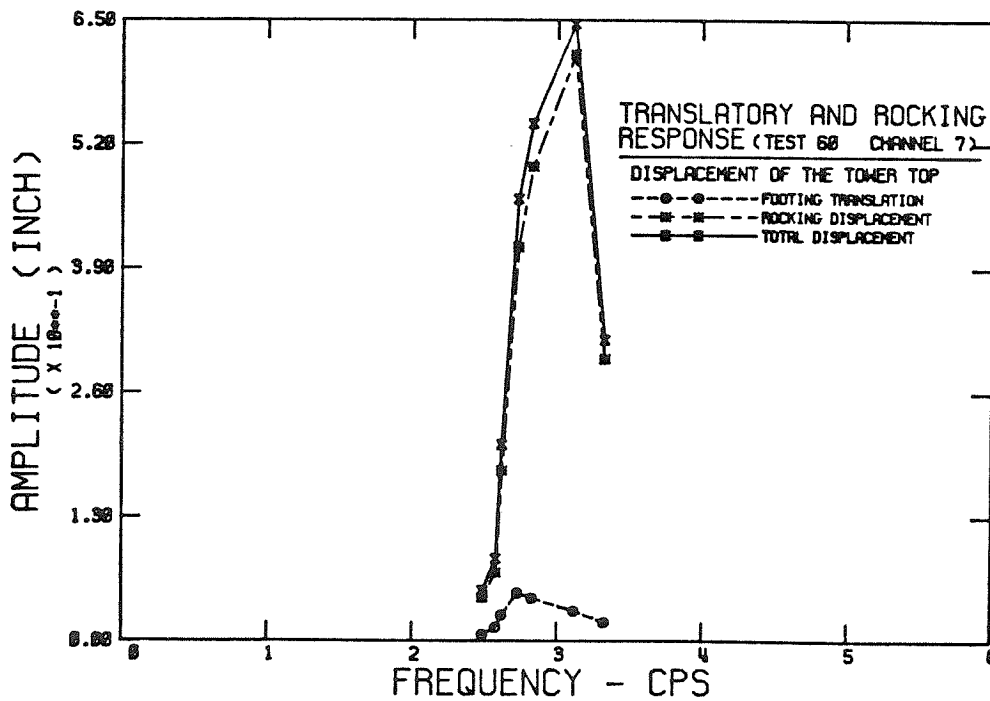


FIG. 7.49 CONTRIBUTION OF SLIDING AND ROCKING MOTIONS TO TOTAL HORIZONTAL DISPLACEMENT OF THE TOWER TOP (HORIZONTAL FORCE ON FOOTING) (MODEL 4, SOIL DEPTH= 33.3 FEET)

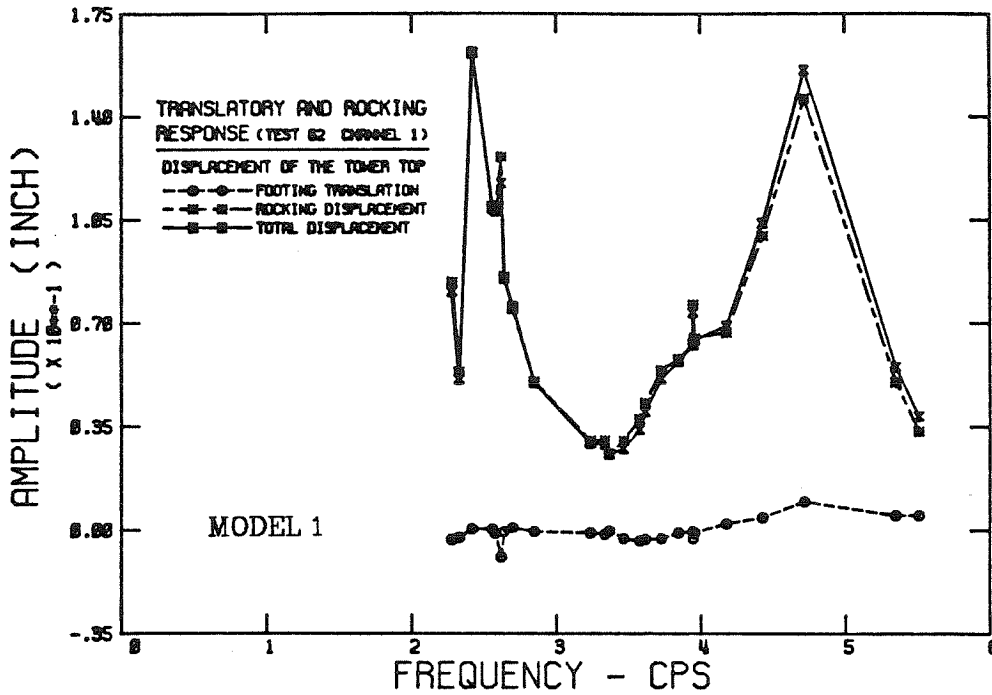


FIG. 7.50 CONTRIBUTION OF SLIDING AND ROCKING MOTIONS TO TOTAL HORIZONTAL DISPLACEMENT OF THE TOWER TOP (HORIZONTAL FORCE ON TOWER TOP)

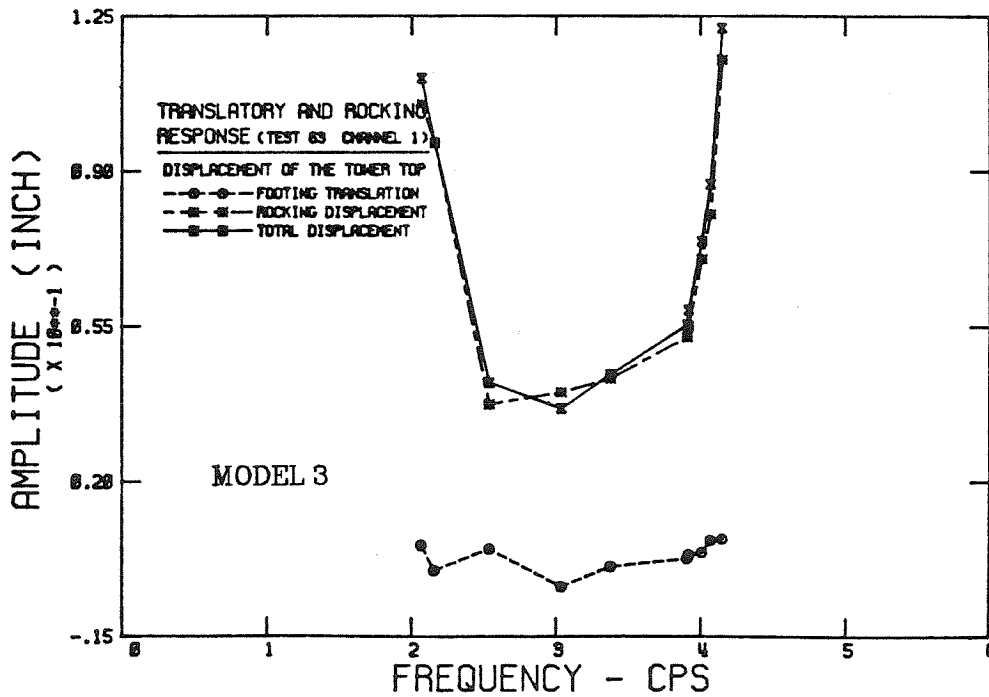


FIG. 7.51 CONTRIBUTION OF SLIDING AND ROCKING MOTIONS TO TOTAL HORIZONTAL DISPLACEMENT OF THE TOWER TOP (HORIZONTAL FORCE ON TOWER TOP)

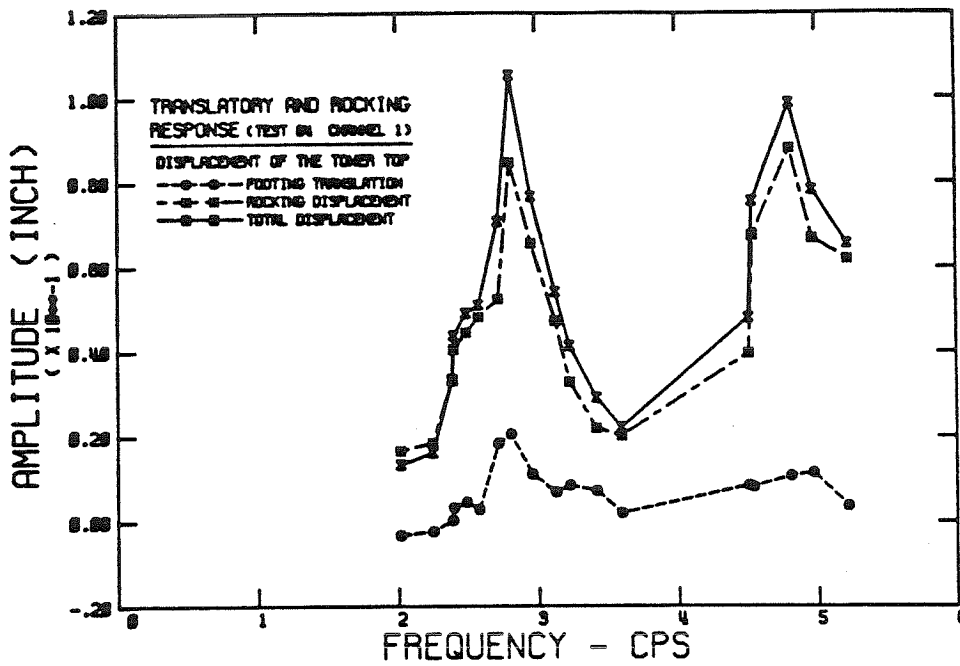


FIG. 7.52a CONTRIBUTION OF SLIDING AND ROCKING MOTIONS TO TOTAL HORIZONTAL DISPLACEMENT (MODEL 4, SOIL DEPTH= 33.3 FEET, EMBEDMENT RATIO = 0.0)

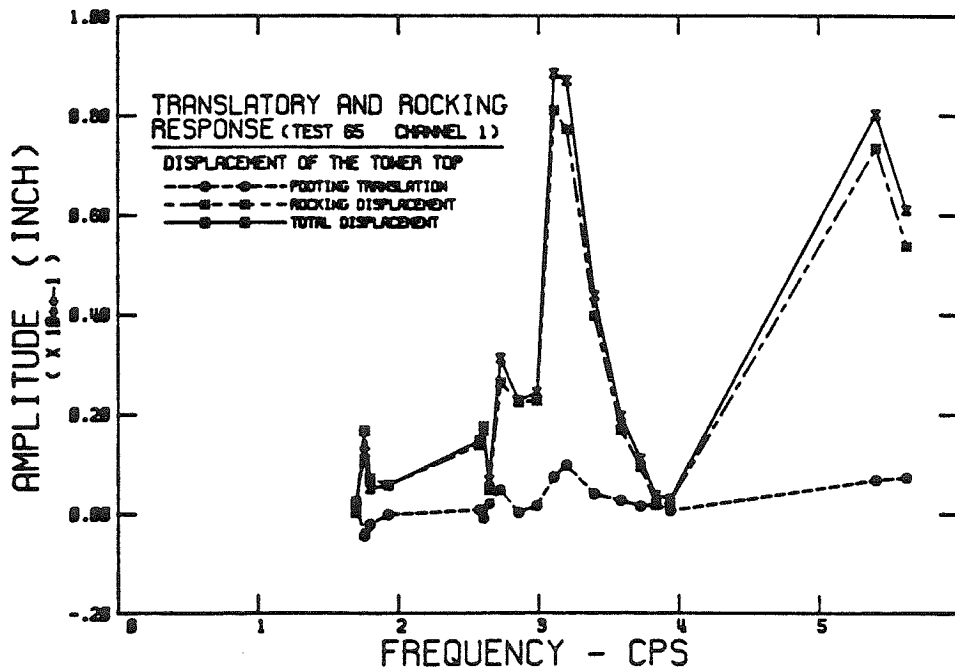


FIG. 7.52b CONTRIBUTION OF SLIDING AND ROCKING MOTIONS TO TOTAL HORIZONTAL DISPLACEMENT (MODEL 4, SOIL DEPTH= 33.3 FEET, EMBEDMENT RATIO = 0.5)

### 7.3. MODEL TESTS IN TRANSIENT HYDRAULIC SHAKER

A few model structures were excited by shaking the whole soil container as was described in Chapters 5 and 6. Natural frequencies and damping ratios for the recorded data (on Visicorder, or floppy disks) were measured by hand, including a large number of cycles to reduce the error of calculations. The models tested, soil depths, and other pertinent test information are summarized in Table 7.9 and the results are compared with some resonant frequencies and damping ratios measured in steady-state vibration tests and the explosion generated free vibration tests on the same models under approximately similar conditions.

Figures 7.53 and 7.54 show the output signals of transducers in two different tests (on Models 2 and 1). Note that in the test on Model 1 (Fig. 7.54) the pressure signals were clipped showing that lift off will happen under sudden high amplitude load. Therefore, it is expected that lift off and separation of surface or shallow footings from the foundation soil would occur under severe seismic loading even when the duration is short. However, in the explosion tests no lift off was observed since the amplitude of vibration was much smaller compared with the amplitude of motion in the above transient tests. Under transient excitation produced by shaking the whole soil bucket, usually the input acceleration was high and therefore large strain amplitudes were produced in soil which reduced the natural frequency of the foundation. Comparing the results of steady-state and transient vibration tests in Table 7.9. shows that in most cases under high amplitude loading the resonant frequency diminishes considerably compared with small amplitude vibration tests. The centrifugal acceleration for all tests listed in the table was 50 g except for the explosion-generated free vibration test on Model 1. The resonant frequency measured in this test was corrected for the g-level as in other tests.

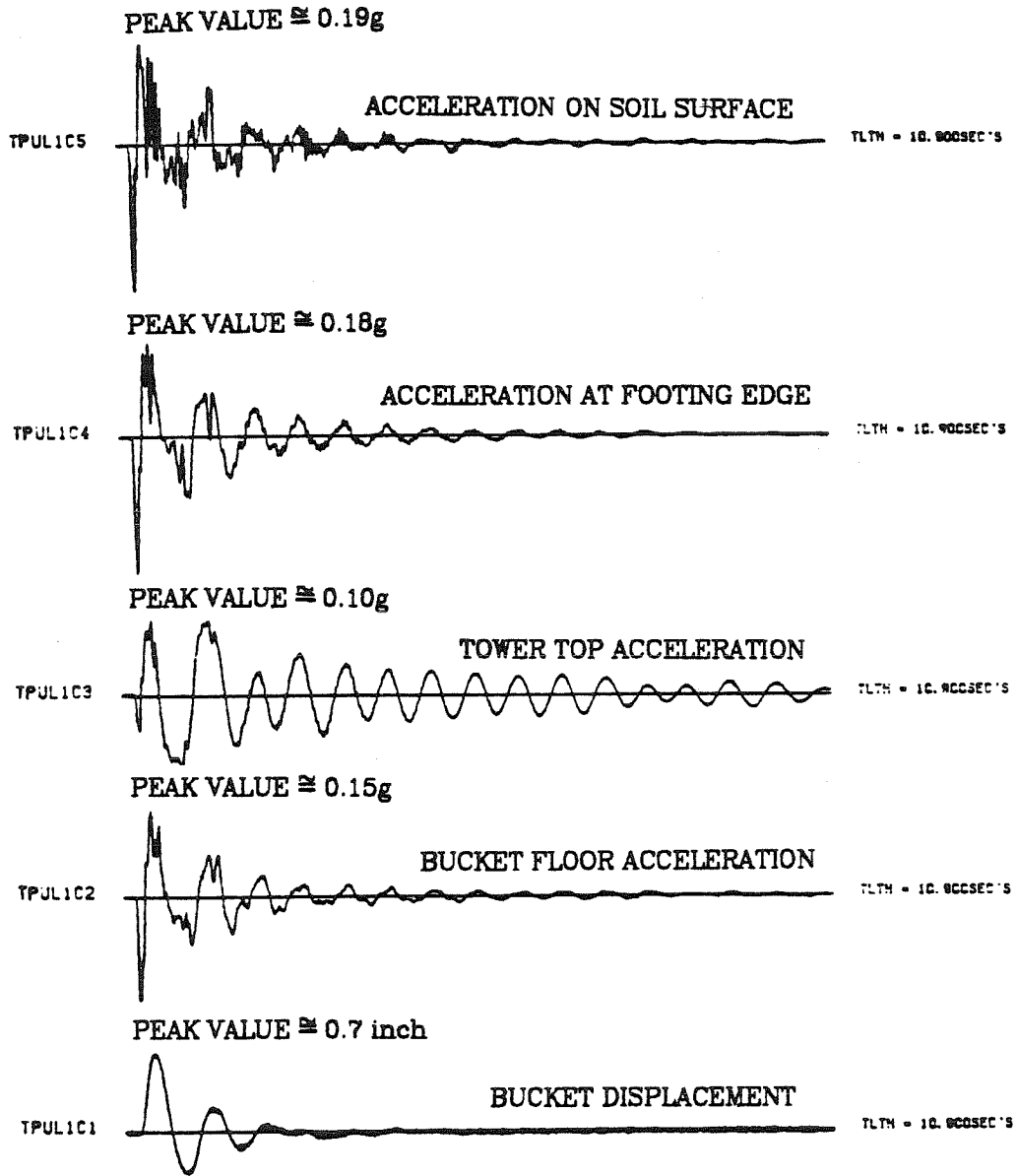


FIG. 7.53 TRANSIENT RESPONSE OF TOWER UNDER PULSE SHAKING OF THE TOWER  
(MODEL 2 SOIL DEPTH= 8.3 FEET)



PRESSURE SCALE: 1 inch  $\approx$  5.0 psi

ACCELERATION SCALE: 1 inch  $\approx$  0.4g

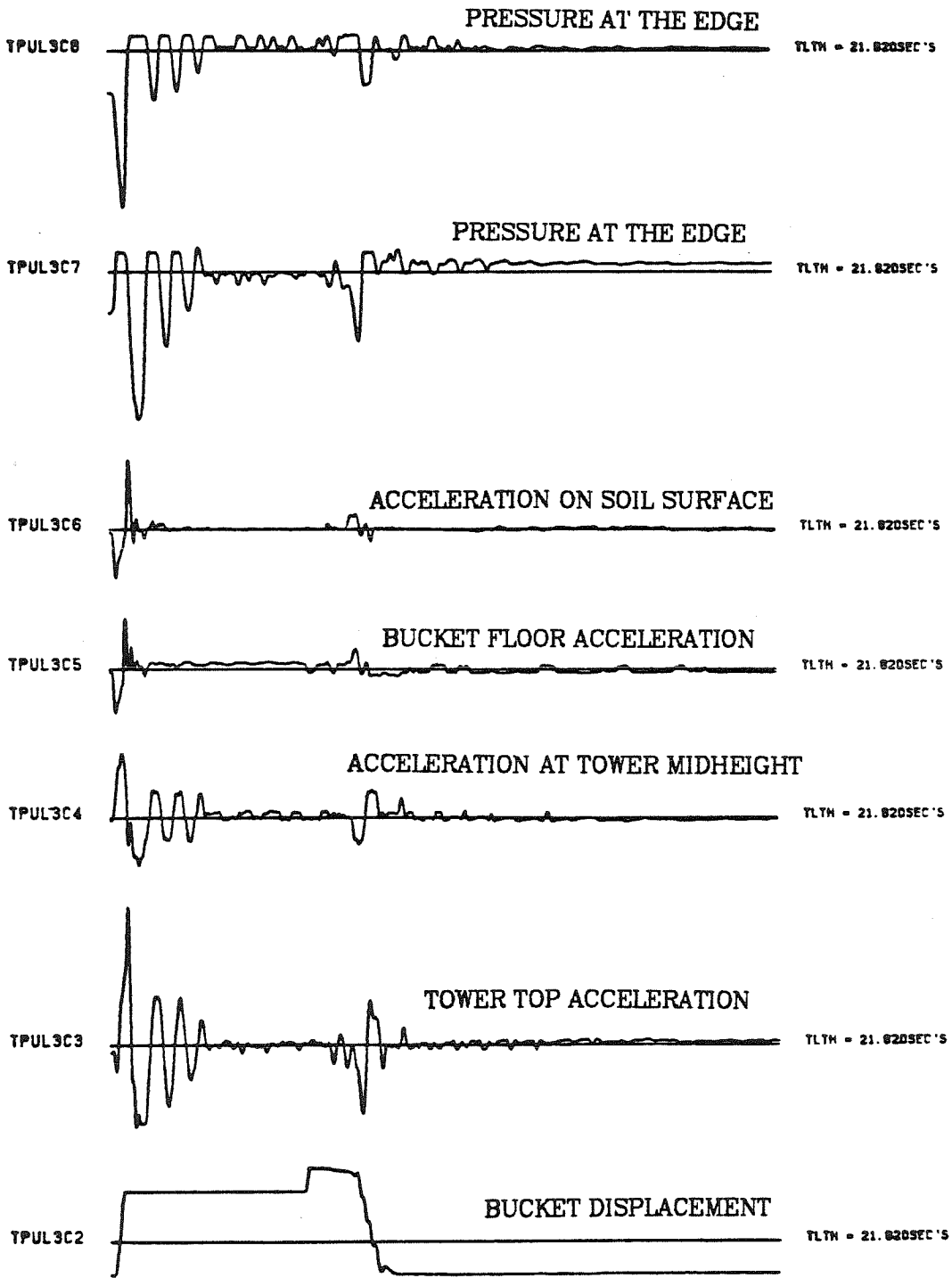


FIG. 7.54 TRANSIENT SHAKING OF THE SOIL CONTAINER (MODEL 1)

A great deal of information can be learned from the data recorded in the above transient tests. One example is the determination of the transfer function for the soil mass in the bucket by a Fourier analysis of acceleration records at the bucket floor and on the soil surface. Because of the large number of experiments performed in this study, further random shaking tests of the soil container simulating earthquake motion were excluded from the test program.

#### 7.4. Modelling at Different Scales

Even though it was not possible to verify the centrifuge modelling laws by comparing the results of experiments with values derived from equivalent tests on full-size structures, it was still possible to test models of different dimensions but similar shapes, at different  $g$ -levels in centrifuge, all representing the same prototype. According to modelling laws the free oscillation frequency of the three models should be in the ratio of their sizes with respect to each other, i.e. for the models used in these tests with the length ratio 1:2:3 frequencies of tower oscillation in model scale should be in the ratio of 3:2:1 to prove the modelling laws. The results derived from the tests involving shaking the whole soil container to study the modelling laws are presented in Table 7.10. The agreement between the measured frequencies and the ratio of centrifugal accelerations is very good. During each test the bucket was shaken with a low amplitude of acceleration; an attempt was made to keep the level of shaking the same for all three tests on the three models. Figure 7.55 shows the acceleration signals recorded (on Visicorder) at top and middle heights of the the model and the input acceleration at the bucket floor for the test on the medium size model.

Table 7.9. Damping Ratios and Resonant Frequencies Measured in Tests Involving Shaking the Soil Bucket compared with other Test Methods

Model	Free Vibration (Shaking of Bucket)				Steady-State Vibration (Air-Driven Shaker)			
No.	Soil Depth (ft)	$f_n$ (Hz)	$\xi$ (%)	$A_{max}^*$ (g)	Soil Depth (ft)	$f_n$ (Hz)	$\xi$ (%)	$A_{max}$ (g)
2	8.30	1.48	2.1	0.090	33.0	1.80	2.0	0.03
3	25.0	2.00	3.0	0.050	33.0	2.30	4.4	0.04
4	25.0	1.48	7.0	0.060	33.0	2.88	7.0	0.02
	Free Vibration (Shaking of bucket)				Free Vibration (explosion generated)			
1 (a)	8.3	1.52	6.0	0.25	30.0	1.90	5.0	0.05
1 (b)	8.3	1.20	6.50	0.30	30.0	1.62	6.0	0.10

\*  $A_{max}$  stands for maximum acceleration amplitude in signal.

Table 7.10. Damping Ratios and Fundamental Resonant Frequencies in "Modelling of Models" Tests

Model No.	Size Ratio	$g$ - Level	$f_n$ (Hz)	$\xi$ (%)
5	1	17.2	3.65	8.0
6	2	25.8	3.7	7.0
7	3	51.5	3.45	8.5

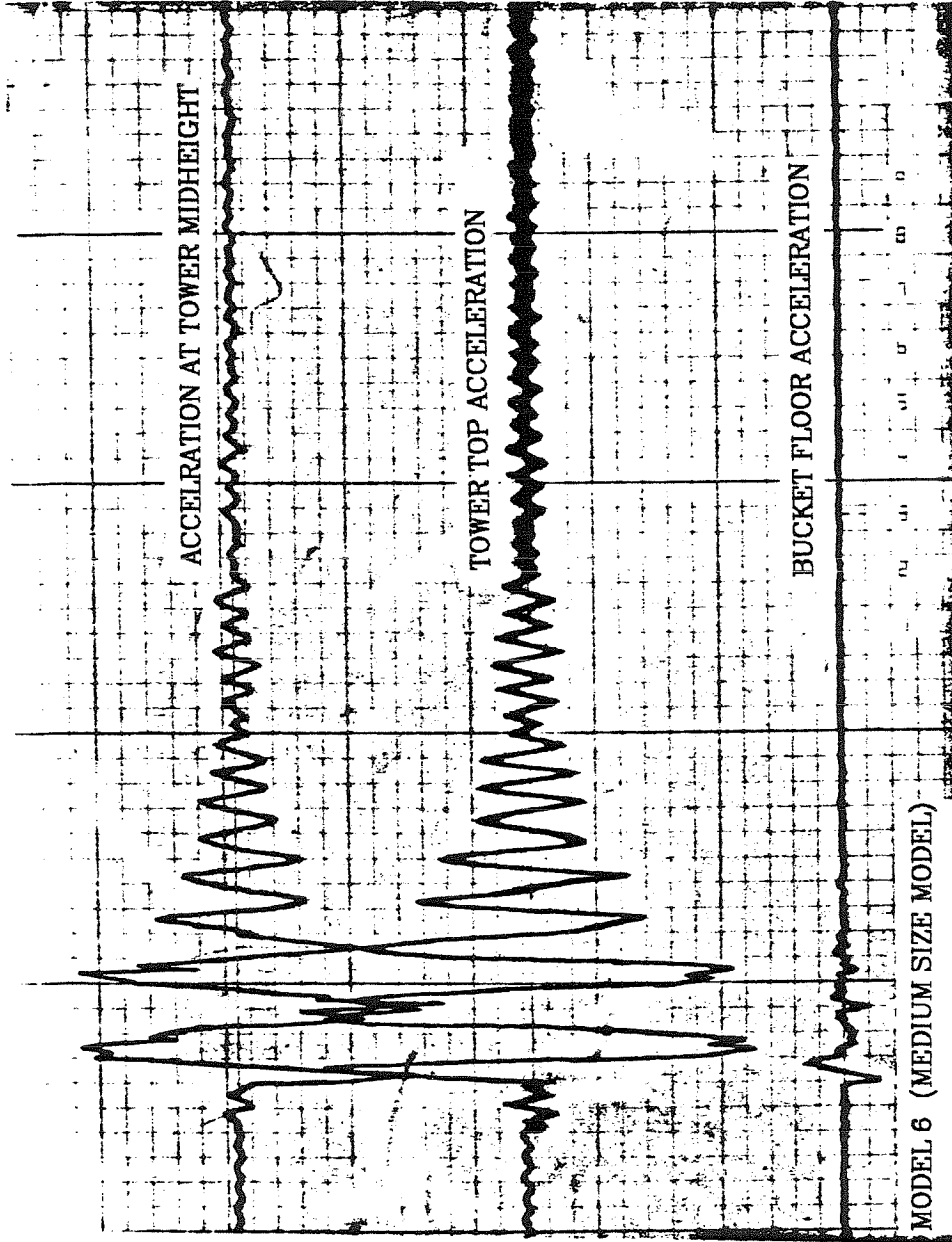


FIG. 7.55 TRANSIENT SHAKING OF SOIL BUCKET IN MODELLING OF MODELS TESTS

## 7.5. CONCLUSION

The following facts and conclusions were learned from these experiments:

- (1) Under small amplitude vibrations (approximately less than .05 g acceleration amplitude) the foundation-soil system behaved in a relatively linear-elastic manner in short duration shakings and the results of parametric studies on the model structures were in reasonable agreement with what was expected from theory and engineering intuition.
- (2) Medium to large amplitude loading did result in yielding of the soil supporting the foundation, starting from the edges where confining stresses are very small and propagating inward with the increase of deformation amplitudes during resonance. More energy dissipated through yielding and deformation of the contact soil, and it was observed that the footing tilted and settled into the soil. Under severe transient shaking the edges of the tower lifted off the soil surface even in a short duration shaking period.
- (3) Almost in every steady-state rocking-sliding test, no matter how small the amplitude of motion, lift-off and consequently footing separation from the foundation soil was observed, particularly at the footing edge. Thus, in these tests even when in some cases the rocking moment amplitude was not high, under a large number of shaking cycles the rigid footing separated from the soil surface which was prepared in a dense state. Lift-off resulted in lengthening of the natural period and in highly nonlinear behavior of the foundation. Footings under small amplitude loads tended to rock on the soil, deforming the soil mainly at the edges. Therefore, the accompanying settlement was very small and

little damping was attributed to the motion. Since the soil used in the experiments was dense, rocking and separation apparently took precedence over gradual yielding and settlement.

- (4) Effect of embedment, change in the foundation size, variation of soil depth, magnitude of the applied load, etc. were all small in the direction of main rocking motion. However, the effect of variation in any of these parameters on the resonant frequency of the system was more obvious in response amplitude plots and resonant frequency data derived in the direction normal to the main rocking motion. This was a result of different load amplitudes and produced strain levels in the soil mass in the two directions of motion.
- (5) Comparison of experimental results derived by different test methods was not very helpful because of the different levels of load amplitudes involved in each test method.

There are two more important facts to be noted which were not mentioned during the main text of the chapter:

- (a) Presence of pressure transducers in tests 1 to 24 on the footing bottom surface, sticking out of the surface and penetrating into the soil, resulted in reduction of the natural frequency of the tower because of disturbance and the yielding of the soil at high concentration stress points around transducer. As the number of transducers on the footing surface increased from one to four or the size of footing was decreased this adverse effect was amplified. However it was observed that the overall behavior of the model towers in tests studying the effect of different parameters did not change very much. This means that the same trend of variation of resonant frequency with the change of the

parameter was observed with or without presence of pressure transducers. It should be noted that in tests 25 to 67 pressure transducers were mounted flush with the footing surface and consequently this adverse phenomenon was not observed.

- (b) In the steady-state tests performed to study vertical and sliding modes of vibration of the footings, because of high values of resonant frequencies of the models the shaker could not reach their resonant frequencies. It was also observed that the amplitude of motion was very small and needed large amplifications. Therefore with the shaker used in this experimental study and with the particular conditions of the soil-structure systems, it was impossible to detect the separate vertical and sliding resonant frequencies of the models. However, tests in lower centrifugal accelerations can be run using the above-mentioned shaker if dynamic behavior of prototype structures with smaller dimensions is of interest.

CHAPTER REFERENCES.

- [1] Beck, J. L., "Determining Modes for Structures from Earthquake Records," EERL 80-01, Caltech, Pasadena, California, June, 1978.
- [2] Gazetas, G., "Analysis of Machine Foundation Vibrations: State of the Art", Soil Dynamic and Earthquake Engineering Journal, Vol. 2, No. 1, 1983.
- [3] Kausel, E., "Forced Vibrations of Circular Foundations on Layered Media," Research Report R74-11, MIT, 1974.
- [4] Lin, A. N., "Experimental Observations of the Effect of Foundation Embedment on Structural Response," Earthquake Engineering Research Laboratory (EERL) 82-01, California Institute of Technology, Pasadena, California, 1982.
- [5] Meyerhof, G. G., "The Ultimate Bearing Capacity of Foundations," Geotechnique, Vol. 2, 1951, pp 301.
- [6] Morris, D. V., "The Centrifugal Modelling of Dynamic Soil-Structure Interaction and Earthquake Behavior," Ph.D. Thesis, University of Cambridge, Cambridge, England, 1979.
- [7] Morris, D. V., "Dynamic Soil-Structure Interaction Modelled Experimentally on a Geotechnical Centrifuge," Canadian Geotechnical Journal, Vol. 18, No. 1, Feb. 1981, pp. 40-51.
- [8] Prakash, S., "Soil Dynamics," McGraw-Hill, 1981, 426pp.
- [9] Richart, F. E., Jr., Hall, J. R., Jr., and Woods, R. D., "Vibrations of Soils and Foundations," Prentice-Hall, Inc., Englewood Cliffs, N.J., 1970, 414pp.
- [10] Stokoe, K. H., II, and Richart, F. E., Jr., "Dynamic Response of Embedded Machine Foundations," Journal of the Geotechnical Engineering Division, A.S.C.E., Vol. 100, No. GT4, April 1974.
- [11] Whitman, R. V., "Analysis of Soil-Structure Interaction,"- a State-of-the-art review, Proceedings, Symposium on Experimental and Theoretical Structural Dynamics, Institute of Sound and Vibration Research, Southampton, England, 1972.



## **CHAPTER 8**

### **THEORETICAL RESULTS, SUMMARY AND CONCLUSIONS**

In this chapter dynamic response of rigid model structures employed in the rocking-sliding tests will be derived theoretically and compared with the experimental results presented in the last chapter. Standard theoretical methods with widespread usage in analysis and design of vibrating foundations will be used in the analysis. Conclusions and recommendations based on the performed comparisons will be presented and discussed in each case. Finally an overall summary and conclusions of the present study will be given and recommendations for future research will be offered.

#### **8.1. INTRODUCTION TO METHODS OF ANALYSIS**

The most widely used theoretical methods in analysis and design of foundations subjected to dynamic loads are analytical methods based on the linear elastic or viscoelastic half-space model. Numerical models, particularly the finite element technique, are capable of solving the foundation vibration boundary value problem with any foundation or boundary geometry. In addition they can easily include the effect of variation in physical properties of the medium as a function of position in space. However, stress-strain relations used in these methods are still very far from real behavior of soils since they usually do not include the yield phenomenon and plastic deformation of the soil mass. In particular in most cases shear modulus of soil is defined as a nonlinear function of stress or strain amplitude derived from laboratory tests and usually a constant value for Poisson's ratio is assumed in analysis. This will not give a correct physical model of the material unless the bulk modulus or Poisson's ratio are also defined at the same time as a function of stress or strain.

All the above-mentioned analytical and numerical methods assume that soil

is a continuum and they usually do not include any effect of yielding and long-term deformations in soil, or lift-off and separation of foundation from the ground surface. In a different approach to the problem following what Winkler envisaged in 1867, soil is assumed as a bed of independent elastic springs supporting the foundation. This model has the advantage of being able to include the plastic deformation of soil and lift off of foundation in a relatively simple manner; however, it suffers from the long-criticized disadvantage of assuming the soil as a discontinuous medium.

In the experiments performed in this study a wide range of strain amplitudes, load intensities, and excitation durations was involved. This resulted, on some occasions, in vibration of model towers without any lift-off or sizeable softening and permanent deformation in soil, but in many other cases lift off and yielding were observed during the tests. Therefore, depending on load amplitude, duration, and frequency of shaking the behavior of the towers under dynamic horizontal force or acceleration was different. However, it was observed that, under approximately constant amplitude vibratory loads, after a while soil behavior tends to a nearly nonlinear elastic one with little energy dissipation or permanent deformation. It is expected that a numerical or analytical model which reasonably predicts the observed behavior of the model towers in the centrifuge tests (which are far preferable to other small scale tests at 1g) can be used with confidence in the analysis and design of vibratory foundations.

In the light of different tower behaviors observed in the tests and available mathematical models for the problem the most common analytical method of "lumped parameters" based on linear elastic or viscoelastic half-space models is used in this study. Of course there exist many shortcomings in the method but what we are interested in is, how far the theoretical and experimental results are from each other and if the difference justifies investing a greater effort in

developing and applying more sophisticated soil models for solving foundation vibration problems.

## 8.2. LUMPED PARAMETER ANALYSIS

The evolution of theories involving the evaluation of dynamic response of rigid plates resting on or embedded in an elastic half-space was reviewed in Chapter 1. As was mentioned the analytical methods based on the elastic or viscoelastic half-space model will result in complicated integral equations which have been solved numerically over the range of dimensionless frequency  $a_0$  of practical interest. Lumped parameter analogs to the elastic half-space models greatly simplify the analysis and design of foundations under vibratory loads. The lumped parameter method of analysis consists of the reduction of a foundation-soil system to a model of a mass and simple spring and dashpot elements. The rigid mass in the model has the same inertial properties as the foundation mass and the springs and dashpots are found from elastic half-space theory by equating response of the elastic half-space model to that of its lumped parameter analog as was shown in Chapter 1. The method is, however, limited to systems with simple geometries. The numerical solutions to the closed-form integral equations will provide us with simple relations, and curves defining the frequency-dependent impedance parameters (damping and stiffness) of the analog model.

In general a rigid axisymmetric foundation resting on the ground surface has four distinct degrees of freedom, namely vertical, and horizontal translations, rocking and torsional rotations. Rocking and horizontal modes of vibration are usually coupled. Thus a two degree of freedom lumped parameter model is needed to simulate the rocking-sliding vibration of the model towers in the experiments. For a relatively tall structure the rocking resonant frequency is

much lower than the resonant frequency for horizontal mode and the damping ratio (excluding material damping) is also much smaller for the rocking mode compared with the horizontal mode. Therefore it is expected that the contribution of foundation translation to the total tower motion at the fundamental resonant frequency of the system, compared with the amplitude of rocking motion about an axis passing through the base, is negligible. This assumption was also experimentally supported as was shown in modal analysis calculations of Chapter 7. Consequently the rigid tower oscillating on an elastic half-space may be idealised as a rotational spring-inertia system of one degree of freedom. The more rigorous two-degree-of-freedom lumped parameter model of the system including the effect of frequency-dependent stiffness and damping coefficients will be considered later.

### 6.2.1. One-Degree-of-Freedom Lumped Parameter Analog

For the simple one degree of freedom system the natural frequency is given by

$$f_n = \frac{1}{2\pi} \sqrt{\frac{K}{I_b}} \quad (8.1)$$

where  $I_b$  is the moment of inertia of the tower about the axis passing through the center of the lower base surface, and  $K$  is the rotational spring stiffness of the elastic half-space.

Assuming a relatively frequency-independent behavior for the model tower (the dimensionless frequency  $a_o$ , defined in Chapter 1, was less than 0.6 in the experiments) the static rotational spring stiffness for a circular base resting on an infinite uniform elastic half-space is defined as (Borowicka, 1963)

$$K = \frac{8 Gr^3}{3(1 - \nu)} \quad (8.2)$$

where  $r$  is radius of the base,  $G$  shear modulus, and  $\nu$  Poisson's ratio of the elastic half-space. Defining the shear modulus  $G$  as an empirical function of void ratio  $e$  and mean confining stress  $\bar{\sigma}_o$ , derived by Hardin and Drnevich (1972), the equation for resonant frequency (Eqn. 8.1) reduces to

$$f_n = 189.5 r^{1.5} \bar{\sigma}_o^{0.22} I_b^{-0.5} \quad (8.3)$$

(in S.I. units only)

Note that in deriving the above relation void ratio of the soil was equal to 0.57, Poisson's ratio was 0.30, and  $G$  was a function of  $\bar{\sigma}_o^{0.44}$  (see Chapter 4 for properties of Nevada Fine Sand). In empirical relations and design curves in the literature, shear modulus  $G$  is usually defined as a function of mean effective stress to the power 0.5. The power 0.5 is derived as the average value from many resonant column tests on different dry cohesionless soils. In addition, Poisson's ratio or bulk modulus of soil is assumed to be constant. Note that this is strictly speaking incorrect. In fact a physically correct soil model requires that shear modulus and Poisson's ratio (or bulk modulus) be functions of both mean and shearing stresses.

The main uncertainty in evaluation of the resonant frequency using the above formula lies in the right choice for the value of mean effective confining stress. Different ways of interpreting the required value of the mean stress have been suggested by several researchers. One common procedure is to use the elastic shear modulus corresponding to a typical point under the footing. Whitman and Richart (1967) recommended that a suitable point for this purpose is at one base radius depth below the edge of circular footing, calculating the stress by the elastic theory including the effect of soil weight itself. Based on this idea the centrifugal accelerations in the experiments reported here were calculated at a radius equal to distance from center axis to one footing radius

depth below the soil surface in the experiments. However, soil is not an elastic material and pressure distributions under a foundation over the contact area and as a function of depth are much different and more complicated than the predictions made by the elastic half-space theory. Morris (1981) noted the uncertainties involved in evaluation of the right value for the mean confining stress and proposed to use the average vertical stress under the footing times a factor  $\alpha$  as the average confining stress. The factor  $\alpha$  was suggested to absorb the effect of all uncertainties in the evaluation of the mean stress. Using this value of mean stress he derived the relation defining the natural frequency as

$$f_n = \sqrt{\frac{\alpha^x M^x r^{3-2x}}{I_b}} n^{x/2} \quad (8.4)$$

where  $x$  is the power of  $\bar{\sigma}_o$  in relation defining  $G$  in terms of mean stress,  $M$  is the mass of foundation, and  $n$  is the scale factor for the centrifuge model (centrifugal acceleration is equal to  $ng$ ). Note that  $x$  is usually taken as 0.5 but its value measured in this study was equal to 0.44. This relation describes how the natural frequency varies with the centrifugal acceleration. In Chapter 7 the experimental results (Fig. 7.25) showed that for a model at different centrifugal accelerations the natural frequency of rocking about the base axis varied as a function of  $n^{0.22}$ . This suggests that the average value of  $x$  (approximately equal to 0.5) derived from resonant column tests performed in this study is supported by the centrifuge experiments. With  $x$  equal to 0.44 the equation for resonant frequency reduces to

$$f_n = 227.5 \alpha^{0.22} \left( \frac{M^{0.44}}{I_b} \right)^{0.5} r^{1.08} n^{0.22} \quad (8.5)$$

(in S.I. units only)

where the factor  $\alpha$ , as was mentioned before, was designed to absorb any

differences between the idealized elastic model and the real foundation response. According to Equation 8.5 the resonant frequency of a rocking foundation is approximately a linear function of  $r$ , radius of the base, and varies approximately as square root of the ratio  $\frac{\sqrt{M}}{I_b}$ . Referring to Figure 7.29 it is observed that on the average the variation of resonant frequency as the square root of  $\frac{\sqrt{M}}{I_b}$  is valid since the experimental curve corresponds to the theoretical predictions within a maximum of 10% error. Experimental results presented in Chapter 7 for variation of natural frequency as a function of foundation size are plotted once more in Figure 8.1 for the purpose of comparison. It is observed from the data for all three test series that for a medium dense sand a straight line can be fitted to the data points with very good correlation. However, the data points related to the tests with constant  $\frac{\sqrt{M}}{I_b}$  and varying footing size (instead of keeping both  $M$  and  $I_b$  independently invariable) are a little scattered around the fitted line. This shows either an experimental scatter of the data points or that, the assumption describing the resonant frequency solely as a function of  $\frac{\sqrt{M}}{I_b}$  and not the  $M$  and  $I_b$  independently is not entirely valid.

Table 8.1 presents the theoretically calculated and experimentally measured values of natural frequencies of the towers in steady-state forced vibration tests. In the above theoretical calculations Equation 8.1 is used and the value of shear modulus  $G$  is taken from resonant column test data (Test 1) in Chapter 4. The mean effective pressure used in derivation of shear modulus is calculated according to Equation 8.8. In tests 5 to 7 the radius of the circular foundation is varied where all other parameters including  $M$  and  $I_b$  were kept independently constant; tests 10 to 12 were performed on model towers with circular foundations of different radius while keeping the ratio  $\frac{\sqrt{M}}{I_b}$  constant; finally in tests 40,

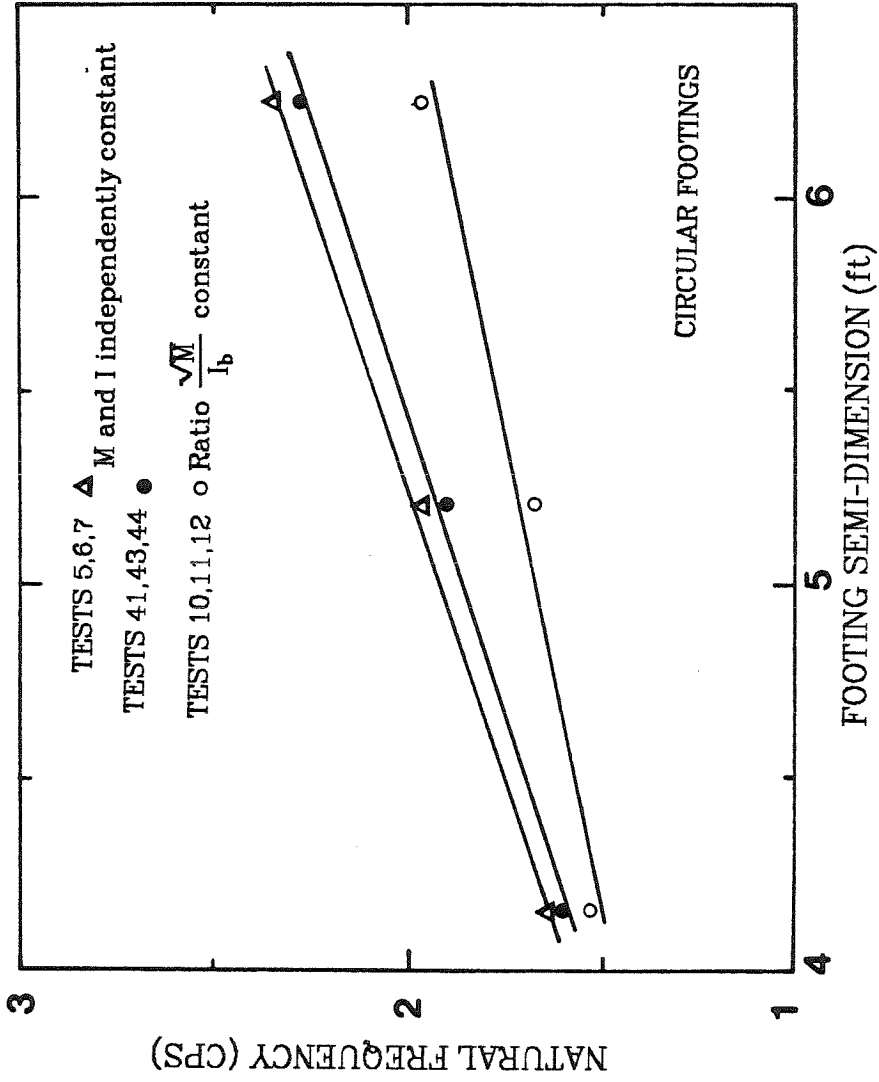


FIG. 8.1 VARIATION OF NATURAL FREQUENCY WITH BASE DIMENSION



42, and 45, in changing the semi-dimension of the square footings, all other parameters were kept constant. Data for tests 29, 31, and 62 are only compared individually with theoretical results to provide more information on the strength and limitations of the theoretical model. The predicted values are generally about 20% to 55% higher than experimental ones. This was also observed in Morris's centrifuge tests but in his tests the difference was smaller (maximum about 20%). The reasons for the large discrepancies observed in the Table 8.1 will be discussed later. However the calculated resonant frequency for the Model II in explosion-generated tests was very close to experimental value of 2.0 Hz. This shows a remarkable agreement between theory and experiment for at least one data point. Comparison at only one point does not prove to be universally valuable but it should be pointed out that this observed agreement is expected since the amplitude and duration of vibration in the explosion tests was very small.

The value of mean confining stress employed in evaluation of  $G$  using empirical relations or the resonant column test results was calculated from linear elastic theory as the minimum mean effective stress value at some depth below the footing edge. The stress value calculated includes the effect of average uniform vertical pressure on the foundation and the weight of soil itself. The minimum stress value occurs at a depth approximately equal to 0.5 radius of the base. This value is used in calculating the mean confining stress. Note that choice of this minimum confining stress compared with the mean stress value at one base radius depth is more justified. This will be discussed more in a later section. The stress distribution due to foundation weight along the depth is given in a tabulated form by Richart, Hall, and Woods (1970). At a depth  $z$  below the footing the vertical stress in soil is calculated from

$$\sigma_{v\text{tot}} = \beta (\bar{\sigma}_z)_{\text{ave}} + \gamma z \quad (8.6)$$

Where  $\gamma$  is the soil unit weight,  $(\bar{\sigma}_z)_{\text{ave}}$ , is the average vertical stress under the footing due to its own weight, and  $\beta$  is the reduction factor (derived from theory of elasticity) which, when multiplied by the average vertical stress at the surface  $(\bar{\sigma}_z)_{\text{ave}}$ , gives the value of vertical stress at the depth  $z$ . Then the horizontal and mean effective confining stresses are given by

$$\sigma_h = \frac{\nu}{1-\nu} (\sigma_v)_{\text{tot}} \quad (8.7)$$

and

$$\bar{\sigma}_o = \frac{1 + \frac{2\nu}{1-\nu}}{3} (\sigma_v)_{\text{tot}} \quad (8.8)$$

A Poisson's ratio  $\nu$  equal to 0.3, derived from ultrasonic wave propagation velocity measurements, was used in stress calculations for the tests in this report. If in Equation 8.5 the value of confining stress calculated according to the above formulation is used then the coefficient  $\alpha$  calculated from Table 8.1 is found to vary from 0.1 to 0.7 in order to give a reasonable agreement between theoretical and experimental results. If according to Morris the average vertical contact stress, due to foundation weight, is employed in the calculations of mean effective stress, then the predicted values for natural frequencies will be even higher than the theoretical results listed in Table 8.1, and the value of  $\alpha$  should then vary from 0.07 to 0.23 in order to give the desired agreement between the theoretical and experimental results. Values of confining stresses calculated according to the above methods, represented as  $\bar{\sigma}_{o1}$  and  $\bar{\sigma}_{o2}$  in the respective order they were defined, are tabulated in Table 8.2. In this table are also given the values of calculated damping ratio and magnification factor for the 1-D analog to the rocking problem (Hall Analog), similar to the Lysmer analog for the vertical vibration introduced in Chapter 1. The damping ratio  $\xi$  and the

Table 8.1. Comparison of Theoretical and Experimental Results for the 1-D Analog

Test No.	Theory $f_n$ (Hz)	Experiment $f_n$ (Hz)
5	4.11	2.25
6	2.38	1.60
7	3.25	1.90
10	2.22	1.55
11	2.86	1.70
12	3.83	2.00
41	3.33	2.35
43	2.05	1.65
44	2.68	1.90
29	3.16	2.30
31	4.35	2.68
62	3.86	2.50

Table 8.2. Calculated Values of Confining Stress, Radiational Damping, and Magnification Factor

Test No.	$\sigma_{c_1}$ (psi)	$\sigma_{c_2}$ (psi)	$\xi$ (%)	$M_m$
5	4.25	3.00	0.32	156.5
6	9.55	4.53	0.02	2500.0
7	6.10	3.48	0.09	555.5
10	13.80	6.12	0.01	5000.0
11	9.33	4.68	0.05	1000.0
12	6.44	3.83	0.22	227.3
41	8.1	4.46	0.15	333.3
43	18.22	7.78	<0.01	>5000.0
44	11.66	5.56	0.04	1250.0
29	7.66	4.30	0.12	416.7
31	7.66	4.30	0.30	166.7
62	7.66	4.30	0.50	100.0

maximum magnification factor  $M_m$  are defined as

$$\xi = \frac{0.15}{(1 + B) \sqrt{B}} \quad (8.9)$$

and

$$M_m \approx \frac{1}{2\xi} \quad (8.10)$$

where  $B = 3(1-\nu)l / 8\rho r^5$ .

### 8.2.2. Two-Degree-of-Freedom Lumped Parameter Analog

The simple one degree of freedom system considered in the previous section seemed to give satisfactory results without any need for a more complicated system. However this can be verified through the analysis of the complete 2-D coupled system by calculating the resonant frequencies of the system or the mode shapes of vibration. In addition response curves for the coupled system can be derived and compared with experimental response plots presented in Chapter 7.

The two-degree-of-freedom lumped parameter analog to the rocking-sliding problem of a rigid block on the surface of the elastic half-space is shown in Figure 8.2. As is seen it consists of a rigid block, one rotational spring and dashpot attached to the block at its base, and one horizontal translational spring and dashpot resisting its sliding motion also attached to the base. The two degrees of freedom are: (1) Rotation of the block about its center of gravity,  $\Phi$  and (2) Translation of center of gravity  $x$ , equal to translational motion of the whole rigid block (see Eqn. 8.19). For steady-state response to a harmonic force the system requires the solution of four simultaneous algebraic equations to obtain both the magnitude and phase of response for each degree of freedom.

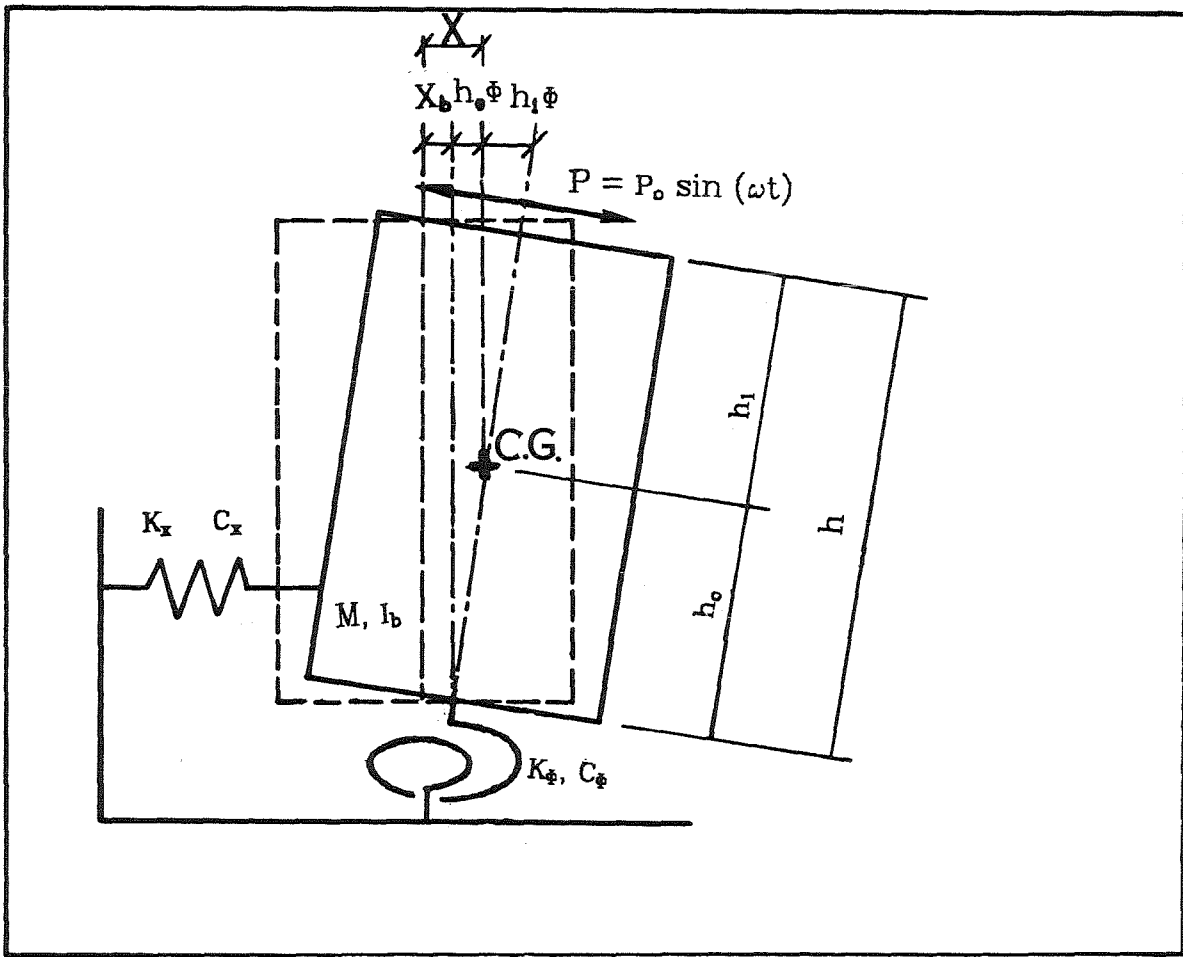


FIG. 8.2 TWO-DEGREE-OF-FREEDOM MODEL FOR LUMPED PARAMETER ANALYSIS OF FOUNDATION TRANSLATION AND ROCKING

Let the applied harmonic force with frequency-dependent amplitude be defined as

$$P = P_o \sin \omega t \quad (8.11)$$

where  $P_o = me\omega^2$ ,  $m$  is eccentric mass of the shaker,  $e$  the eccentricity, and  $\omega$  is angular frequency of the excitation. Then the equations of motion for the system shown in Figure 8.2 are:

For translation,

$$M\ddot{x} + C_x\dot{x} + K_x x - h_o C_x \dot{\phi} - h_o K_x \phi = P(t) \quad (8.12)$$

and for rotation

$$I\ddot{\phi} + (C_\phi + h_o^2 C_x)\dot{\phi} + (K_\phi + h_o^2 K_x)\phi - h_o C_x \dot{x} - h_o K_x x = P(t)h_1 \quad (8.13)$$

For the steady state solutions given by

$$x(t) = A_1 \sin \omega t + A_2 \cos \omega t \quad (8.14a)$$

$$\phi(t) = B_1 \sin \omega t + B_2 \cos \omega t \quad (8.14b)$$

the following matrix equation can be written

$$[K] \begin{Bmatrix} A_1 \\ A_2 \\ B_1 \\ B_2 \end{Bmatrix} = \{F\} \quad (8.15)$$

where  $[K]$  is given by the following equation:

$$[K] = \begin{bmatrix} -m\omega^2 + K_x & -C_x\omega & -h_o K_x & h_o C_x\omega \\ C_x\omega & -m\omega^2 + K_x & -h_o C_x\omega & -h_o K_x \\ -h_o K_x & h_o C_x\omega & -I\omega^2 + K_\phi + h_o^2 K_x & -C_\phi\omega - C_x h_o^2 \omega \\ -h_o C_x\omega & -h_o K_x & C_\phi\omega + C_x h_o^2 \omega & -I\omega^2 + K_\phi + h_o^2 K_x \end{bmatrix} \quad (8.16)$$

and  $\{F\}$  is given by,

$$\{F\} = \begin{Bmatrix} P_o \\ 0 \\ P_o h_1 \\ 0 \end{Bmatrix} \quad (8.17)$$

Solution of Equation 8.15 for the quantities  $A_1$ ,  $A_2$ ,  $B_1$ , and  $B_2$  leads to the following response magnitudes and phases,

$$|x| = \sqrt{A_1^2 + A_2^2} \quad (8.18a)$$

$$\Theta_x = \tan^{-1} \frac{A_2}{A_1} \quad (8.18b)$$

and

$$|\Phi| = \sqrt{B_1^2 + B_2^2} \quad (8.18c)$$

$$\Theta_\Phi = \tan^{-1} \frac{B_2}{B_1} \quad (8.18d)$$

Translation of the base of the footing is designated by

$$x_b = x - h_o \Phi \quad (8.19)$$

If  $x_b$  is negligible compared with rotational amplitude,  $x_\Phi = (h_1 + h_o) \Phi$  about an axis passing through the base, then the simple 1-D system in Section 8.2.1 would be sufficient for the analysis of the fundamental mode of the rocking-sliding system.

The next step in calculating the response is to define the foundation-soil impedances and inertial-geometrical properties of the rigid block. Dynamic properties of the soil and the rigid towers employed in the theoretical analyses are defined in Chapters 4,5,6, and 7 and will not be repeated here. Therefore it is only needed to define the impedance functions for the soil and calculate them using the known dynamic properties.

### 8.2.3. Foundation-Soil Impedances

The foundation-soil impedances which introduce the effect of soil-structure interaction in dynamic analysis of structures under any vibratory load or acceleration input, were defined in Chapter 1. Equations 1.6a and 1.6b define stiffness and damping coefficients of the analog system for the vertical or horizontal translational motion of a rigid foundation on the elastic or viscoelastic half-space. Similarly equations 1.8 and 1.9 define the rocking impedance functions. For simplicity in presentation of the impedance functions the following relations are defined

$$k = \frac{f_1}{f_1^2 + f_2^2} \quad (8.20)$$

$$c = \frac{-1}{a_0} \left( \frac{f_1}{f_1^2 + f_2^2} \right) \quad (8.21)$$

By defining the above relations the frequency-dependent part of the impedance functions will be collected in closed form functions  $k$  and  $c$  and the impedance functions for the horizontal and rocking vibrations of the foundation reduce to

$$K_x = Gr_0 k, \quad (8.22)$$

$$C_x = \sqrt{G\rho} r_0^2 c \quad (8.23)$$

and

$$K_\phi = Gr_0^3 k, \quad (8.24)$$

$$C_\phi = \sqrt{G\rho} r_0^4 c \quad (8.25)$$

Since the impedance functions  $k$  and  $c$  are frequency-dependent, the frequency domain is usually used for dynamic analysis. The values of these coefficients must be calculated at any given frequency before the four simultaneous equations are solved for that value of frequency. Lin (1982) presented a detailed comparison of different expressions for the impedance functions which have been derived by different researchers. Since all the formulations found in



the literature are at least valid for the case of  $\nu = 0$ , he compared the impedance functions for this case and in the final format he obtained a single formulation for the case of  $\nu = 0.33$  (the site conditions in his experiments). In some cases the impedance functions (stiffness and damping coefficients K and C) were not directly given in the literature and it was necessary to calculate them knowing the compliance functions (Equations 8.20 to 8.25). Impedance functions for rigid circular footings on the surface of the linear elastic half-space were compared and formulations given by Veletsos and Wei were chosen. These formulations are frequency dependent and are defined for a wide range of dimensionless frequency. In both horizontal translation and rocking vibration the formulations given by Veletsos and Wei would not lead to major differences with the other formulations discussed there. These formulas for the horizontal translation and the case of  $\nu = 0.3$  (for the sand used in this study) are given as

$$K_x = 4.80Gr_o (1.0 - 0.001802a_o - 0.03271a_o^2 - 0.1749a_o^3 + 0.02135a_o^4 - 0.004195a_o^5) \quad (8.26)$$

$$C_x = 4.80\sqrt{G\rho} r_o^2 (0.580 + 0.001954a_o - 0.0130a_o^2 + 0.01118a_o^3 - 0.00841a_o^4 + 0.001262a_o^5) \quad (8.27)$$

and in the case of the rocking oscillation for  $\nu = 0.3$  the impedance functions are

$$K_\phi = 4.00Gr_o^3 (1.0 + 0.1058a_o - 0.400a_o^2 + 0.3026a_o^3 - 0.1010a_o^4 + 0.02181a_o^5) \quad (8.28)$$

$$C_\phi = 4.00\sqrt{G\rho} r_o^4 (-0.0002 - 0.006734a_o + 0.3240a_o^2 - 0.2542a_o^3 + 0.08173a_o^4 - 0.00969a_o^5) \quad (8.29)$$

The above impedance functions are valid over the range of  $0 < a_0 < 2.5$ . Horizontal translation impedance functions show very little frequency dependence over the entire frequency range, but rocking impedance functions, particularly the damping coefficient, have greater dependence on frequency than those of horizontal translation. In the above formulations for the impedance functions coupling between translation and rocking of the footing (a flat plate) on the surface of the elastic-half space and excited by a horizontal force or a rocking moment is negligible and therefore the coupling terms are not considered in the discussions of this section.

#### **8.2.4. Impedance Functions for Viscoelastic Foundations**

Damping predicted by linear elastic half-space theory, in a rocking-sliding system, vibrating in its fundamental resonant frequency (mainly rocking motion) is very small as was shown in Section 8.2.1. The only form of energy dissipation in the above theoretical model is geometrical or radiation damping. Therefore, there is a great need to use a mathematical model which accounts for the effects of material energy dissipation in the halfspace material. Such effects are particularly important for high-intensity excitations associated with large strains in the supporting material. In fact this is the case in most moderate to severe earthquakes which induce large strains and permanent deformations in the soil mass supporting foundations. This large amplitude deformation and increased material damping was also observed in the centrifuge tests conducted in this study. To include the effect of material damping in the analysis, the half space will be idealized as a linear viscoelastic solid, and two models will be considered: the standard Voigt model and the constant hysteretic model. Veletsos and Verbic ( 1973) have addressed the problem in a report on

vibration of viscoelastic foundations. Derivation of impedance functions for the above model is based on the application of the correspondence principle applied to analytical approximations of numerically obtained solutions for the corresponding elastic problem. It should be noted that it is extremely difficult to apply the above-mentioned principle to the complicated integral equations derived for the exact solution of the elastic half-space problem.

The stress-strain relation for the harmonically oscillating halfspace is defined by

$$\tau = G^* \gamma \quad (8.30)$$

where

$$G^* = G \left[ 1 + i \frac{\omega G'}{G} \right] \quad (8.31)$$

In the above equations  $\tau$ ,  $\gamma$  are shear stress and shear strain respectively, and  $G$ ,  $G'$  are the shear moduli of elasticity and coefficient of viscosity, respectively. The correspondence principle requires that the elastic moduli in closed form solutions to the elastic problem be substituted by their viscoelastic counterparts as defined in 8.31. The value of  $G'$  is related to the energy loss in the system represented by the area enclosed in the strain-stress loading-unloading loop. How the value of  $G'$  changes with frequency, determines if the model is a viscous or a hysteretic one. For a Voigt solid,  $G'$  is considered to be constant, whereas for constant hysteretic solid the product  $\omega G'$  is considered to be constant.

Let the loss coefficient  $\tan \delta$  be defined as

$$\tan \delta = \frac{\omega G'}{G} = \frac{1}{2\pi} \frac{\Delta W_h}{W} \quad (8.32)$$

where  $W$  is the strain energy stored in a perfectly elastic material with maximum

deformation amplitude the same as in the viscoelastic one, and  $\Delta W_h$  is the energy lost in a complete stress-strain cycle. Then provided the values of  $\tan \delta$  (or  $\frac{\Delta W_h}{W}$ ) for the soil and the viscoelastic solid are taken the same, the simple viscoelastic models will adequately simulate the damping properties of actual soils. Note that the hysteretic solid is also called the constant  $\tan \delta$  model.

In deriving the impedance functions for the viscoelastic model for simplicity in presentation of future relations the new functions  $k_x$ ,  $c_x$  for horizontal translation; and  $k_\varphi$ ,  $c_\varphi$  for the rocking motion are introduced. These functions differ from the  $k$  and  $c$  defined in Section 8.2.2. by only a factor which is a function of Poisson's ratio; they are defined as

$$k_x = \frac{2-\nu}{8} k \quad (8.33)$$

$$c_x = \frac{2-\nu}{8} c \quad (8.34)$$

$$k_\varphi = \frac{3(1-\nu)}{8} k \quad (8.35)$$

$$c_\varphi = \frac{3(1-\nu)}{8} c \quad (8.36)$$

Neglecting the small coupling between the horizontal and rocking motions, Veletsos and Verbic defined the following approximate relations for the impedance functions related to horizontal translation and rocking motions of a rigid massless disk on the surface of elastic half-space:

For the horizontally excited disk,

$$k_x = 1, \quad (8.37)$$

$$c_x = \alpha_1 \quad (8.38)$$

for the disk in rocking motion

$$k_{\varphi} = 1 - \beta_1 \frac{(\beta_2 a_0^2)}{1 + (\beta_2 a_0^2)} - \beta_3 a_0^2 \quad (8.39)$$

$$c_{\varphi} = \beta_1 \beta_2 \frac{(\beta_2 a_0^2)}{1 + (\beta_2 a_0^2)} \quad (8.40)$$

where  $\alpha_i$  and  $\beta_i$  are numerical coefficients which depend on Poisson's ratio,  $\nu$  (see Veletsos and Verbic, 1973).

Assuming that Poisson's ratio is the same for elastic and viscoelastic material then the impedance functions for the viscoelastic half-space are determined merely by replacing the real-valued shear modulus  $G$  by the complex modulus  $G^*$  in the relations for  $K$ 's and  $C$ 's (Equations 8.22 to 8.25 and 8.37 to 8.40). The resulting stiffness and damping functions for the viscoelastic model are then defined as:

For the horizontally excited disk,

$$k_x^v = 1 - \sqrt{\frac{R-1}{2}} \alpha_1 a_0 \quad (8.41)$$

$$c_x^v = \frac{\sqrt{R+1}}{2} \alpha_1 + \xi \quad (8.42)$$

where

$$\xi = \frac{V_s}{r} \frac{G^*}{G} = \frac{1}{a_0} \tan \delta \quad (8.43)$$

and

$$R = \sqrt{1 + a_0^2 \xi^2} = \sqrt{1 + \tan^2 \delta} \quad (8.44)$$

For the disk in rocking motion, the corresponding equations obtained by use of Equations 8.39 and 8.40 are

$$k_{\varphi}^v = 1 - \chi_{\varphi} - \beta_3 a_0^2 \quad (8.45)$$

$$c_{\varphi}^v = \psi_{\varphi} + \xi \quad (8.46)$$

where

$$X_{\varphi} = \frac{\beta_1 \left[ R + \sqrt{\frac{R-1}{2}} (\beta_2 a_0)^2 \right]}{R + 2 \sqrt{\frac{R-2}{2}} (\beta_2 a_0) + (\beta_2 a_0)^2} \quad (8.47)$$

and

$$\psi_{\varphi} = \frac{\beta_1 \beta_2 \sqrt{\frac{R+1}{2}} (\beta_2 a_0)^2}{R + 2 \sqrt{\frac{R-2}{2}} (\beta_2 a_0) + (\beta_2 a_0)^2} \quad (8.48)$$

In the above equations  $V_s$  is the shear wave velocity in the half-space medium,  $r$  is the radius of the rigid disk on the surface of half-space, and superscript  $v$  represents the viscoelastic impedance functions.

### 8.2.5. Impedance Functions for Analysis of Embedded Foundations

Embedment effect increases the stiffness and consequently the resonant frequency of the foundation-soil system. This property of embedment is usually included in analysis by increasing the foundation-soil impedance values.

Two different approaches to include the effect of embedment have been undertaken. The first method (Baranov, 1967) assumes that the foundation rests on the surface of an elastic half-space and is embedded in an elastic layer which may have different properties from the elastic half-space. Using this approach it is possible to include the effect of separation between foundation and the soil in an approximate fashion by reducing the shear modulus of the side layer compared with the modulus of the half-space. In another method (Parmalee and Kudder, 1974; Elsabee and Morray, 1977; Luco, Wong, and Tri-funac, 1975), the foundation is assumed to be embedded in a homogeneous medium; therefore there is no provision for the reduction in stiffness values of

the side layer to account for the effect of foundation and soil separation. In the first method the added terms to the impedance functions accounting for the effect of embedment are frequency-dependent, and are different for stiffness and damping effects in horizontal and rocking vibration. Beredugo and Novak (1972) reported impedance functions for translation and rocking which account for the effect of embedment using the above method.

In the second method the additional stiffness and damping terms introduced by the effect of embedment are assumed to be frequency-independent. Static impedance values are merely increased by a factor which is a function of embedment depth to obtain the impedance properties of the embedded foundations. Usually in this method the effect of embedment is considered by using similar functions for stiffness and damping terms for all modes of vibration. These simplifications greatly reduce the cost and time required for the analysis, but diminish the accuracy of the solution and normally predict a greater stiffness of the system produced by embedment compared with predictions using the first method.

Lin (1982) in a review of the advantages and disadvantages of the formulations presented by the above authors, lists the different impedance functions and presents plots comparing the predictions made by these methods.

Experimental results reported in the present study are compared with theoretical predictions based on the formulations offered by all the above-mentioned authors.

#### **8.2.6. Presentation of Theoretical Results for the 2-D Model**

A computer program called "2DSYS" was written which computes the response amplitudes of a rigid circular foundation resting on the surface of a

linear elastic or viscoelastic half-space. The program can also analyze the dynamic response of a rigid circular footing embedded in a linearly elastic infinite medium. For the embedded case four different formulations including the effect of embedment were considered. These relations for the increased stiffness and damping coefficients because of embedment effect were derived from the references mentioned in the former section.

The analysis process consists of the following steps:

- (1) Input the dynamic properties of the soil and model structure, and the mode of analysis. The mode of analysis can be any of the following options:
  - (a) Rigid foundation on elastic half-space
  - (b) Rigid foundation on viscoelastic half-space with viscous damping
  - (c) Rigid foundation on viscoelastic half-space with hysteretic damping
  - (d) Embedded foundation in elastic half-space
    - (d.1) Beredugo and Novak formulation
    - (d.2) Parmalee and Kudder formulation
    - (d.3) Elsabee and Morray formulation
    - (d.4) Luco, Wong, Trifunac formulation

(the above formula are listed in the report by Lin, 1982)
- (2) Increment the frequency and at each value compute all the frequency dependent terms (i.e.,  $a_0$ , force amplitude, damping and stiffness coefficients for the particular mode of analysis).
- (3) Assemble the complex stiffness matrix of the two-degree-of-freedom analog and the load vector.
- (4) Solve the four algebraic equations for the phases and amplitudes of the response (i.e., the horizontal displacement of the center of gravity and



the rotation of the block about its center of gravity). Repeat steps 1 to 4 and derive the solution for the range of frequency of interest. Theoretical response functions derived from this analysis can be compared with the response curves derived for the experimental data in Chapter 7.

- (5) Repeat the same procedure used for experimental data in Chapter 7 to derive resonant frequencies and damping ratios for the theoretical data. That is, using the system identification program described in Chapter 7, derive the best fit of the response of a single-degree-of-freedom oscillator to the theoretical amplitude-frequency curve of the tower at the fundamental resonant frequency of the system. The damping and frequency of the fitted oscillator will then be compared with experimental data of Chapter 7.

There are some particular features of the input data that need to be addressed at this stage. These features include,

- (1) Since the above theory is only valid for a semi-infinite medium, a theoretical analysis was not carried out for the tests on the effect of soil depth. Therefore, only results of tests with maximum soil depth were theoretically checked.
- (2) Since the theoretical model is linear amplitude of the generalized displacement vector will vary as a linear function of load magnitude. Thus, tests on the nonlinear effect of increasing load amplitude were not modeled theoretically.
- (3) Damping ratios employed in the analysis were derived from the damping values measured in low amplitude resonant column tests (strain  $\leq 10^{-4}$ ). These values varied from approximately 1% for high confining

teretic damping ratio was used in the analysis of all model towers. Only in the modelling of one test, was viscous damping used in the analysis.

- (4) Mean confining stress in the soil supporting the tower was derived in the same fashion as described for the 1-D simple oscillator analog (Section 8.2.1).
- (5) Poisson's ratio was taken as 0.3 and the shear modulus was obtained from data in Table 4.2 for test 1 of the resonant column tests. Mass, mass moment of inertia, and height of center of gravity for the models were all found from Table 6.2 and the tables in Chapter 7.

#### 8.2.6.1 Theoretical Values of Resonant Frequencies

Theoretical values of resonant frequencies for the fundamental mode of rocking-sliding are tabulated in Table 8.3. The test numbers are in groups related to each parametric study (i.e., tests studying the effect of foundation size, the moment of inertia, and the ratio  $\frac{\sqrt{M}}{I_b}$ ). Also included in the table are the experimental values derived for the resonant frequencies and damping ratios. Overall comparison of the theoretical and measured resonant frequencies shows that theory will always predict resonant frequencies of the foundation-soil system about 15% to 55% higher than the experimental values. It is observed that agreement between theoretical and experimental results gets worse as the size of foundation or the embedment ratio increases. This means that changing foundation-soil parameters in order to increase the stiffness of the system will not produce an increase in the resonant frequency as appreciable as that predicted by theory. The probable reasons for this discrepancy between theoretical and experimental data will be discussed later in this chapter.

The damping values show a closer agreement between theory and experiment. The uncertainty in exact damping values, measured by the resonant column tests, and their scattered variation with confining pressure suggests that a value of 2% to 5% for hysteretic damping ratio of soil will yield the correct damping contribution to the soil-structure system. Figure 8.3 depicts the response amplitude of the theoretical solution for a model tower resting on the soil surface (theoretical modelling of Tests 19 and 11 to 14). Material damping was not included in this case and loss of energy in the model occurred because of geometrical damping only. Figure 8.3 and Table 8.2 show that the second mode of rocking-sliding vibration is extremely damped, while damping for the fundamental mode of vibration is very small. Therefore, introduction of rigid boundaries around the soil mass in the centrifuge tests will not affect substantially the geometrical damping of the fundamental mode of the system. However, geometrical damping in higher rocking-sliding modes will be reduced significantly by the presence of the rigid boundaries. In addition, the small value of radiational damping for the modes of the bounded soil-foundation system, emphasizes the importance of inclusion of material damping in response amplitude analysis.

A comparison of theoretical values of resonant frequencies in Tables 8.1 and 8.3 shows an excellent agreement between the calculated values using either the 1-D lumped-parameter model or the 2-D lumped-parameter one. The resonant frequency values in Table 8.3 are a little smaller because of inclusion of the material damping. Therefore the simple 1-D analog will produce approximately the same results as the 2-D model in predicting the fundamental resonant frequency of the model or prototype.

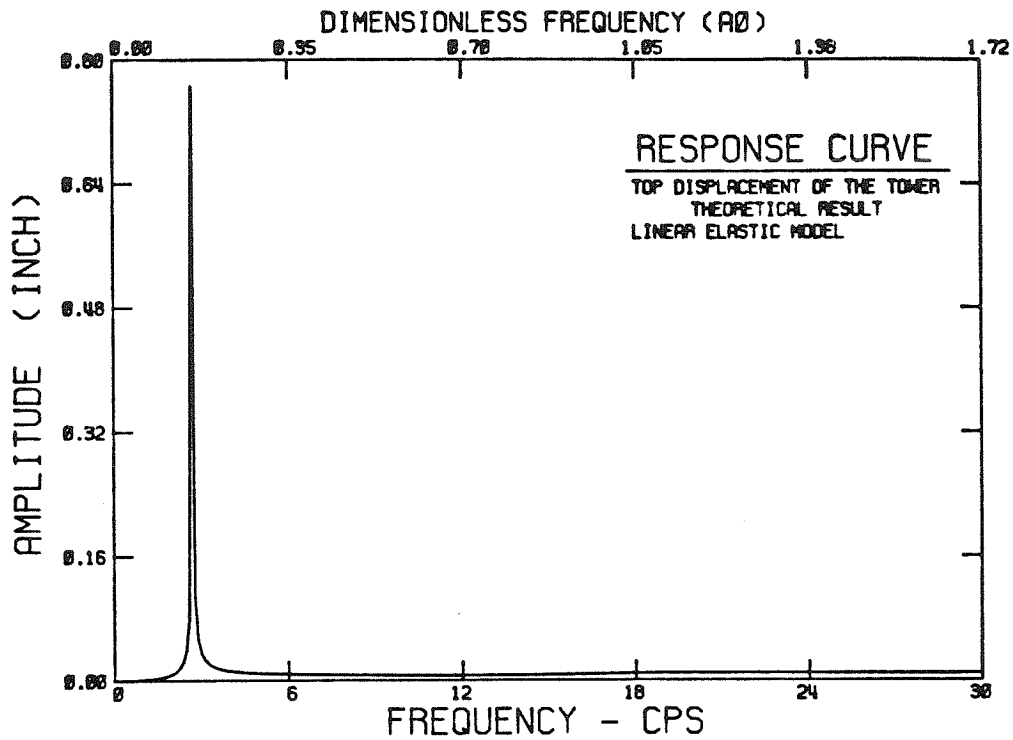


FIG. 8.3 RESPONSE CURVE OF THE TWO-DEGREE-OF-FREEDOM OSCILLATOR

Table 8.3. Comparison of Theoretical and Experimental Results for the 2-D Lumped Parameter Analog

Test No.	Theory $f_n$ (Hz)	Theory $\xi$ (%)	Experiment $f_n$ (Hz)	Experiment $\xi$ (%)
5	3.93	2.13	2.25	
6	2.32	2.7	1.6	
7	3.19	1.8	1.90	
10	2.19	1.6	1.55	3.0
11	2.62	1.6	1.70	2.5
12	3.89	2.2	2.00	3.0
41	3.20	2.0	2.35	3.0
43	1.90	1.7	1.65	1.0
44	2.55	2.0	1.90	4.0
29	3.07	2.0	2.50	2.8
31	4.13	2.5	2.68	3.0
62	3.69	2.2	2.50	3.0

### 8.2.6.2 Comparison of Experimental and Theoretical Response Amplitudes

Figures 8.4 and 8.5 compare the response amplitudes derived by the theoretical model and the experimental observations in Test 19. Both viscous (Fig. 8.4) and hysteretic damping (Fig. 8.5) were considered. The difference between the theoretical response amplitudes with the two different damping types was negligible and therefore only hysteretic damping was considered for the rest of this analysis. It is observed from the figures that inclusion of material damping does not considerably influence the values of resonant frequencies but it does cause a big change in the amplitude of motion. Therefore the major reason for the observed discrepancy between theoretical and experimental results is the stiffness of the system which is much higher in the theoretical model. The amplitude of experimental response curve is in good agreement with the amplitude of theoretical model with about 0.5% hysteretic damping ratio. The second rocking mode in experimental data, produced by the boundary effects, is not observed in the theoretical response curves since the model assumes a semi-infinite medium.

### 8.2.6.3. Theoretical Modal Analysis

A method similar to the one in Chapter 7 was used to calculate the theoretical amplitude contributions of the base translation and the rigid body rotation about an axis through the base, to the total displacement of the tower top. Results of these calculations for a few test models with different physical properties and different loading conditions (different positions of the applied horizontal force) are shown in Figures 8.6 to 8.12. A comparison of these figures with Figures 7.46 to 7.52 shows that theory and experiment are in good agreement in predicting the contribution of the translational and rotational motions to the total amplitude of the tower. In addition it is shown that assuming the fundamental mode of vibration as a purely rotational motion about an axis

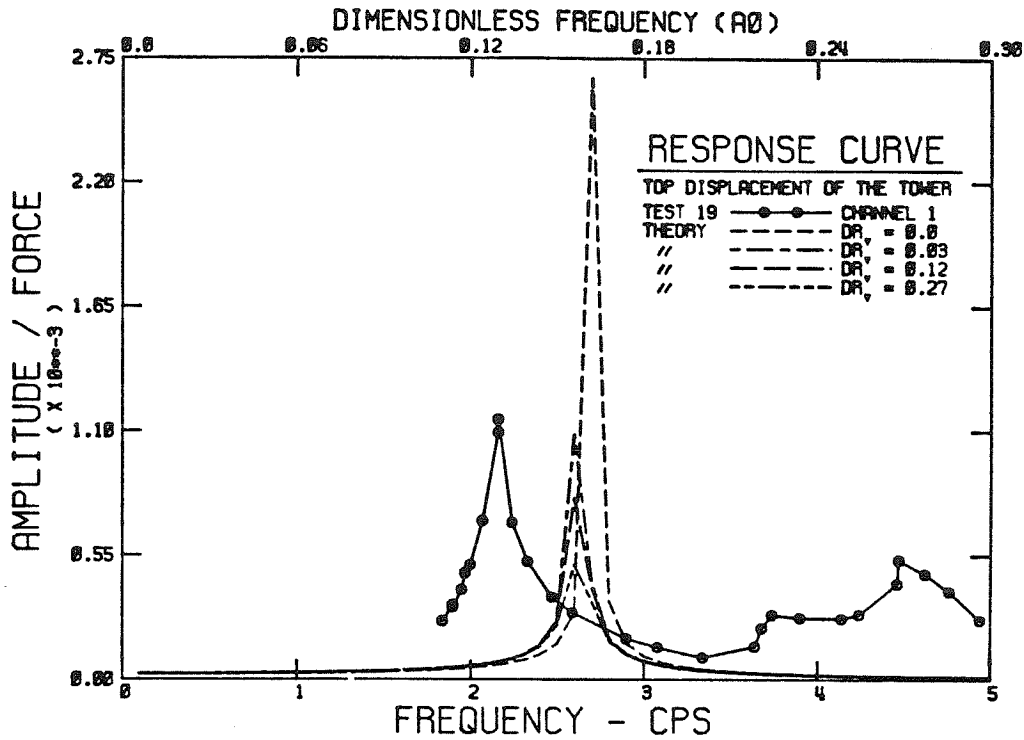


FIG. 8.4 THEORETICAL RESPONSE CURVES COMPARED WITH EXPERIMENTAL OBSERVATIONS (VISCOUS MODEL)

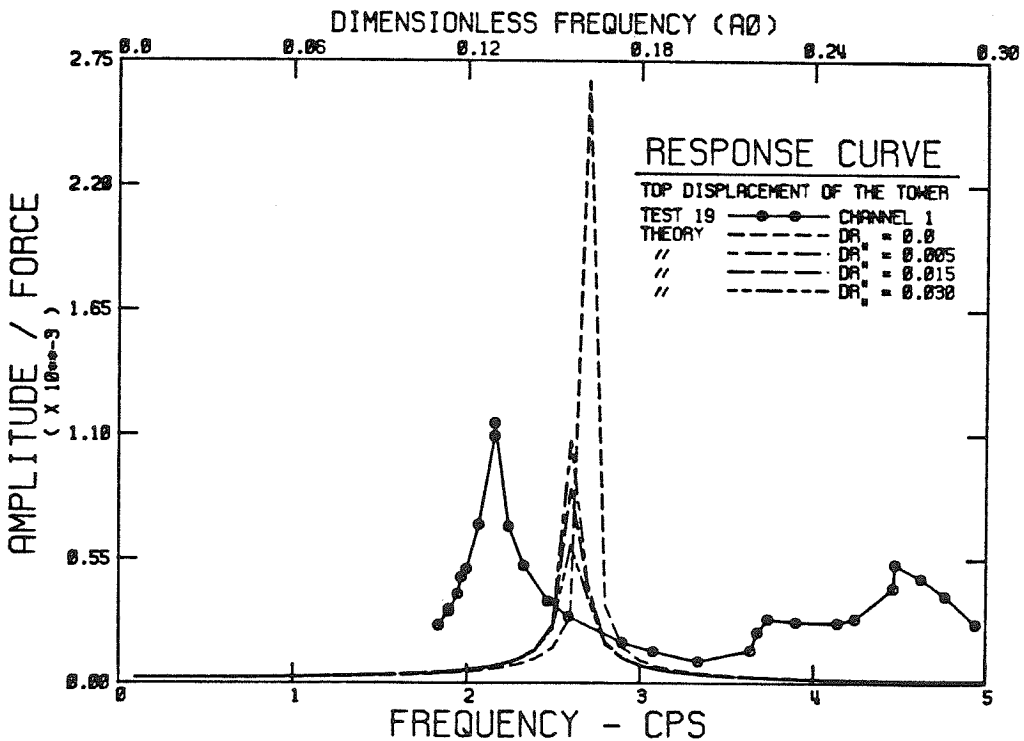


FIG. 8.5 THEORETICAL RESPONSE CURVES COMPARED WITH EXPERIMENTAL OBSERVATIONS (HYSTERETIC MODEL)

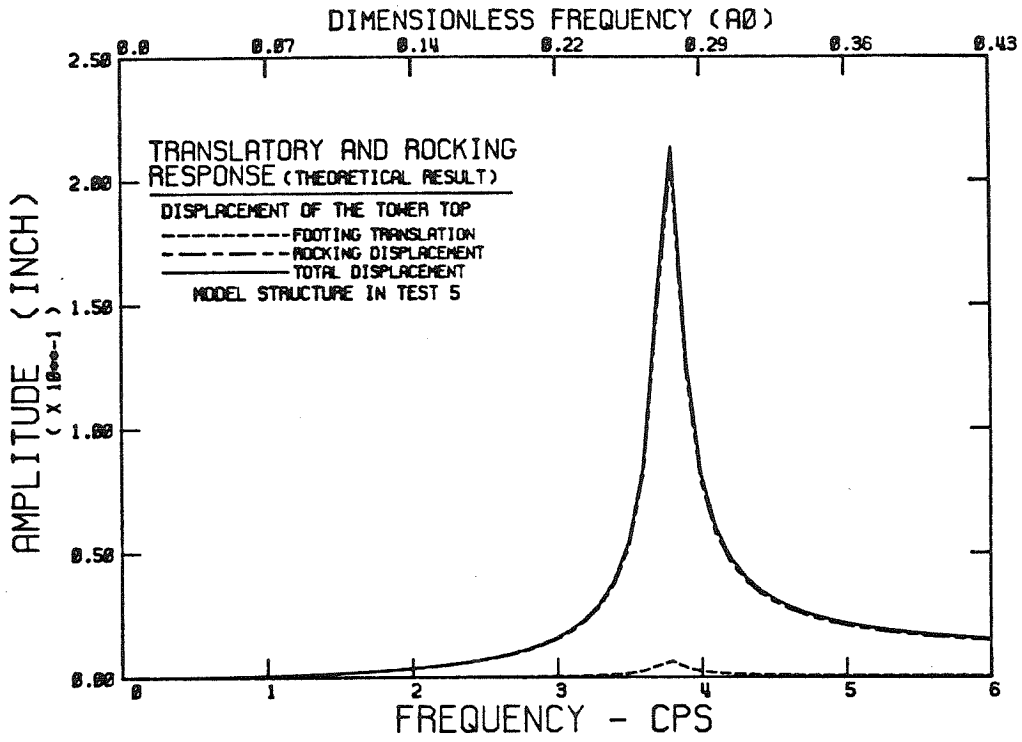


FIG. 8.6 CONTRIBUTION OF TRANSLATIONAL AND ROCKING MOTION TO THE TOTAL DISPLACEMENT OF THE TOWER TOP

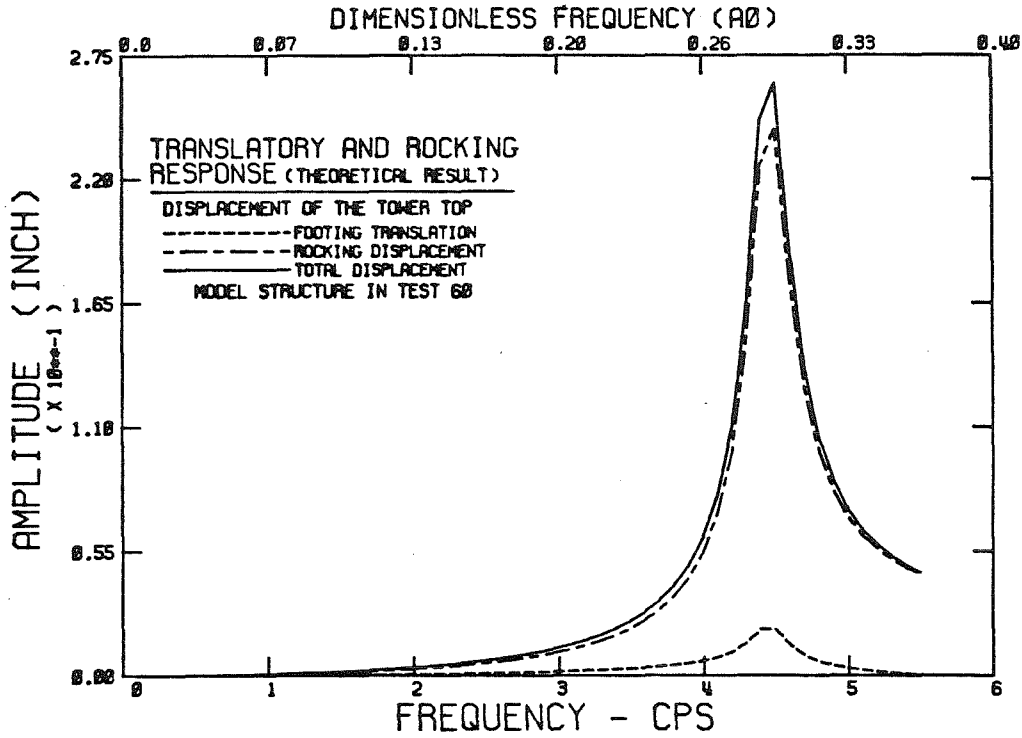


FIG. 8.7 CONTRIBUTION OF TRANSLATIONAL AND ROCKING MOTION TO THE TOTAL DISPLACEMENT OF THE TOWER TOP

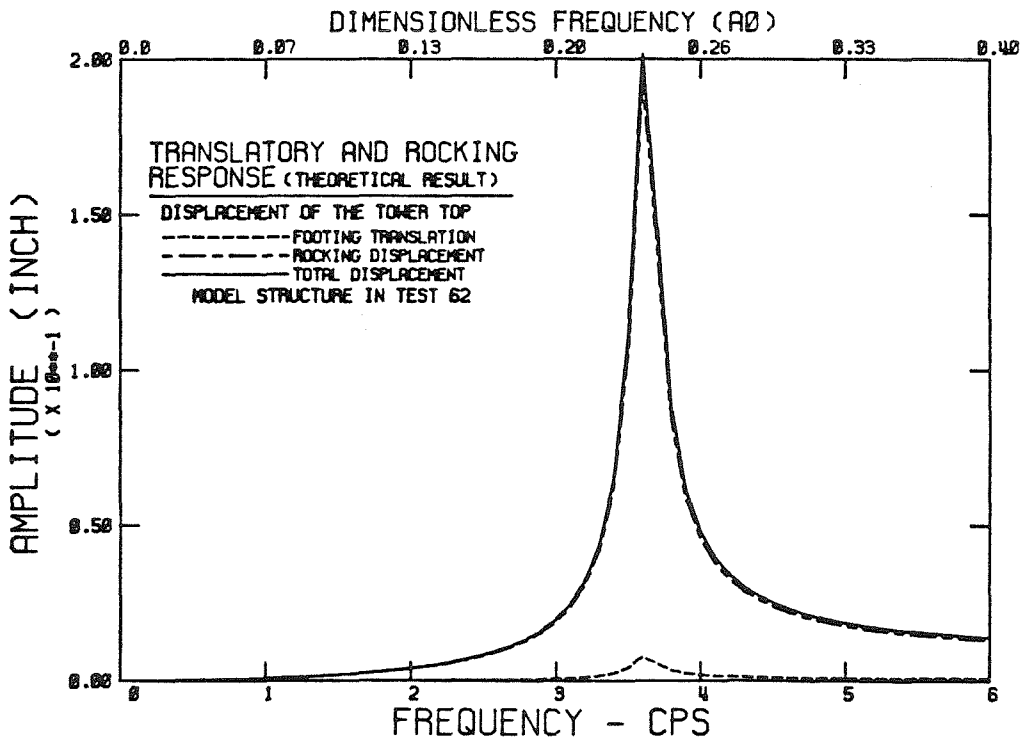


FIG. 8.8 CONTRIBUTION OF TRANSLATIONAL AND ROCKING MOTION TO THE TOTAL DISPLACEMENT OF THE TOWER TOP



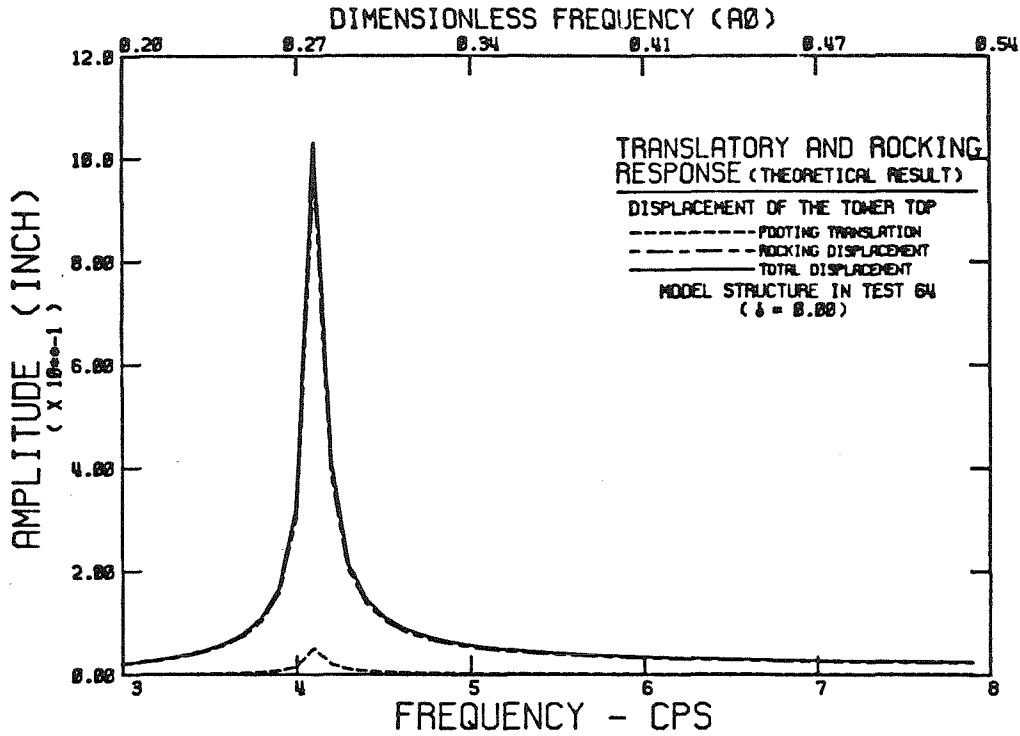


FIG. 8.9 CONTRIBUTION OF TRANSLATIONAL AND ROCKING MOTION TO THE TOTAL DISPLACEMENT OF THE TOWER TOP

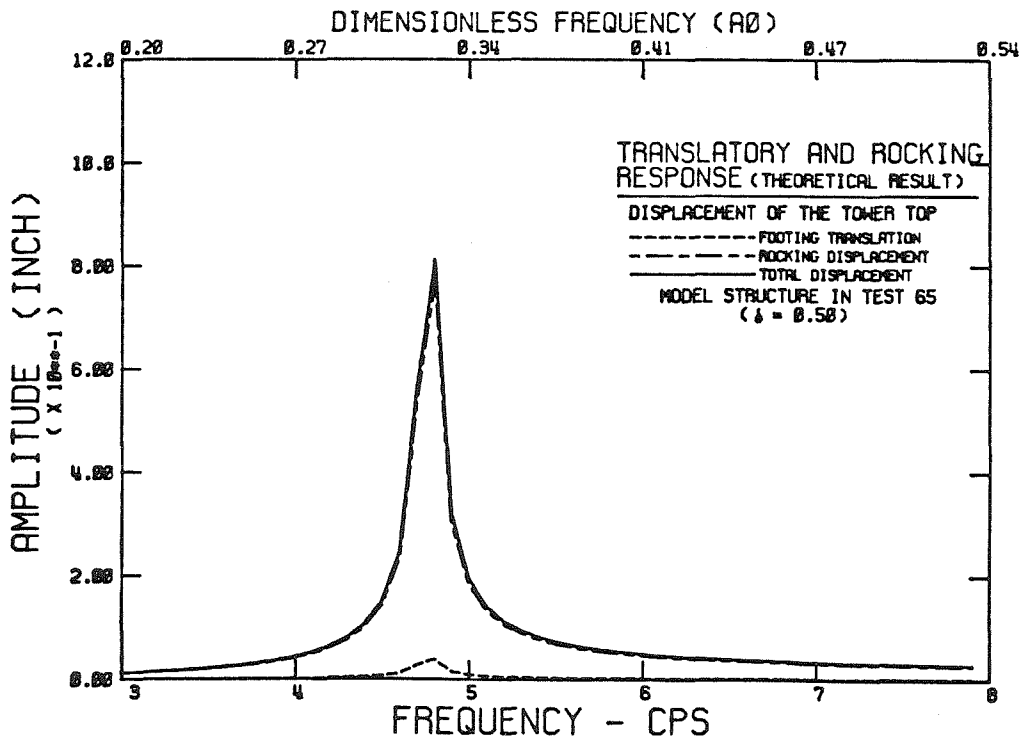


FIG. 8.10 CONTRIBUTION OF TRANSLATIONAL AND ROCKING MOTION TO THE TOTAL DISPLACEMENT OF THE TOWER TOP

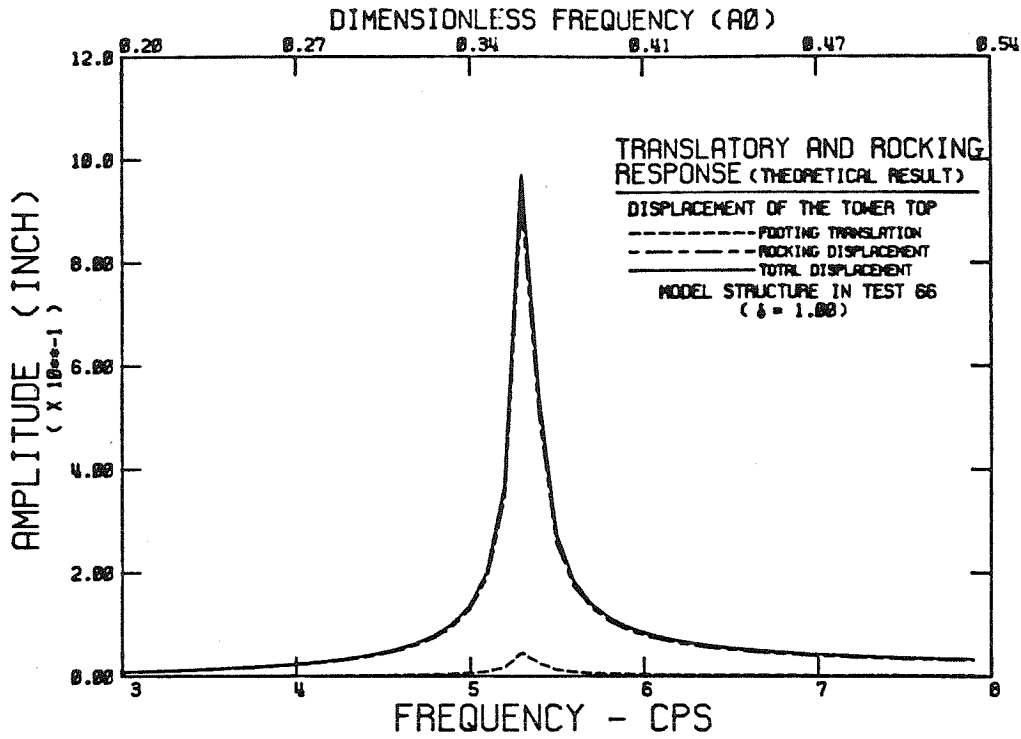


FIG. 8.11 CONTRIBUTION OF TRANSLATIONAL AND ROCKING MOTION TO THE TOTAL DISPLACEMENT OF THE TOWER TOP

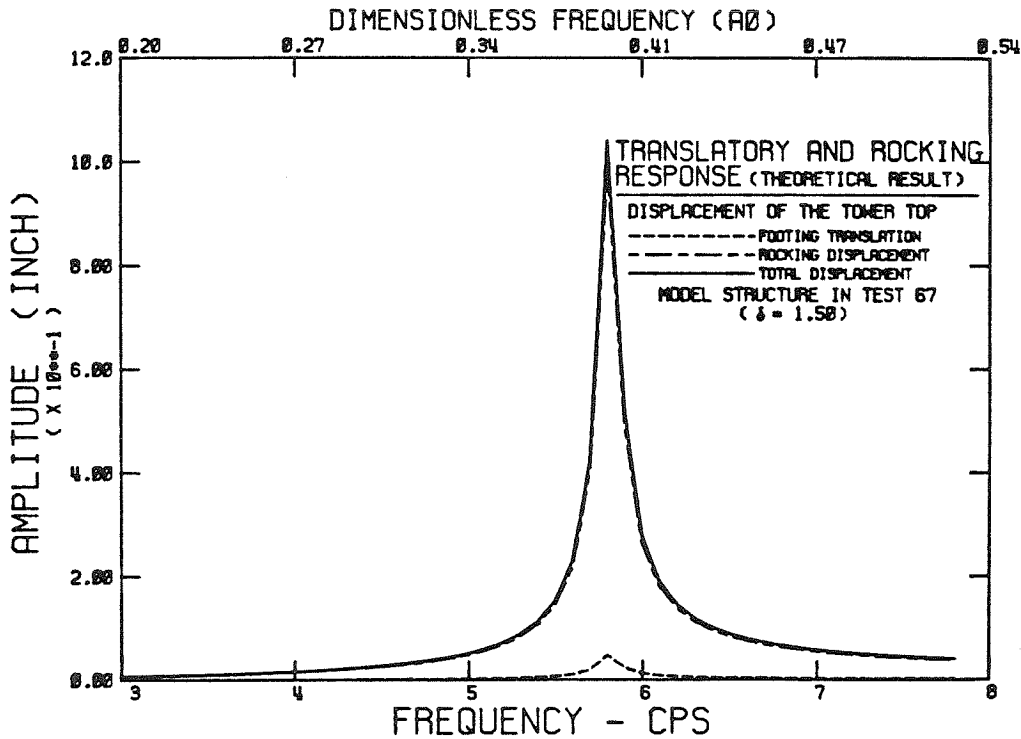


FIG. 8.12 CONTRIBUTION OF TRANSLATIONAL AND ROCKING MOTION TO THE TOTAL DISPLACEMENT OF THE TOWER TOP

passing through the center of the base is a reasonable assumption. Maximum predicted contribution of the translational motion to the total displacement of the tower top is observed for Test 60 where the horizontal force was applied directly to the footing top surface and not to the tower top as in the other tests. In this case the applied load is closer to the footing base and consequently the moment amplitude with respect to the base is much smaller compared to the case where the horizontal force is applied to the tower top.

#### **8.2.6.4 Theoretical Results for Embedded Footings**

Except for the theoretical results derived from the Novak and Beredugo formulation all other formulations resulted in very high resonant frequencies compared with experimental values; therefore they will not be discussed here. The theoretical resonant frequencies for the models of Tests 64, 65, 66, and 67 assuming the same material for the side layer as the half-space were derived to be: 4.0 Hz, 4.77 Hz, 5.3 Hz, and 5.8 Hz respectively compared to the experimental values in Table 7.8. This shows a great difference between individual theoretical and experimental resonant frequencies, but the percentages of increase in frequencies because of embedment are close in the two cases, i.e. 37% increase from theory compared with 27% increase in experiments from 0 embedment ratio to 1.5. If it is assumed that the shear modulus of the side layer is half of the value for the half-space then the theoretical values will be equal to 4.0 Hz, 4.47 Hz, 4.77 Hz, and 5.10 Hz respectively. In this case theory will predict only 25 % increase in resonant frequency for the largest depth of embedment which is in good agreement with the experimental result. Figure 8.13 shows the amplitude response curves for the tests 64 to 67 as calculated theoretically by the Novak and Beredugo formulation (see Chapter 4 for the soil and Table 6.2 for the model properties respectively). It is observed that the amplitude of

vibration decreases considerably from 0 (surface footing) to 0.5 embedment ratio. From 0.5 to 1.5 embedment ratio amplitude decreases gradually at a slower rate than the initial reduction from surface footing to embedded one. This shows that there is a large increase in the radiational damping ratio when the footing is embedded in the elastic medium. Figure 8.14 compares the experimental results shown in Figure 7.30 with theoretical predictions using the Beredugo and Novak formulations for the two cases of  $G_s/G = 1.0$ , and  $G_s/G = 0.5$  (here  $G_s$  and  $G$  represent the shear modulus of the side layer and the half-space respectively).

#### 8.2.6.5. Theoretical Results for Foundations of Different Sizes

Figure 8.15 shows the calculated response curves for three foundations with different sizes. The soil-foundation parameters and particularly the three different footing sizes used in these theoretical calculations are the same as data in tests 41, 43, and 44 (see Tabl. 6.2). Therefore, the theoretically calculated resonant frequencies from Figure 8.15 can be compared with their experimental counterparts in Figure 7.22 (or Tabl. 7.2). The theoretical results in general predict the same trend of behavior as experimental ones but they show a much higher increase in resonant frequencies with increase of foundation size compared with experimental results. Amplitude of vibration decreases considerably as the footing size increases. This shows an increase in geometrical damping ratio when footing dimensions become larger. Note that there was no appreciable change in amplitude of motion for the corresponding experimental results. This is mainly because of uplift and nonlinear behavior of the footing-soil system which prevents appreciable changes of the geometrical damping. The interference of the rigid boundaries of the soil bucket reducing the geometrical damping of the system is another reason for the above-mentioned

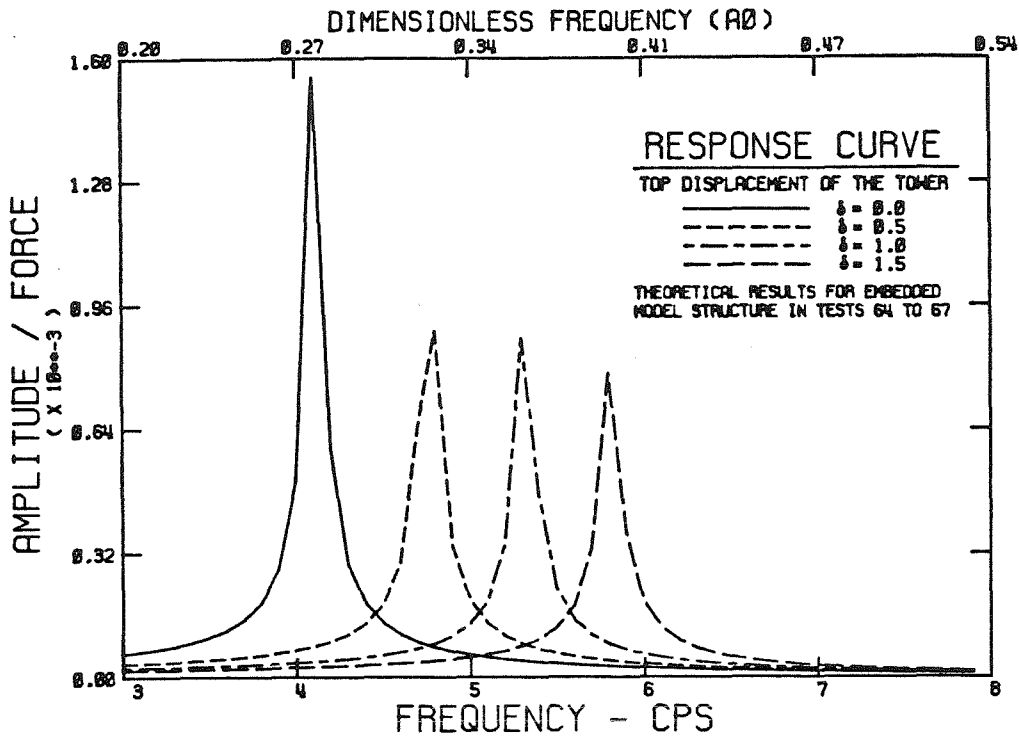


FIG. 8.13 EFFECT OF EMBEDMENT ON RESPONSE OF FOUNDATIONS

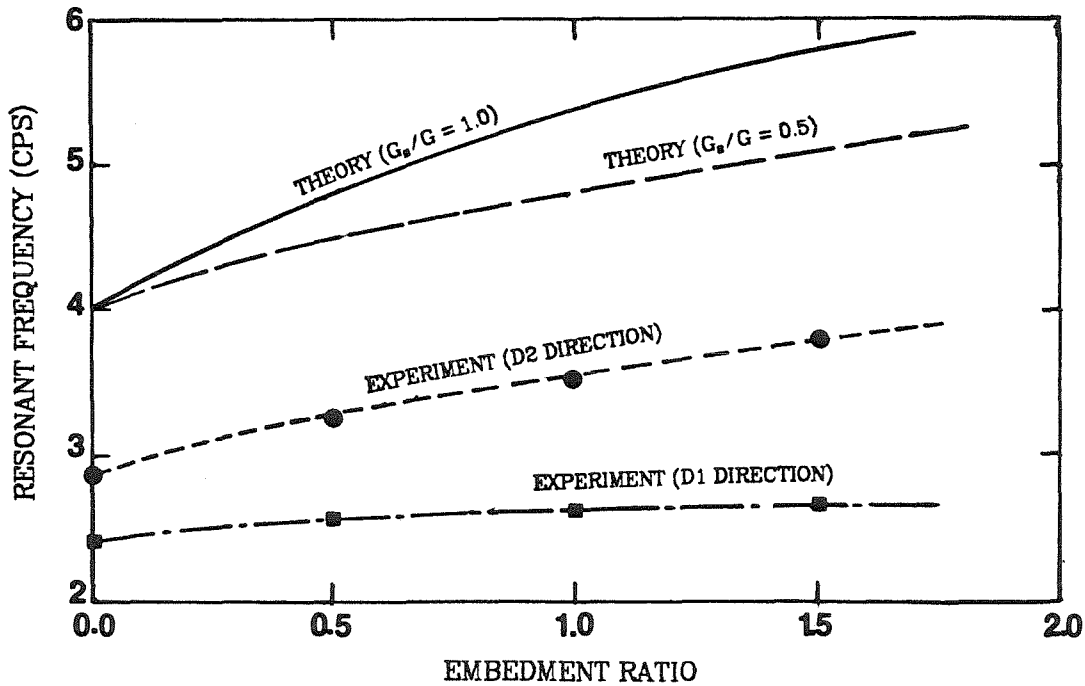


FIG. 8.14 COMPARISON OF THE EXPERIMENTAL AND THEORETICAL RESULTS FOR THE EFFECT OF EMBEDMENT

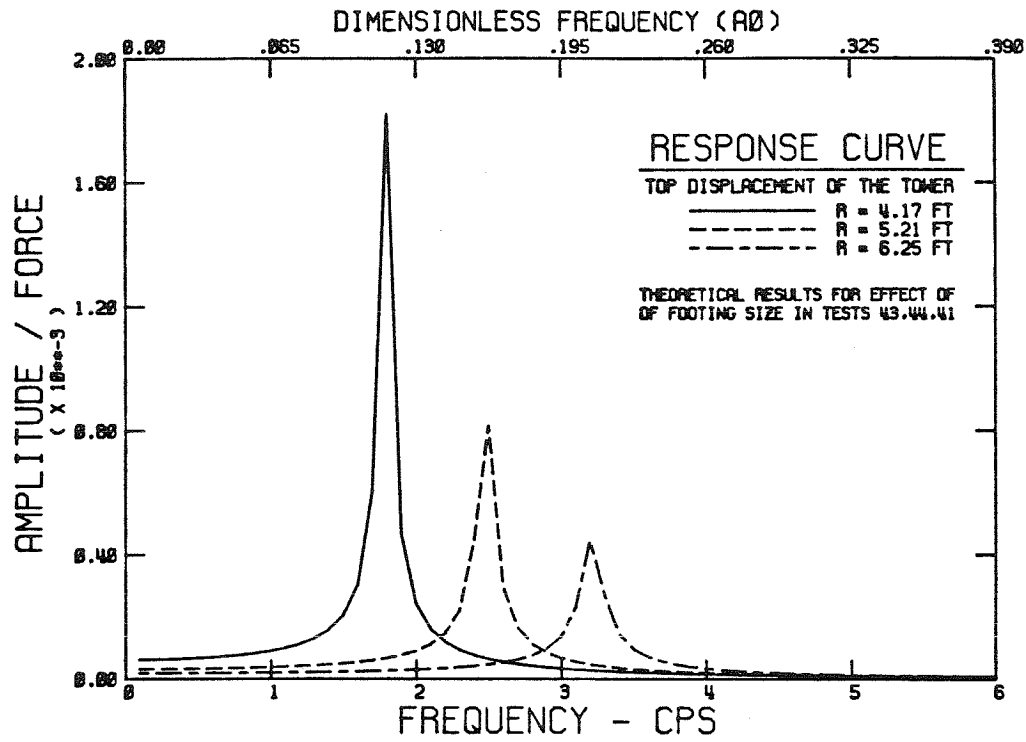


FIG. 8.15 EFFECT OF FOUNDATION SIZE ON RESPONSE OF CIRCULAR FOOTINGS

phenomenon.

#### **8.2.6.6. Reasons for Discrepancy between Predicted and Measured Results**

There are several reasons for the difference in theoretical and experimental results; these are:

- (1) The permanent deformations (settlement and tilting of the tower) observed in many steady-state forced vibration tests and in the tests involving shaking the bucket suggests that plastic deformation was sufficient to soften the soil and reduce its effective elastic modulus.
- (2) Reduction of the pressure amplitude at footing edges during large amplitude vibration at resonance in steady-state forced vibration tests and at the beginning of some transient pulse shaking tests is a sign of lift-off and separation of the foundation from the soil surface. Evidently lift-off will reduce the natural frequency of the structure. This is in great contrast to the elastic half-space theory which assumes a rigid bond between footing and half-space.
- (3) In the case of embedded foundations separation of footing and soil around the sides will drastically diminish the effect of embedment. Thus the major contribution of embedment is the increase of the confining pressure under the footing particularly at the edges because of overburden soil pressure.
- (4) The value of shear modulus employed in the theoretical analysis has a great influence on the results. The critical choice of the confining pressure for which the shear modulus is calculated or measured determines the reliability of the results. The actual stress distribution under a footing and with soil depth is very complicated and different from

theoretical prediction. Because of large local effects in rocking mode due to: i) uplift; ii) yielding of the contact soil; iii) shallow dynamic "pressure bulb" (produced by 'constructive interference' of downward propagating waves); and iv) disturbance of the near surface soil layer; estimating a reliable value for soil strength is very difficult. Therefore, it is suspected that a reasonable value of shear modulus for soil in the half-space model can be used. It was also seen that reduction of shear modulus by using a single factor in order to match the theoretical and experimental results is not possible. Under special conditions where uplift and plastic deformations are particularly absent, some approximate methods such as what was suggested by Morris can be used.

Therefore, the elastic half-space model is not an adequate theoretical tool for analyzing the foundation vibration problem in most practical conditions of interest and more rigorous methods of analysis and soil stress-strain constitutive models are required.

### 8.3. SUMMARY AND CONCLUSIONS

This study has been concerned with the the effect of different foundation-soil parameters on the response of rigid foundations of different shapes subjected to random pulse shakings or steady-state forced vibration. Experiments on different model structures were performed in a geotechnical centrifuge, thereby simulating the true behavior of prototype foundations of reasonable size. Effect of depth of the soil supporting the foundation, foundation shape and size, mass moment of inertia, load amplitude, and depth of embedment were the major parameters studied in this report. Tower structures of different shapes, size and mass were built for this experimental study and were used in the above



parametric studies. All models were rigid since the main goal of the study was to determine the dynamic behavior of the foundation and not the structure. The diameters of the model footings were in a range of 2.0 to 3.0 inches in model scale corresponding to 4.2 feet to 6.25 feet the prototype. Model structures were placed on a bed of dry, dense sand called Nevada Fine Sand. Properties of the sand were measured in a series of resonant column tests and ultrasonic wave propagation velocity measurement experiments.

Before starting the centrifuge experiments a number of tests studying the dynamic behavior of foundations on a large piece of foam rubber simulating the elastic half-space were performed. These tests were conducted in the soil mechanics laboratory at 1g gravitational acceleration and served as an initial effort to understand the foundation vibration problem.

In the centrifuge tests free vibrations of the models were measured in two ways: 1) by detonating a small amount of explosive powder on the tower top (active loading), and 2) by shaking the whole soil bucket with centrifuge in flight (passive loading). In addition a comprehensive parametric study was performed in a series of steady-state forced vibration tests using a tiny but powerful air-driven shaker. Accelerations and displacements of the tower were measured using a number of transducers so that response curves, and mode shapes of the system and dynamic characteristics of the soil-structure interaction problem could be derived. Dynamic and static pressure distributions under surface and embedded foundations were measured. The experimental results were compared with the solutions of linearly elastic and linearly viscoelastic half-space theories and the reasons for discrepancies between theoretical and experimental results were discussed.

The following conclusions were learned from the experimental results and a

comparison with elastic half-space and viscoelastic half-space theoretical solutions.

- (1) Experimental results in many cases accorded with intuition except in case of the soil depth effect where it was learned that in large amplitude rocking vibration of a tall structure resting on the soil surface the vibration effect is very much local and change of depth does not appreciably affect the resonant frequency of the structure. Therefore for narrow slender structures vibrating in their fundamental resonant frequency in the rocking-sliding mode of vibration, the zone of vibration influence under the foundation is small. This is because the foundation mat of a slender structure has a greater tendency to uplift, resulting in a greater separation of the soil and foundation.
- (2) Lift-off, yielding of the soil, imperfections of the model, and soil inhomogeneity account for the major differences between theoretical and experimental results. These factors, which have great influence on the behavior of the vibrating system, have not been included in analysis by most of the theories available at present. Therefore in order to fill the existing gap between theoretical and experimental predictions, development of an analytical or numerical method capable of considering the above effects is essential. Most theoretical work assumes none of the above phenomena are important in small amplitude vibrations such as vibration problems in machine foundations. However, from the test results it was concluded that even under small amplitude loading, after many cycles of vibration, the foundation will lift off the soil and this will cause a reduction in the natural frequency of the structure; this is often beneficial to structural response during severe ground shaking.

- (3) Differences between theoretical and experimental results were more than what was reported in other experimental studies cited in this report. In part this was because of the lift-off effect and also because of higher amplitude loading in the tests which should be of more interest to those researching in earthquake engineering field. It was observed that it is impossible to match the theoretical values of resonant frequencies for both surface and embedded footings to experimental values by just considering a single factor multiplied by soil shear modulus and reducing its value. Therefore, a more logical way of interpreting and reducing the discrepancy between the theoretical and experimental data is necessary.

To this end it is recommended that future experimental and theoretical research be centered on more realistic foundation-soil behavior, that is, to include the effect of lift off, nonlinearity, and inelastic soil behavior in the analysis and experimental studies. At present, for example, an extension of the Winkler foundation model to problems involving the dynamic response of foundations is capable of including the effect of lift-off and yielding of the soil; this has been used in some recent research. Such a model is recommended in contrast to elastic half-space theory when the probability of foundation lift-off and yielding in the soil is high. The other powerful theoretical tool is the finite element technique. The finite element method can incorporate inhomogeneity, anisotropy, advanced soil constitutive models, and the contact condition between soil and footing. It is also of interest to extend the above experimental research to cases where different soil conditions are studied i.e., loose and saturated sands and other soil kinds, in particular, clays.

It is expected that the results and conclusions of this study will be a guide in development of new theories emphasizing the inclusion of real soil behavior and other realistic features of the foundation vibration problems described in this report.

CHAPTER REFERENCES.

- [1] Baranov, V. A., "On the Calculation of Excited Vibrations of an Embedded Foundation," (in Russian) *Voprosy Dynamiki i Prochnosti Polytechnical Institute of Riga*, No. 14, 1967, pp. 195-206.
- [2] Beredugo, Y. O., and Novak, M., "Coupled Horizontal and Rocking Vibration of Embedded Footings," *Canadian Geotechnical Journal*, Vol. 9, Nov. 1972, pp 477-497.
- [3] Borowicka, H., "Concerning Essentrically Loaded Rigid Discs on an Isotropic Elastic Foundation," (in German), *Ingenieur - Archiv*, 1, 1963, pp. 1-8.
- [4] Elsabee, F., and Morray, J. P., "Dynamic Behavior of Embedded Foundations," Civil Engineering Department Report R77-33, Massachusetts Institute of Technology (MIT), Cambridge, Massachusetts, Sept. 1977.
- [5] Hardin, B. O., and Drnevich, V. P., "Shear Modulus and Damping in Soils: Design Equations and Curves," *ASCE, Journal of the Soil Mechanics and Foundations Division*, 98 (SM7), 1972.
- [6] Lin, A. N., "Experimental Observations of the Effect of Foundation Embedment on Structural Response," Earthquake Engineering Research Laboratory (EERL) 82-01, California Institute of Technology, Pasadena, California, 1982.
- [7] Luco, J. E., Wong H. L., and Trifunac, M. D., "A Note on the Dynamic Response of Rigid Embedded Foundations," *International Journal of Earthquake Engineering and Structural Dynamics*, Vol. 4, No. 2, Oct.-Dec. 1975, pp. 119-125.
- [8] Morris, D. V., "Dynamic Soil-Structure Interaction Modelled Experimentally on a Geotechnical Centrifuge," *Canadian Geotechnical Journal*, Vol. 18, No. 1, Feb. 1981, pp. 40-51.
- [9] Parmalee, R. A., and Kudder, R. J., "Seismic Soil-Structure Interaction of Embedded Buildings," *Proceedings of the Fifth WCEE, Rome, 1974*, pp. 1941-1950.
- [10] Richart, F. E., Jr., Hall, J. R., Jr., and Woods, R. D., "Vibrations of Soils and Foundations," Prentice-Hall, Inc., Englewood Cliffs, N.J., 1970, 414pp.
- [11] Veletsos, A. S., and Wei, Y. T., "Lateral and Rocking Vibrations of Footings," *Structural Research at Rice*, 8, Department of Civil Engineering, Rice University, Houston, Jan. 1971.
- [12] Veletsos, A. S., and Verbic, B., "Vibration of Viscoelastic Foundations," *International Journal of Earthquake Engineering and Structural Dynamics*, Vol. 2, No. 1, 1973, pp. 87-102.
- [13] Whitman, R. V., and Richart, F. E., "Design Procedures for Dynamically Loaded Foundations," *Journal of the Soil Mechanics and Foundations Division, ASCE*, 93 (SM6), 1967, pp. 169-193.

## APPENDIX A

### SCALE MODELING

For a model to behave like its prototype counterpart, it should be similar to it in various ways. These similarity conditions can be derived systematically as the output of a dimensional analysis (Bridgman, 1931). The following sections outline a summary of dimensional analysis and its application to scale modelling theory.

#### *A.1. Dimensions, Homogeneous Equations, Dimensional Analysis*

Physical phenomena are described by making use of quantities such as mass, acceleration, force, stress, temperature, viscosity, etc. These can be described in terms of three primary quantities; mass (M), length (L), and time (T). However, using Newton's second law of motion viz. Force = Mass x Acceleration, one can alternatively use force (F), as one of the primary quantities instead of mass. Once a set of primary quantities is chosen, all the others (i.e. derived quantities) can be expressed, from their definitions, in terms of primary quantities. The expression for a derived unit of measurement in terms of the primary units is called "dimension of the physical quantity". Table A.1 gives the dimensions of various physical quantities of interest in modeling of geotechnical problems. In a dimensionally homogeneous equation every term in the equation has the same dimensions as the other ones. Thus the equation does not depend on the units of measurements. All physical equations are dimensionally homogeneous.

According to "Buckingham's  $\pi$  Theorem", if there are  $n$  variables which govern a certain phenomenon and if these variables involve  $m$  primary quantities, then the phenomenon can be described by  $(n-m)$  independent dimensionless parameters. A dimensionally homogeneous equation among these  $n$  variables can be reduced to a relationship between the complete set of  $(n-m)$  dimensionless products.

TABLE A.1  
DIMENSIONS OF PHYSICAL QUANTITIES

Quantity	Dimensions	Quantity	Dimensions
Displacement, Length	L	Momentum	$MLT^{-1}$
Velocity	$LT^{-1}$	Angular Momentum	$ML^2T^{-1}$
Angular Velocity	$T^{-1}$	Elastic Moduli	$ML^{-1}T^{-2}$
Acceleration	$LT^{-2}$	Pressure, Stress	$ML^{-1}T^{-2}$
Angular Acceleration	$T^{-2}$	Strain	$M^{\circ}L^{\circ}T^{\circ}$
Mass Density	$ML^{-3}$	Torque	$ML^2T^{-2}$
Force	$MLT^{-2}$	Surface Tension	$MT^{-2}$
Specific Weight	$ML^{-2}T^{-2}$	Dynamic Viscosity	$ML^{-1}T^{-1}$
Work of Energy	$ML^2T^{-2}$	Kinematic Viscosity	$L^2T^{-1}$
Power	$ML^2T^{-3}$	Heat	$ML^2\Theta^{-2}$
Period	T	Specific Heat	$L^2\Theta^{-2}T^{-1}$
Frequency	$T^{-1}$	Coefficient of Consolidation	$L^2T^{-1}$

Note: in the above table primary quantities are mass [M], length [L], and time [T].

### A.2. *Application of Dimensional Analysis to Modeling*

As the first step in model testing, physical quantities influencing the solution of a problem should be identified by writing the equations governing the behavior of the system or if this is not possible they should be guessed by intuition. Next, using dimensional analysis theorems, a relation between the independent dimensionless parameters formed by the problem variables must be constructed. This equation governs the behavior of both model and prototype whatever the units of measurement. The dimensionless products (usually called  $\pi$ -terms) are represented by  $\pi_1, \pi_2, \pi_3$ , etc. If  $\pi_1$  is the independent variable and the others are the dependent ones, then the dimensionless equation for model and prototype can be written as (Housner and Hudson, 1950)

$$\pi_{1p} = f(\pi_{2p}, \pi_{3p}, \dots) \quad (\text{A.1})$$

$$\pi_{1m} = f(\pi_{2m}, \pi_{3m}, \dots) \quad (\text{A.2})$$

where subscripts 'p' and 'm' refer to prototype and model respectively. For the two systems, model and prototype, to be physically similar the arguments of  $f$  in these two equations must have equal values in model and prototype. These equations will lead to similarity conditions, which dictate the requirements for design and method of testing of the model. A direct application of this technique in deriving model ratios for general geotechnical and especially centrifuge modelling tests is presented next.

### A.3. *Example*

It is intended to design and test a model structure resting on soil to study the problem of deflection and stress distribution in it under the combined effect of its own weight and other applied stresses (Panek 1952, Hoek 1965).

From the knowledge of strength of materials we know that in general, for a structure in a state of thermal and static equilibrium, and behaving within its elastic limits, deflection  $u$  and stress  $\sigma$  at a point of interest depend on the fol-

lowing groups of variables:

1.) Geometry of the structure

Other than variables  $x, y, z$  for the location of the point at which deflections and stresses are desired, other variables related to geometry are defined by:

$L$  : a characteristic length dimension specifying size and shape of structure.

$h/L, w/L, \text{ etc.}$  : group of ratios of other dimensions to length dimension  $L$ .

2.) Structural material

These variables for the case of a linearly elastic isotropic material can be defined by:

$E$  : modulus of elasticity

$\mu$  : Poisson's ratio

$\gamma$  : unit weight of the material

If the structure includes more than one material, the others may be specified by

the dimensionless ratios  $\frac{E'}{E}, \frac{E''}{E}, \text{ etc.}; \frac{\mu'}{\mu}, \frac{\mu''}{\mu}, \frac{\gamma'}{\gamma}, \frac{\gamma''}{\gamma},$

3.) Applied stress conditions

Stresses in a body other than those generated by gravity forces are defined by:

$P$  : externally applied load.

$Q$  : externally applied stresses.

$\sigma_0$  : internal stresses.

$u_0$  : imposed displacement on a part of structure.

Other loads, stresses, and displacements may be specified by a set of dimension-

less ratios such as  $\frac{P'}{P}, \frac{P''}{P}, \dots, \frac{Q'}{Q}, \frac{Q''}{Q}, \dots, \frac{\sigma_0'}{\sigma_0}, \frac{\sigma_0''}{\sigma_0}, \dots, \text{ etc.}$

The above 13 physical quantities including stress  $\sigma$  and displacement  $u$  can be derived from two primary quantities force and length. According to Buckingham



theorems a series of  $13-2=11$  independent dimensionless parameters can be formed from the above variables. Taking L and E as the repeating variables in the dimensionless groups the following set will result:

$$\frac{x}{L}, \frac{y}{L}, \frac{z}{L}, \frac{u}{L}, \frac{u_0}{L}, \frac{\gamma L}{E}, \frac{P}{EL^2}, \frac{Q}{E}, \frac{\sigma}{E}, \frac{\sigma_0}{E}, \mu$$

Note that Poisson's ratio  $\mu$  was already dimensionless.

The governing dimensionally homogeneous equation containing all variables will be

$$f(x, y, z, u, L, \frac{h}{L}, w_L, \dots, E, \frac{E'}{E}, \frac{E''}{E}, \dots, \gamma, \frac{\gamma'}{\gamma}, \frac{\gamma''}{\gamma}, \dots,$$

$$\mu, \mu', \mu'', \dots, \sigma, Q, \sigma_0, u_0, P, \frac{P'}{P}, \frac{P''}{P}, \dots, \frac{\sigma_0'}{\sigma_0}, \frac{\sigma_0''}{\sigma_0},$$

$$\frac{Q'}{Q}, \frac{Q''}{Q}, \dots, \frac{u_0'}{u_0}, \frac{u_0''}{u_0}, \dots) = 0 \tag{A.3}$$

(the above variables appear in dimensionally homogeneous arguments in the equation) or in terms of the dimensionless products, displacement u and stress  $\sigma$  are defined by equations

$$\frac{u}{L} = F\left[\frac{x}{L}, \frac{y}{L}, \frac{z}{L}, \frac{h}{L}, \frac{w}{L}, \dots, \frac{E'}{E}, \frac{E''}{E}, \dots, \frac{\gamma L}{E}, \frac{\gamma'}{\gamma}, \frac{\gamma''}{\gamma}, \dots,$$

$$\mu, \mu', \mu'', \dots, \frac{Q}{E}, \frac{\sigma_0}{E}, \frac{u_0}{L}, \frac{P}{EL^2}, \frac{P'}{P}, \frac{P''}{P}, \dots\right] \tag{A.4}$$

$$\frac{\sigma}{E} = G\left[\frac{x}{L}, \frac{y}{L}, \dots, \frac{P}{EL^2}, \frac{P'}{P}, \frac{P''}{P}, \dots\right] \tag{A.5}$$

in which F and G are undetermined functions.

For similarity of model and prototype we equate the arguments of these functions for both systems. Through equating the ratios  $\frac{w}{L}, \frac{h}{L}, \dots$  we require geometrical similarity of the systems. Equal values of  $\frac{x}{L}, \frac{y}{L}$ , and  $\frac{z}{L}$  means that

stresses and displacements are desired at similar points in the model and prototype. Equality of stress and load ratios  $\frac{P'}{P}$ ,  $\frac{P''}{P}$ , etc. requires similarity of load and stress distributions throughout the two systems. Also, ratios  $\mu, \mu', \mu'', \dots, \frac{E'}{E}, \frac{E''}{E}, \dots$ , and  $\frac{\gamma'}{\gamma}, \frac{\gamma''}{\gamma}, \dots$ , should be the same for both systems, which means that the distribution of material properties must be the same in the model as in the prototype. Finally equating the remaining dimensionless groups, i.e.,  $\frac{\gamma L}{E}, \frac{P}{EL^2}, \frac{Q}{E}, \frac{\sigma_o}{E}$ , and  $\frac{u_o}{L}$  for both model and prototype we arrive at following model ratio relationships

$$\text{Length} \quad \frac{L_p}{L_m} = \frac{\gamma_m}{\gamma_p} \cdot \frac{E_p}{E_m} \quad (\text{A.6})$$

$$\text{Force} \quad \frac{P_p}{P_m} = \frac{L_p^2}{L_m^2} \cdot \frac{E_p}{E_m} \quad (\text{A.7})$$

$$\text{Stress} \quad \frac{Q_p}{Q_m} = \frac{\sigma_{op}}{\sigma_{om}} = \frac{E_p}{E_m} \quad (\text{A.8})$$

$$\text{Displacement} \quad \frac{u_{op}}{u_{om}} = \frac{L_p}{L_m} \quad (\text{A.9})$$

Having all arguments of the functions F and G equal for model and prototype then,

$$\frac{\sigma_p}{E_p} = \frac{\sigma_m}{E_m} \quad (\text{A.10})$$

$$\frac{u_p}{L_p} = \frac{u_m}{L_m} \quad (\text{A.11})$$

Once two of the model ratios are arbitrarily selected, scale factor of modelling for the rest of physical quantities of interest will follow from the definition of their dimensions or from equations (A.6) to (A.9). If the model material is identical to prototype material ( $\mu_m = \mu_p$ ;  $E_m = E_p$ ;  $\rho_m = \rho_p$ , where  $\rho$  is mass density of the material) and the model is subjected to an artificial gravitational acceleration  $N.g$  in a centrifuge ( $g$  is gravitational acceleration and  $N$  is the scale factor)

then:

$$\frac{L_p}{L_m} = \frac{\gamma_m}{\gamma_p} = \frac{\xi_m \cdot \rho_m}{\xi_p \cdot \rho_p} = \frac{\xi_m}{\xi_p} = N \quad (\text{A.12})$$

$$\frac{P_p}{P_m} = \frac{L_p^2}{L_m^2} = N^2 \quad (\text{A.13})$$

$$\frac{Q_p}{Q_m} = \frac{\sigma_{op}}{\sigma_{om}} = \frac{E_p}{E_m} = 1 \quad (\text{A.14})$$

$$\frac{u_{op}}{v_{om}} = \frac{L_p}{L_m} = N \quad (\text{A.15})$$

Thus by the use of centrifuge and scale models manufactured of the prototype material, stresses and strains are identical to those in the prototype at homologous points. Therefore, for a nonlinear anisotropic hysteretic and inelastic material such as soil, it is also expected that the model will follow the prototype behavior.

Dynamic time scale:

In the case of dynamic testing similarity conditions for forces must hold true for inertia forces as well. The extra variables in this case are the externally applied acceleration  $a$ , the time  $t$ , and gravity acceleration  $g$ . In this case the primary quantities are force, length, and time, so there are three independent variables ( $m = 3$ ), and sixteen dependent ones ( $n = 16$ ). The number of independent dimensionless groups will be thirteen ( $n - m = 13$ ), thus, two more dimensionless products will be added to the former list. These can be for example  $\frac{a}{g}$  and  $\frac{L^2 \rho}{t^2 E}$ . We can equate any of these two dimensionless parameters in the model and prototype, for example equating the second term

$$\left( \frac{L^2 \rho}{t^2 E} \right)_m = \left( \frac{L^2 \rho}{t^2 E} \right)_p \quad (\text{A.16})$$

from which

$$\frac{t_m}{t_p} = \left[ \frac{\rho_m}{\rho_p} \cdot \frac{E_p}{E_m} \right]^{\frac{1}{2}} \frac{L_m}{L_p} \quad (\text{A.17})$$

Using a centrifuge model made from the same material as in the prototype and subjected to N.g centrifugal acceleration, the time scale for dynamic model tests will be

$$\frac{t_m}{t_p} = \frac{L_m}{L_p} = \frac{1}{N} \text{ or } t_p = N \cdot t_m \quad (\text{A.18})$$

and the frequency scale is

$$\frac{\omega_m}{\omega_p} = N \text{ or } \omega_m = N \cdot \omega_p \quad (\text{A.19})$$

where  $\omega$  is the angular frequency.

Consolidation time scale (Rowe, 1975):

In order to simulate consolidation process and water diffusion through soil structure the consolidation time factor T should be identical in the model and prototype. The time factor T of one-dimensional consolidation is defined by:

$$T = \frac{c_v t_c}{(nH)^2} \quad (\text{A.20})$$

in which

c is the coefficient of consolidation

t is the consolidation time

H is the height of the layer under consolidation

n is the number of drainage boundaries (1 or 2)

The time factor T must be constant namely

$$\left[ \frac{c_v t}{H^2} \right]_m = \left[ \frac{c_v t}{H^2} \right]_p \quad (\text{A.21})$$

For the same soil and a length scale factor  $\frac{H_p}{H_m} = N$ , it will reduce to

$$\frac{t_{cm}}{t_{cp}} = \frac{1}{N^2} \text{ or } t_{cp} = N^2 \cdot t_{cm} \quad (\text{A.22})$$

Which means that the drainage time in a centrifuge soil model is N times shorter than the time required in prototype.

In this study dynamic tests on model structures resting on dry sand were performed which requires inclusion of only the dynamic time scale, while consolidation time effects were absent.

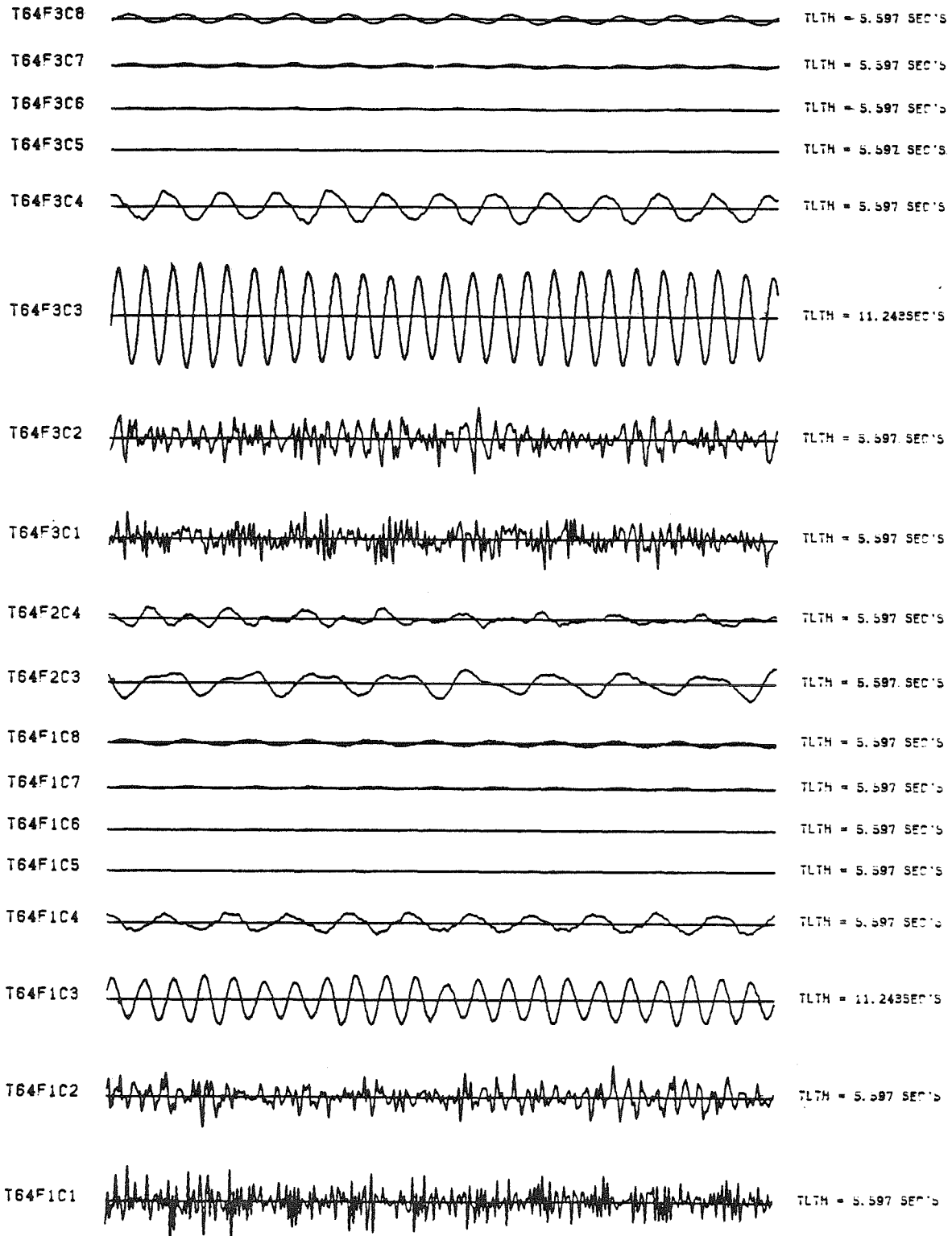
Appendix References.

- [1] Bridgman, P.W., "Dimensional Analysis," Yale University Press, Revised Ed., 1931, 113 pp.
- [2] Hoek, E., "The Design of a Centrifuge for the Simulation of Gravitational Force Fields in Mine Models," Journal of the South African Institute of Mining and Metallurgy, Vol. 65, No. 9, 1965, pp. 455-487.
- [3] Housner, G. W., and Hudson, D. E., "Applied Mechanics Dynamics," Division of Engineering, California Institute of Technology, 2nd edition, 1959, 392 pp.
- [4] Panek, L.A., "Centrifugal Testing Apparatus for Mine-Structure Stress Analysis," U.S. Bureau of Mines, Report of Investigations 4883, 1952.
- [5] Rowe, P.W., "Applications of Centrifugal Models to Geotechnical Structures," Proceedings of Symposium on Geotechnical Structures, University of New South Wales, Australia, July 1975, Preprint 25 pages.

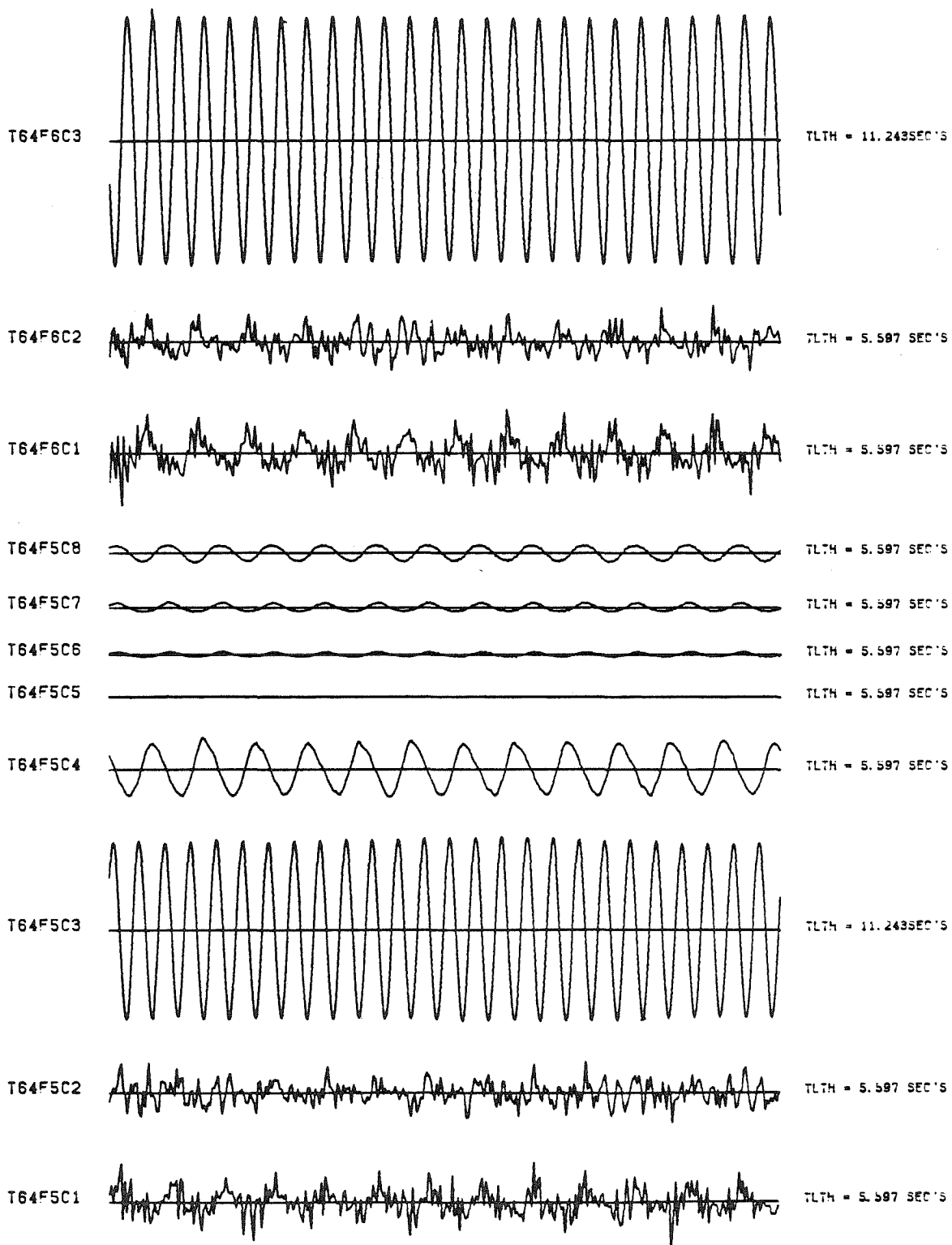
## APPENDIX B

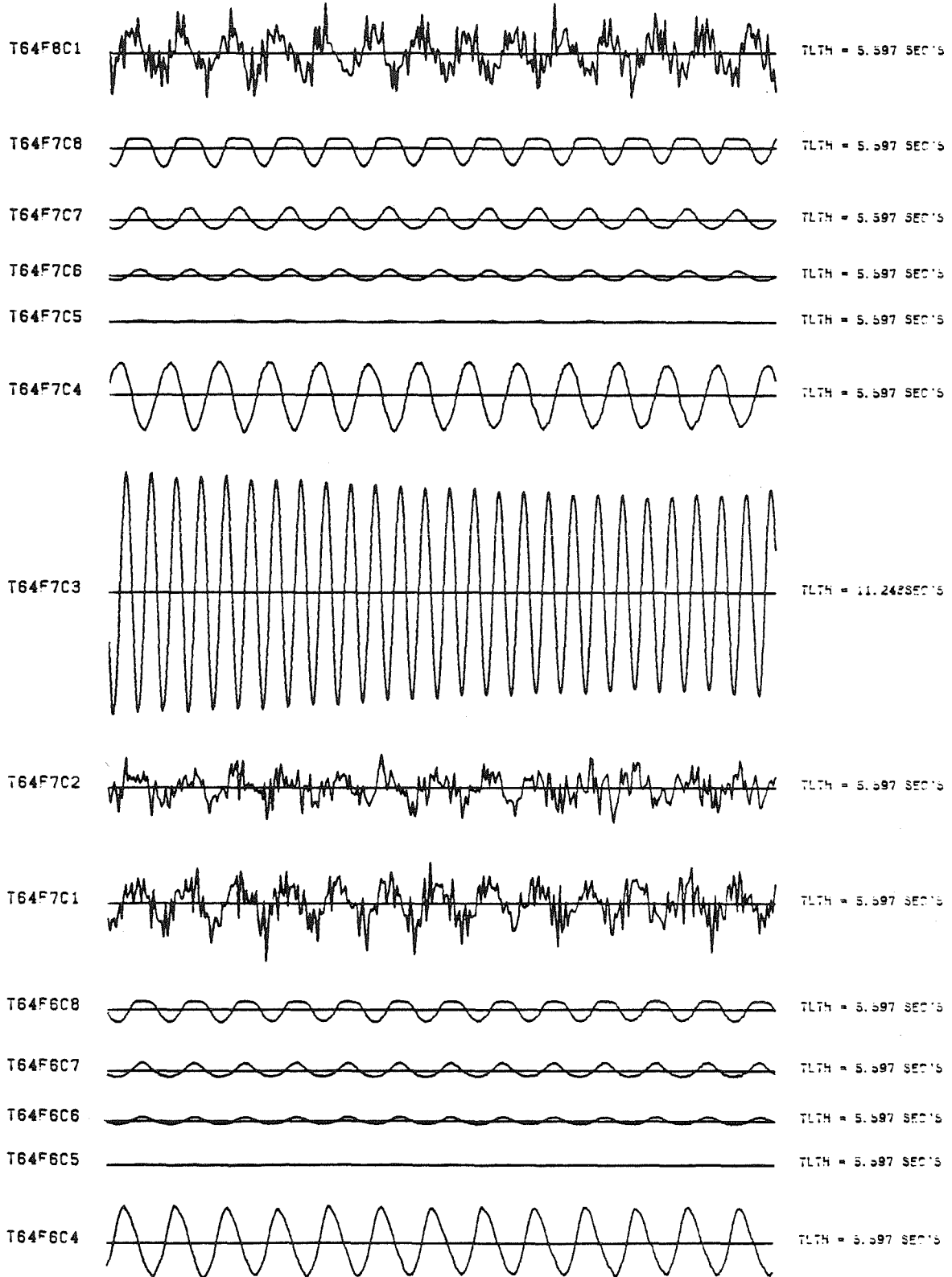
### RECORDED TRANSDUCER DATA IN TEST 64

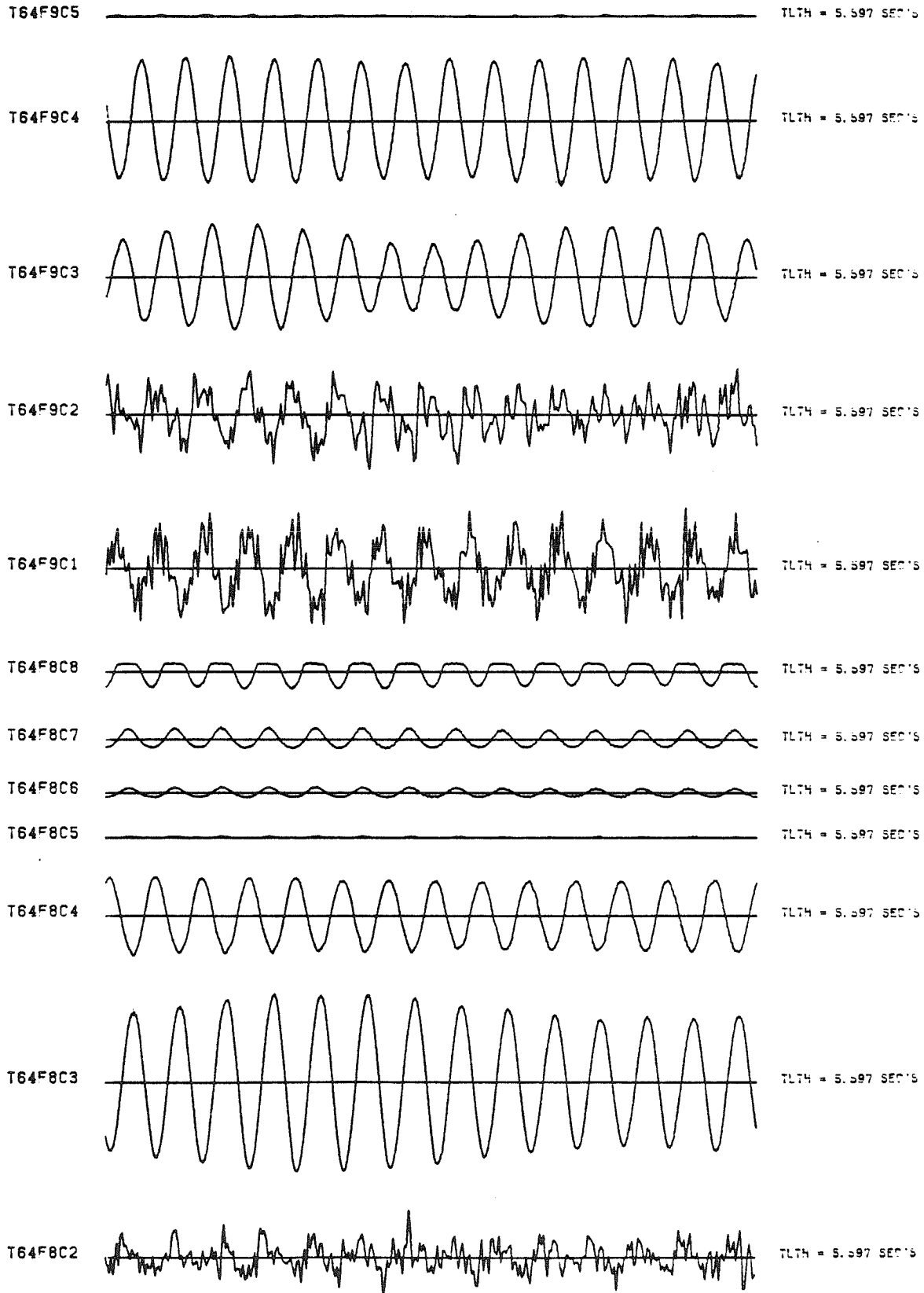
The digitized transducer data recorded at different frequencies of vibration during the test are plotted and presented in this appendix. At each frequency 8 transducer signals are recorded, 2 accelerations (Channels 1 and 2), 2 displacements (Channels 3 and 4), and 4 pressure signals (Channels 4 to 8). To the left of each plot the abbreviated name of the signal is shown (see Chapter 6 for definition of the signal name). The total time length of each record in prototype scale is printed to the right of the plot. Approximate value of the frequency of each record can be estimated by dividing the number of cycles by the time length of the record. The total number of frequencies at which the data was sampled is 21. Note that at some of the sampling frequencies all the signals are not plotted. This is because their amplitudes were very small compared with other signals, and they were comparable to the magnitude of electrical noise present in the signal. The main reason for plotting the raw data was to check their contents before further data processing. Few real time analog records were usually plotted during each test to provide a mean for checking the digitized data.

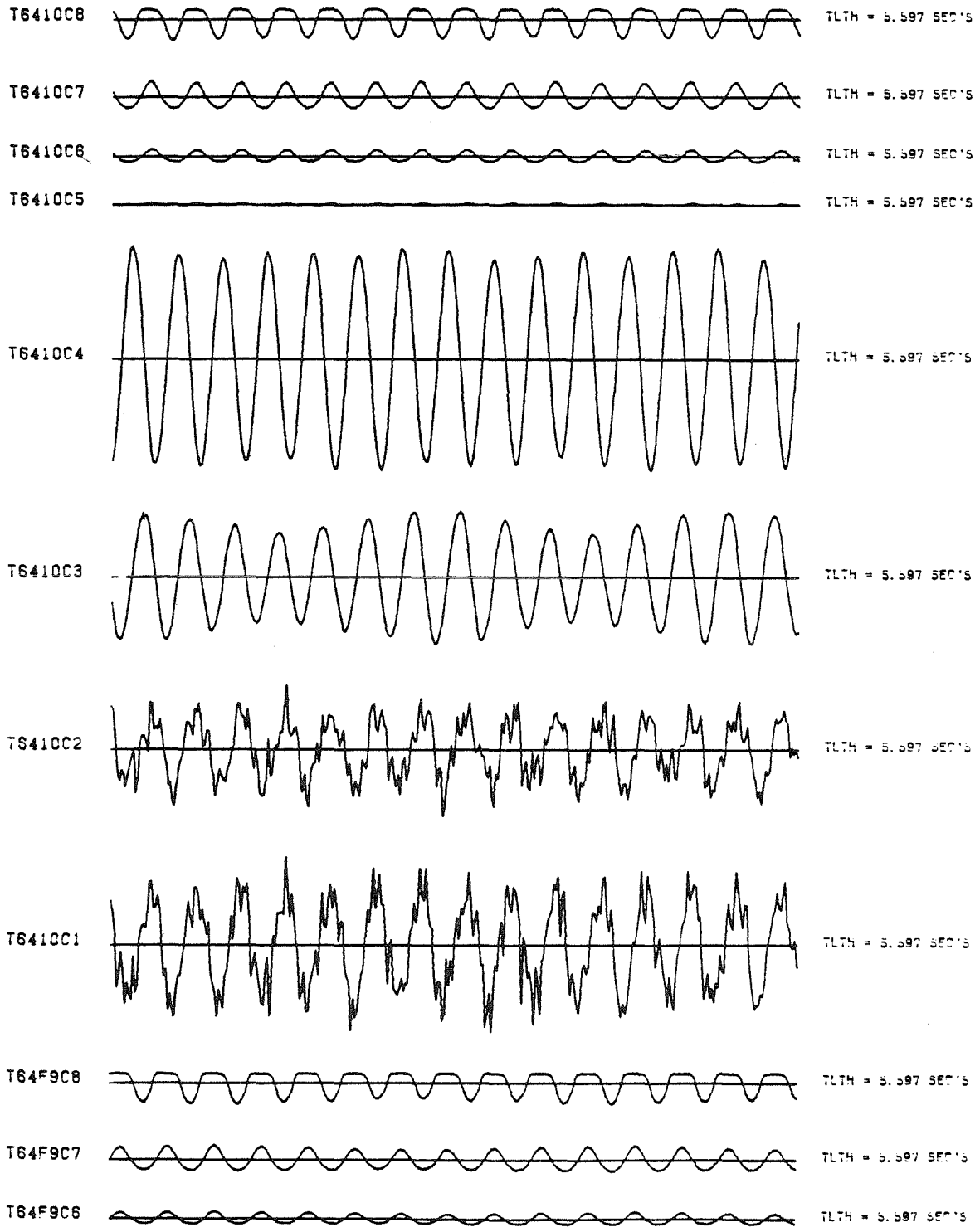


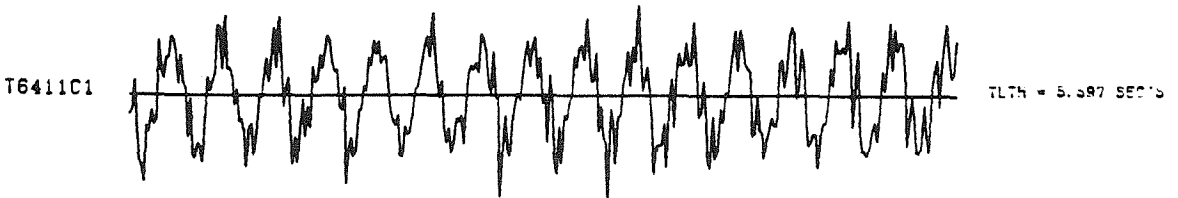
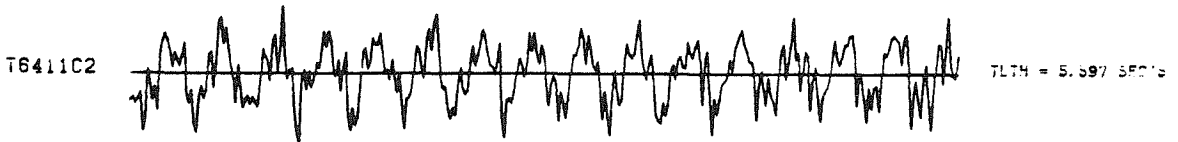
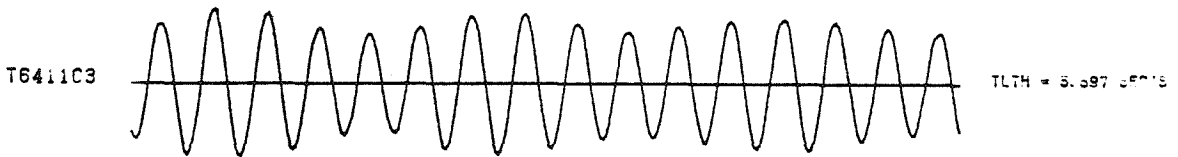
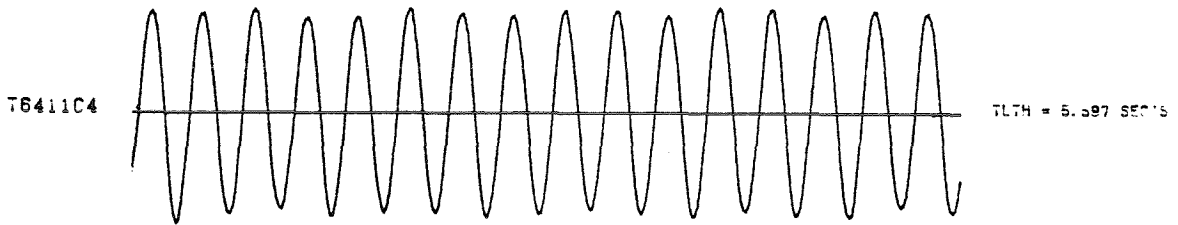
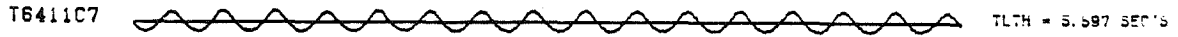
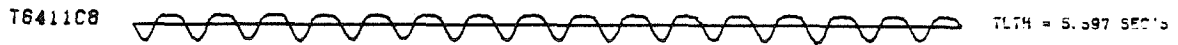
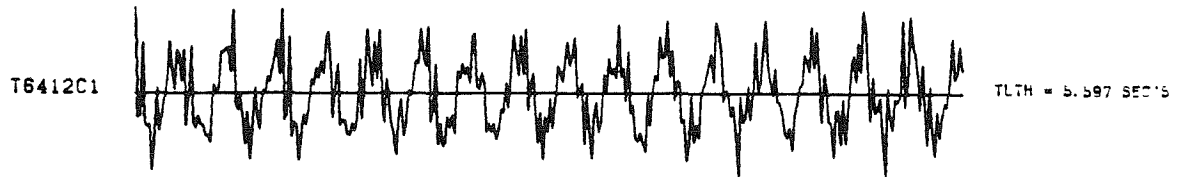
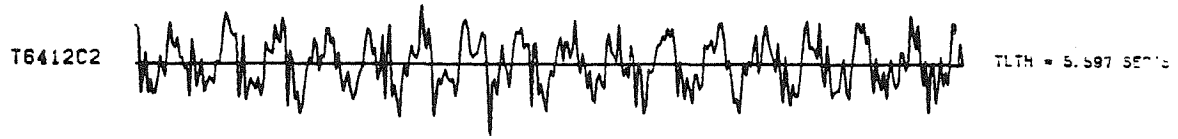


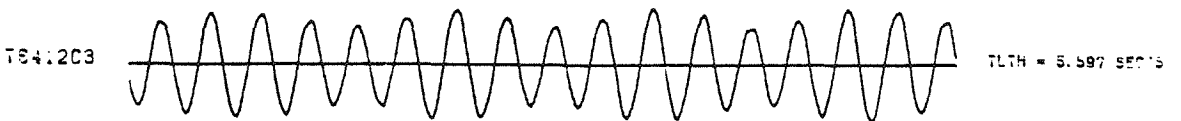
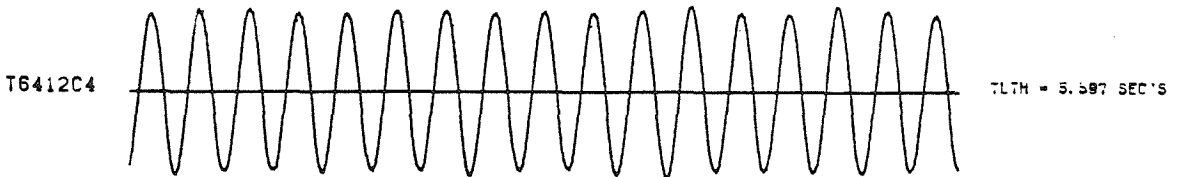
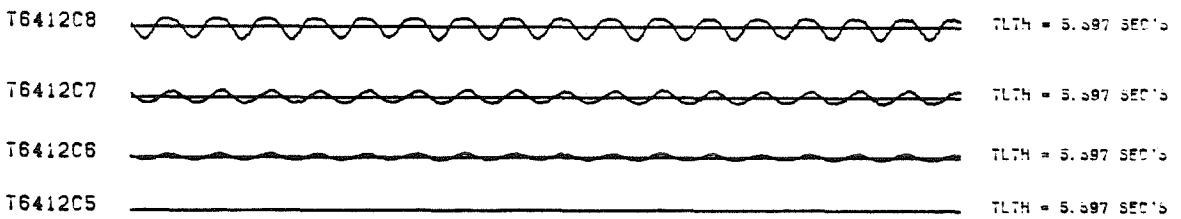
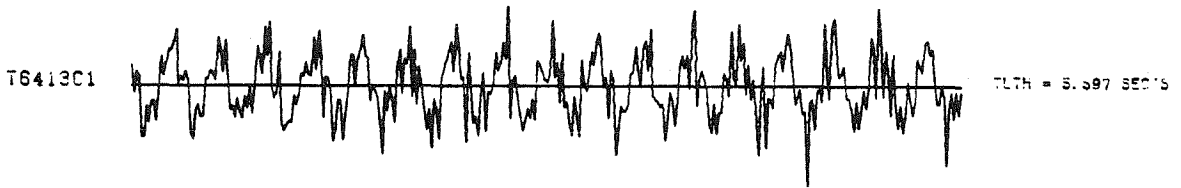
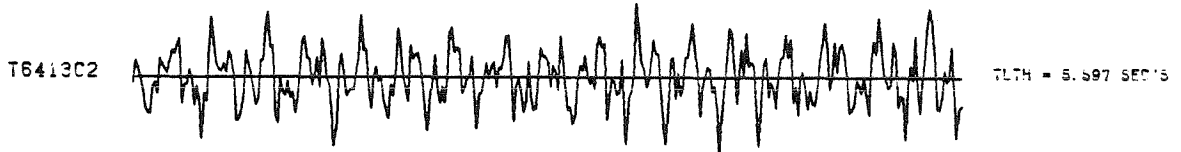
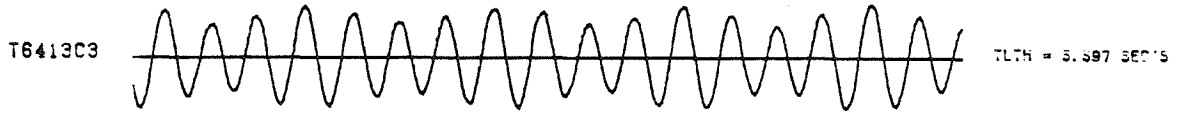
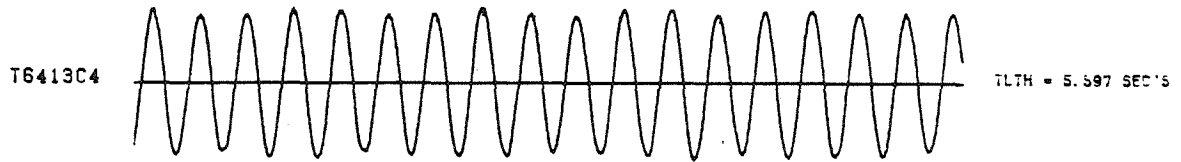
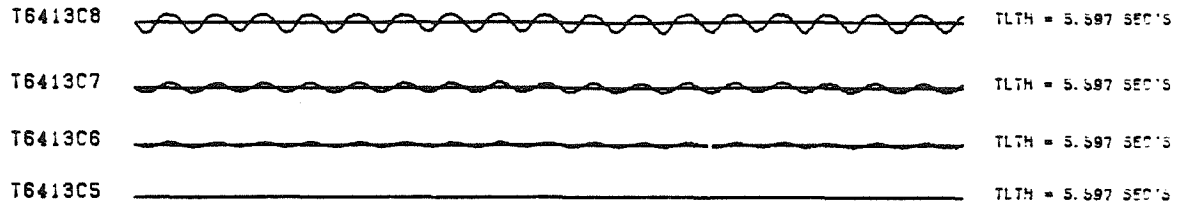






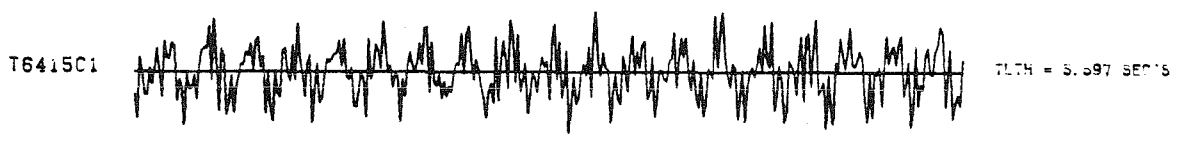
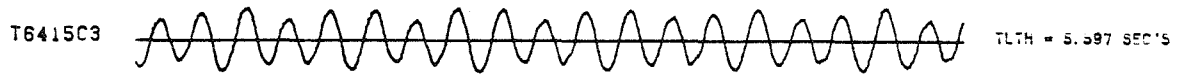
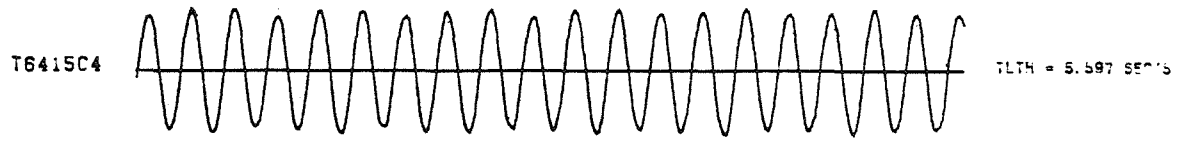


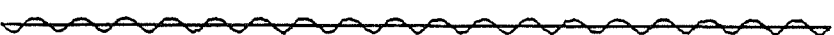




T6415C6 \_\_\_\_\_ TLTH = 5.597 SEC'S

T6415C5 \_\_\_\_\_ TLTH = 5.597 SEC'S

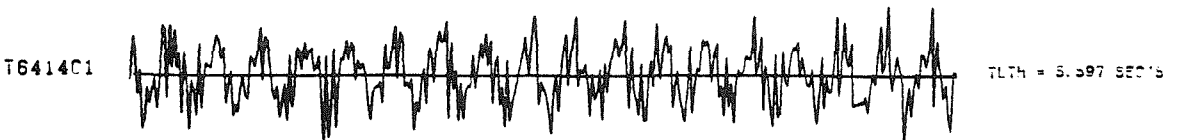
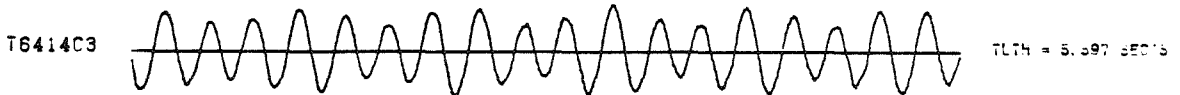
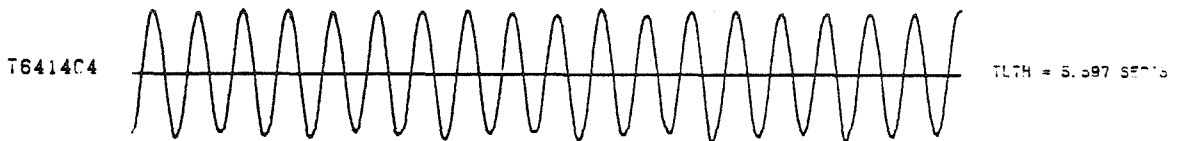


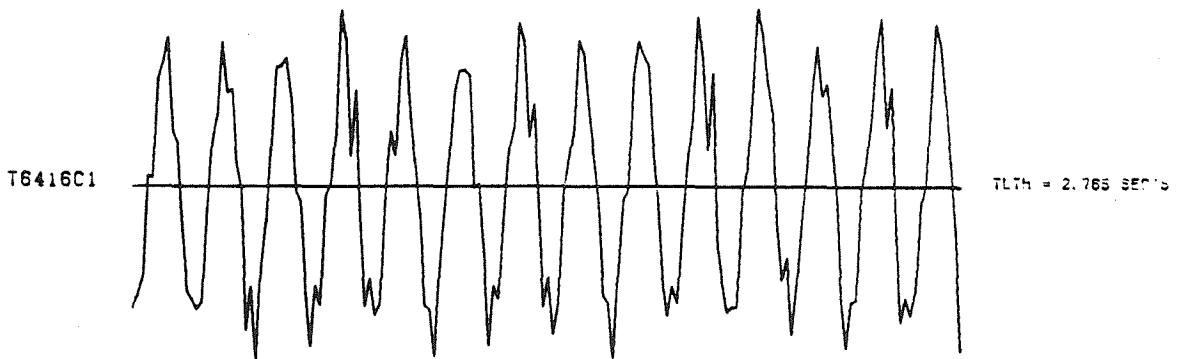
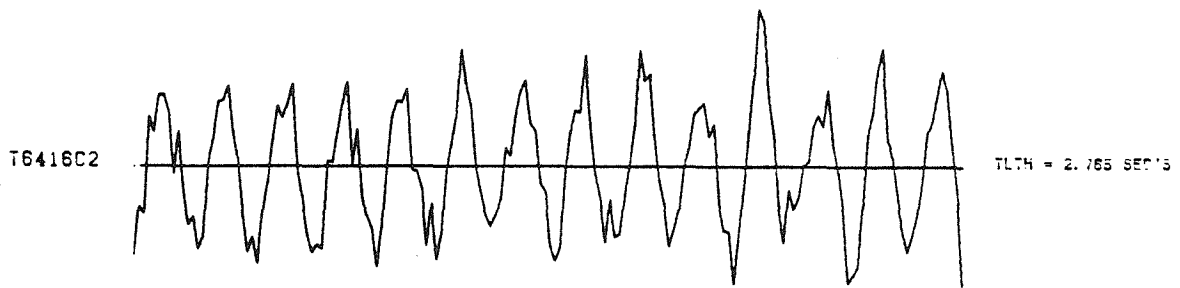
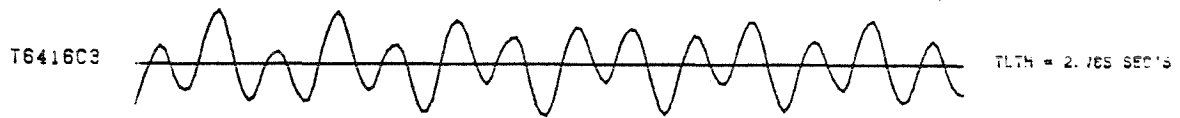
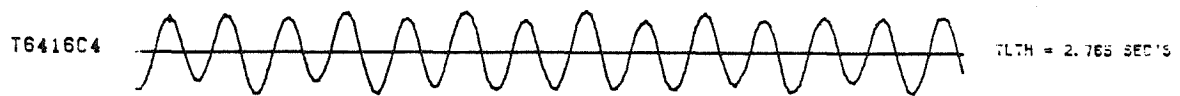
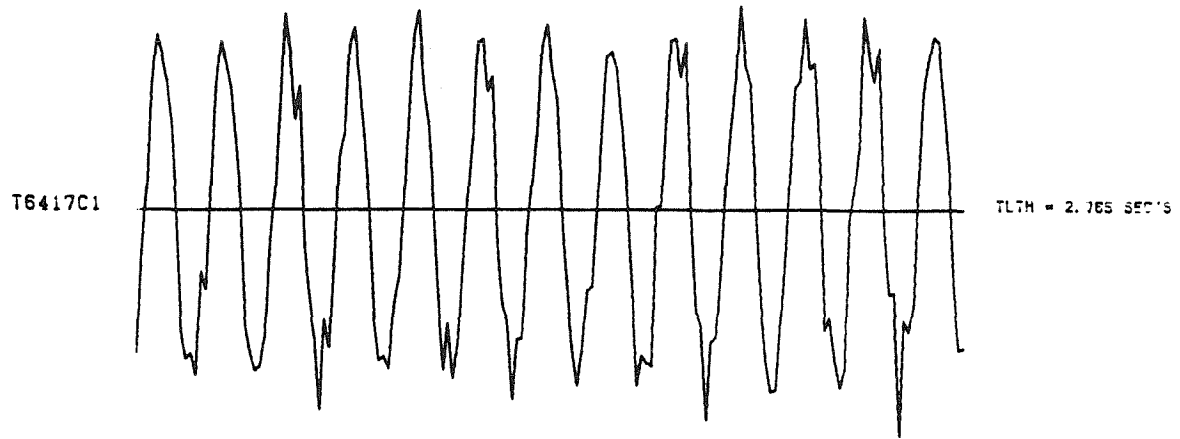
T6414C8  TLTH = 5.597 SEC'S

T6414C7  TLTH = 5.597 SEC'S

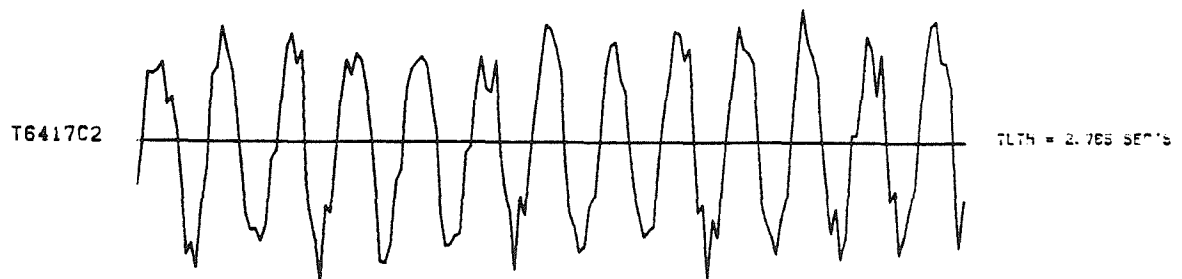
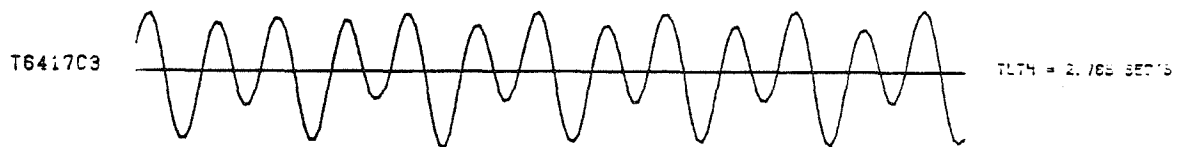
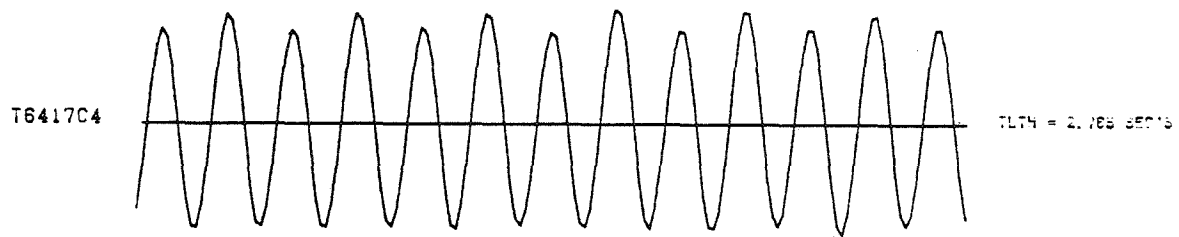
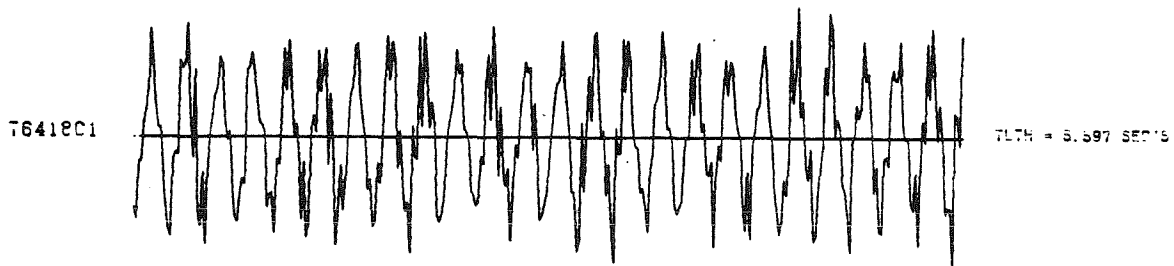
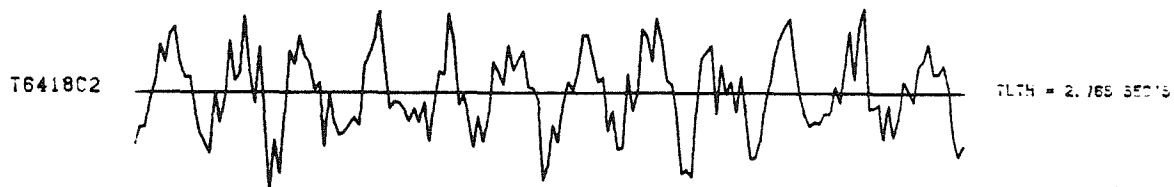
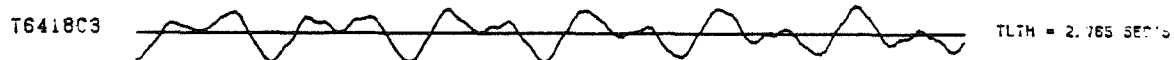
T6414C6 \_\_\_\_\_ TLTH = 5.597 SEC'S

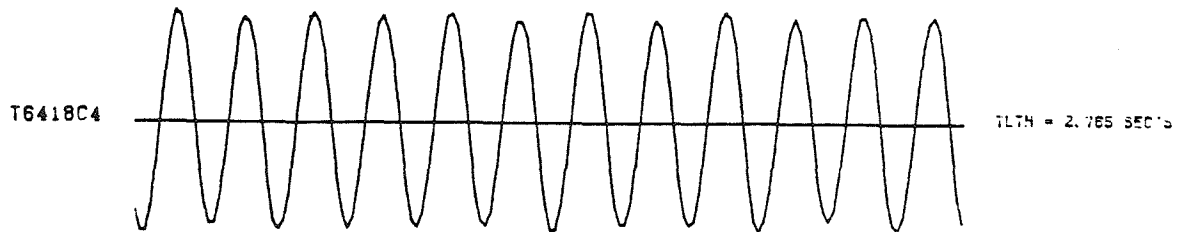
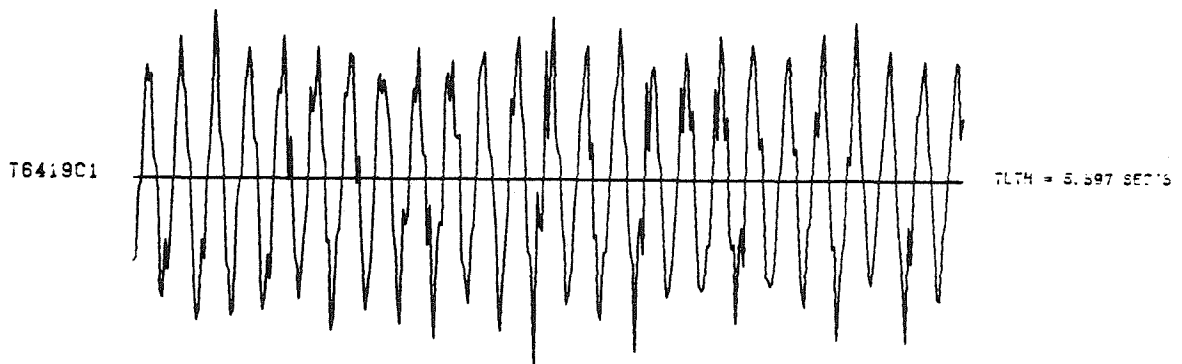
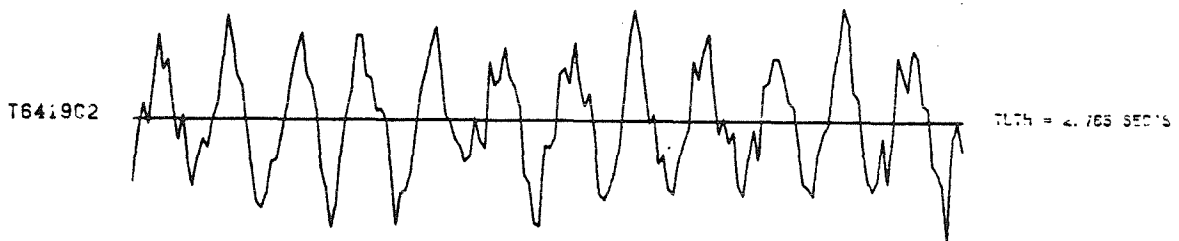
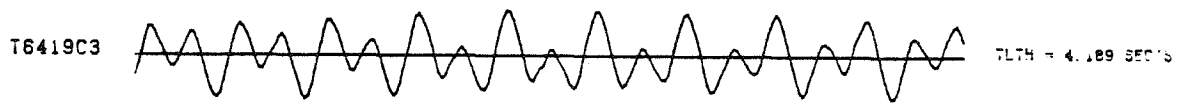
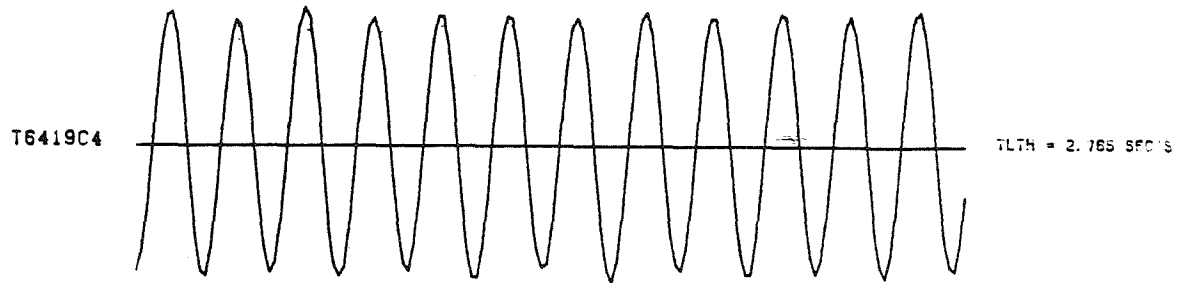
T6414C5 \_\_\_\_\_ TLTH = 5.597 SEC'S

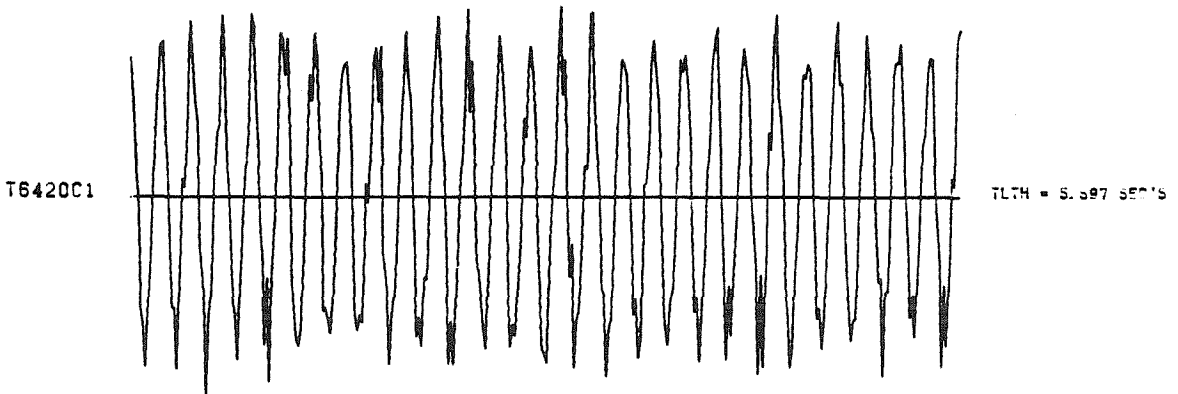
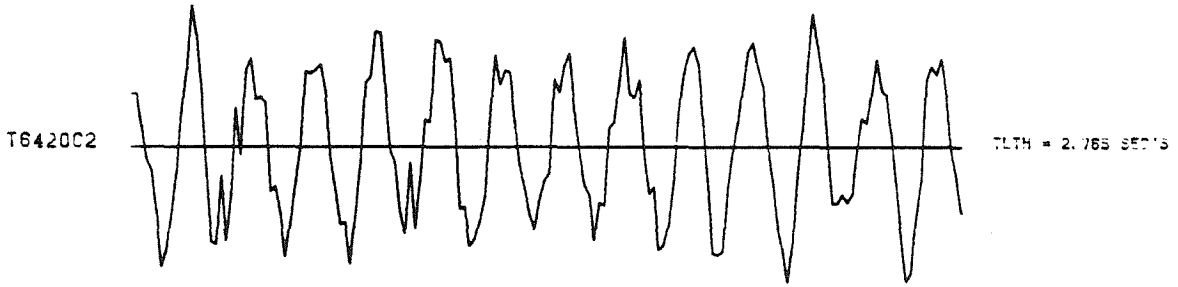
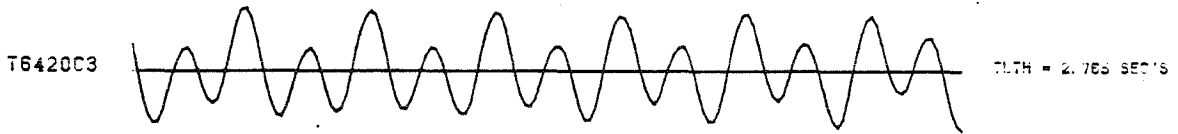
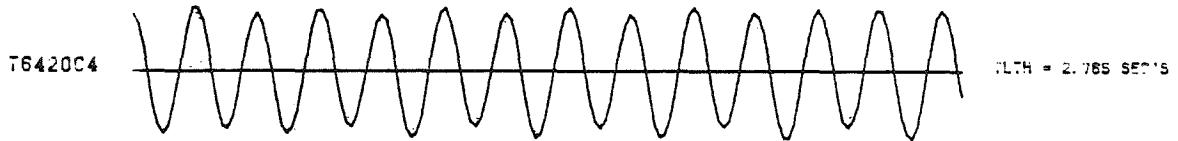
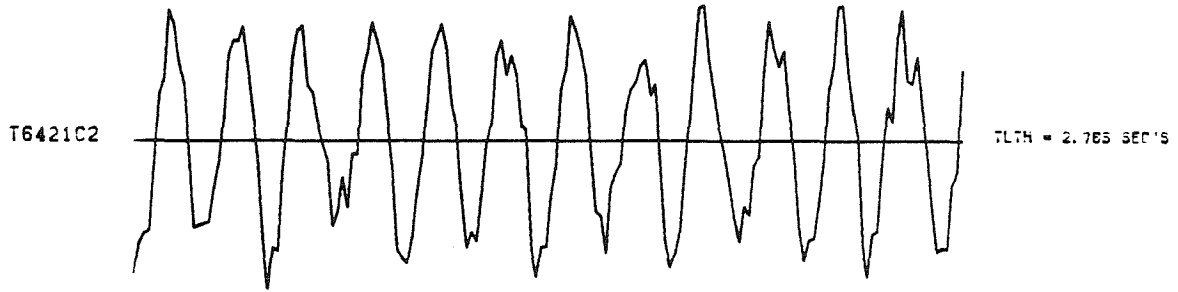
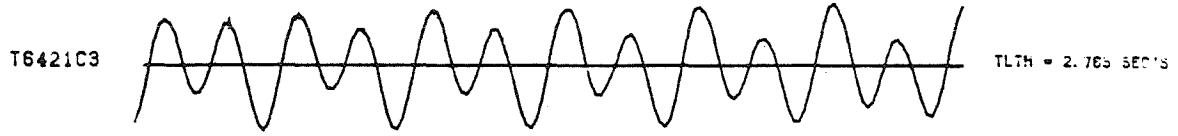










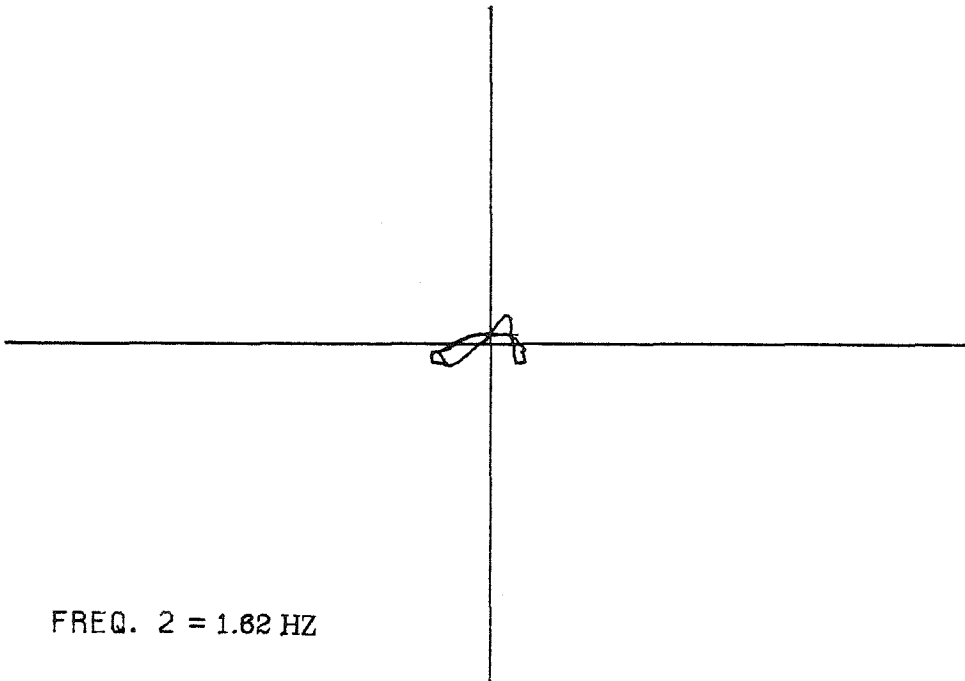


## APPENDIX C

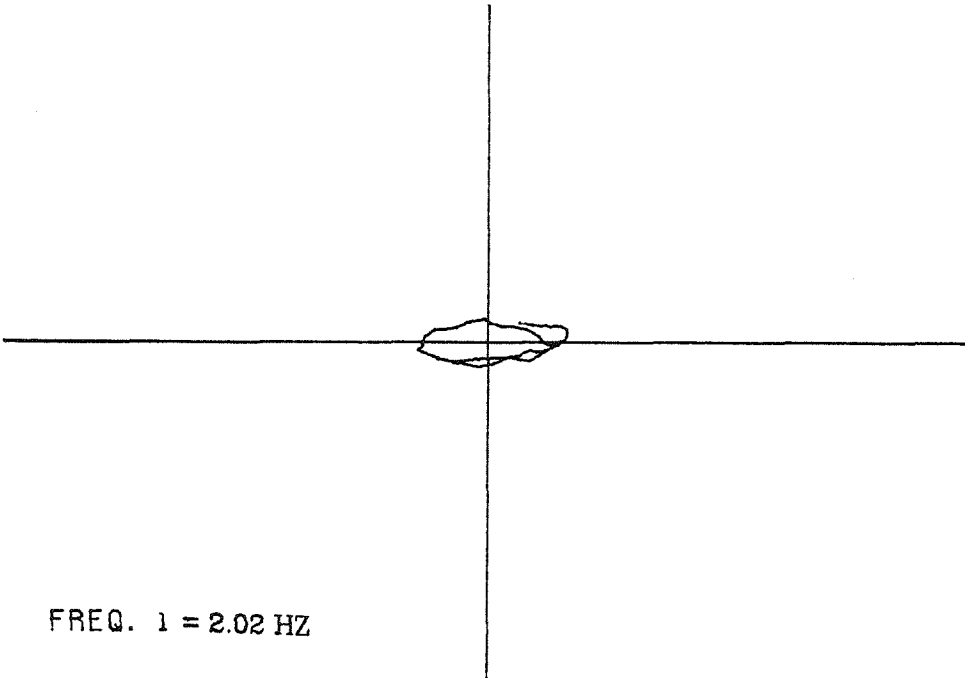
### DISPLACEMENT PATH OF TOWER TOP IN THE HORIZONTAL PLANE

In this appendix the actual path of tower top motion in the horizontal plane (plane parallel to soil surface) during steady-state rocking-sliding vibration is shown. The X-Y plots in the next few pages show the motion of the tower top at different frequencies during Test 64. In these plots horizontal axis represents the displacement in D1 direction (main direction of rocking) and the vertical axis is the displacement in D2 direction (normal to the main direction). Relative amplitudes of displacements in the normal directions D1 and D2 are sufficient to produce the path of tower top motion. Therefore, having similar scales for displacement components on X and Y axes, absolute values of displacements are not required. As is observed from the figures amplitude of tower motion in D1 direction is much bigger than D2 amplitude before and during first resonant frequency. However, close to the resonance in D2 direction amplitudes of motion components are comparable. The approximate angle between direction of applied force and displacement transducer axes can be derived from the plots. Refer to Chapter 7 for more discussion about the reasons of this approximate elliptical motion of the tower top.

TEST 64

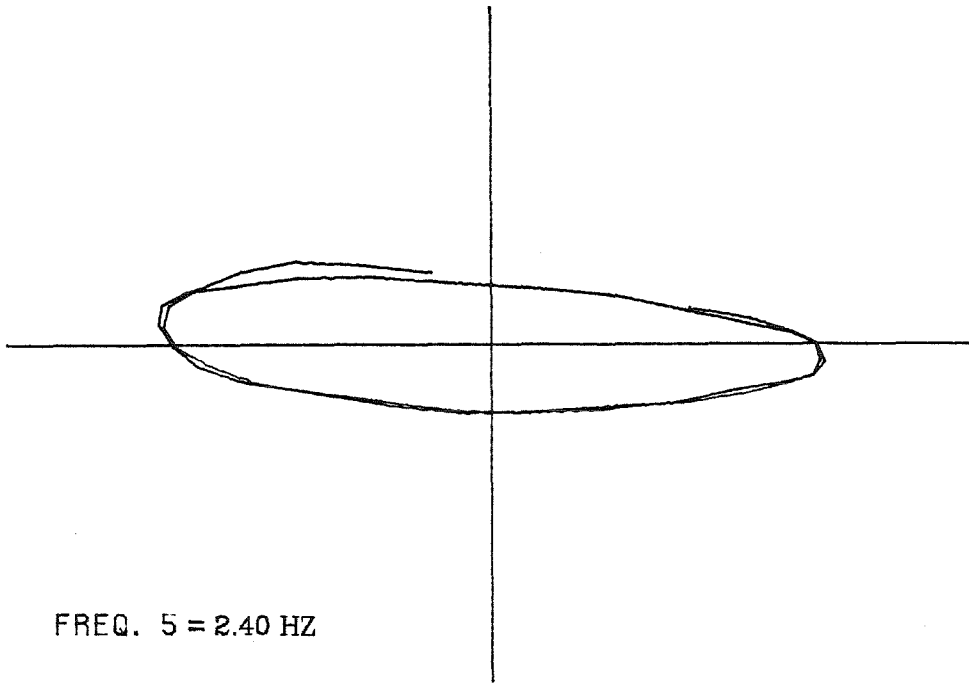


FREQ. 2 = 1.62 HZ

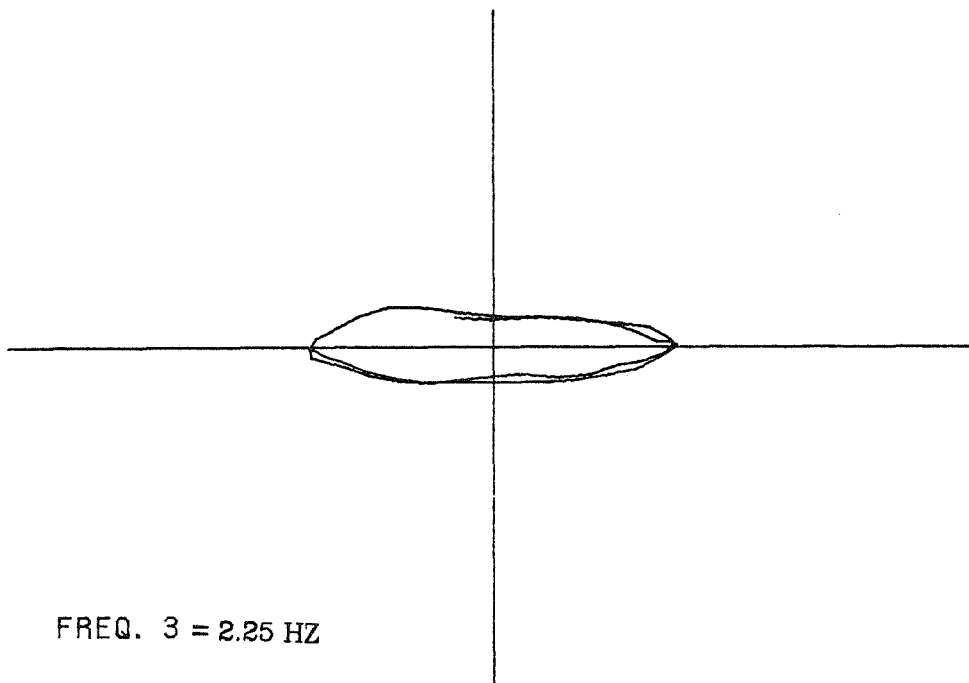


FREQ. 1 = 2.02 HZ

TEST 64

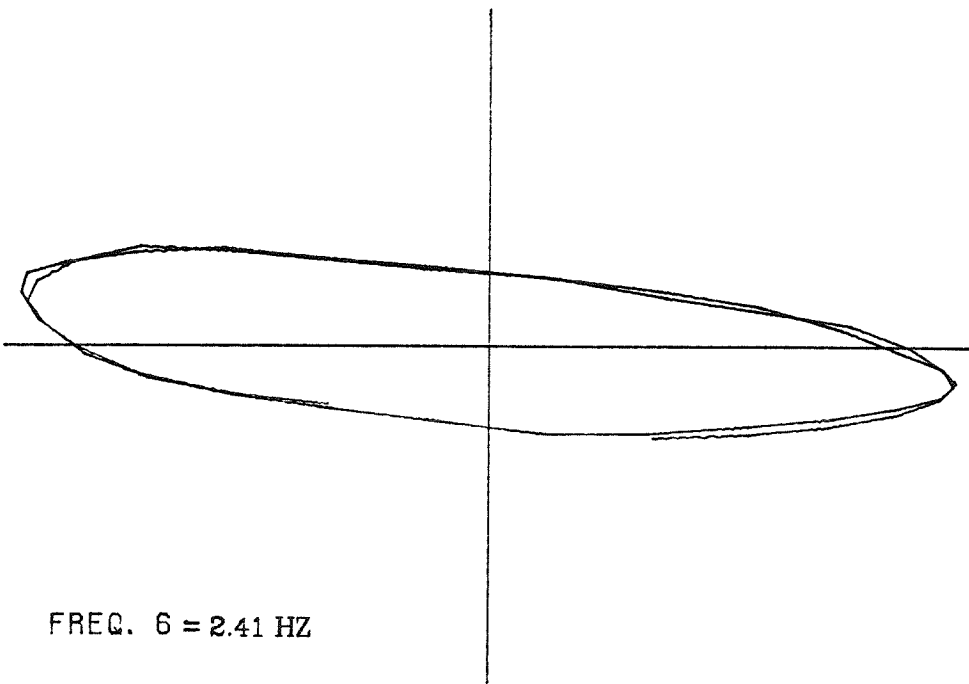
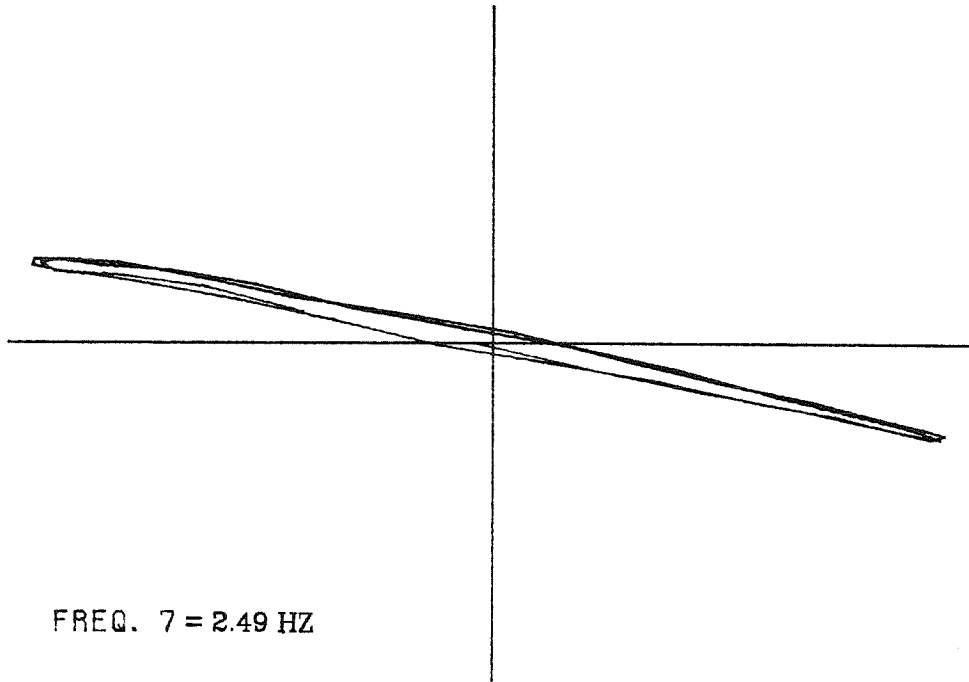


FREQ. 5 = 2.40 HZ

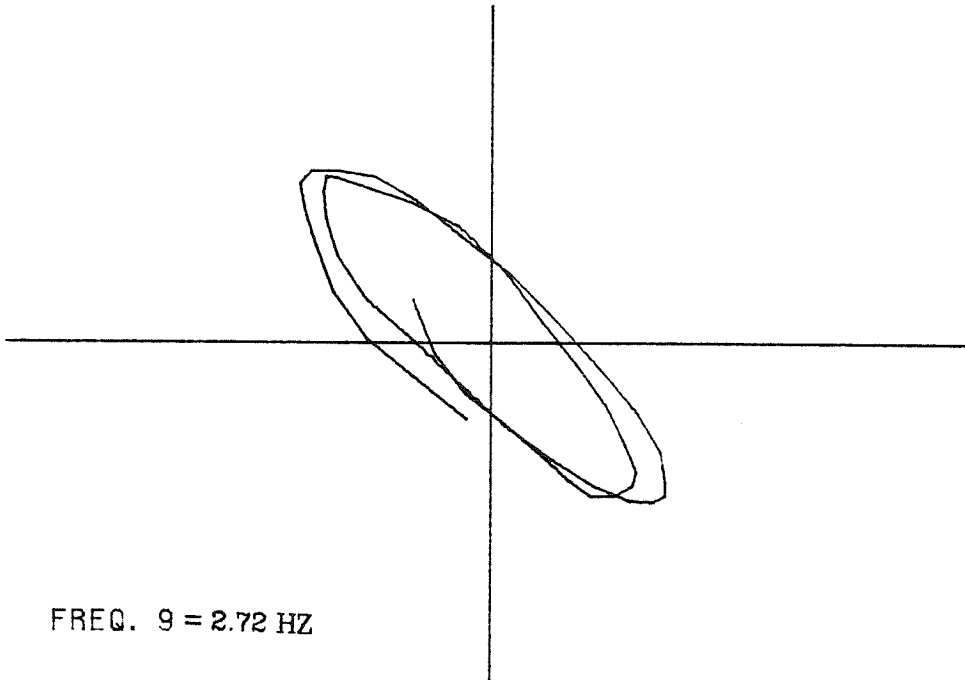


FREQ. 3 = 2.25 HZ

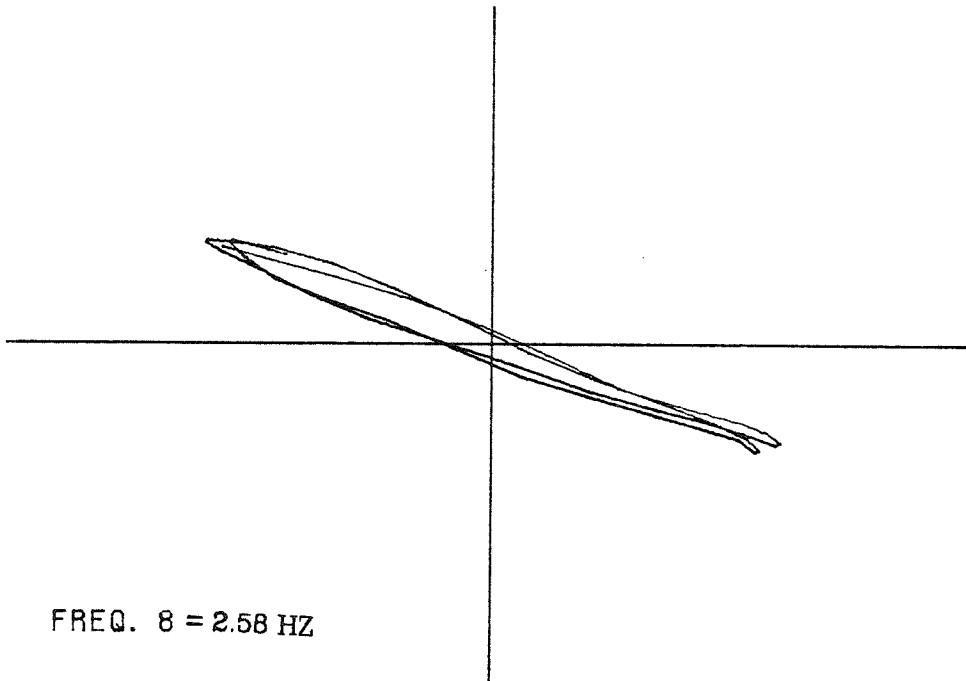
TEST 64



TEST 64



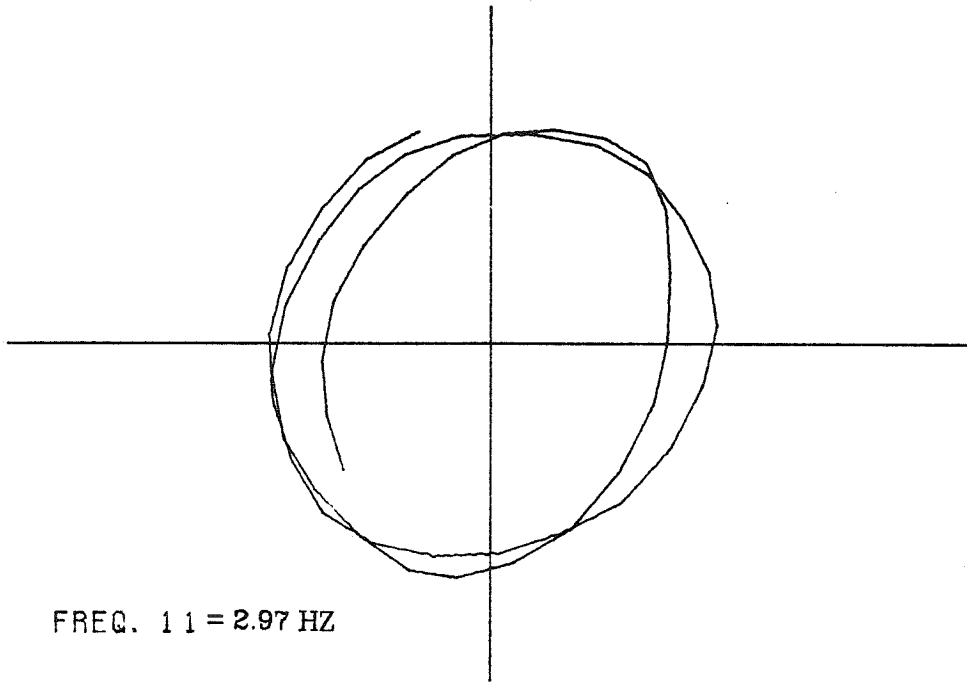
FREQ. 9 = 2.72 HZ



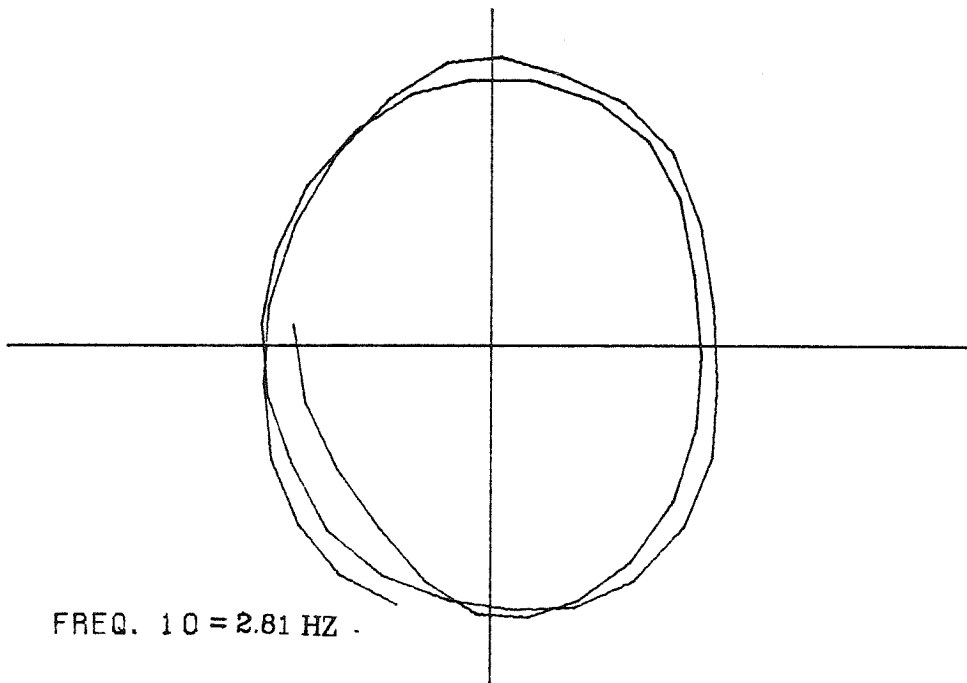
FREQ. 8 = 2.58 HZ



TEST 64

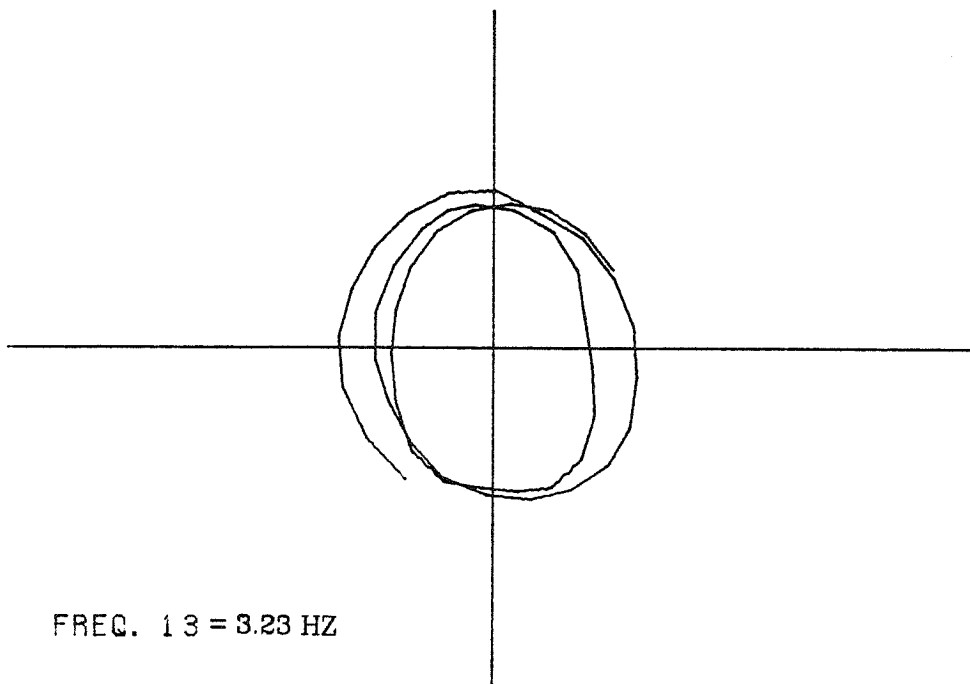


FREQ. 11 = 2.97 HZ

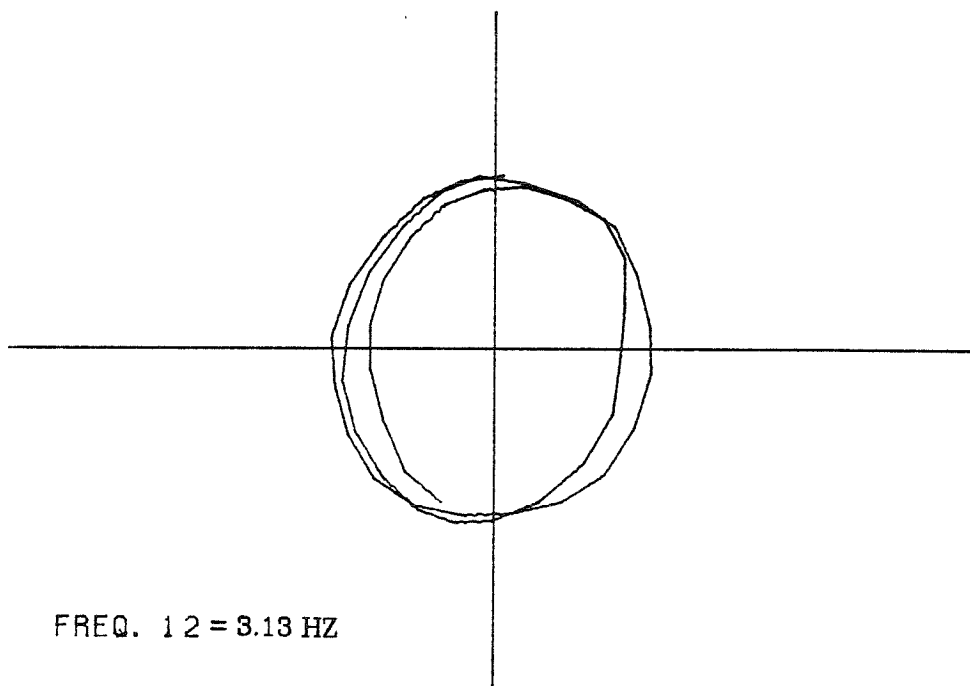


FREQ. 10 = 2.81 HZ .

TEST 64

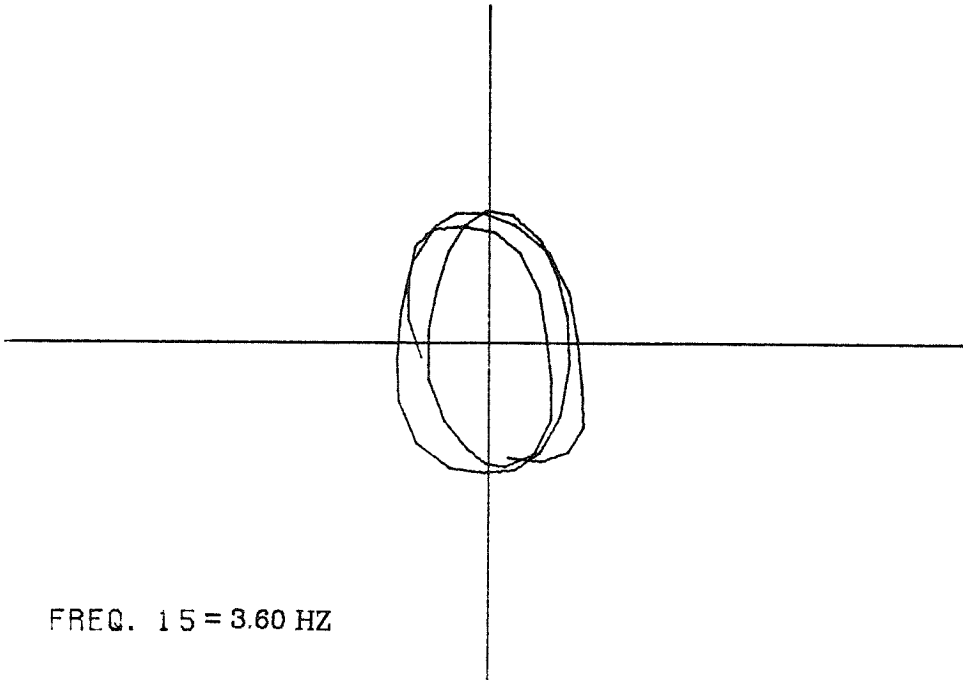


FREQ. 13 = 3.23 HZ

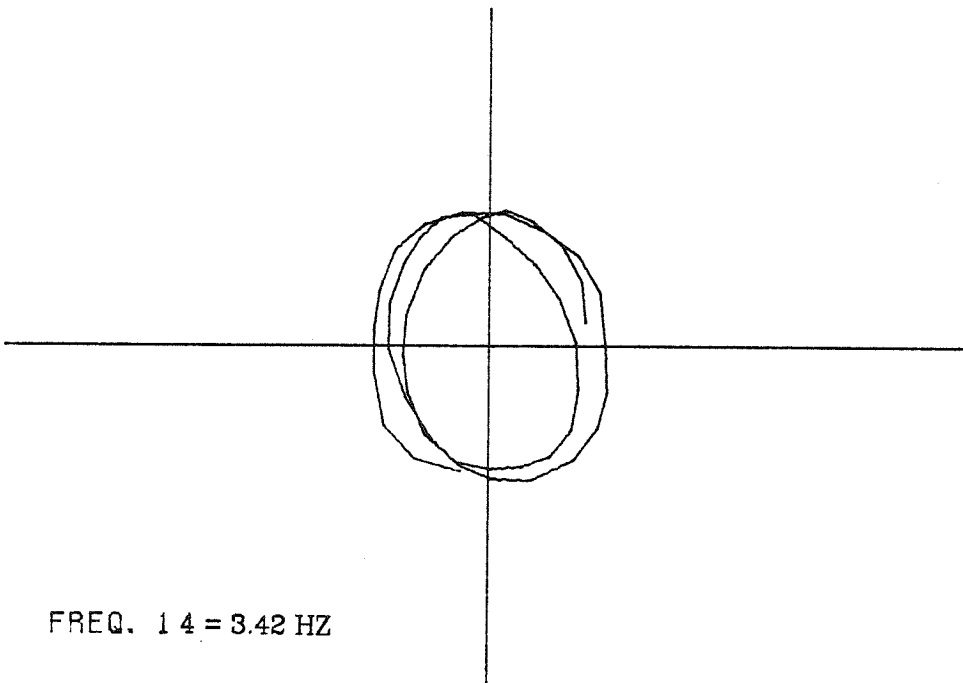


FREQ. 12 = 3.13 HZ

TEST 64



FREQ. 15 = 3.60 HZ



FREQ. 14 = 3.42 HZ